# Synthesis of Heterogeneous Heparan Sulfate Oligosaccharides to Investigate Structure-Activity Relationship (SAR)

**A Thesis**

**Submitted in partial fulfillment of the requirements for the degree of Doctor of Philosophy**

**By**
**Prashant Jain**
**ID- 20142014**

**Under the Guidance of**
**Dr. Raghavendra Kikkeri**


**Indian Institute of Science Education and Research, Pune**

*I would like to dedicate my thesis to my beloved family*

# CERTIFICATE

This is to certify that the work incorporated in this thesis entitled "***Synthesis of Heterogeneous Heparan Sulfate Oligosaccharides to Investigate Structure- Activity Relationship (SAR)***" submitted by **Prashant Jain** was carried out by candidate at Indian Institute of Science Education and Research, Pune under my supervision. The work presented here or any part of it has not been included in any other thesis submitted previously for the award of any degree or diploma from any other university or institution.

Date: 16-02-2021

Dr. Raghavendra Kikkeri
Associate Professor
IISER, Pune

# DECLARATION

I hereby declare that the thesis entitled ***"Synthesis of Heterogeneous Heparan Sulfate Oligosaccharides to Investigate Structure- Activity Relationship (SAR)"*** submitted for Doctor of Philosophy in Chemistry at Indian Institute of Science Education and Research, Pune, has not been submitted by me to any other university or institution. This work presented here was carried out at the, Indian Institute of Science Education and Research, Pune, India under the supervision of **Dr. Raghavendra Kikkeri.**

Date: 16-02-2021

Prashant Jain
ID: 20142014

# Acknowledgements

*I would like to express my sincere gratitude to my supervisor Dr. Raghavendra Kikkeri. More than me, this thesis belongs to him. It is his continuous efforts, dedication, and patience that have helped me throughout my Ph.D. tenure. I could not have asked for a better supervisor than him. His "never give up" attitude has helped me keep moving during the most challenging and stressful times in my Ph.D. His passion and creative thinking is something that has always motivated me to work better and smarter. His continuous faith in me, even during my failures, has helped me grow as an individual and confident person.*

*I would like to thank my collaborators, Dr. Vered and Shani, from Tel-Aviv University, Israel, for their time and efforts. The thesis would not have completed without their cooperation. I would also like to thank my RAC members, Prof. S.G. Srivatsan, from IISER, and Dr. Deepa Subramanyam from NCCS, Pune, for their valuable suggestions.*

*I would like to thank IISER Pune for providing me financial support. My heartfelt thanks to Prof. Jayant Udgaonkar, Director IISER Pune, Prof K.N. Ganesh (former Director IISER Pune) and Prof. H.N. Gopi, Chair Chemistry for providing excellent research facilities. A big thanks to all the chemistry technical team and instrument operators, especially Mr. Sandeep (for mass spectrometry, Mr. Nitin (for NMR) and, Mr. Saurav (for FACS) for making the Ph.D. process much more comfortable.*

*I would like to thank my lab mates (which I consider my family now) for their unlimited support throughout my Ph.D. Special thanks to my senior, Chethan, for making me do the chemistry the right way. It is his contribution and hard work in his initial days that made things easy for us. Preeti ma'am for teaching me the biological techniques and for being a good mentor to me. Thanks to Bala and Suraj for the incredible support. A big thanks to lab mates Sandhya, Vijendra, Trimbak, Rakesh, Saurabh, Sharath, Deepak, Haritha, and Keerthana for keeping the lab atmosphere alive and joyful. Huge thanks to lab alumni Rohan, Sivakoti, Harikrishna, Madhuri, Phani and Catherine for supporting me during my initial days.*

*I am indebted to my friends Girish and Om for their unbelievable support, love, and care. The journey would not have completed without them. I consider myself fortunate to have friends for life, special thanks to Puneeta (for the memorable moments), Mayur (the only roommate), Deepak, Yashwant, Preeti, Konoya and IPh.D. batch 2014 for a cherished time spent together.*

*Lastly, I would like to acknowledge my family and friends (Shwet, Shubham, Abhishek, Praveen and Sharvani) for their encouragement and support all through my studies. I am grateful to GOD almighty for the blessings and strength.*

*Prashant Jain*

# Contents

## *Chapter-3: Identification of a High Affinity Heparan Sulfate Ligands for Vascular Endothelial Growth Factor to Modulate Angiogenesis*

## *Chapter-4: Rational Designing of Glyco-nanovehicles to Target Cellular Heterogeneity*

# Abbreviations

## A

| | |
|---|---|
| AD | Alzheimer Disease |
| $AF_{555}$ | Alexa Fluor 555 |
| AM | Acetoxymethyl |
| AT | Antithrombin |
| ATP | Adenosine Triphosphate |
| APP | Amyloid Precursor Protein |

## B

| | |
|---|---|
| BAIB | Bis(acetoxy)iodobenzene |
| BMP-2 | Bone Morphogenetic Protein 2 |
| BACE-1 | Beta-site APP Cleaving Enzyme 1 |

## C

| | |
|---|---|
| CAMs | Cell Adhesion Molecules |
| CBDs | Carbohydrate Binding Domains |
| CM5 | Carboxymethylated |
| CS | Chondroitin Sulfate |
| CVDs | Cardiovascular Disease |

## D

| | |
|---|---|
| DDQ | 2,3-Dichloro-5,6-dicyano-1,4-benzoquinone |
| DMAP | 4-Dimethylaminopyridine |
| DMEM | Dulbecco's Modified Eagle's Medium |
| DMF | Dimethylformamide |

| | |
|---|---|
| DPPC | Diphenyl Phosphoryl Chloride |
| DS | Dermatan Sulfate |
| DTI | Direct Thrombin Inhibitor |

## E

| | |
|---|---|
| EBM-2 | Endothelial Basal Medium-2 |
| ECM | Extracellular Matrix |
| EDTA | Ethylenediaminetetraacetic acid |
| EGF | Epidermal Growth Factor |
| EGFR | Epidermal Growth Factor Receptor |
| ELISA | Enzyme-Linked Immunosorbent Assay |
| ESL-1 | E-Selectin Ligand 1 |

## F

| | |
|---|---|
| FBS | Fetal Bovine Serum |
| FDA | Food and Drug Administration |
| aFGF | acidic Fibroblast Growth Factor |
| bFGF | basic Fibroblast Growth Factor |
| FGFR | Fibroblast Growth Factor Receptor |
| FITC | Fluorescein isothiocyanate |

## G

| | |
|---|---|
| GAGs | Glycosaminoglycans |
| Gal | Galactose |
| GalN | Galactosamine |
| GlcA | Glucuronic Acid |
| GFs | Growth Factors |
| GPCRs | G-Protein Coupled Receptors |

## H

| | |
|---|---|
| HB-EGF | Heparin Binding- EGF -like Growth Factor |
| HCA | Hierarchical Cluster Analysis |
| Hep | Heparin |
| HR-ESI-MS Spectrometry | High Resolution Electrospray Ionisation Mass |
| HRP | Horseradish Peroxidase |
| HS | Heparan Sulfate |
| HSBPs | Heparan Sulfate Binding Proteins |
| HSPGs | Heparan Sulfate Proteoglycans |
| HUVECs | Human Umbilical Vein Endothelial Cells |

## I

| | |
|---|---|
| IdoA | Iduronic Acid |
| ITC | Isothermal Titration Calorimetry |

## K

| | |
|---|---|
| KS | Keratan Sulfate |

## L

| | |
|---|---|
| LMWH | Low Molecular Weight Heparin |

## M

| | |
|---|---|
| MAPK | Mitogen-activated Protein Kinases |
| MCP | Monocyte Chemoattractant Protein |
| MS | Molecular Sieves |

## N

| | |
|---|---|
| NA | N-Acetyl |
| NAP-Br | 2-(Bromomethyl)naphthalene |
| NFT | Neurofibrillary tangles |
| NHS | N-Hydroxysuccinimide |
| NIS | N-Iodosuccinimide |
| NMR | Nuclear Magnetic Resonance |
| NU | N-Unsubstituted |

## P

| | |
|---|---|
| PBS | Phosphate Buffered Saline |
| PHF | Paired Helical Filaments |
| PMSF | Phenylmethane Sulfonyl Fluoride |
| PSGL-1 | P-Selectin Glycoprotein Ligand -1 |
| PTSA | p-Toluenesulfonic Acid |
| PVDF | Polyvinylidene Fluoride |
| py | Pyridine |

## R

| | |
|---|---|
| RANTES | Regulated on activation, normal T cell expressed and secreted |
| RFU | Relative Fluorescence Units |
| RPMI | Roswell Park Memorial Institute |
| RT | Room Temperature |

## S

| | |
|---|---|
| SAR | Structure-Activity Relationship |

| | |
|---|---|
| SD | Standard Deviation |
| SDS | Sodium Dodecyl Sulfate |
| SEM | Standard Error of the Mean |
| SPR | Surface Plasmon Resonance |

## T

| | |
|---|---|
| TBAI | Tetrabutylammonium Iodide |
| TBDPS-Cl | tert-Butyldiphenylsilyl Chloride |
| TEM | Transmission Electron Microscopy |
| TEMPO | 2,2,6,6-Tetramethyl-1-piperidinyloxy |
| THF | Tetrahydrofuran |
| T-HP | Texas red- Heparin |
| TLC | Thin-layer Chromatography |
| TMB | 3,3′,5,5′-Tetramethylbenzidine |
| TME | Tumor Microenvironment |
| TMSSPh | Phenyl Trimethylsilyl Sulphide |
| TNBCs | Triple Negative Breast Cancer Cells |

## U

| | |
|---|---|
| UFH | Unfractionated Heparin |

## V

| | |
|---|---|
| VEGF | Vascular Endothelial Growth Factor |

# Abstract

Understanding the relationship between the chemical structure of a molecule and its biological activity holds tremendous potential for drug candidates' development in several pathophysiological conditions. Carbohydrates, the most diverse biomolecules present on cell surfaces or extracellular matrix spaces, remains the least explored molecules in this scenario due to their structural complexity and bioavailability. Heparan sulfate (HS), a carbohydrate polymer accompanied by a broad range of biological activities, is undisputedly the most complex polysaccharide present in living systems. Despite decades of research investigating HS's structure-activity relationship, our current understanding is limited by its extensive microheterogeneity. Identification of the structural epitopes of HS that are responsible for orchestrating various cellular processes could enable us to fine-tune the interactions among those processes that modulate biological activities. Inspired by this, we have synthesized a combinatorial library of HS tetrasaccharides and investigated their structural relationships with chemokines, growth factors, P-selectin, and Tau protein.

Chapter 1 briefly introduces cell surface glycans and discusses the structural details of glycosaminoglycans, one of the major classes of surface glycans, with a focus on HS heterogeneity. Also, with the help of a literature review, the chapter introduces the aim of the thesis by reviewing the previously known structure-activity relationship (SAR) details of HS with heparan sulfate binding proteins (HSBPs).

Chapter 2 summarizes the synthesis of the novel heparin tetrasaccharides (HT) library used to investigate structure-activity relationship. To discover the new binding epitopes responsible for selectively activating chemokines, comprehensive microarray and surface plasmon resonance (SPR) analyses were conducted using a broad spectrum of chemokines. Surprisingly, the rare *N*-unsubstituted (NU) domain carrying the HT ligands HT-2,6S-NH and HT-3,6S-NH was found to modulate the activities of CCL2 and CCL5. Furthermore, HT-3,6S-NH was successfully used to inhibit CCL2-mediated cancer cell proliferation, migration, and invasion. We believe that CCL2 and CCL5 are only the fourth and fifth proteins that have been found to recognize HS's NU domain.

Chapter 3 describes the systematic investigation method used to identify high-affinity HS ligands that modulate angiogenesis. The HS library described in Chapter 2 was used to determine their binding affinities with the growth factors, namely BMP-2, amphiregulin, HB-EGF, $VEGF_{165}$, and FGF-2. Glycan microarray and SPR analysis identified the wide binding preferences of HS ligands with growth factors. However, the unexpectedly high binding of HT-6S-NAc and HT-2,6S-NAc with the growth factor $VEGF_{165}$ was observed, which suggested that HT ligands can be used to target the cellular signaling mediated by $VEGF_{165}$. To substantiate the binding profiles of $VEGF_{165}$ and the HT ligands 6S-NAc and 2,6S-NAc, *in vitro* experiments with human umbilical vein endothelial cells (HUVECs) were conducted. The successful inhibition of $VEGF_{165}$-mediated HUVEC cell proliferation, migration, and endothelial tube formation in the presence of synthetic HT ligands revealed the hidden structural features of HS that could be crucial for the development of antiangiogenic agents.

Chapter 4 addresses a new aspect to study structure-activity relationship of HT ligands with HSBPs wherein the multivalent fluorescent glyco-gold nanovehicle is constructed to target the epidermal growth factor receptors (EGFR) present on triple-negative breast cancer cells (TNBCs). A series of confocal images using HT-6S-NAc- and HT-6P-modified nanovehicles showed that HT-6S-NAc-capped gold nanoparticles in the two-dimensional cell culture model had uptake that was preferential compared with that of HT-6P. Also, this preferential uptake was in good agreement with the cell-surface EFGR expression on the TNBCs, with MDA-MB-468 (which had the highest EGFR expression) showing remarkably high uptake compared to that of SK-Br-3 (which had the lowest EGFR expression). Furthermore, the results were validated by selectively targeting cancer cells in the tumor microenvironment using the three-dimensional cell culture technique. Overall, the results support the use of HT ligands in targeted cancer therapy.

Finally, Chapter 5 summarizes HT ligands' high-throughput screening profiles with P-selectin and Tau protein acquired by glycan microarray. We have identified a structurally well-defined *N*- unsubstituted HT ligand (HT-2S-NH) with exceptionally high P-selectin binding for the first time. The results support the decades-old theory that suggests selectin binding preferences with non-sulfated glucosamine residues containing HS

oligosaccharides. In addition, the microarray binding profiles of HT ligands with Tau protein are summarized and discussed in detail.

# Publications

1. **Jain, P**.; Shanthamurthy, C. D.; Ben-Arye, S. L.; Woods, R. J.; Kikkeri, R.; Padler-Karavani, V. Discovery of Rare Sulfated N-Unsubstituted Glucosamine Based Heparan Sulfate Analogs Selectivly Activating Chemokines. *Chem Sci.* ***(Accepted 2021)***. *DOI: 10.1039/d0sc05862a*
2. **Jain. P**.; Shanthamurthy. C. D.; Chaudhary. P.M.; Kikkeri, R. Rational Designing of Glyco-nanovehicles to Target Cellular Heterogeneity *Chem Sci.* ***(Accepted 2021)***. *DOI: 10.1039/D1SC00140J*
3. Danielson, E.; Dindo, M.; Porkovich, A. J.; Kumar, P.; Wang, Z.; **Jain, P.**; Mete, T.; Ziadi, Z.; Kikkeri, R.; Laurino, P., Non-enzymatic and highly sensitive lactose detection utilizing graphene field-effect transistors. *Biosens. Bioelectro.* **2020,** *165*, 112419.
4. Bhingardeve, P.; Madhanagopal, B. R.; Naick, H.; **Jain, P**.; Manoharan, M.; Ganesh, K. Receptor-Specific Delivery of Peptide Nucleic Acids Conjugated to Three Sequentially Linked N-Acetyl Galactosamine Moieties into Hepatocytes. *J. Org. Chem.* **2020,** *85* (14), 8812-8824.
5. Anand, S.; Mardhekar, S.; Raigawali, R.; Mohanta, N.; **Jain, P**.; D. Shanthamurthy, C.; Gnanaprakasam, B.; Kikkeri, R., Continuous-Flow Accelerated Sulfation of Heparan Sulfate Intermediates. *Org. Lett.* **2020,** *22* (9), 3402-3406.
6. Shanthamurthy, C. D.; **Jain, P**.; Yehuda, S.; Monteiro, J. T.; Ben-Arye, S. L.; Subramani, B.; Lepenies, B.; Padler-Karavani, V.; Kikkeri, R. ABO Antigens Active Tri-and Disaccharides Microarray to Evaluate C-type Lectin Receptor Binding Preferences. *Sci. Rep.* **2018,** *8* (1), 1-7.
7. **Jain, P**.; Shanthamurthy, C. D.; Ben-Arye, S. L.; Padler-Karavani, V.; Kikkeri, R., Identification of a High Affinity Heparan Sulfate Ligand for Vascular Endothelial Growth Factor to Modulate Angiogenesis *(Under Revision).*
8. Shanthamurthy, C. D.; Gimeno, A.; Ben-Arye, S. L.; Kumar, N. V.; **Jain, P.**; Padler-Karavani, V.; Jiménez-Barbero, J.; Kikkeri, R. The Next Generation Heparan Sulfate Mimics for Modulating Biological Activities *(Under Revision).*

**9.** Kikkeri, R.; **Jain. P.**; Shanthamurthy. C. D.; Kumar, N. V.; Raigawali, R.; Ben-Arye, S. L.; Padler-Karavani, V. Heparan Sulfate Compounds As Chemokine Inhibitors. PCT patent **(filed 2021).**

**10.** Bhingardeve, P.; **Jain P**.; Ganesh, K. Formation of Conjoined Triplex of Duplexes by Homothymine- Homocytosinyl C$\gamma$(*S/R*)- Bimodal Peptide Nucleic Acids (C$\gamma$-*bm*-PNA) with DNA $dA_8/dG_6$ and Cell Permeability. **2021.** (Manuscript Submitted)

# CHAPTER- 1

## Introduction

# 1.1 Introduction:

Cell surface glycans offer an abundance of opportunities to study the cell's physiological process. These glycans are mostly present on the cell surfaces in the form of glycocalyx: [1, 2] the hair-like structures covering virtually all the mammalian cells (Figure 1). Glycocalyx composition can be broadly classified into two categories; glycolipids and glycoproteins that work together as a cell-protective coat. Mainly, the carbohydrate portion of these molecules helps in cell-cell recognition, communication, and intracellular adhesion. Additionally, they represent the first defense line against several bacteria, viruses, or pathogens entering our body.[3]

Structurally, glycoprotein consists of a core protein chain covalently modified/ glycosylated with carbohydrate units either at serine/ threonine or an asparagine residue of

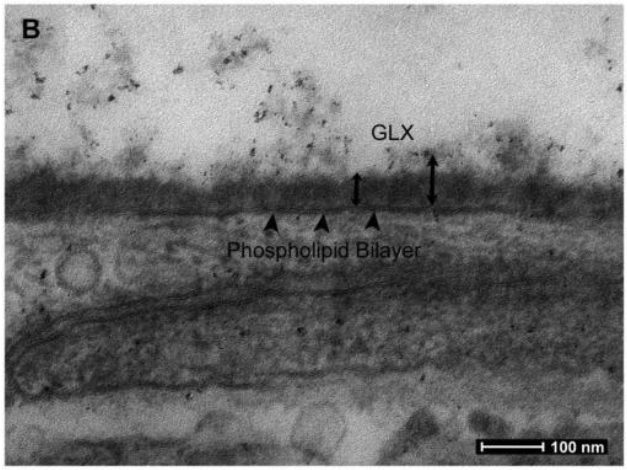


**Figure 1:** Transmission electron micrograph of fetal endothelial cells. (Adapted with permission from reference 2)

proteins fabricating O- or N- glycans, respectively.[4-6] The carbohydrate composition can vary from monosaccharide units to complex branch oligosaccharides giving rise to macromolecular structures on the cell surfaces. A subset of glycoprotein, which makes up to 50- 90 % of glycocalyx composition, are categorized as proteoglycans (Figure 2).

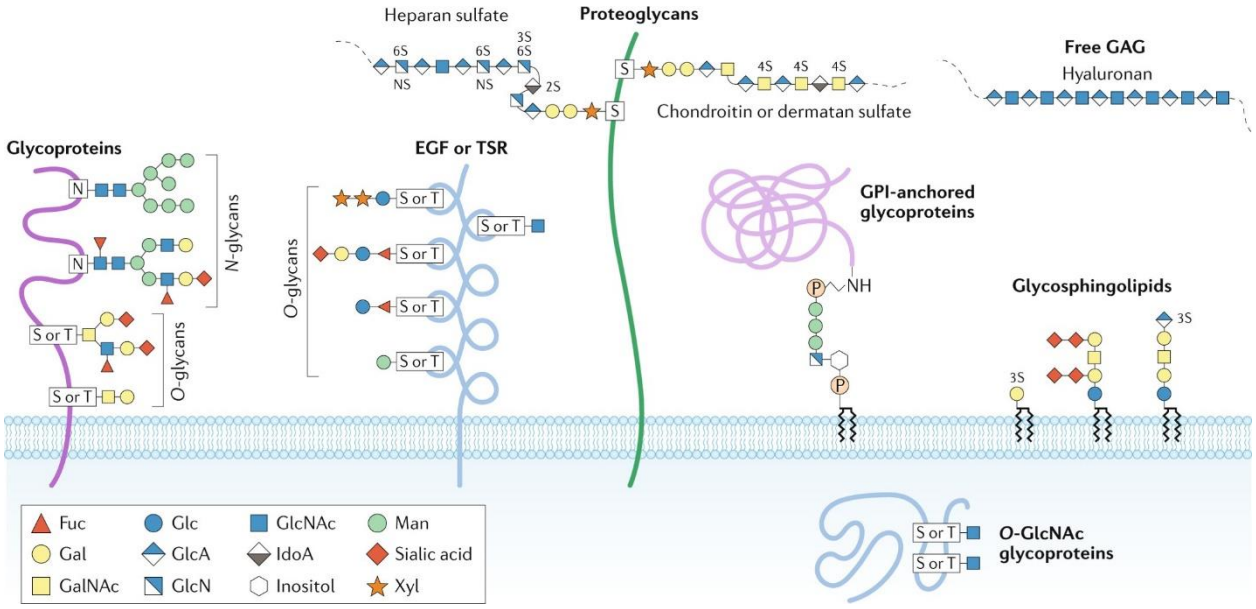


**Figure 2:** Cell surface arrangement of glycoprotein, glycolipids and proteoglycans. (Adapted with permission from reference 3)

In proteoglycans, proteins cores are heavily glycosylated with polysaccharides, a.k.a. glycosaminoglycans (GAGs). GAGs are linear carbohydrate polymer comprising of disaccharide repeating units having an amino sugar (either glucosamine or galactosamine) and a uronic acid (either glucuronic or iduronic acid) as monosaccharide building blocks. These polysaccharides are negatively charged that arises due to the sulfate or carboxylate groups present within the backbone.[7] Based on the disaccharide assembly; GAGs are generally divided into five major categories (Figure 3). For instance, Dermatan Sulfate (DS) consists of iduronic acid (IdoA) and galactosamine (GalN) as disaccharide repeating units, whereas Chondroitin Sulfate (CS) assembly is made up of glucuronic acid (GlcA) and GalN. Likewise, Keratan Sulfate (KS) belongs to a GAG family but does not contain uronic acid as a backbone unit and instead has galactose (Gal) and GalN as their disaccharide repeating units. Hyaluronan (HA), the only GAG molecule lacking sulfate moieties, is generally present as free polysaccharides within the extracellular matrix space and is not attached to any protein cores. [8-11]

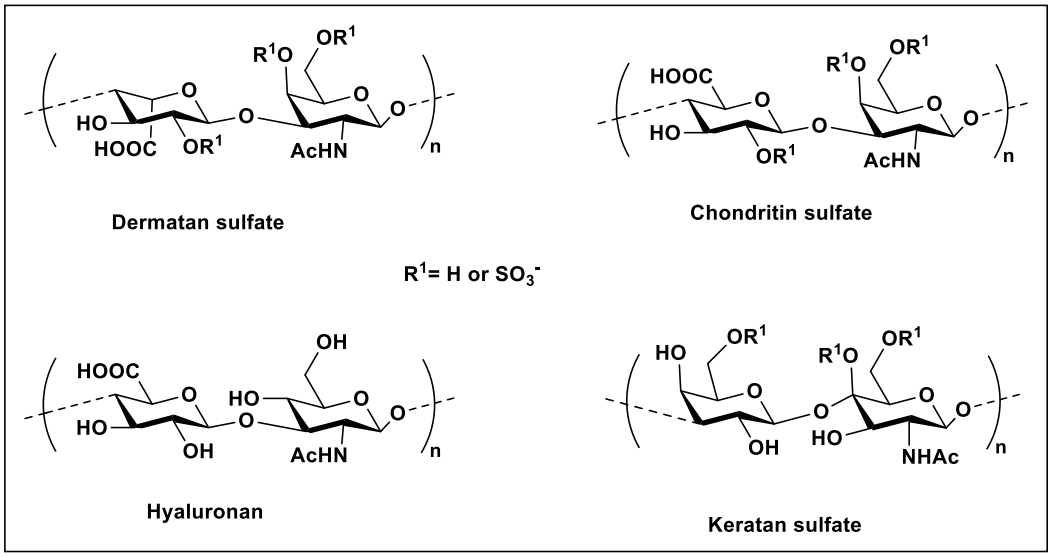


**Figure 3:** Glycosaminoglycans (DS, CS, HA & KS) repeating units.

Finally, the most heterogeneous carbohydrate polymer predominantly present on all mammalian cell membranes and extracellular matrix space is Heparan Sulfate Proteoglycans (HSPGs). Similar to other GAG family member Heparan Sulfate (HS) contains disaccharide repeats of GlcN and uronic acid (both IdoA and GlcA) along with negatively charged sulfate moieties unevenly distributed throughout the backbone that ultimately regulates a broad range of biological activities.

## 1.2 Heparan Sulfate (HS)/ Heparin:

Heparan Sulfate (HS) / Heparin, a negatively charged biomolecules that are generally found on the cell surfaces or extracellular matrix (ECM), belongs to a proteoglycan's family. Approximately 17 HSPGs have been identified so far, which includes both cell membrane attached and secreted molecules.[12] The glycated part of the protein present in all animal tissues is linear polysaccharide having repeating disaccharide unit composed of glucosamine and uronic acid. The amino sugar alpha linked to uronic acid (glucuronic or iduronic acid) may be *N*-acetylated or *N*- sulfated, whereas free amine (*N*- unsubstituted) are very rarely found. In addition to it, the uronic acid composition varies extensively. Glucuronic acid, a critical unit of HS, is beta linked to glucosamine residue to make around 50 % of the total disaccharide repeats, while iduronic acid is majorly present in heparin is alpha linked (Figure 4). [13, 14]

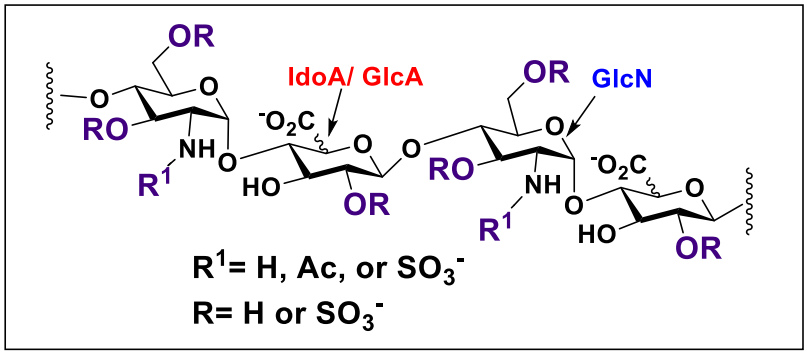


**Figure 4:** Heparan Sulfate (HS)/ Heparin chemical structure. R/ $R^1$ depicts potential sites of sulfation

Along with the *N*-sulfate, the sugar moieties are often modified with *O*-sulfate at 6- and 3- *O* position of glucosamine and 2- *O* position of iduronic acid. This differential sulfation in the backbone and the mixed uronic acid composition substantially increases HS microheterogeneity. HS or heparin is being used interchangeably among the scientific community; however, there are some key structural difference between them. For example, HS is synthesized virtually by all cells, whereas heparin synthesis is carried out exclusively by connective tissue-type mast cells. In addition to that, size and sulfation patterns vary extensively, with heparin displaying higher order of negative charges within the backbone compared to HS. HS is known to bind with hundreds of proteins present on cell surfaces or extracellular matrix space, thereby regulating various cellular processes, including cell differentiation, morphogenesis, blood coagulation, inflammation, angiogenesis, stem cell renewal, etc.[15, 16] However, despite the immense growth in HS or heparin synthesis literature, the Structure-Activity Relationship (SAR) of HS is poorly understood.

In the past, several research groups have synthesized broad and well-defined HS oligosaccharides to explore the structure-activity relationship with HSBPs. Pioneer work is done by Linhardt et al. to create chemoenzymatically well-controlled HS oligosaccharide libraries.[17] Synthesis of homogeneous LMWH as an anti-coagulant drug provides an alternative to naturally occurring HS procured from animals to reduce the severe side effects.[18] In addition to it, synthesis of a combinatorial library of 66 HS oligosaccharide covering a broad range of sulfation pattern and sizes were reported by the same group to facilitate SAR studies.[19] Similarly, Boons et al. reported the modular synthesis of HS oligosaccharide sequences, which were further employed to study HS's structural

requirements to inhibit the protease BACE-1, a precursor enzyme that generates neurotoxic amyloid beta-peptide.[20] The library was further expanded to a larger oligosaccharide size, which could uncover active HS epitopes.[21, 22]

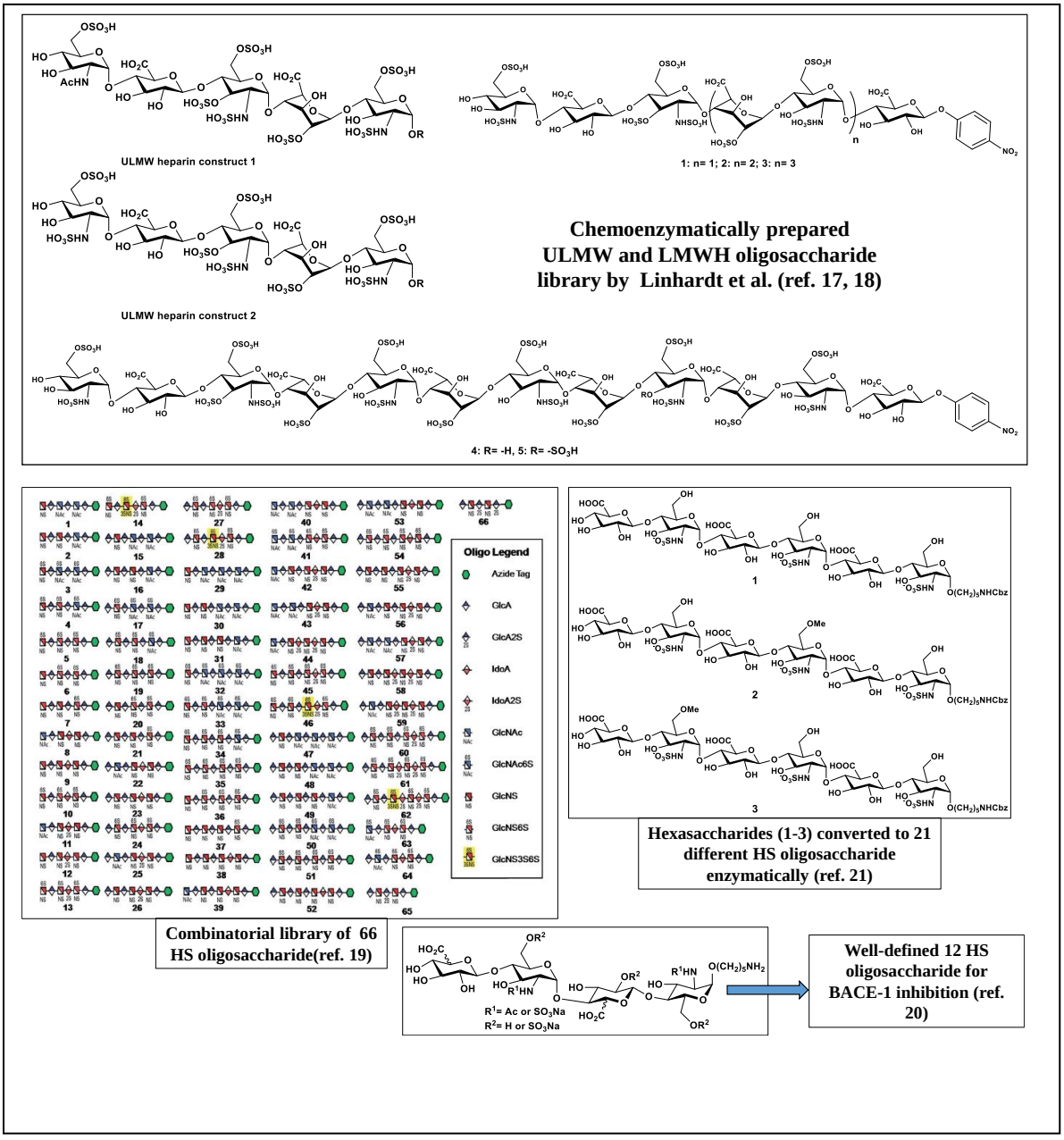


**Figure 5**: Structurally well-defined HS/ Heparin oligosaccharide library

In a similar fashion, libraries constructed by Seeberger, Liu, and others revealed the crucial binding repeats of HS to fine-tune heparin- protein interactions (Figure 5).[23- 26]

Construction of chemically synthesized heparin oligosaccharide libraries is often limited to the shorter chain length or fewer analogs of higher complex polysaccharides chains due to inherent difficulties in synthesis and heterogeneity associated with HS structure.[27] For instance, a simple disaccharide repeat of HS can generate 48 different HS analog with an exclusive sulfation pattern (Figure 6). Moreover, switching the reducing and non-reducing would yield another 48 repeats, thereby generating 96 unique HS epitopes that can be utilized for studying SAR. The complexity further increases exponentially upon an increase in the chain length. Therefore, the synthesis of precisely controlled HS oligosaccharides of higher-order remains a challenging task to date.

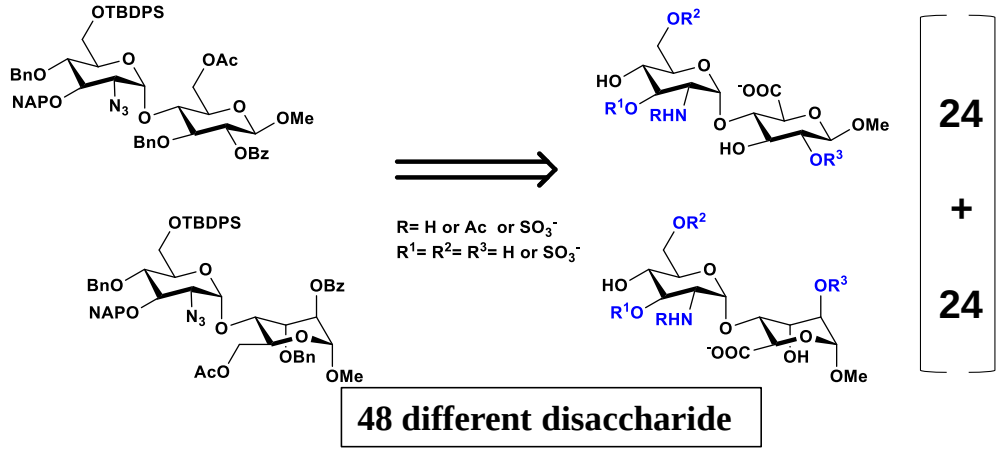


**Figure 6**: Maximum possible structurally unique HS epitopes at disaccharide level.

## 1.2.1 Structure-Activity Relationship (SAR) of Heparan Sulfate with HSBPs:

**1.2.1.1 Historical Aspect (Antithrombin):** World Health Organization reports cardiovascular diseases (CVDs) as the number one cause of death worldwide, accounting for almost 18 million lives in 2016, out of which 85% were due to heart attack and stroke. This pernicious disease's original genesis is blood clots forming in the arteries or veins of the heart, brain, lungs, kidney, and limbs. The circumstances in which excessive blood clotting occurs include deep vein thrombosis and peripheral artery diseases. Thrombin (also known as Factor IIA) is the serine protease, which cleaves fibrinogen to fibrin followed by platelet activation, leading to clot formation in the classical coagulation

cascade. During thrombosis, anticoagulants are required in a larger concentration to inhibit the serine proteases, which ultimately inhibits the cascade and clot formation. [28-31] Thrombin inhibitor can be broadly classified into two categories, namely, direct or indirect thrombin inhibitor. For instance, Bivalirudin, an FDA-approved drug, falls under the direct thrombin inhibitor (DTI) category, whereas heparin is an indirect thrombin inhibitor.[32]

Heparin binds to antithrombin (AT), a serine protease enzyme inhibitor, and activates it. The activated AT-Heparin complex then inhibits thrombin and other enzymes involved in its formation, particularly Factor Xa. The use of clinically approved Unfractionated Heparin (UFH) and Low Molecular Weight Heparin (LMWH) isolated from porcine mucosa as an anticoagulant is under the limelight for many years now.[33-35] However, it was not until the early 1980s when researchers discovered structural features of the anticoagulant heparin.[36] Efforts led by various research groups revealed a unique pentasaccharide sequence essential for AT binding (Figure 7). In addition to that, the role of 3-*O* sulfation at reducing end glucosamine residue within the pentasaccharide sequence was found to be critical. The removal of 3-*O* sulfate in pentasaccharide reduced the AT activity by 20000-fold upon binding.[37] Identification of the pentasaccharide sequence with a precise sulfation pattern remains the earliest example of the relationship between heparin structure and its activity with protein. The particular finding led to the discovery of only FDA approved drug in the market, commonly known as Fondaparinux (Arixtra).[38]

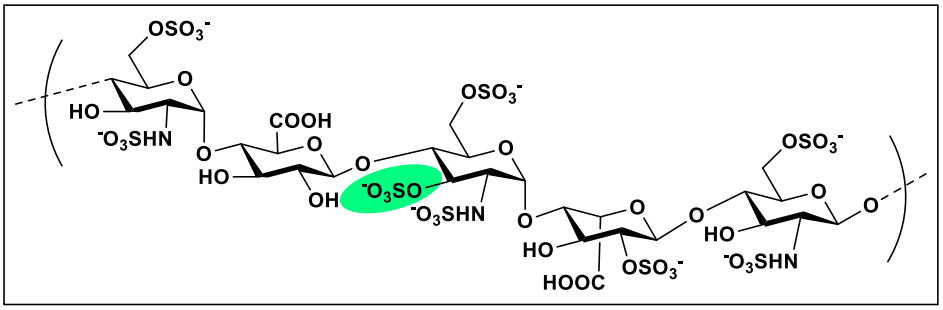


**Figure 7:** High affinity Heparin pentasaccharide for antithrombin binding. (Highlighted part shows the crucial sulfate moiety responsible for binding)

**1.2.2.2 Growth Factors:** Growth factors (GFs) represent a naturally occurring wide range of proteins/ signaling molecules capable of maintaining cell proliferation, migration,

differentiation, and survival. Aberrant GFs signaling can lead to diverse pathological conditions, including cancer. Lately, it has been observed that the binding of GFs with HSPGs plays a crucial role in regulating these cellular processes.[39, 40] For example, the formation of a ternary complex constituting FGF/FGFR/HS is crucial for FGFs signaling pathways. It has been proposed that HS protects FGFs from inactivation as well as from proteolytic degradation. However, similar to the antithrombin, there exist structural domains within the HS backbone critical for FGFs activation.[41, 42] Lindahl et al. showed that FGF-2 (bFGF) binds selectively with glucosaminyl 6-*O*-desulfated heparin but poorly with iduronosyl 2-*O*-desulfated analogs.[43] In addition to that, chemically fragmented natural HS with subsequent enzymatic O or N sulfation demonstrated the potential of oligosaccharides library to probe binding affinity with HSBPs.[44]

Further, Kimata et al. generated a well-defined sulfated octasaccharide library from naturally occurring sources to investigate the structural features of heparin required for GFs binding.[45] However, as obtained, HS from animal sources possesses batch to batch variation.[46] Moreover, chemical and enzymatic digestion of HS often leads to a heterogeneous mixture, which sometimes is difficult to purify and characterize. Besides, most libraries were randomly generated with minimum to no control over installing site-selective sulfate groups within the backbone and lacking the systematic investigation. Hung et al., in 2014, reported the divergent chemical synthesis of 48 different HS based disaccharide analog covering the maximum possible combination at disaccharide level and studied FGF-1 (aFGF) interactions. Among 48 disaccharides, only four could bind with FGF-1 determined through ITC, thereby exploring SAR at the disaccharide level.[47] The following study represented the synthetic sugar libraries as a powerful tool to unravel HS's accurate binding epitopes for systematized exploration.

Glycan microarray offers an effective platform for screening a large pool of oligosaccharides with proteins within a short period. The technique is robust and requires a significantly lower amount of substrates to study.[48, 49] Boons et al. synthesized a well-defined 47 different heparin tetrasaccharide library and recognized the structural requirements essential for FGF-2 binding using a glycan microarray platform, thereby expanding the database investigating heparin's SAR present currently.[50] However, as

quoted by them, "*the library does not cover the entire chemical space of HS-tetrasaccharides*." There is always a scope to expand the existing database. In addition to the above, binding affinities and SAR with other growth factors, including BMP-2, HB-EGF, VEGFs, are well documented.[41] HS oligosaccharides are widely known to play a crucial role in controlling $VEGF_{165}$ activity during angiogenesis and will be discussed in more detail later in the thesis.

**1.2.2.3 Chemokines:** Chemokines are small secreted proteins (8- 17 kDa) belonging to cytokine superfamily.[51] Like its parent family, they maintain cellular homeostasis and development through the different signaling cascades. In addition to that, chemokines are widely known to mediate cell migration, mainly white blood cells (leukocytes) through G-protein coupled receptors (GPCRs) during inflammation. Leukocytes are needed in larger concentrations and must be present at the right place for an appropriate immune response. Inflammatory chemokines, also known as chemoattractants, regulate leukocyte trafficking at the sites of inflammation in a well-organized chemotaxis pathway.

The role of HS in inflammation is well established. [52, 53] Chemokines secreted upon immune cells activation tether themselves to the endothelial cell surface with the aid of HS that ultimately binds with GPCRs present on leukocytes, facilitating its migration at the site of injury (Figure 8). However, during pathological conditions that include chronic inflammation and other autoimmune diseases, chemotaxis needs to be inhibited. Identification of the HS epitope responsible for chemokine attachment on surfaces could lead to novel drug candidates' development to inhibit chemokine-mediated cell movement.

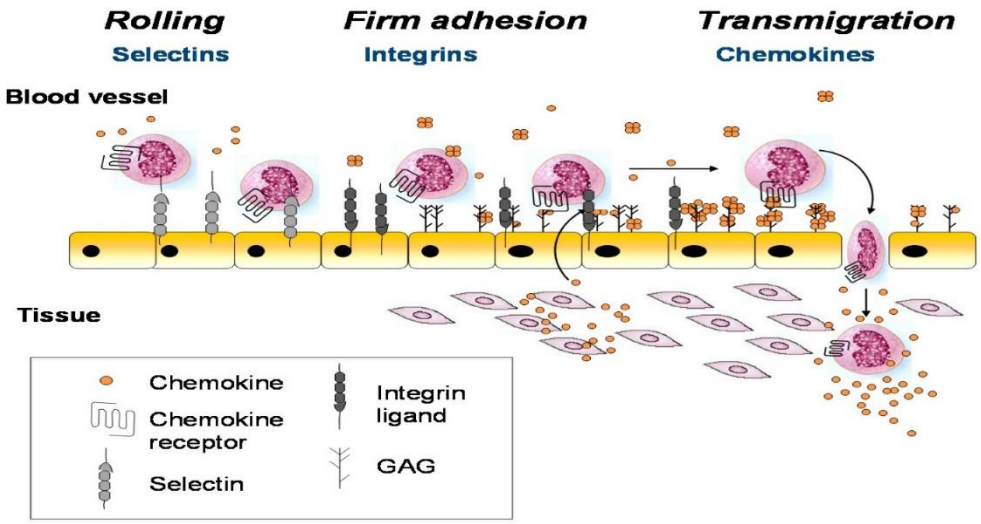


**Figure 8:** Role of GAGs in cell (leukocytes) recruitment during inflammation. (Adapted with permission from reference 42).

Seeberger et al. studied the binding profiles of synthetic HS analog with chemokines taking advantage of glycan microarray technology to understand the HS's structural features requirement. Surprisingly, it was observed that a simple 2,4- *O*- disulfate iduronic acid had strong comparable binding profiles as complex higher oligosaccharides, again demonstrating the use of synthetic libraries as a powerful approach to discover cryptic binding pocket ligands of HSBPs.[54] In addition to that, *in vitro* chemotaxis inhibition by a structurally defined hexasaccharide suggested the use of oligosaccharides as a potential drug candidate to modulate chemokine activity. Tetrasaccharide HS library, created by Boons et al., revealed distinct structural requirements to regulate chemokine activities.[50]

Though chemotaxis during inflammation is touted as the most dominant biological process regulated by chemokines and their receptors, several other processes, including angiogenesis, metastasis, embryonic development, etc., are highly influenced by the chemokines and its signaling network.[55] The role of inflammatory chemokine CCL5 and its receptor CCR5 in cancer progression is well documented.[56] Zlotnik et al. reported that the expression of CXCR4 and CCR7 is highly upregulated in human breast cancer cells, thereby controlling the metastasis upon interaction with their respective chemokines ligands.[57] Targeting the chemokine-receptor signaling axis in cancer metastasis by

synthetic HS analog could lead to the next generation drug molecules for therapeutic use. Therefore, understanding the SAR of synthetic HS analog with chemokines would be the first step for novel drug designing and discussed in more detail further in the thesis.

**1.2.2.4 Tau Protein**: Around 50 million lives worldwide are affected by dementia, adding nearly 10 million new cases every year. Alzheimer's disease (AD), a pathological condition with the deteriorated memory loss, is the most common form of dementia, accounting for almost 60- 70 % of total cases. Dysfunction or accumulation of Tau protein is among the major biological event involved in this life-threatening disease. Tau is a microtubule-associated protein (MAP) required to stabilize the microtubule network formed by tubulin within the nerve cells. The activity of Tau is regulated through a degree of phosphorylation accomplished by a microtubule-associated protein kinase. The activity of kinase and phosphatase is balanced in the normal adult brain, maintaining standard physiological conditions. However, in AD, Tau is abnormally hyperphosphorylated than the typical adult brain and results in the formation of paired helical filaments (PHFs) that self assembles to form neurofibrillary tangles (NFTs) (Figure 9). Phosphorylation of Tau results in its detachment from the microtubule, which in turn destabilizes the assembly. While normal Tau is soluble, the self-assembled structures are insoluble and form aggregates in the brain. This hyperphosphorylated Tau or aggregates does not bind to tubulin, disrupting the microtubule network, and leads to clinically significant Alzheimer's disease. [58, 59]

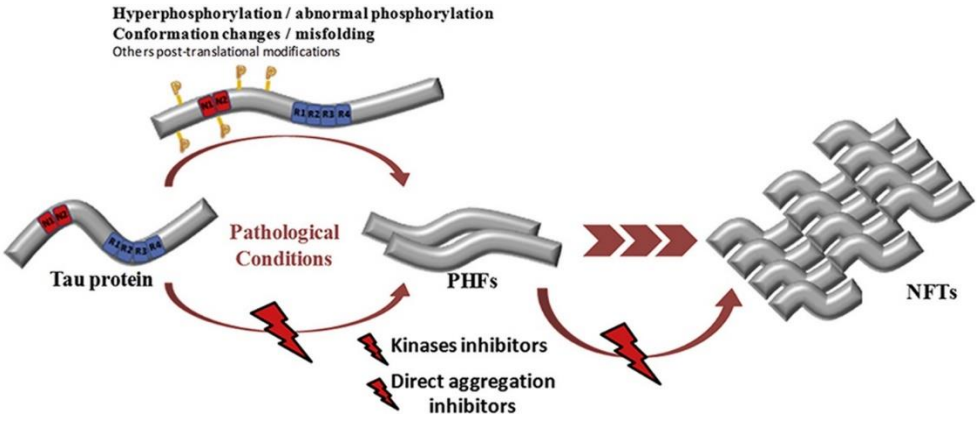


**Figure 9:** Tau protein aggregation mechanism (Adapted with permission from reference 48).

Recent studies suggest that this neurodegenerative disease's progression takes place in a "prion-like" manner wherein protein aggregates upon its release in the extracellular matrix space enters the neighboring cells to seed further aggregation.[60] In addition to that, prior work indicates that HSPGs are involved in this transcellular migration of Tau aggregates. Binding of protein aggregates to cell surface HS facilitates the seeding of aggregates in nearby cells.[61, 62] However, like other HSBPs, the structure-activity relationship of HS with Tau or its phosphorylated counterpart remains poorly understood. Some of the previous examples and newly found structural features of HS that may regulate Tau protein behavior are discussed further in more detail.

**1.2.2.5 P- Selectin**: Selectins are recognized as a separate class of carbohydrate-binding proteins (CBDs), or simply lectins, belong to a family of cell adhesion molecules (or CAMs). Based on the cell type on which it was initially being identified, they have been divided into three types, namely, L- selectin (identified first on lymphocytes), P- selectin (identified first on Platelets), and E- selectin (identified first on endothelium).[63, 64] The role of these transmembrane glycoproteins in inflammation and disease is well explored since their discovery in the late 1980s. Crucial initial adhesive events, for example, lymphocytes homing and leukocyte interaction with endothelium (discussed above under "chemokine" section), are some of the pivotal events mediated by selectins.[65] Therefore, selectins serve as an exciting target in inflammation-related diseases such as multiple sclerosis, rheumatoid arthritis, and cancer.[66, 67]

Selectin recognizes its ligand in a calcium-dependent manner and hence sometimes is also termed as C-type lectins. Carbohydrate ligand such as sialyl-Lewis$^x$ is one of the most studied ligands for selectin to date (Figure 10). PSGL-1 and ESL-1 are two glycoproteins that express these carbohydrate ligands and bind to P and E selectin, respectively, wherein PSGL-1 remains the most extensively studied glycoprotein at the molecular and cellular level. However, the binding of pure sialyl-Lewisx tetrasaccharide with P and L-selectins is weak, limiting the use of these carbohydrate ligands in therapeutics.[65]

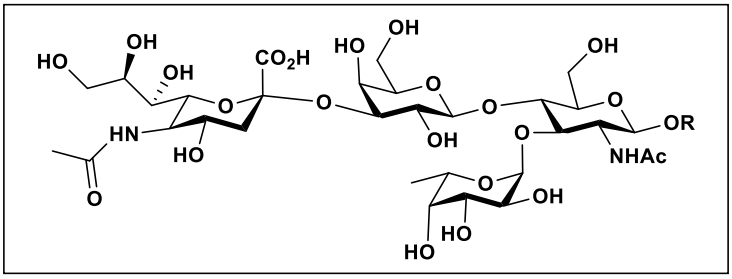


**Figure 10:** sialyl Lewis X (sLex) chemical structure.

Several studies in the early 1990s observed the binding of selectins with sulfated polysaccharides such as heparin, fucoidan, and dextran sulfate that opened new avenues for selectin targeting and this might be viable as a surrogate for the native Sia binding moiety.[68, 59] The research focused on studying HS's role in inflammation and immune-related disease involving selectin as a targeted ligand offers an attractive approach for exploring HS's therapeutic use.[70] However, the structural feature requirements for binding to P-selectins or selectins, in general, remains a challenging task. There exist only a few reports in the literature that explores the SAR of heparin with selectins.[71] This thesis presents the newly discovered structure features of HS oligosaccharides with P-selectin that could further lead to novel drug candidates' development.

The following chapters in the thesis summarize the synthesis of newly designed heterogeneous heparan sulfate oligosaccharides and subsequently explore its structure-activity relationship, mainly focusing on two different heparin sulfate binding proteins (HSBPs); growth factors and chemokines. In addition to that, newly discovered structural feature requirements for P-selectin and Tau protein were discussed briefly. Identifying optimal structural features essential for HSBPs activity could pave the path for the development of modern diagnostic agents or drugs.

## 1.3 References:


1. Reitsma, S.; Slaaf, D. W.; Vink, H.; Van Zandvoort, M. A.; oude Egbrink, M. G., The endothelial glycocalyx: composition, functions, and visualization. *Pflügers Arch.* **2007,** *454* (3), 345-359.
2. Fabre-Gray, A. C.; Down, C. J.; Neal, C. R.; Foster, R. R.; Satchell, S. C.; Bills, V. L., Imaging the placental glycocalyx with transmission electron microscopy. *Placenta.* **2018,** *74*, 59-61.
3. Reily, C.; Stewart, T. J.; Renfrow, M. B.; Novak, J., Glycosylation in health and disease. *Nature Rev. Nephrol.* **2019**, 1.
4. Roberts, K.; Grief, C.; Hills, G.; Shaw, P., Cell wall glycoproteins: structure and function. *J. Cell Sci.* **1985,** *1985* (Supplement 2), 105-127.
5. Hughes, R. C., *Membrane glycoproteins: a review of structure and function*. Elsevier: 2014.
6. Roberts, K.; Shaw, P.; Hills, G., High-resolution electron microscopy of glycoproteins: the crystalline cell wall of Lobomonas. *J. Cell Sci.* **1981,** *51* (1), 295-313.
7. Kjellén, L.; Lindahl, U., Proteoglycans: structures and interactions. *Ann. Rev. Biochem.* **1991,** *60* (1), 443-475.
8. Iozzo, R. V.; Schaefer, L., Proteoglycan form and function: a comprehensive nomenclature of proteoglycans. *Matrix Biol.* **2015,** *42*, 11-55.
9. Mende, M.; Bednarek, C.; Wawryszyn, M.; Sauter, P.; Biskup, M. B.; Schepers, U.; Bräse, S., Chemical synthesis of glycosaminoglycans. *Chem. Rev.* **2016,** *116* (14), 8193-8255.
10. Gandhi, N. S.; Mancera, R. L., The structure of glycosaminoglycans and their interactions with proteins. *Chemical Biol. Drug Des.* **2008,** *72* (6), 455-482.
11. Raman, R.; Sasisekharan, V.; Sasisekharan, R., Structural insights into biological roles of protein-glycosaminoglycan interactions. *Chem. Biol.* **2005,** *12* (3), 267-277.
12. Sarrazin, S.; Lamanna, W. C.; Esko, J. D., Heparan sulfate proteoglycans. *Cold Spring Harbor perspectives in biology* **2011,** *3* (7), a004952.

13. Shriver, Z.; Capila, I.; Venkataraman, G.; Sasisekharan, R., Heparin and heparan sulfate: analyzing structure and microheterogeneity. In *Heparin-A Century of Progress*, Springer: 2012; pp 159-176.
14. Rabenstein, D. L., Heparin and heparan sulfate: structure and function. *Nat. Prod. Rep.* **2002,** *19* (3), 312-331.
15. Bernfield, M.; Götte, M.; Park, P. W.; Reizes, O.; Fitzgerald, M. L.; Lincecum, J.; Zako, M., Functions of cell surface heparan sulfate proteoglycans. *Ann. Rev. Biochem.* **1999,** *68* (1), 729-777.
16. Xu, D.; Esko, J. D., Demystifying heparan sulfate–protein interactions. *Ann. Rev. Biochem.* **2014,** *83*, 129-157.
17. Xu, Y.; Masuko, S.; Takieddin, M.; Xu, H.; Liu, R.; Jing, J.; Mousa, S. A.; Linhardt, R. J.; Liu, J., Chemoenzymatic synthesis of homogeneous ultralow molecular weight heparins. *Science* **2011,** *334* (6055), 498-501.
18. Xu, Y.; Cai, C.; Chandarajoti, K.; Hsieh, P.-H.; Li, L.; Pham, T. Q.; Sparkenbaugh, E. M.; Sheng, J.; Key, N. S.; Pawlinski, R., Homogeneous low-molecular-weight heparins with reversible anticoagulant activity. *Nat. Chem. Biol.* **2014,** *10* (4), 248-250.
19. Zhang, X.; Pagadala, V.; Jester, H. M.; Lim, A. M.; Pham, T. Q.; Goulas, A. M. P.; Liu, J.; Linhardt, R. J., Chemoenzymatic synthesis of heparan sulfate and heparin oligosaccharides and NMR analysis: paving the way to a diverse library for glycobiologists. *Chem. Sci.* **2017,** *8* (12), 7932-7940.
20. Arungundram, S.; Al-Mafraji, K.; Asong, J.; Leach III, F. E.; Amster, I. J.; Venot, A.; Turnbull, J. E.; Boons, G.-J., Modular synthesis of heparan sulfate oligosaccharides for structure− activity relationship studies. *J. Am. Chem. Soc.* **2009,** *131* (47), 17394-17405.
21. Lu, W.; Zong, C.; Chopra, P.; Pepi, L. E.; Xu, Y.; Amster, I. J.; Liu, J.; Boons, G. J., Controlled chemoenzymatic synthesis of heparan sulfate oligosaccharides. *Angew. Chem. Int. Ed.* **2018,** *130* (19), 5438-5442.
22. Sun, L.; Chopra, P.; Boons, G.-J., Modular Synthesis of Heparan Sulfate Oligosaccharides Having N-Acetyl and N-Sulfate Moieties. *J. Org. Chem.* **2020**.

23. Xu, Y.; Wang, Z.; Liu, R.; Bridges, A. S.; Huang, X.; Liu, J., Directing the biological activities of heparan sulfate oligosaccharides using a chemoenzymatic approach. *Glycobiology* **2012,** *22* (1), 96-106.
24. de Paz, J. L.; Noti, C.; Seeberger, P. H., Microarrays of synthetic heparin oligosaccharides. *J. Am. Chem. Soc.* **2006,** *128* (9), 2766-2767.
25. Hecht, M.-L.; Rosental, B.; Horlacher, T.; Hershkovitz, O.; De Paz, J. L.; Noti, C.; Schauer, S.; Porgador, A.; Seeberger, P. H., Natural cytotoxicity receptors NKp30, NKp44 and NKp46 bind to different heparan sulfate/heparin sequences. *J. Proteome Res.* **2009,** *8* (2), 712-720.
26. Maza, S.; Macchione, G.; Ojeda, R.; López-Prados, J.; Angulo, J.; De Paz, J. L.; Nieto, P. M., Synthesis of amine-functionalized heparin oligosaccharides for the investigation of carbohydrate–protein interactions in microtiter plates. *Org. Biomol. Chem.* **2012,** *10* (10), 2146-2163.
27. Dulaney, S. B.; Huang, X., Strategies in synthesis of heparin/heparan sulfate oligosaccharides: 2000–present. In *Adv. Carbohydr. Chem. Biochem.*, Elsevier: 2012; Vol. 67, pp 95-136.
28. Harter, K.; Levine, M.; Henderson, S. O., Anticoagulation drug therapy: a review. *West. J. Emerg.* **2015,** *16* (1), 11.
29. Dahlbäck, B., Blood coagulation. *The Lancet* **2000,** *355* (9215), 1627-1632.
30. Crawley, J.; Zanardelli, S.; Chion, C.; Lane, D., The central role of thrombin in hemostasis. *J. Thromb. Haemost.* **2007,** *5*, 95-101.
31. Mann, K. G.; Butenas, S.; Brummel, K., The dynamics of thrombin formation. *Arterioscler. Thromb. Vasc. Biol.* **2003,** *23* (1), 17-25.
32. Di Nisio, M.; Middeldorp, S.; Büller, H. R., Direct thrombin inhibitors. *N. Engl. J. Med.* **2005,** *353* (10), 1028-1040.
33. Gray, E.; Hogwood, J.; Mulloy, B., The anticoagulant and antithrombotic mechanisms of heparin. In *Heparin-A century of progress*, Springer: 2012; pp 43-61.
34. Kishimoto, T. K.; Viswanathan, K.; Ganguly, T.; Elankumaran, S.; Smith, S.; Pelzer, K.; Lansing, J. C.; Sriranganathan, N.; Zhao, G.; Galcheva-Gargova, Z.,

Contaminated heparin associated with adverse clinical events and activation of the contact system. *N. Engl. J. Med.* **2008,** *358* (23), 2457-2467.

35. Guerrini, M.; Beccati, D.; Shriver, Z.; Naggi, A.; Viswanathan, K.; Bisio, A.; Capila, I.; Lansing, J. C.; Guglieri, S.; Fraser, B., Oversulfated chondroitin sulfate is a contaminant in heparin associated with adverse clinical events. *Nature Biotechnol.* **2008,** *26* (6), 669-675.
36. van Boeckel, C. A.; Petitou, M., The unique antithrombin III binding domain of heparin: a lead to new synthetic antithrombotics. *Angew. Chem. Int. Ed.* **1993,** *32* (12), 1671-1690.
37. Thacker, B. E.; Xu, D.; Lawrence, R.; Esko, J. D., Heparan sulfate 3-O-sulfation: a rare modification in search of a function. *Matrix Biol.* **2014,** *35*, 60-72.
38. Giangrande, P., Fondaparinux (Arixtra): a new anticoagulant. *Int. J. Clin.* **2002,** *56* (8), 615-617.
39. Turner, N.; Grose, R., Fibroblast growth factor signalling: from development to cancer. *Nat. Rev. Cancer* **2010,** *10* (2), 116-129.
40. Amann, J.; Kalyankrishna, S.; Massion, P. P.; Ohm, J. E.; Girard, L.; Shigematsu, H.; Peyton, M.; Juroske, D.; Huang, Y.; Salmon, J. S., Aberrant epidermal growth factor receptor signaling and enhanced sensitivity to EGFR inhibitors in lung cancer. *Cancer Res.* **2005,** *65* (1), 226-235.
41. Forsten-Williams, K.; Chu, C. L.; Fannon, M.; Buczek-Thomas, J. A.; Nugent, M. A., Control of growth factor networks by heparan sulfate proteoglycans. *Ann. Biomed. Eng.* **2008,** *36* (12), 2134-2148.
42. Mohammadi, M.; Olsen, S. K.; Ibrahimi, O. A., Structural basis for fibroblast growth factor receptor activation. *Cytokine Growth Factor Rev.* **2005,** *16* (2), 107-137.
43. Maccarana, M.; Casu, B.; Lindahl, U., Minimal sequence in heparin/heparan sulfate required for binding of basic fibroblast growth factor. *J. Biol. Chem.* **1993,** *268* (32), 23898-23905.
44. Jemth, P.; Kreuger, J.; Kusche-Gullberg, M.; Sturiale, L.; Giménez-Gallego, G.; Lindahl, U., Biosynthetic Oligosaccharide Libraries for Identification of Protein-binding Heparan Sulfate Motifs Exploring The Structural Diversity By Screening

For Fibroblast Growth Factor (Fgf) 1 And Fgf2 Binding. *J. Biol. Chem.* **2002,** *277* (34), 30567-30573.

45. Ashikari-Hada, S.; Habuchi, H.; Kariya, Y.; Itoh, N.; Reddi, A. H.; Kimata, K., Characterization of growth factor-binding structures in heparin/heparan sulfate using an octasaccharide library. *J. Biol. Chem.* **2004,** *279* (13), 12346-12354.
46. der Meer, V.; Kellenbach, E.; Van den Bos, L. J., From farm to pharma: an overview of industrial heparin manufacturing methods. *Molecules* **2017,** *22* (6), 1025.
47. Hu, Y.-P.; Zhong, Y.-Q.; Chen, Z.-G.; Chen, C.-Y.; Shi, Z.; Zulueta, M. M. L.; Ku, C.-C.; Lee, P.-Y.; Wang, C.-C.; Hung, S.-C., Divergent synthesis of 48 heparan sulfate-based disaccharides and probing the specific sugar–fibroblast growth factor-1 interaction. *J. Am. Chem. Soc.* **2012,** *134* (51), 20722-20727.
48. Park, S.; Gildersleeve, J. C.; Blixt, O.; Shin, I., Carbohydrate microarrays. *Chem. Soc. Rev.* **2013,** *42* (10), 4310-4326.
49. Disney, M. D.; Seeberger, P. H., The use of carbohydrate microarrays to study carbohydrate-cell interactions and to detect pathogens. *Chem. Biol.* **2004,** *11* (12), 1701-1707.
50. Zong, C.; Venot, A.; Li, X.; Lu, W.; Xiao, W.; Wilkes, J.-S. L.; Salanga, C. L.; Handel, T. M.; Wang, L.; Wolfert, M. A., Heparan sulfate microarray reveals that heparan sulfate–protein binding exhibits different ligand requirements. *J. Am. Chem. Soc.* **2017,** *139* (28), 9534-9543.
51. Hughes, C. E.; Nibbs, R. J., A guide to chemokines and their receptors. *FEBS J.* **2018,** *285* (16), 2944-2971.
52. Farrugia, B. L.; Lord, M. S.; Melrose, J.; Whitelock, J. M., The role of heparan sulfate in inflammation, and the development of biomimetics as anti-inflammatory strategies. *J. Histochem. Cytochem.* **2018,** *66* (4), 321-336.
53. Proudfoot, A. E.; Johnson, Z.; Bonvin, P.; Handel, T. M., Glycosaminoglycan interactions with chemokines add complexity to a complex system. *Pharmaceuticals* **2017,** *10* (3), 70.

54. de Paz, J. L.; Moseman, E. A.; Noti, C.; Polito, L.; von Andrian, U. H.; Seeberger, P. H., Profiling heparin–chemokine interactions using synthetic tools. *ACS Chem. Biol.* **2007,** *2* (11), 735-744.
55. Raman, D.; Sobolik-Delmaire, T.; Richmond, A., Chemokines in health and disease. *Exp. Cell Res.* **2011,** *317* (5), 575-589.
56. Aldinucci, D.; Colombatti, A., The inflammatory chemokine CCL5 and cancer progression. *Mediators Inflamm.* **2014,** *2014*.
57. Müller, A.; Homey, B.; Soto, H.; Ge, N.; Catron, D.; Buchanan, M. E.; McClanahan, T.; Murphy, E.; Yuan, W.; Wagner, S. N., Involvement of chemokine receptors in breast cancer metastasis. *Nature* **2001,** *410* (6824), 50-56.
58. Iqbal, K.; Liu, F.; Gong, C.-X.; Grundke-Iqbal, I., Tau in Alzheimer disease and related tauopathies. *Curr. Alzheimer Res.* **2010,** *7* (8), 656-664.
59. Jouanne, M.; Rault, S.; Voisin-Chiret, A.-S., Tau protein aggregation in Alzheimer's disease: an attractive target for the development of novel therapeutic agents. *Eur. J. Med. Chem.* **2017,** *139*, 153-167.
60. Brettschneider, J.; Del Tredici, K.; Lee, V. M.-Y.; Trojanowski, J. Q., Spreading of pathology in neurodegenerative diseases: a focus on human studies. *Nature Rev. Neurosci.* **2015,** *16* (2), 109-120.
61. Zhao, J.; Zhu, Y.; Song, X.; Xiao, Y.; Su, G.; Liu, X.; Wang, Z.; Xu, Y.; Liu, J.; Eliezer, D., 3-O-Sulfation of Heparan Sulfate Enhances Tau Interaction and Cellular Uptake. *Angew. Chem. Int. Ed.* **2020,** *59* (5), 1818-1827.
62. Wang, P.; Cascio, F. L.; Gao, J.; Kayed, R.; Huang, X., Binding and neurotoxicity mitigation of toxic tau oligomers by synthetic heparin like oligosaccharides. *Chem. Commun.* **2018,** *54* (72), 10120-10123.
63. Bevilacqua, M. P.; Nelson, R. M., Selectins. *J. Clin. Investig.* **1993,** *91* (2), 379-387.
64. McEver, R. P., Selectins. *Curr. Opin. Immunol.* **1994,** *6* (1), 75-84.
65. Ley, K., The role of selectins in inflammation and disease. *Trends Mol. Med.* **2003,** *9* (6), 263-268.

66. Barthel, S. R.; Gavino, J. D.; Descheny, L.; Dimitroff, C. J., Targeting selectins and selectin ligands in inflammation and cancer. *Expert Opin. Ther. Targets* **2007,** *11* (11), 1473-1491.
67. Impellizzeri, D.; Cuzzocrea, S., Targeting selectins for the treatment of inflammatory diseases. *Expert Opin. Ther. Targets* **2014,** *18* (1), 55-67.
68. Skinner, M. P.; Fournier, D. J.; Andrews, R. K.; Gorman, J. J.; Chesterman, C. N.; Berndt, M. C., Characterization of human platelet GMP-140 as a heparin-binding protein. *Biochem. Biophys. Res. Commun.* **1989,** *164* (3), 1373-1379.
69. Skinner, M. P.; Lucas, C.; Burns, G.; Chesterman, C.; Berndt, M. C., GMP-140 binding to neutrophils is inhibited by sulfated glycans. *J. Biol. Chem.* **1991,** *266* (9), 5371-5374.
70. Nelson, R. M.; Cecconi, O.; Roberts, W. G.; Aruffo, A.; Linhardt, R. J.; Bevilacqua, M. P., Heparin oligosaccharides bind L-and P-selectin and inhibit acute inflammation. *Blood* **1993**, 82 (11), 3253- 3258.
71. Norgard-Sumnicht, K. E.; Varki, N. M.; Varki, A., Calcium-dependent heparin-like ligands for L-selectin in nonlymphoid endothelial cells. *Science* **1993,** *261* (5120), 480-483.

# CHAPTER- 2

## Discovery of Rare Sulfated *N*-Unsubstituted Glucosamine Based Heparan Sulfate Analogs Selectively Activating Chemokines

## Abstract:

Achieving selective inhibition of chemokines with structurally well-defined heparan sulfates (HS) oligosaccharide can provide important insights into cancer cells migration and metastasis. However, HS is highly heterogeneous in chemical composition, which limits its therapeutic use. Here, we report the rational design and synthesis of *N*-unsubstituted (NU) and *N*-acetyl (NA) heparan sulfate tetrasaccharides that selectively inhibit structurally homologous chemokines. HS analogs were produced by divergent synthesis, where fully protected HS tetrasaccharide precursor was subjected to selective deprotection and regioselectively *O*-sulfated, and *O*-phosphorylated to obtain 13 novel HS tetrasaccharides. HS microarray and SPR analysis with a wide range of chemokines revealed the structural significance of sulfation patterns and NU domain in chemokines activities for the first time. Particularly, HT-3,6S-NH displayed an unprecedented binding capacity to CCL2 chemokine. Further systematic interrogation of the role of HT-3,6S-NH in cancer demonstrated an effective blockade of CCL2 and its receptor CCR2 interactions, thereby impairing cancer cell proliferation, migration and invasion, a step towards designing novel drug molecules.

## 2.1 Introduction:

Chemokines are endogenous signalling peptides essential for immuno-surveillance, homeostasis, inflammation, infection and tissue repair.[1-5] Chemokines and their receptor activities depend on how they bind and oligomerize in the presence of glycosaminoglycans (GAGs).[6-8] Humans express 47 chemokines and 20 receptors, and most of the chemokines are highly basic proteins. It has been therefore hypothesized elsewhere that chemokine-GAG binding is non-specific.[9-10] However, after the discovery of acidic CCL3 and CCL4 chemokines binding to GAGs, it had become clearer that their interaction proceeds in a sequence- dependent manner.[11, 12] Moreover, chemokines have shown different interaction strengths with various GAGs, including heparan sulfate (HS), chondroitin sulfate and dermatan sulfate, illustrating that microheterogeneity in GAG structures can modulate binding patterns, for example through uronic acid composition, sulfation patterns and oligosaccharide length.[13]

This has prompted the synthesis of well-described, homogeneous GAG structures, and more specifically HS oligosaccharides, to regulate chemokine activity. For example, Gallagher et al. reported that the CXCL4 chemokine requires HS 2-*O*-sulfated iduronic acid (IdoA) for tetramerization and binding to its cell surface receptors.[14] Elsewhere, Lindahl et al. had shown that interleukin-8 (CXCL8 or IL-8) prefers the IdoA(2-$OSO_3^-$)-GlcN$SO_3^-$(6$OSO_3^-$) repeating unit to activate neutrophil trafficking,[15] while Gardiner et al. reported the elegant role of 6-*O*-sulfation in switching the binding between CXCL12 and IL-8.[16] Hesieh-Wilson et al. demonstrated that the trisulfated IdoA(2-$OSO_3^-$)-GlcN$SO_3^-$ (6-$OSO_3^-$)-conjugated polymer strongly inhibited RANTES (CCL5)-CCR3-receptor-mediated cell migration.[17] In addition, Seeberger et al. showed that CCL21 strongly binds to a hexasaccharide containing the GlcN$SO_3^-$ (6-$OSO_3^-$)-IdoA(2-$OSO_3^-$) repeating unit as compared to CXCL12, while CCL19 does not bind to it at all.[18] Boons et al. discovered that CCL2 binds to highly sulfated HS compounds and exhibits no preference for the uronic acid component, while both CCL2 and CCL13 displayed promiscuous binding with most of the HS glycans.[19] These data suggest that well-defined HS oligosaccharides can provide structural details to target chemokine- GAG interaction to modulate its activities. However, HS is highly heterogeneous in its

structure and the majority of the HS libraries that have been used for chemokine studies are composed of *N*-sulfated and *N*-acetylated (NA) glucosamine domains.[17-19] Native HS also expresses an *N*-unsubstituted (NU) domains, but this region has not been fully investigated in existing studies.[20, 21] To address this gap, and to decipher the sulfation code of chemokine heparin binding, here we report the divergent synthesis of a limited number of NU- and NA domains HS tetrasaccharides (Figure 1).

High-throughput screening of these synthetic HS ligands with a wide range of chemokines revealed selective chemokine binder, which can be used to block chemokine activity to target cancer biology. However thus far, only few heparin binding proteins have been reported to bind NU-domain-containing HS ligands,[22- 26] and here we provide the first such example where chemokines activity was interrogated systematically with NU domain ligands.

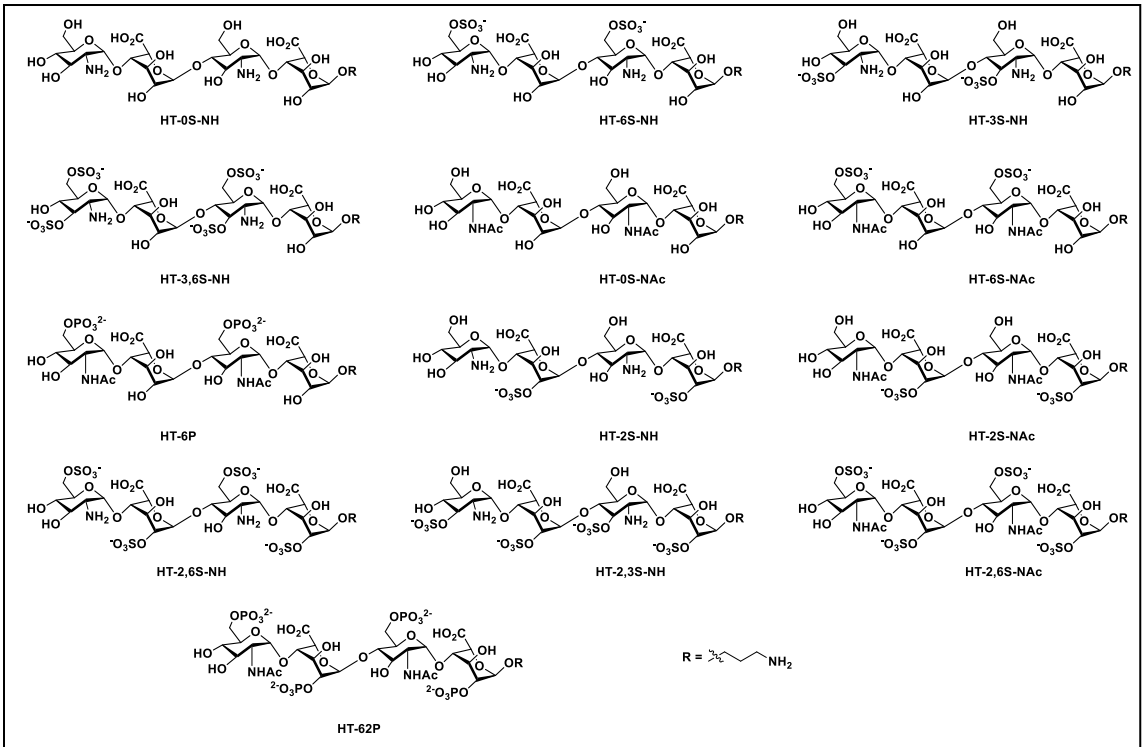


**Figure 1:** Structures of heparan sulfate tetrasaccharide analogs.

## 2.2 Results and Discussion:

### 2.2.1 Synthesis of orthogonally protected tetrasaccharides:

*N*-unsubstituted and *N*-acetylated HS analog library with regioselective sulfate modifications at 2-*O* (IdoA), 3-*O* (GlcN), and 6-*O* (GlcN) were obtained by single tetrasaccharide **27** and its *N*- acetate counterpart **28** (Scheme 1) using the divergent synthetic approach. Synthesis of **27** required a carefully designed technique that allowed us to do selective site modifications along the tetrasaccharide backbone in a controlled manner.

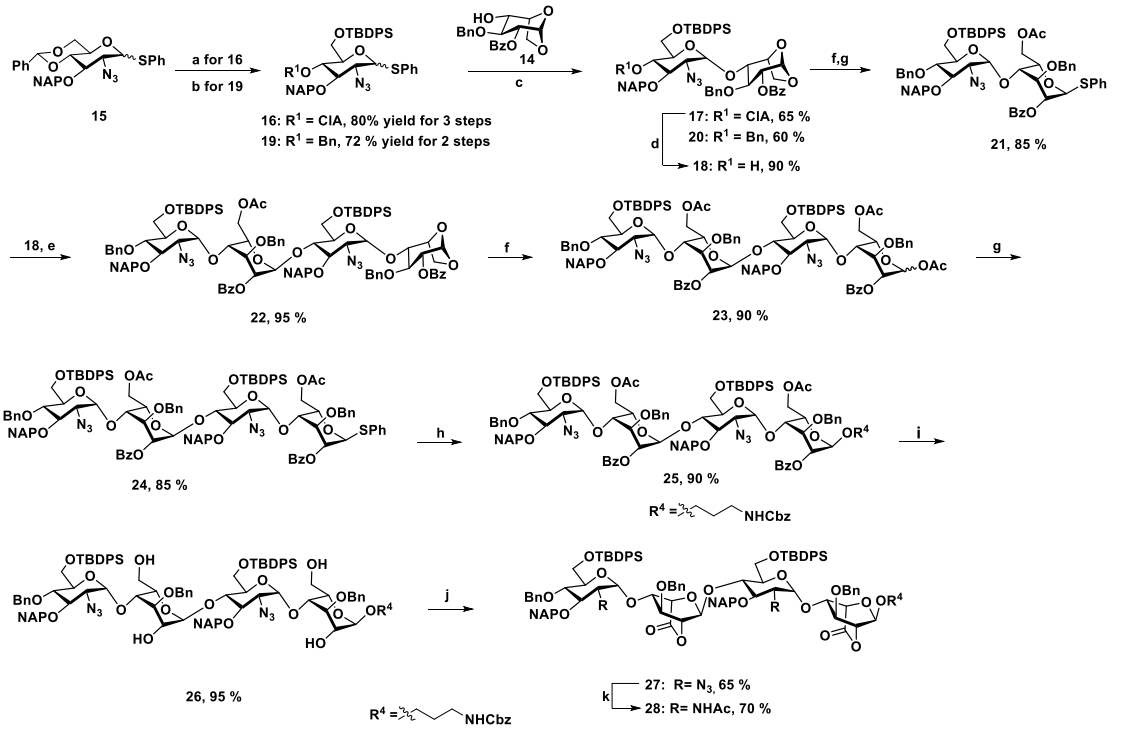


**Scheme 1:** (a) (i) PTSA, $CH_2Cl_2$/MeOH (1:2), rt, 6 h; (ii) TBDPSCl, imidazole, DMAP, $CH_2Cl_2$, 0 °C, 12 h; (iii) $(ClAc)_2O$, $CH_2Cl_2$/py (4:1), 0 °C, 20 min. (b) (i) $BH_3$•THF, TMSOTf, $CH_2Cl_2$, 0 °C, 6 h; (ii) TBDPSCl, imidazole, DMAP, $CH_2Cl_2$, 0 °C, 12 h. (c) NIS, TMSOTf, 4 Å MS, -78 °C to -20 °C, $CH_2Cl_2$, 30 min. (d) Thiourea, MeOH/ py (1:1), 80 °C, 1 h. (e) NIS, TMSOTf, 4 Å MS -10 °C, $CH_2Cl_2$, 30 min. (f) $Ac_2O$, $Cu(OTf)_2$, rt, 12 h. (g) TMSSPh, $ZnI_2$, $CH_2Cl_2$, rt, 2 h. (h) Benzyl (3-hydroxypropyl)carbamate, NIS, TfOH, 4 Å MS, rt, $CH_2Cl_2$, 30 min. (i) NaOMe, $CH_2Cl_2$/MeOH (1:1), rt, 12 h. (j) TEMPO, $CH_2Cl_2$/MeOH (1:1), rt, 12 h. (k) Zn, THF/AcOH/$Ac_2O$ (3:2:2), rt, 12 h.

Efforts led by various research groups revolutionized heparin sulfate synthesis in the past decade.[27-31] Using a similar strategy as Hung[28] et al. with slight modifications in the protecting group, synthesis of **27** was carried out by disaccharide building blocks **21** and

**18**. Notably, the use of 4-*O*-chloroacetate (ClA) at non reducing GlcN residue as a temporary protecting group in **17** was found to be vital for chain elongation than other previously reported 4-*O* protecting groups such as TCA[29] / Fmoc[30]/ Lev[31]. Disaccharides (**21 and 18**) and monosaccharide precursors were synthesized from glucosamine and iduronic acid building blocks **14, 16, 19 & 20**, as previously described.[28, 32] Next, we adopted [2+2] glycosylation approach with **21** (glycosyl donor) and **18** (glycosyl acceptor) to obtain 1,6 anhydrous tetrasaccharide **22** in excellent yield. Acetolysis of the reducing end IdoA residue of **22** with the aid of acetic anhydride and copper trifluoromethanesulfonate as catalyst followed by phenyl trimethylsulfide and $ZnI_2$ treatment afforded **24** as a thiophenol glycosyl donor. Linker glycosylation of **24**, followed by sequential deacetylation and TEMPO mediated oxidation of **25**, yielded **27** (72 % for three steps). Finally, C-2 azide of glucosamine moieties in **27** was converted into acetate in the presence of Zn/AcOH/$Ac_2O$ to develop tetrasaccharide **28**, which was further used to synthesize HS analogs with *N*-acetate backbone (Scheme 1).

### 2.2.2 Orthogonal deprotection and sulfation:

A divergent synthetic approach was followed to develop a combinatorial library of HS oligosaccharides. For instance, silyl protecting group TBDPS was deprotected selectively using 70 % HF.py for 6-*O*-sulfate derivatives precursors (**29 & 36**). Similarly, NAP deprotection with the help of DDQ yielded 3-*O*-sulfated precursors (**31 & 34**). The lactone ring was first opened for the derivatives carrying 2-*O*-sulfated IdoA, followed by the benzyl esterification to yield **39 & 42** in moderate yield (Scheme 2). Subsequent, selective deprotection was carried out in a similar manner for oligosaccharides having multiple *O*-2,6 or *O*-2,3 sulfate modifications (**45, 47 & 50**). $SO_3.NEt_3$ was used for introducing sulfate group in the backbone (**30, 32, 35, 37, 40, 43, 46, 48 & 51**), whereas for the phosphate derivative (**38 & 52**) diphenylphsphoryl chloride (DPPC) was utilized.

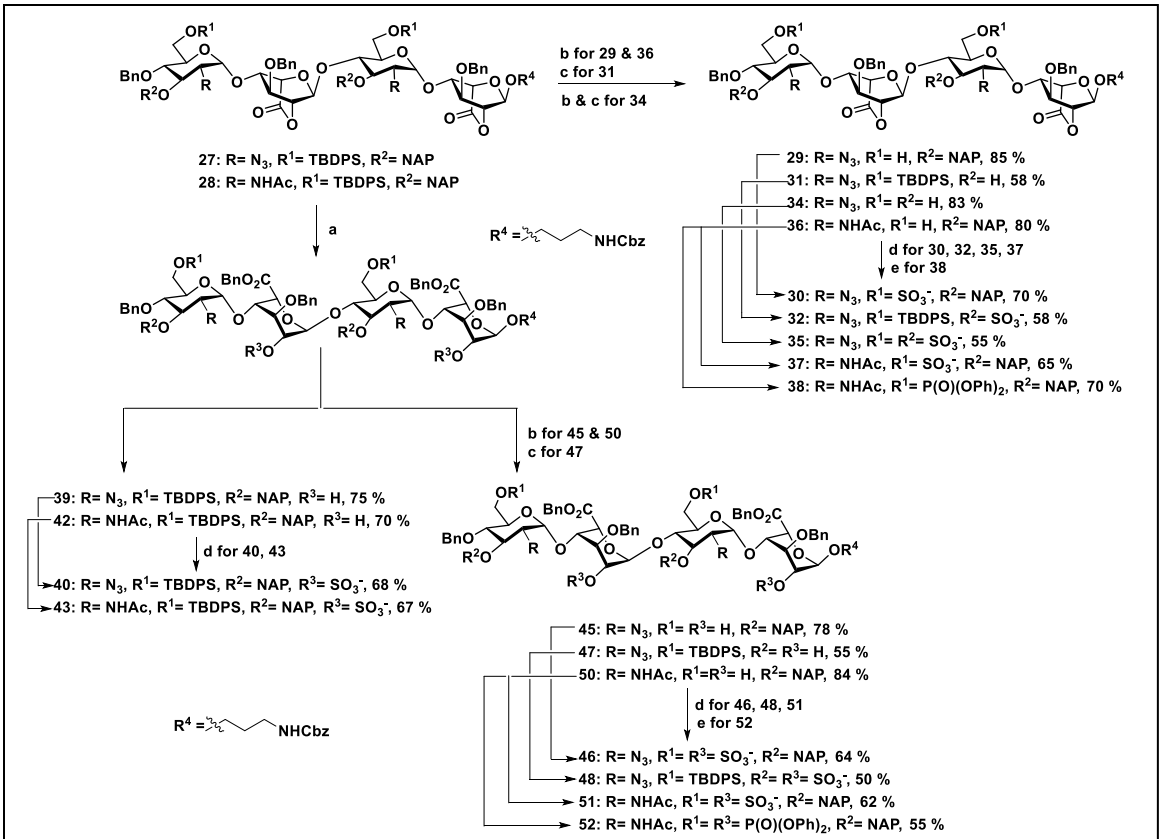


**Scheme 2:** (a) (i) LiOH•$H_2O$, THF/$H_2O$ (1:1), rt, 2 h; (ii) BnBr, TBAI, $NaHCO_3$, DMF, 60 °C, 2 h. (b) 70 % HF•py, py, 0 °C, 12 h. (c) DDQ, $CH_2Cl_2$/ $H_2O$ (18:1), rt, 1 h. (d) $SO_3$•$NEt_3$, DMF, 60 °C, 72 h. (e) DPPC, DMAP, $NEt_3$, $CH_2Cl_2$/py (1:1), 0 °C, 12 h.

Finally, global deprotection of all the sulfated derivatives, including non- sulfated analogs (**29 & 36**) yielded desired HS tetrasaccharide **1-13** with the amine linker at the reducing for the generation of HS microarray (Scheme 3). Final HS oligosaccharides and intermediates were characterized by $^{1}H$, $^{13}C$, DEPT and $^{31}P$ NMR. Additionally, molecular weights for all the compounds were confirmed by high-resolution mass spectroscopy.

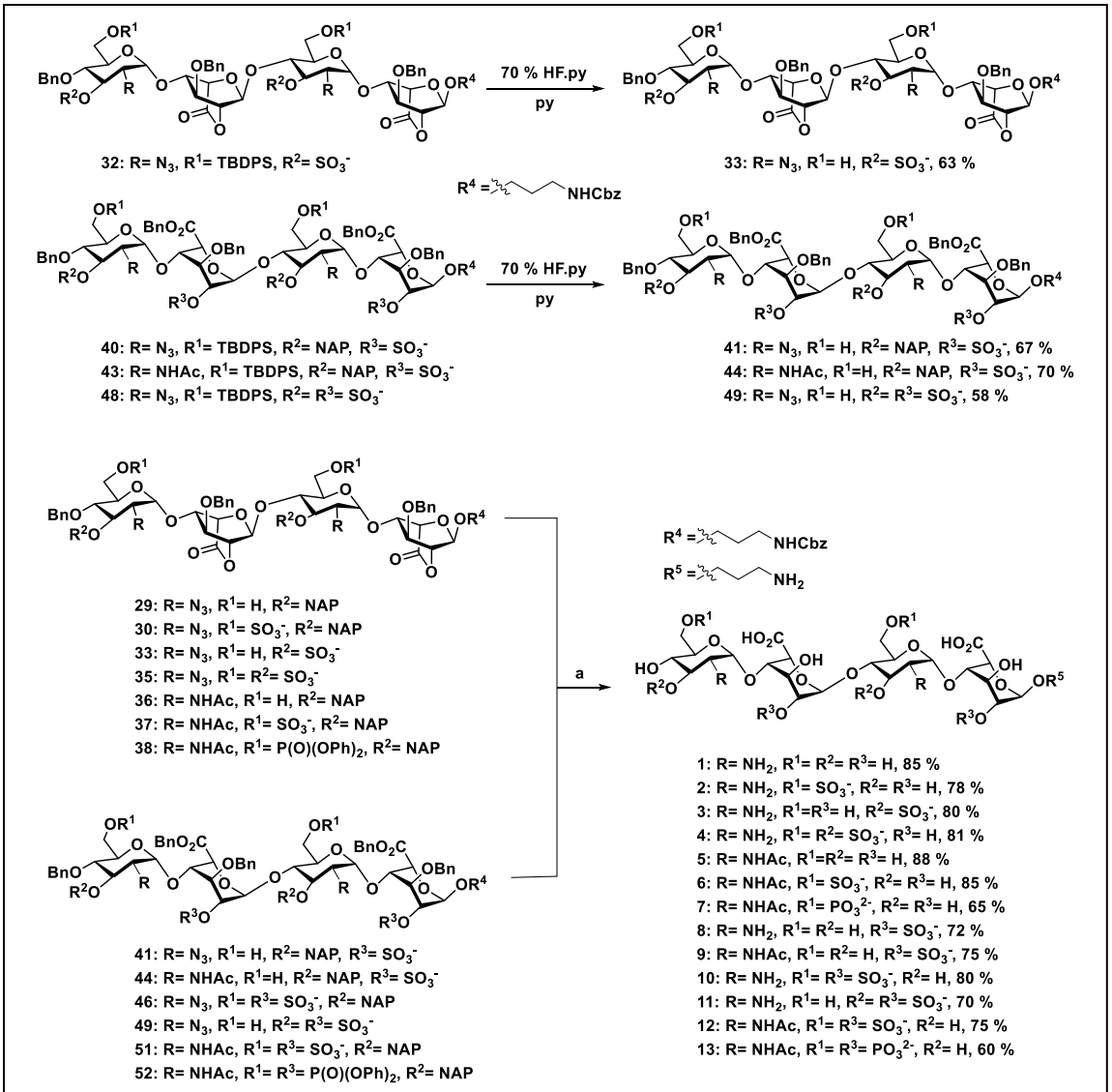


**Scheme 3:** (a) For **1-6** (i) LiOH•$H_2O$, THF/$H_2O$ (1:1), rt, 2 h; (ii) $H_2$, $Pd(OH)_2$, MeOH, 36 h; For **9-12** (i) $H_2$, $Pd(OH)_2$, MeOH, 36 h; For **7** and **13** (i) LiOH•$H_2O$, THF/$H_2O$ (1:1), rt, 2 h; (ii) $H_2$, $Pd(OH)_2$, MeOH, 36 h; (iii) $H_2$, $PtO_2$, MeOH, 24 h.

## 2.2.3 Microarray analysis:

To unravel HS-chemokines binding patterns, heparin microarray was fabricated and examined with various biotinylated chemokines as described in experimental section, at three different concentrations, followed by detection with Cy3-tagged streptavidin. We interrogated the binding affinity of HS analogs on three homeostatic chemokines (CCL28, CXCL12 and CCL21) and six inflammatory chemokines [CXCL8 (IL-8), CXCL10 (IP-10), CCL2 (MCP-1) CCL7 (MCP-3), CCL13 (MCP-4) and CCL5

(RANTES)]. To rationalize the binding patterns of oligosaccharides, each HS-chemokines interaction was ranked according to percentage of maximal binding. Based on ranking and chemokine binding patterns, they were segregated into four groups (A, B, C and D) (Figure 2, Figure R1 (experimental section)).

**(a)**

| Substituent | Structure | Group / ID | A | | | B | C | | D | | |
|---|---|---|---|---|---|---|---|---|---|---|---|
| | | | CCL13 | CCL21 | CXCL12 | CCL28 | CCL7 | CXCL10 | CXCL8 | CCL5 | CCL2 |
| None | GlcNAcα(1-4)IdoAα(1-4)GlcNAcα(1-4)IdoA-proNH2 | HT-0S-NAc | 24 | 27 | 16 | 22 | 2 | 14 | 3 | 1 | 0 |
| | GlcNHα(1-4)IdoAα(1-4)GlcNHα(1-4)IdoA-proNH2 | HT-0S-NH | 64 | 62 | 51 | 36 | 45 | 39 | 13 | 3 | 3 |
| IdoA(2S) | GlcNAcα(1-4)IdoA(2S)α(1-4)GlcNAcα(1-4)IdoA(2S)-proNH2 | HT-2S-NAc | 21 | 23 | 11 | 21 | 1 | 11 | 2 | 1 | 0 |
| | GlcNHα(1-4)IdoA(2S)α(1-4)GlcNHα(1-4)IdoA(2S)-proNH2 | HT-2S-NH | 70 | 69 | 69 | 43 | 56 | 52 | 37 | 31 | 13 |
| GlcNAc(6S) | GlcNAc(6S)α(1-4)IdoAα(1-4)GlcNAc(6S)α(1-4)IdoA-proNH2 | HT-6S-NAc | 81 | 79 | 66 | 79 | 73 | 41 | 19 | 24 | 13 |
| GlcNH(6S) | GlcNH(6S)α(1-4)IdoAα(1-4)GlcNH(6S)α(1-4)IdoA-proNH2 | HT-6S-NH | 45 | 25 | 25 | 38 | 11 | 15 | 5 | 3 | 1 |
| GlcNAc(6P) | GlcNAc(6P)α(1-4)IdoAα(1-4)GlcNAc(6P)α(1-4)IdoA-proNH2 | HT-6P | 70 | 81 | 75 | 39 | 40 | 48 | 10 | 5 | 1 |
| GlcNAc(6S)-IdoA(2S) | GlcNAc(6S)α(1-4)IdoA(2S)α(1-4)GlcNAc(6S)α(1-4)IdoA(2S)-proNH2 | HT-2,6S-NAc | 79 | 71 | 69 | 66 | 86 | 64 | 53 | 54 | 30 |
| GlcNH(6S)-IdoA(2S) | GlcNH(6S)α(1-4)IdoA(2S)α(1-4)GlcNH(6S)α(1-4)IdoA(2S)-proNH2 | HT-2,6S-NH | 74 | 66 | 79 | 79 | 91 | 89 | 79 | 95 | 80 |
| GlcNAc(6P)-IdoA(2P) | GlcNAc(6P)α(1-4)IdoA(2P)α(1-4)GlcNAc(6P)α(1-4)IdoA(2P)-proNH2 | HT-6,2P | 87 | 78 | 59 | 78 | 56 | 55 | 29 | 14 | 2 |
| GlcNH(3S) | GlcNH(3S)α(1-4)IdoAα(1-4)GlcNH(3S)α(1-4)IdoA-proNH2 | HT-3S-NH | 58 | 83 | 84 | 62 | 78 | 65 | 51 | 20 | 28 |
| GlcNH(3S, 6S) | GlcNH(3S,6S)α(1-4)IdoAα(1-4)GlcNH(3S,6S)α(1-4)IdoA-proNH2 | HT-3,6S-NH | 69 | 73 | 80 | 54 | 89 | 96 | 94 | 82 | 95 |
| GlcNH(3S)-IdoA(2S) | GlcNH(3S)α(1-4)IdoA(2S)α(1-4)GlcNH(3S)α(1-4)IdoA(2S)-proNH2 | HT-2,3S-NH | 64 | 48 | 45 | 66 | 35 | 27 | 9 | 4 | 1 |

| % |
|---|
| 100 |
| 75 |
| 50 |
| 25 |
| 0 |

**(b)**

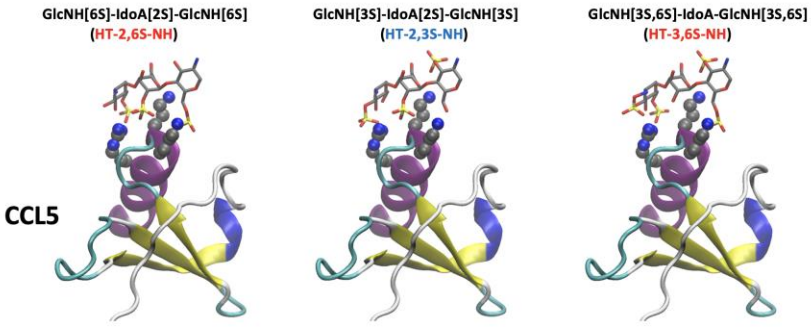


**Figure 2.** Chemokine glycan microarray binding assay. (a) Arrays were fabricated on epoxide-activated slides as described.[33, 34] Binding was tested at 3 serial dilutions, then detected with the relevant biotinylated secondary antibody (1 μg/ml) followed by Cy3-Strepavidin (1.5 μg/ml) (Table 1). Arrays were scanned, relative fluorescent units (RFU) obtained, and maximum RFU determined and set as 100% binding. Then rank binding (per printed glycan per concentration, per each chemokine dilution, per printed block) was determined. Since each glycans was printed at 2 concentration, 100% binding was set separately for each concentration. Then, binding to all the other glycans at the same concentration was ranked in comparison to the maximal binding, and the average rank binding and SEM for each glycan across the two glycan concentrations and three examined dilutions of each chemokine was calculated (n=6, 2 glycan concentrations, across 3 chemokine dilutions). This analysis allowed to compare the glycan binding profiles of the different chemokines and dissect their binding preferences. The mean rank is shown as a heat map of all the examined binding assays together (red highest, blue lowest and white 50$^{th}$ percentile of ranking). (b) Sulfate groups were added or deleted from the ligand in the crystal structure of the co-complex of a heparin trisaccharide with CCL5 (PDB ID: 5DNF, Chain I) using Chimera (UCSF Chimera--a visualization system for exploratory research and analysis.[35] No other changes to the orientation of the ligand or protein were made. Based on glycan microarray screening, binding to CCL5 was high for GAG fragments **HT-2,6-NH** and **HT-3,6S-NH** (red), but low to **HT-2,3S-NH** (blue), consistent with expectations based on the co-complex crystal structure models.

In this analysis, group A chemokines CCL13 (an inflammatory chemokine), CXCL12 and CCL21 (homeostatic chemokine) shared several of the conserved binding patterns, which suggest that these chemokines share several homologous binding pockets. For instance, group A chemokines bind to non-sulfated **HT-0S-NH** and phosphated ligands (**HT-62P** and **HT-6P**) (Figure 2), suggesting that the HS-based structure-activity relationship of these chemokines do not solely depend on the sulfate group. Moreover, group A chemokines showed strong binding with di- sulfated analogs such as **HT-2S-NH** and **HT-6S-NAc**. However, its respective NU and NA counterpart (**HT-6S-NH** and **HT-2S-NAc)** displayed weak binding (Figure 2), illustrating that NU and NA domains display switchable binding patterns *via* sulfation codes. It is noted that highly sulfated HS ligands displayed moderate to strong binding regardless of sulfation pattern or NU/NA domains. These trends clearly demonstrate that group A chemokines are sensitive to di-sulfation codes, while the highly sulfated HS ligands may improve the binding strength, but with poor selectivity.

In group B, CCL28 chemokine displayed weak binding with non-sulfated analogs (ranked 36% for **HT-0S-NH** and 22% **HT-0S-NAc**) and moderate to strong binding with sulfated ligands. Unlike, group A chemokines, CCL28 displayed poor binding with 2-*O*-sulfated NU ligand (ranked 43% for **HT-2S-NH**). Whereas, **HT-6S-NAc** (ranked 79%) and **HT-3S-NH** (ranked 62%) di-sulfated ligands**, H-2,6S-NH** (ranked 79%), **HT-2,6-NAc** (ranked 66%), **HT-3,6S-NH** (ranked 54%) tetra-sulfated ligands and **HT-2,6P** (ranked 78%) phosphate ligand displayed moderate to strong binding (Figure 2a). These results suggest that group A and group B chemokine binding patterns may require a more complex HS library to establish selectivity.

In group C, CCL7 and CXCL10 displayed a sulfation pattern-based binding. Unlike group A and group B chemokines, CCL7 and CXCL10 displayed weak binding with non-sulfated and phosphate HS ligands (ranked between 2%- 56%). Among six di-sulfated ligands, only **HT- 3S-NH** (ranked 78% for CCL7 and 65% for CXCL10) and **HT-6S-NAc** (ranked 73% for CCL7) displayed strong binding as compared to the other analogs. Similarly, among four tetra-sulfated HS ligand, **HT-2,3S-NH** (ranked 35% for CCL7 and 27% for CXCL10) displayed weak binding, whereas **HT-2,6S-NH** (ranked

91% for CCL7 and 89% for CXCL10), **HT-2,6S-NAc** (ranked 86% for CCL7 and 64% for CXCL10) and **HT-3,6S-NH** (ranked 89% for CCL7 and 96% for CXCL10) ligands displayed strong binding (Figure 2). These results illustrate that group C chemokines have some selectivity to di-sulfated ligands. Larger HS-disulfated library could further allow to fine-tune their binding patterns characteristics.

Finally, all members of D group chemokines (CXCL8, CCL5 and CCL2) displayed exclusive strong binding to high-sulfated ligands and weak binding with di-sulfated ligands, nonsulfated or phosphorylated ligands. Among high-sulfate ligands, group D chemokines displayed high selecitivity to NU domain over NA domain. Notably, CXCL8 and CCL2 displayed strong binding preference to **HT-3,6S-NH** (ranked 94% for CXCL8 and 95% for CCL2) ligand, whereas, CCL5 showed strong binding to **HT-2,6S-NH** (ranked 95%) ligand (Figure 2a), suggesting that NU domain is highly significant in modulating these chemokines activities, particularly of group D chemokines. It had previously been shown that the interaction of heparin tetrasaccharides with CCL5 is modulated by sulfation pattern and pH, however these studies also emphasized the dynamic and often non-specific nature of the ionic GAG-protein contacts.[36] Nevertheless, to provide further insights into the interactions between CCL5 and HT compounds of varying sulfation patterns, we used a co-crystal structure of CCL5 co-complexed with a heparin trisaccharide (PDB ID: 5DNF, Chain I), in which sulfate groups were added or deleted from the ligand (Figure 2b). This analysis revealed that sulfation at the 6 position in GlcNH is preferred over sulfation at the 3 position, because the 6S group can interact with both R59 and K55, whereas the 3S only interacts with R59. For this reason, both GlcNH[6S]-IdoA[2S]-GlcNH[6S] and GlcNH[3S,6S]-IdoA-GlcNH[3S,6S] (related to **HT-2,6S-NH** and **HT-3,6S-NH**, ranked 95% and 82% by glycan microarrays, respectively) are stronger binders than GlcNH[3S]-IdoA[2S]-GlcNH[3S] (related to **HT-2,3S-NH,** ranked 4%) (Figure 2a).

### 2.2.4 SPR and cell proliferation assay:

To quantitatively evaluate the binding patterns between HS ligands and chemokines, SPR experiment was performed with **H-3,6S-NH** CXCL10, CXCL8, CCL5 and CCL2), which showed strong selective and sensitive binding in microarray experiments. The

equilibrium binding constants ($K_D$) measured from steady state fits are listed in Table 2 (experimental section). **HT-3,6S-NH** displayed strong binding with inflammatory chemokine CCL2 (1.89 µM) (Figure 3). This strong binding is attributed to the fast association ($K_{on}$) as compared to chemokine-CCL2 interaction.

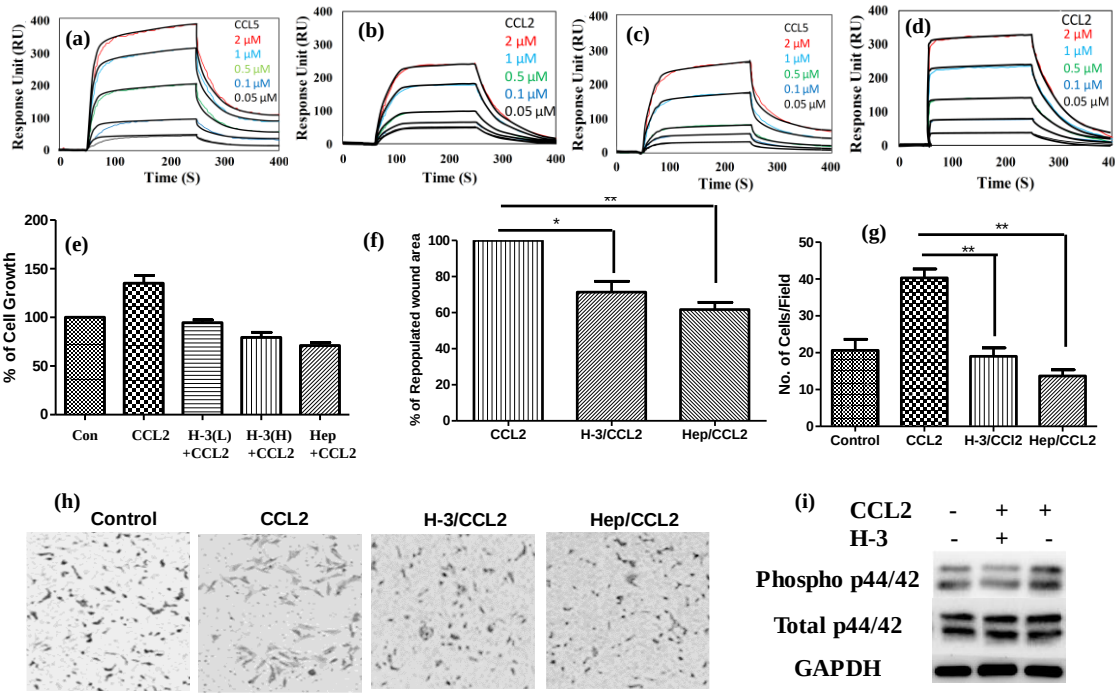


**Figure 3.** SPR analysis of chemokines binding profile on sensor chip having **HT** ligands: (a) & (b) SPR binding analysis of the interaction between **HT-2,6S-NH** with CCL5 and CCL2 respectively; (c) & (d) SPR binding analysis of the interaction between **HT-3,6S-NH** with CCL5 and CCL2 respectively. Concentrations of chemokines were 0.05–2 µM. A global fit according to a 1:1 binding model was applied (black curves); (e) MCF-7 Cell proliferation was quantified by WST assay after 72 hrs treatment with **HT-3,6S-NH (H-3)** at different concentration with CCL2chemokine. The bar graphs indicated percentage of cell growth. **L** corresponds to 10 µg/ml conc; **H** corresponds to 50 µg/ml conc of ligands **((H-3)** and Heparin (**Hep**)). **CCL2** chemokines (50 ng); (f) Cell migration assay: Area repopulated in 8 h with CCL2 chemokine is considered as 100% wound heal and Data expressed as mean ± SD (n=3; *P<0.05, *P<0.01 ); (g) Boyden chamber assay was performed in presence of **HT-3,6S-NH** and **Hep** (50 µg/ml) with or without CCL2 (50 ng); (h) bright field images of Boyden chamber assay; (i) MAPK pathway analysis: MCF-7 Cells were treated with **CCL2** (50 ng) with or without **HT-3,6S-NH (H-3)** ligands (50 µg/ml) and cell lysate was prepared at 30 min time points and P-p44/42 and Total p44/42 was imaged.

In contrast, **HT-2,6SNH** displayed strong binding to CCL5 (2.34 µM) (Figure 3). Interestingly, CXCL8, CCL7 and CXCL10 showed weak binding constants (10-15 µM) for both NU domain ligands (Figure 5, experimental section). Furthermore, SPR analysis of CCL5 and CCL2 displayed 3-fold stronger binding with **H-3,6S-NH** and **HT-2,6S-NH**

ligands, respectively. Thus, for the first time, we were able to identify key NU domain sulfation pattern that can modulate chemokines activity.

Given the high affinity binding of **HT-3,6S-NH** to CCL2 chemokines, and the link between CCL2 and cancer metastasis, investigating inhibitor effect on CCL2 cancer cell signaling is considered a novel approach to demonstrate the therapeutic potential of HS mimics.[37] To this end, we first studied cancer cells proliferation in the presence of **HT-3,6S-NH (H-3)** ligand and CCL2. Native heparin was used as a positive control. Cell proliferation was analyzed by WST assay using MCF-7 cell line, as they express high level of the CCL2 specific chemokine receptor (CCR2).[38] It was observed that high concentration of **HT-3,6S-NH** ligand moderately inhibited cell proliferation (Figure 3e). To understand the mechanism of inhibition, we performed cell-cycle analysis in the presence and absence of HS ligand and CCL2 chemokine, then quantified the DNA content of each cell state by flow-cytometry. The cell cycle analysis clearly revealed that addition of CCL2 induced S and G2/M phase cell-cycles, while high concentration of **HT-3,6S-NH** and heparin reduced G2/M state from 15% to 10%, indicating that **HT-3,6S-NH** moderately to poorly activate the cell cycle. Further studies with **HT-3,6S-NH** multivalent probes are ideal for modulating cancer cell proliferation.

### 2.2.5 Cell migration assay:

We next examined cell migration by wound healing assay (Figure 3f) and by Boyden-chamber assay (Figure 3g & 3h). Addition of **HT-3,6S-NH** ligand reduced chemokine activity, where a 24% reduction in cell migration rate and 41% reduction in the wound healing was observed. In addition, a substantial reduction in cell migration was observed in the Boyden chamber assay. Finally, the mechanism of invasiveness was examined further by analyzing the level of phosphorylation of MAP kinase pathway. Western blot analysis of p42/44 showed that MCF-7 cells treated with **HT-3,6S-NH**/CCL2 expressed low level of MAPK compared to CCL2 treated cells (Figure 3i). Overall, all these results suggest that **HT-3,6S-NH** is a potential ligand that can modulate CCL2 chemokine activities.

## 2.3 Conclusions:

Here, we describe the divergent synthesis of 13 new HS ligands, displaying different sulfate/phosphate patterns with NU/NA glucosamine residue. The binding interactions between HS ligands and chemokines on microarray platform displayed several cryptic binding pockets for sulfation patterns with NU domain, which was not identified with previous HS synthetic ligands. Among them, **HT-3,6S-NH** ligand displayed a marked selectivity and sensitivity to CCL2 chemokine. The biological relevance of such structural binding studies was illustrated by incubating **HT-3,6S-NH** ligand with cancer cells: the HS ligand inhibited cancer cells proliferation, migration and invasion. Thus, NU domain is important to regulate specific chemokine biological activities, thereby demonstrating potential novel therapeutic applications of HS ligands. To the best of our knowledge, we have identified CCL2 and CCL5 chemokines as only the fourth and fifth proteins currently known to recognize NU-domain HS ligands with different sulfation patterns.

## 2.4 Experimental part:

### 2.4.1 General information

All chemicals were reagent grade and used as supplied except where noted. Analytical thin layer chromatography (TLC) was performed on Merck silica gel 60 F254 plates. Compounds were visualized by UV irradiation or dipping the plate in CAM/ninhydrin solution followed by heating. Column chromatography was carried out using force flow of the indicated solvent on Fluka Kieselgel 60 (230–400 mesh). $^{1}H$ and $^{13}C$ NMR spectra of all compounds were recorded on Jeol 400 MHz, and Bruker 600 MHz with cryo probe using residual solvents signals as an internal reference ($CDCl_3$ δH, 7.26 ppm, δC 77.3 ppm, $CD_3OD$ δH 3.31 ppm, δC 49.0 ppm and $D_2O$ δH 4.79 ppm). The chemical shifts (δ) are reported in ppm and coupling constants (J) in Hz.

## 2.4.2 Synthesis of HS tetrasaccharide (1-13):

**Synthesis of HS tetrasaccharide precursor:**

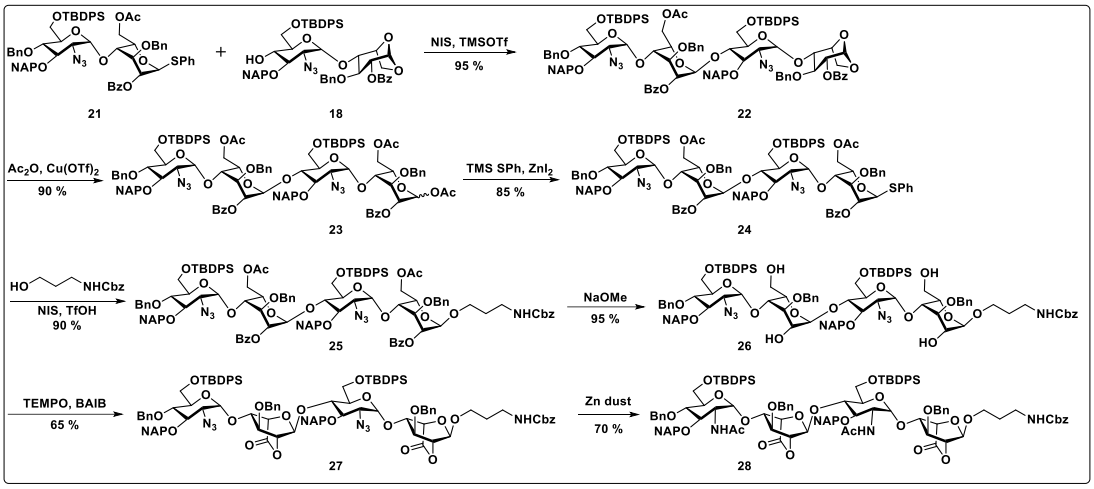


**4-Methylphenyl 2-azido-4-*O*-chloroacetyl-6-*O*-*tert*-butyldiphenylsilyl-3-*O*-(2-naphthylmethyl)-2-deoxy-1-thio-*α*/*β*-D-glucopyranoside (16)**

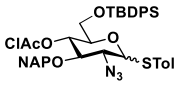
16

To a solution of compound **15** (1.5 g, 2.78 mmol) in $CH_2Cl_2$ (5 mL) and MeOH (10 mL) was added PTSA (0.95 g, 5.56 mmol) and stirred for 6 h. Upon completion, the reaction mixture was quenched using $Et_3N$ and extracted with ethyl acetate and brine. The organic layer was collected, dried over $Na_2SO_4$, filtered, concentrated and purified through flash silica gel column chromatography (ethyl acetate/ hexane= 1/1, v/v) Next, the obtained compound (1 g, 2.21 mmol) was dissolved in $CH_2Cl_2$ (10 mL) and stirred at ice cold temperature under $N_2$ atmosphere followed by the addition of imidazole (0.45 g, 6.64 mmol) and DMAP (0.10 g, 0.88 mmol). Finally, TBDPS-Cl was added dropwise and reaction mixture was left for stirring. After 12 h, the reaction was quenched using MeOH and extracted with brine. The combined organic layer was collected, dried over $Na_2SO_4$, filtered, concentrated and purified through silica gel column chromatography (ethyl acetate/ hexane= 1/10, v/v). Further, the solution of 6-*O*-TBDPS compound (1 g, 1.45 mmol) in $CH_2Cl_2$ (8 mL) and pyridine (2 mL) was stirred at ice cold temperature for 15 minutes under $N_2$ atmosphere before the addition of chloroacetic anhydride (0.32 g, 1.85 mmol). Reaction completion was monitored by TLC

(approx. 20 min). After the completion of reaction, the mixture was washed with 1 N HCl and brine. The organic layer was collected, dried over $Na_2SO_4$, filtered, concentrated and purified through silica gel column chromatography (ethyl acetate/ hexane= 1/20, v/v) to obtain compound **16** in 95 % yield. $^1$H NMR (400 MHz, Chloroform-d) **(α anomer)** δ 7.87 – 7.83 (m, 3H), 7.78 (s, 1H), 7.64 – 7.61 (m, 4H), 7.51 – 7.48 (m, 2H), 7.43 – 7.30 (m, 9H), 7.06 (d, *J* = 7.9 Hz, 2H), 5.59 (d, *J* = 5.4 Hz, 1H), 5.28 – 5.23 (m, 1H), 5.07 (d, *J* = 11.6 Hz, 1H), 4.80 (d, *J* = 11.6 Hz, 1H), 4.37 (ddd, *J* = 10.1, 4.2, 2.3 Hz, 1H), 4.03 (dd, *J* = 10.2, 5.4 Hz, 1H), 3.86 – 3.81 (m, 1H), 3.67 (qd, *J* = 11.7, 3.3 Hz, 2H), 3.53 – 3.44 (m, 2H), 2.33 (s, 3H), 1.02 (s, 9H). $^{13}$C NMR (101 MHz, Chloroform-d) δ 165.85, 138.06, 135.81, 135.67, 134.92, 134.89, 133.28, 133.12, 133.11, 132.96, 132.43, 130.01, 129.81, 129.72, 129.65, 128.47, 128.13, 127.79, 127.70, 127.17, 126.40, 126.31, 126.15, 87.46, 79.35, 75.46, 71.68, 71.56, 64.24, 62.35, 40.43, 26.77, 21.24, 19.28. **(β anomer)** $^1$H NMR (400 MHz, Chloroform-*d*) δ 7.87- 7.85 (m, 3H), 7.78 – 7.74 (m, 3H), 7.70 (dd, *J* = 7.7, 1.4 Hz, 2H), 7.57 (d, *J* = 8.1 Hz, 2H), 7.54 – 7.51 (m, 2H), 7.47 – 7.41 (m, 7H), 7.09 (d, *J* = 8.0 Hz, 2H), 5.21 (t, *J* = 6.8 Hz, 1H), 5.03 (d, *J* = 11.5 Hz, 1H), 4.80 (d, *J* = 11.6 Hz, 1H), 4.43 (d, *J* = 10.0 Hz, 1H), 3.80 (dd, *J* = 11.6, 1.9 Hz, 1H), 3.68 – 3.64 (m, 1H), 3.58 (dd, *J* = 13.2, 5.4 Hz, 1H), 3.51 – 3.45 (m, 4H), 2.36 (s, 3H), 1.10 (s, 9H). $^{13}$C NMR (101 MHz, Chloroform-d ) δ 165.67, 139.07, 135.79, 135.78, 134.83, 134.54, 133.25, 133.12, 132.99, 132.92, 130.01, 129.90, 129.81, 128.48, 128.08, 127.83, 127.78, 127.25, 126.51, 126.40, 126.33, 126.16, 86.05, 82.60, 78.65, 75.49, 70.67, 64.75, 62.20, 26.80, 21.29, 19.26. HR-ESI-MS *(m/z)*: $[M+Na]^+$ calcd for $C_{42}H_{44}ClN_3O_5SSiNa$, 788.2357; found, 788.2358.

**1,6-Anhydro-[2-azido-4-*O*-chloroacetyl-6-*O*-*tert*-butyldiphenylsilyl-3-*O*-(2 naphthylmethyl)-2-deoxy-*α*-D-glucopyranosyl]-(1→4)-*O*-2-*O*-benzoyl-3-*O*-benzyl-*β*-L- idopyranose (17)**

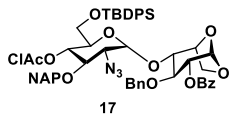

17

A solution of donor **16** (1 g, 1.30 mmol) and acceptor **14** (0.41 g, 1.17 mmol) in $CH_2Cl_2$ (20 mL) was stirred under $N_2$ atmosphere in round bottom flask containing freshly dried 4 Å molecular sieves for 2 h. The mixture solution was cooled down to -78 $^o$C followed by the addition of NIS (0.46 g, 2.08 mmol) and TMSOTf (71 µL, 0.39 mmol). The temperature was gradually increased to -20 $^o$C and reaction mixture was left for stirring for another 15 minutes. After 15 minutes

reaction completion was monitored by TLC and quenched using few drops of $Et_3N$. Molecular sieves were filtered using celite and organic layer was washed with aqueous $Na_2S_2O_3$ and brine. The collected organic layer was dried over $Na_2SO_4$, filtered, concentrated and purified through silica gel column chromatography (ethyl acetate/ hexane= 1/12, v/v) to obtain compound **17** in 65 % yield. $^1$H NMR (400 MHz, Chloroform-d) δ 8.08 – 8.06 (m, 2H), 7.85 (td, *J* = 7.0, 6.4, 2.9 Hz, 3H), 7.78 (s, 1H), 7.64 (dt, *J* = 8.0, 1.4 Hz, 4H), 7.61 – 7.58 (m, 1H), 7.51 – 7.36 (m, 12H), 7.30 – 7.27 (m, 2H), 7.26 – 7.22 (m, 2H), 5.55 (d, *J* = 1.7 Hz, 1H), 5.36 (d, *J* = 3.8 Hz, 1H), 5.16 – 5.09 (m, 2H), 5.06 (d, *J* = 11.5 Hz, 1H), 4.91 (d, *J* = 10.8 Hz, 1H), 4.80 (dd, *J* = 11.0, 9.5 Hz, 2H), 4.65 (t, *J* = 4.5 Hz, 1H), 4.19 (d, *J* = 7.6 Hz, 1H), 4.12 (t, *J* = 8.0 Hz, 1H), 4.07 (dd, *J* = 8.1, 4.0 Hz, 1H), 4.03 – 3.98 (m, 1H), 3.77 – 3.72 (m, 2H), 3.67 (dd, *J* = 11.4, 5.3 Hz, 1H), 3.62 – 3.59 (m, 1H), 3.57 (d, *J* = 2.1 Hz, 2H), 3.51 (dd, *J* = 10.3, 3.8 Hz, 1H), 1.06 (s, 9H). $^{13}$C NMR (101 MHz, Chloroform-d) δ 165.84, 165.80, 137.92, 135.73, 135.68, 134.87, 133.55, 133.28, 133.14, 132.86, 132.74, 129.97, 129.47, 128.60, 128.52, 128.50, 128.07, 127.93, 127.89, 127.87, 127.82, 127.01, 126.45, 126.34, 125.96, 99.48, 99.37, 79.51, 78.94, 75.07, 74.96, 74.24, 71.75, 71.41, 65.77, 63.36, 62.64, 40.41, 26.82, 19.22. HR-ESI-MS *(m/z)*: $[M+Na]^+$ calcd for $C_{55}H_{56}ClN_3O_{11}SiNa$, 1020.3270; found, 1020.3271.

**1,6-Anhydro-[2-azido-6-*O*-*tert*-butyldiphenylsilyl-3-*O*-(2-naphthylmethyl)-2-deoxy-*α*-D-glucopyranosyl]-(1→4)-*O*-2-*O*-benzoyl-3-*O*-benzyl-*β*-L-idopyranose (18)**

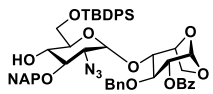

18

To a solution of compound **17** (0.70 g, 0.7 mmol) in MeOH (5 mL) and pyridine (5 mL) was added thiourea (0.10 g, 1.4 mmol) and refluxed at 80 $^o$ C. After 1 h, volatiles were evaporated and residue was extracted with ethyl acetate, 1 N HCl and brine. The collected organic layer was dried over $Na_2SO_4$, filtered, concentrated and purified through silica gel column chromatography (ethyl acetate/ hexane= 1/8, v/v) to obtain compound **18** in 90 % yield. $^1$H NMR (400 MHz, Chloroform-d) δ 8.06 (dd, *J* = 8.3, 1.2 Hz, 2H), 7.86 (dq, *J* = 9.6, 4.2 Hz, 4H), 7.68 (td, *J* = 7.6, 7.0, 1.5 Hz, 4H), 7.62 – 7.55 (m, 2H), 7.53 – 7.38 (m, 11H), 7.26 – 7.20 (m, 4H), 5.54 (d, J = 1.7 Hz, 1H), 5.26 (d, *J* = 3.7 Hz, 1H), 5.12 (d, *J* = 11.3 Hz, 1H), 5.08 – 5.03 (m, 2H), 4.90 (d, *J* = 10.9 Hz, 1H), 4.76 (d, *J* = 10.9 Hz, 1H), 4.56 (t, *J* = 4.6 Hz, 1H), 4.17 (d, *J* = 7.7 Hz, 1H), 4.08 (t, *J* = 8.1 Hz, 1H), 4.00 (dd, *J* = 8.1, 4.1 Hz, 1H), 3.91 – 3.82 (m,

3H), 3.72 (t, *J* = 6.2 Hz, 2H), 3.61 (dt, *J* = 9.4, 4.5 Hz, 1H), 3.37 (dd, *J* = 10.3, 3.7 Hz, 1H), 2.66 (s, 1H), 1.08 (s, 9H). $^{13}$C NMR (101 MHz, Chloroform-d) δ 165.83, 137.98, 135.69, 135.68, 135.45, 133.51, 133.42, 133.22, 132.83, 132.71, 130.14, 130.10, 129.98, 129.48, 128.62, 128.57, 128.47, 128.09, 127.98, 127.96, 127.85, 127.83, 127.07, 126.35, 126.22, 125.98, 99.76, 99.33, 79.50, 79.44, 78.90, 75.33, 75.05, 74.32, 72.61, 71.89, 65.75, 64.36, 62.96, 26.93, 19.27. HR-ESI-MS *(m/z)*: $[M+Na]^+$ calcd for $C_{53}H_{55}N_3O_{10}SiNa$, 944.3555; found, 944.3540.

**Phenyl-[2-azido-4-*O*-benzyl-6-*O*-*tert*-butyldiphenylsilyl-3-*O*-(2-naphthylmethyl)-2-deoxy-*α*-D-glucopyranosyl]-(1→4)-*O*-2-*O*-benzoyl-3-*O*-benzyl-6-*O*-acetyl-1-thio-*α*-L-idopyranoside (21)**

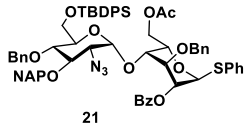

21

A solution of compound **20** (1 g, 0.98 mmol) in $Ac_2O$ (10 mL) was stirred at ice cold temperature for 15 minutes before the addition of $Cu(OTf)_2$ (0.035 g, 0.098 mmol). After 16 h, the reaction mixture was concentrated under reduced pressure and the residue was extracted with ethyl acetate, $NaHCO_3$ and washed with brine. The combined organic layer was dried over $Na_2SO_4$, filtered, concentrated and preceded further without any purification. Next, the as obtained acetylated solution of compound (0.98 g, 0.88 mmol), $ZnI_2$ (0.59 g, 1.84 mmol) and phenyl trimethylsilyl sulphide (0.50 g, 2.72 mmol) in $CH_2Cl_2$ (15 mL) was stirred under $N_2$ atmosphere for 2 h. Upon completion, the reaction mixture was filtered through celite, evaporated and purified through silica gel column chromatography (ethyl acetate/ hexane= 1/5, v/v) to obtain compound **21** in 85 % yield. $^1$H NMR (400 MHz, Chloroform-d ) δ 8.20 (dd, *J* = 6.8, 2.9 Hz, 2H), 7.87 – 7.77 (m, 3H), 7.72 (s, 1H), 7.71 – 7.68 (m, 2H), 7.68 – 7.66 (m, 1H), 7.61 – 7.58 (m, 3H), 7.54 – 7.48 (m, 4H), 7.44- 7.41 (m, 4H), 7.40 (s, 1H), 7.38 (d, *J* = 2.2 Hz, 4H), 7.37 – 7.35 (m, 4H), 7.34- 7.32 (m, 4H), 7.31- 7.29 (m, 2H), 7.21-7.19 (m, 2H), 5.64 (s, 1H), 5.42 (s, 1H), 5.01 (d, *J* = 11.6 Hz, 1H), 4.92 (dt, *J* = 6.9, 4.0 Hz, 1H), 4.83 (d, *J* = 10.9 Hz, 1H), 4.78 (d, *J* = 11.7 Hz, 1H), 4.72 (d, *J* = 10.8 Hz, 1H), 4.65 (d, *J* = 3.6 Hz, 1H), 4.57 (d, *J* = 10.6 Hz, 1H), 4.44 (dd, *J* = 11.5, 8.1 Hz, 1H), 4.26 (d, *J* = 10.6 Hz, 1H), 4.20 (dd, *J* = 10.7, 3.6 Hz, 2H), 4.02 (dd, *J* = 11.6, 2.1 Hz, 1H), 3.91 (d, *J* = 11.5 Hz, 1H), 3.81 (s, 1H), 3.79 – 3.76 (m, 1H), 3.73 (d, *J* = 9.8 Hz, 1H), 3.68 (s, 1H), 3.38 (dd, *J* = 9.9, 3.6 Hz, 1H), 1.93 (s, 3H), 1.08 (s, 9H). $^{13}$C NMR (101 MHz, Chloroform-d )

δ 170.36, 165.76, 138.04, 137.34, 135.88, 135.61, 135.54, 135.09, 133.48, 133.27, 133.05, 133.03, 131.71, 129.88, 129.70, 129.69, 128.90, 128.61, 128.48, 128.43, 128.24, 128.12, 128.07, 127.98, 127.77, 127.73, 127.67, 127.59, 127.49, 127.00, 126.11, 126.06, 125.98, 98.96, 85.87, 80.76, 77.80, 75.34, 75.12, 75.05, 73.17, 72.83, 71.95, 69.74, 66.42, 64.12, 63.11, 62.18, 26.88, 20.72, 19.36. HR-ESI-MS *(m/z)*: $[M+Na]^+$ calcd for $C_{68}H_{69}N_3O_{11}SSiNa$, 1186.4320; found, 1186.4319

**1,6-Anhydro-[(2-azido-4-*O*-benzyl-6-*O*-*tert*-butyldiphenylsilyl-3-*O*-(2-naphthylmethyl)-2-deoxy-*α*-D-glucopyranosyl)-(1→4)-*O*-(2-*O*-benzoyl-3-*O*-benzyl-6-*O*-acetyl-*α*-L-idopyranosyl)-(1→4)-*O*-(2-azido-6-*O*-*tert*-butyldiphenylsilyl-3-*O*-(2-naphthylmethyl)-2-deoxy-*α*-D-glucopyranosyl)]-(1→4)-*O*-2-*O*-benzoyl-3-*O*-benzyl-*β*-L-idopyranose (22)**

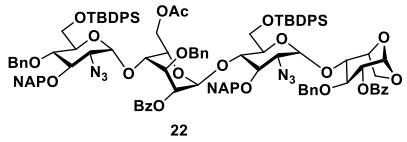

22

A solution of donor **21** (0.87 g, 0.74 mmol) and acceptor **18** (0.55 g, 0.60 mmol) in $CH_2Cl_2$ (15 mL) was stirred under $N_2$ atmosphere in round bottom flask containing freshly dried 4 Å molecular sieves for 2 h. The mixture solution was cooled down to -10 $^o$ C followed by the addition of NIS (0.26 g, 1.18 mmol) and TMSOTf (26 µL, 0.148 mmol). After 15 minutes reaction completion was monitored by TLC and quenched using few drops of $Et_3N$. Molecular sieves were filtered using celite and organic layer was washed with aqueous $Na_2S_2O_3$ and brine. The collected organic layer was dried over $Na_2SO_4$, filtered, concentrated and purified through silica gel column chromatography (ethyl acetate/ hexane= 1/6, v/v) to obtain compound **22** in 95 % yield. $^1$H NMR (400 MHz, Chloroform-d) δ 8.03 (dd, *J* = 6.5, 1.4 Hz, 4H), 7.83 – 7.81 (m, 1H), 7.78 – 7.75 (m, 1H), 7.71- 7.58 (m, 15H), 7.48 – 7.27 (m, 29H), 7.22-7.19 (m, 9H), 5.51 (d, *J* = 1.7 Hz, 1H), 5.36 (s, 1H), 5.22 (s, 1H), 5.18 (d, J = 3.9 Hz, 1H), 5.13 (d, *J* = 11.3 Hz, 1H), 5.04 (dd, *J* = 8.2, 1.7 Hz, 1H), 4.87 (d, *J* = 11.3 Hz, 1H), 4.83 (d, *J* = 4.2 Hz, 1H), 4.81 – 4.80 (m, 1H), 4.75 (s, 1H), 4.73 – 4.67 (m, 3H), 4.63 (d, J = 10.6 Hz, 1H), 4.50 (dt, J = 6.8, 3.5 Hz, 1H), 4.41- 4.38 (m, 1H), 4.36 (d, J = 4.78 Hz, 1H), 4.18 – 4.06 (m, 4H), 4.01 (tt, *J* = 7.0, 3.9 Hz, 2H), 3.93 – 3.86 (m, 4H), 3.83 (dd, *J* = 9.4, 2.9 Hz, 2H), 3.74 (t, *J* = 9.8 Hz, 3H), 3.66 – 3.61 (m, 2H), 3.59 – 3.51 (m, 2H), 3.38 (dd, *J* = 10.4, 3.8 Hz, 1H), 3.31 (dd, *J* = 10.1, 3.5

Hz, 1H), 1.41 (s, 3H), 1.03 (s, 9H), 1.00 (s, 9H). $^{13}$C NMR (101 MHz, Chloroform-d) δ 170.07, 165.75, 138.11, 137.91, 137.44, 135.87, 135.82, 135.66, 135.59, 135.45, 135.21, 133.43, 133.37, 133.29, 133.21, 133.15, 133.03, 132.98, 132.86, 129.89, 129.82, 129.76, 129.72, 129.55, 129.43, 128.66, 128.55, 128.48, 128.44, 128.40, 128.36, 128.21, 128.15, 127.98, 127.84, 127.79, 127.76, 127.71, 127.67, 127.62, 127.53, 127.00, 126.94, 126.30, 126.08, 126.06, 125.97, 125.76, 125.72, 99.35, 99.21, 98.32, 97.35, 80.38, 79.21, 79.04, 78.45, 77.70, 77.25, 76.95, 75.35, 75.30, 75.10, 74.95, 74.13, 73.46, 73.34, 73.00, 72.95, 72.90, 72.83, 68.87, 65.52, 65.34, 64.04, 62.42, 62.36, 61.98, 26.86, 26.80, 20.20, 19.35, 19.33. HR-ESI-MS *(m/z)*: $[M+Na]^+$ calcd for $C_{115}H_{118}N_6O_{21}Si_2Na$, 1997.7787; found, 1997.7722.

**Acetyl-*O*-[(2-azido-4-*O*-benzyl-6-*O*-*tert*-butyldiphenylsilyl-3-*O*-(2-naphthylmethyl)-2-deoxy-*α*-D-glucopyranosyl)-(1→4)-*O*-(2-*O*-benzoyl-3-*O*-benzyl-6-*O*-acetyl-*α*-L-idopyranosyl)-(1→4)-*O*-(2-azido-6-*O*-*tert*-butyldiphenylsilyl-3-*O*-(2-naphthylmethyl)-2-deoxy-*α*-D-glucopyranosyl)]-(1→4)-*O*-2-*O*-benzoyl-3-*O*-benzyl-6-*O*-acetyl-*α/β*-L- idopyranoside (23)**

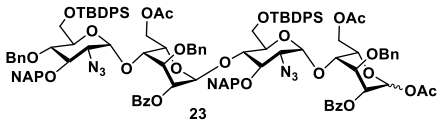

23

A solution of compound **22** (1 g, 0.98 mmol) in $Ac_2O$ (10 mL) was stirred at ice cold temperature for 15 minutes before the addition of $Cu(OTf)_2$ (0.035 g, 0.098 mmol). After 16 h, the reaction mixture was concentrated under reduced pressure and the residue was extracted with ethyl acetate, $NaHCO_3$ and washed with brine. The combined organic layer was dried over $Na_2SO_4$, filtered, concentrated and purified through silica gel column chromatography (ethyl acetate/ hexane= 1/5, v/v) to obtain compound **23** in 90 % yield.. $^1$H NMR (400 MHz, Chloroform-d ) δ 8.16 – 8.11 (m, 3H), 8.05 (d, *J* = 7.7 Hz, 3H), 7.86 – 7.77 (m, 4H), 7.64 (ddq, *J* = 22.1, 13.3, 7.6, 6.4 Hz, 21H), 7.56 – 7.29 (m, 50H), 7.28 – 7.14 (m, 17H), 6.24 (d, *J* = 2.3 Hz, 1H), 5.42 (s, 1H), 5.25 – 5.16 (m, 3H), 4.95 – 4.67 (m, 13H), 4.61 (dd, *J* = 7.2, 3.4 Hz, 2H), 4.41 (dq, *J* = 16.1, 6.1, 5.4 Hz, 5H), 4.30 – 4.10 (m, 8H), 4.09 – 4.01 (m, 3H), 3.93 – 3.63 (m, 18H), 3.52 (s, 1H), 3.35 – 3.30 (m, 3H), 2.12 (d, *J* = 3.9 Hz, 2H), 1.97 (s, 2H), 1.90 (s, 3H), 1.28 (s, 2H), 1.25 (s, 3H), 1.05 (s, 15H), 1.00 (s, 13H). $^{13}$C NMR (101 MHz, Chloroform-d ) δ 170.44, 170.31, 169.98, 169.97, 169.04, 168.91, 166.05, 165.76, 165.71, 138.18, 137.52, 137.51, 137.24, 135.90,

135.87, 135.64, 135.60, 135.49, 135.45, 135.23, 133.46, 133.40, 133.36, 133.34, 133.28, 133.25, 133.22, 133.17, 133.16, 133.02, 132.99, 132.74, 132.71, 129.90, 129.80, 129.76, 129.72, 129.65, 129.63, 129.50, 128.72, 128.69, 128.63, 128.60, 128.52, 128.47, 128.44, 128.36, 128.23, 128.18, 128.15, 128.13, 128.09, 128.05, 128.00, 127.98, 127.84, 127.76, 127.75, 127.71, 127.66, 127.63, 127.53, 127.43, 127.41, 127.37, 126.94, 126.10, 126.04, 126.00, 125.94, 125.88, 125.86, 125.69, 125.67, 125.61, 125.58, 98.52, 98.13, 97.91, 97.00, 96.98, 91.74, 90.56, 80.36, 79.11, 78.91, 77.64, 77.27, 75.31, 75.04, 73.97, 73.88, 73.83, 73.33, 73.29, 73.26, 72.93, 72.80, 72.68, 72.55, 72.46, 71.98, 68.63, 68.54, 67.80, 67.25, 64.65, 64.37, 64.29, 64.06, 62.48, 62.33, 62.26, 61.94, 26.87, 26.79, 21.01, 20.73, 20.66, 20.01, 19.95, 19.44, 19.34. HR-ESI-MS *(m/z)*: $[M+Na]^+$ calcd for $C_{119}H_{124}N_6O_{24}Si_2Na$, 2100.8137; found, 2100.8171.

**Phenyl-[(2-azido-4-*O*-benzyl-6-*O*-*tert*-butyldiphenylsilyl-3-*O*-(2-naphthylmethyl)-2-deoxy-*α*-D-glucopyranosyl)-(1→4)-*O*-(2-*O*-benzoyl-3-*O*-benzyl-6-*O*-acetyl-*α*-L-idopyranosyl)-(1→4)-*O*-(2-azido-6-*O*-*tert*-butyldiphenylsilyl-3-*O*-(2-naphthylmethyl)-2-deoxy-*α*-D-glucopyranosyl)]-(1→4)-*O*-2-*O*-benzoyl-3-*O*-benzyl-6-*O*-acetyl-1-thio-*α*-L-idopyranoside (24)**

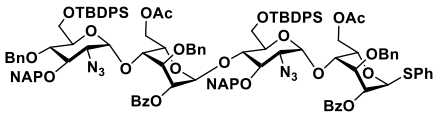

24

A solution of compound **23** (0.98 g, 0.88 mmol), $ZnI_2$ (0.59 g, 1.84 mmol) and phenyl trimethylsilyl sulphide (0.50 g, 2.72 mmol) in $CH_2Cl_2$ (15 mL) was stirred under $N_2$ atmosphere for 2 h. Upon completion, the reaction mixture was filtered through celite, evaporated and purified through silica gel column chromatography (ethyl acetate/ hexane= 1/5, v/v) to obtain compound **24** in 85 % yield. $^1$H NMR (400 MHz, Chloroform-d) δ 8.12 (ddd, J = 5.7, 3.0, 1.6 Hz, 2H), 8.03 (s, 1H), 8.01 (d, J = 1.3 Hz, 1H), 7.82 – 7.79 (m, 1H), 7.77 – 7.74 (m, 1H), 7.67 – 7.56 (m, 15H), 7.48 – 7.43 (m, 7H), 7.40 – 7.37 (m, 7H), 7.35 – 7.33 (m, 4H), 7.31 – 7.28 (m, 14H), 7.25- 7.21 (m, 5H), 7.17 (d, *J* = 7.5 Hz, 2H), 7.14 – 7.10 (m, 4H), 5.62 (s, 1H), 5.38 (s, 1H), 5.34 (s, 1H), 5.18 (s, 1H), 4.94 – 4.83 (m, 3H), 4.79 (d, *J* = 10.8 Hz, 1H), 4.75 (d, *J* = 4.0 Hz, 1H), 4.72 (d, *J* = 4.1 Hz, 1H), 4.70 (d, *J* = 2.4 Hz, 1H), 4.67 (d, *J* = 3.2 Hz, 1H), 4.64 (d, *J* = 3.5 Hz, 1H), 4.56 (d, *J* = 10.6 Hz, 1H), 4.47 (d, J = 3.8 Hz, 1H), 4.38 (dd, *J* = 5.5, 3.2 Hz, 1H), 4.36 – 4.32 (m, 2H), 4.14 – 4.08 (m, 2H), 4.05 – 4.02 (m, 3H), 3.99 (t, *J* = 5.4 Hz, 1H), 3.91 (dd, *J* =

5.6, 1.9 Hz, 1H), 3.88 – 3.85 (m, 2H), 3.83 (t, *J* = 3.4 Hz, 1H), 3.79 (d, *J* = 10.2 Hz, 1H), 3.74 (d, *J* = 9.9 Hz, 1H), 3.71 – 3.66 (m, 2H), 3.63 – 3.57 (m, 2H), 3.54 – 3.51 (m, 1H), 3.47 (s, 1H), 3.28 (d, J = 3.5 Hz, 1H), 3.26 (d, J = 3.6 Hz, 1H), 1.86 (s, 3H), 1.20 (s, 3H), 1.02 (s, 9H), 0.97 (s, 9H). $^{13}$C NMR (101 MHz, Chloroform-d ) δ 170.26, 169.96, 165.86, 165.70, 138.18, 137.54, 137.31, 135.90, 135.87, 135.65, 135.59, 135.46, 135.45, 135.23, 133.46, 133.39, 133.28, 133.26, 133.21, 133.14, 133.02, 133.00, 132.70, 131.73, 129.90, 129.82, 129.76, 129.71, 129.66, 129.63, 128.91, 128.69, 128.60, 128.47, 128.43, 128.36, 128.25, 128.18, 128.12, 128.09, 127.98, 127.85, 127.82, 127.76, 127.75, 127.70, 127.66, 127.63, 127.52, 127.40, 127.34, 126.93, 126.10, 126.03, 125.99, 125.94, 125.85, 125.69, 125.57, 98.16, 98.03, 96.96, 85.84, 80.36, 79.15, 77.63, 77.25, 75.30, 75.04, 74.97, 74.22, 73.28, 72.91, 72.83, 72.80, 72.59, 72.42, 71.58, 69.80, 68.54, 66.30, 64.62, 64.46, 64.06, 62.89, 62.27, 61.93, 26.87, 26.80, 20.65, 19.95, 19.44, 19.33. HR-ESI-MS *(m/z)*: $[M+Na]^+$ calcd for $C_{123}H_{126}N_6O_{22}SSi_2Na$, 2149.8080; found, 2149.8088.

**N-benzyloxycarbonyl-3-aminopropyl-*O*-[(2-azido-4-*O*-benzyl-6-*O*-*tert*-butyldiphenylsilyl-3-*O*-(2-naphthylmethyl)-2-deoxy-*α*-D-glucopyranosyl)-(1→4)-*O*-(2-*O*-benzoyl-3-*O*-benzyl-6-*O*-acetyl-*α*-L-idopyranosyl)-(1→4)-*O*-(2-azido-6-*O*-*tert*-butyldiphenylsilyl-3-*O*-(2-naphthylmethyl)-2-deoxy-*α*-D-glucopyranosyl)]-(1→4)-*O*-2-*O*-benzoyl-3-*O*-benzyl-6-*O*-acetyl-*α*-L-idopyranoside (25)**

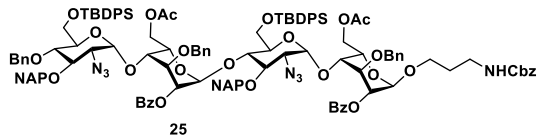

25

A solution of donor **24** (0.90 g, 0.42 mmol) and linker benzyl (3-hydroxypropyl)carbamate (0.097 g, 0.46 mmol) in $CH_2Cl_2$ (15 mL) was stirred under $N_2$ atmosphere in round bottom flask containing freshly dried 4 Å molecular sieves for 2 h. Next, NIS (0.15 g, 0.67 mmol) and TfOH (7.4 µL, 0.084 mmol) was added at room temperature and reaction completion was monitored by TLC, quenched using few drops of $Et_3N$. Molecular sieves were filtered using celite and organic layer was washed with aqueous $Na_2S_2O_3$ and brine. The collected organic layer was dried over $Na_2SO_4$, filtered, concentrated and purified through silica gel column chromatography (ethyl acetate/ hexane= 1/3, v/v) to obtain compound **25** in 90 % yield. $^1$H NMR (400 MHz, Chloroform-d) δ 8.09 (dd, J = 6.4, 3.1 Hz, 2H), 8.01 – 7.99 (m, 1H), 7.82 – 7.78 (m, 1H), 7.76 – 7.74 (m, 1H), 7.67 – 7.54 (m, 14H), 7.49 (s, 1H), 7.47 –

7.45 (m, 2H), 7.43 (s, 1H), 7.40 (s, 1H), 7.39 (s, 2H), 7.37 (s, 2H), 7.34 – 7.27 (m, 24H), 7.24 – 7.20 (m, 6H), 7.17 – 7.11 (m, 6H), 5.63 (s, 1H), 5.37 (s, 1H), 5.18 (s, 1H), 5.08 (s, 2H), 5.03 (s, 1H), 4.96 (s, 1H), 4.88 (dd, *J* = 11.4, 4.5 Hz, 1H), 4.78 (d, *J* = 10.7 Hz, 2H), 4.74 (d, *J* = 11.3 Hz, 2H), 4.68 (d, *J* = 10.8 Hz, 1H), 4.64 (d, *J* = 3.6 Hz, 1H), 4.58 (dd, *J* = 17.4, 11.3 Hz, 2H), 4.39 (dt, *J* = 8.6, 4.4 Hz, 1H), 4.33 (dt, *J* = 11.2, 3.9 Hz, 2H), 4.27 – 4.24 (m, 2H), 4.10 (t, *J* = 9.4 Hz, 2H), 4.03 (d, *J* = 12.5 Hz, 1H), 3.99 – 3.93 (m, 3H), 3.89 (s, 1H), 3.87 – 3.80 (m, 5H), 3.74 (d, J = 11.9 Hz, 1H), 3.68 (t, *J* = 9.7 Hz, 2H), 3.61 (d, *J* = 10.3 Hz, 2H), 3.57 – 3.54 (m, 3H), 3.47 (s, 1H), 3.39 (s, 1H), 3.28 (d, *J* = 3.6 Hz, 1H), 3.25 (d, *J* = 3.3 Hz, 1H), 3.24 – 3.18 (m, 2H), 1.86 (s, 3H), 1.18 (s, 3H), 1.01 (s, 9H), 0.97 (s, 9H). $^{13}$C NMR (101 MHz, Chloroform-d) δ 170.37, 169.91, 165.79, 165.68, 156.55, 138.18, 137.54, 137.50, 136.72, 135.88, 135.86, 135.61, 135.58, 135.47, 135.23, 133.46, 133.42, 133.28, 133.23, 133.19, 133.14, 133.01, 132.70, 129.88, 129.84, 129.74, 129.69, 129.64, 129.63, 129.61, 129.59, 128.70, 128.66, 128.58, 128.54, 128.45, 128.38, 128.34, 128.30, 128.25, 128.17, 128.13, 128.10, 128.01, 127.97, 127.82, 127.74, 127.72, 127.68, 127.64, 127.61, 127.58, 127.51, 127.40, 127.34, 126.91, 126.08, 126.01, 125.95, 125.92, 125.84, 125.65, 125.56, 98.15, 98.11, 97.84, 96.93, 80.36, 79.09, 77.63, 77.24, 75.28, 75.02, 74.97, 73.82, 73.25, 73.16, 72.89, 72.80, 72.56, 72.50, 72.40, 72.38, 71.63, 68.79, 68.56, 67.01, 66.57, 65.12, 64.59, 64.42, 64.07, 63.04, 62.34, 62.21, 61.94, 39.64, 29.41, 26.86, 26.78, 20.63, 19.90, 19.44, 19.32. HR-ESI-MS *(m/z)*: $[M+Na]^+$ calcd for $C_{128}H_{135}N_7O_{25}Si_2Na$, 2248.8944; found, 2248.9016.

**N-benzyloxycarbonyl-3-aminopropyl-*O*-[(2-azido-4-*O*-benzyl-6-*O*-*tert*-butyldiphenylsilyl-3-*O*-(2-naphthylmethyl)-2-deoxy-*α*-D-glucopyranosyl)-(1→4)-*O*-(3-*O*-benzyl-*α*-L-idopyranosyl)-(1→4)-*O*-(2-azido-6-*O*-*tert*-butyldiphenylsilyl-3-*O*-(2-naphthylmethyl)-2-deoxy-*α*-D-glucopyranosyl)]-(1→4)-*O*-3-*O*-benzyl-*α*-L-idopyranoside (26)**

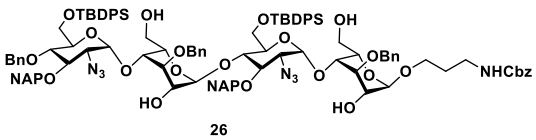

26

To a solution of compound **25** (0.84 g, 0.37 mmol) in $CH_2Cl_2$ (7 mL) and MeOH (7 mL) was added NaOMe (0.06g, 1.11 mmol) and stirred at room temperature. After 12 h, reaction mixture was quenched using Amberlite IR 120H$^+$ resin, filtered, evaporated and purified through silica gel column chromatography

(ethyl acetate/ hexane= 1/2.5, v/v) to obtain compound **26** in 95 % yield. $^{1}$H NMR (400 MHz, Chloroform-d) δ 7.81 – 7.68 (m, 13H), 7.57 (d, J = 8.5 Hz, 2H), 7.51 – 7.44 (m, 15H), 7.41 – 7.35 (m, 11H), 7.33 – 7.30 (m, 4H), 7.29 – 7.27 (m, 6H), 7.17 – 7.14 (m, 3H), 5.72 (s, 1H), 5.10 (s, 1H), 5.05 (s, 3H), 5.01 – 4.94 (m, 2H), 4.88 – 4.84 (m, 2H), 4.80 (dd, *J* = 10.6, 4.7 Hz, 2H), 4.73 (d, *J* = 11.3 Hz, 2H), 4.68 (dd, *J* = 10.9, 3.7 Hz, 2H), 4.63 – 4.51 (m, 2H), 4.25 (dt, *J* = 14.0, 6.9 Hz, 2H), 3.99 (t, *J* = 9.5 Hz, 1H), 3.89 – 3.83 (m, 7H), 3.81 – 3.71 (m, 8H), 3.61 – 3.54 (m, 8H), 3.48 (d, J = 11.5 Hz, 1H), 3.36 (d, *J* = 8.3 Hz, 1H), 3.22 (ddt, *J* = 18.0, 13.6, 5.6 Hz, 2H), 2.70 (dt, *J* = 10.7, 5.2 Hz, 1H), 2.16 (s, 1H), 1.85 (s, 2H), 1.10 (s, 9H), 1.05 (s, 9H). $^{13}$C NMR (101 MHz, Chloroform-d) δ 156.68, 138.02, 137.50, 137.48, 136.61, 136.00, 135.84, 135.79, 135.60, 135.10, 134.86, 133.44, 133.32, 133.30, 133.15, 133.14, 133.08, 132.84, 132.64, 129.87, 129.82, 129.79, 129.69, 128.72, 128.51, 128.48, 128.45, 128.43, 128.27, 128.07, 128.04, 128.02, 127.90, 127.84, 127.79, 127.70, 127.67, 127.60, 127.56, 127.52, 127.08, 126.61, 126.32, 126.07, 126.00, 125.59, 100.99, 100.07, 94.79, 94.36, 81.25, 79.86, 77.75, 77.26, 76.02, 75.52, 75.06, 73.64, 72.94, 72.47, 72.32, 72.02, 71.69, 70.87, 70.30, 69.56, 66.99, 66.95, 66.88, 66.86, 66.85, 66.63, 66.51, 66.36, 64.61, 63.99, 62.76, 62.49, 61.79, 61.44, 39.68, 29.72, 26.93, 26.83, 19.46, 19.31. HR-ESI-MS *(m/z)*: $[M+Na]^{+}$ calcd for $C_{110}H_{123}N_7O_{21}Si_2Na$, 1957.8242; found, 1957.8326.

**N-benzyloxycarbonyl-3-aminopropyl-*O*-[(2-azido-4-*O*-benzyl-6-*O*-*tert*-butyldiphenylsilyl-3-*O*-(2-naphthylmethyl)-2-deoxy-*α*-D-glucopyranosyl)-(1→4)-*O*-(3-*O*-benzyl-*α*-L-idopyranosylurono-6,2-lactone)-(1→4)-*O*-(2-azido-6-*O*-*tert*-butyldiphenylsilyl-3-*O*-(2-naphthylmethyl)-2-deoxy-*α*-D-glucopyranosyl)]-(1→4)-*O*-3-*O*-benzyl-*α*-L-idopyranosidurono-6,2-lactone (27)**

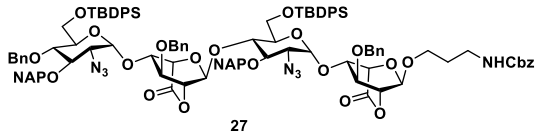

27

To a solution of compound **26** (0.67 g, 0.34 mmol) in $CH_2Cl_2$ (5 mL) and $H_2O$ (5 mL) was added TEMPO (0.01g, 0.07 mmol), BAIB (0.54 g, 1.70 mmol) and stirred at room temperature. After 16 h, the reaction mixture was extracted using saturated aqueous $NH_4Cl$. The collected organic layer was dried over $Na_2SO_4$, filtered, concentrated and purified through silica gel column chromatography (ethyl acetate/ hexane= 1/3, v/v) to obtain

compound **27** in 65 % yield. $^{1}$H NMR (400 MHz, Chloroform-d) δ 7.89 – 7.78 (m, 7H), 7.71 – 7.68 (m, 4H), 7.65 – 7.61 (m, 4H), 7.51 – 7.29 (m, 36H), 7.22 – 7.17 (m, 3H), 5.84 (s, 1H), 5.47 (s, 1H), 5.25 (d, J = 12.0 Hz, 1H), 5.20 – 5.05 (m, 4H), 4.99 (d, J = 10.7 Hz, 1H), 4.95 (s, 1H), 4.92 (s, 1H), 4.87 (d, J = 11.6 Hz, 1H), 4.82 (d, *J* = 11.5 Hz, 1H), 4.76 (d, *J* = 8.9 Hz, 1H), 4.70 (d, *J* = 20.3 Hz, 1H), 4.65 – 4.62 (m, 1H), 4.49 (d, *J* = 12.4 Hz, 2H), 4.32 (d, *J* = 2.8 Hz, 1H), 4.24 (s, 1H), 4.21 – 4.14 (m, 3H), 4.01 – 3.85 (m, 5H), 3.82 – 3.76 (m, 3H), 3.71 (dt, *J* = 8.0, 3.3 Hz, 3H), 3.65 – 3.59 (m, 3H), 3.53 (dd, *J* = 14.1, 3.7 Hz, 1H), 3.48 – 3.45 (m, 2H), 3.34 (dt, *J* = 13.6, 6.6 Hz, 1H), 2.77 (dd, *J* = 9.4, 4.4 Hz, 1H), 1.89 – 1.87 (m, 2H), 1.07 (s, 18H). $^{13}$C NMR (101 MHz, Chloroform-d) δ 167.43, 167.04, 156.60, 138.13, 137.02, 136.86, 136.70, 136.21, 136.00, 135.88, 135.58, 135.56, 135.19, 133.65, 133.34, 133.30, 133.14, 133.01, 132.77, 132.74, 130.02, 129.85, 129.73, 129.70, 129.64, 128.52, 128.49, 128.42, 128.32, 128.23, 128.21, 128.19, 128.11, 128.08, 128.03, 127.93, 127.81, 127.70, 127.65, 127.53, 127.52, 127.19, 126.49, 126.19, 126.09, 126.02, 125.91, 124.87, 124.68, 99.84, 98.98, 96.78, 96.74, 80.99, 80.27, 80.00, 78.32, 78.06, 77.87, 77.77, 77.24, 76.10, 75.82, 74.95, 74.34, 72.65, 72.57, 72.49, 72.35, 72.25, 71.82, 69.42, 69.37, 69.11, 66.64, 63.34, 61.69, 61.47, 39.89, 29.48, 26.91, 19.36, 19.28. HR-ESI-MS *(m/z)*: $[M+Na]^+$ calcd for $C_{110}H_{115}N_7O_{21}Si_2Na$, 1949.7616; found, 1949.7651.

**N-benzyloxycarbonyl-3-aminopropyl-*O*-[(2-acetamido-4-*O*-benzyl-6-*O*-*tert*-butyldiphenylsilyl-3-*O*-(2-naphthylmethyl)-2-deoxy-*α*-D-glucopyranosyl)-(1→4)-*O*-(3-*O*-benzyl-*α*-L-idopyranosylurono-6,2-lactone)-(1→4)-*O*-(2-acetamido-6-*O*-*tert*-butyldiphenylsilyl-3-*O*-(2-naphthylmethyl)-2-deoxy-*α*-D-glucopyranosyl)]-(1→4)-*O*-3-*O*-benzyl-*α*-L-idopyranosidurono-6,2-lactone (28)**

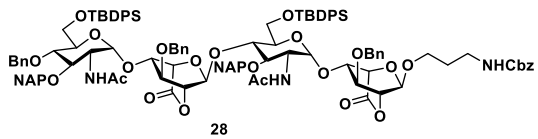

28

To a solution of compound **27** (0.40 g, 0.20 mmol) in THF (3 mL), AcOH (2 mL) and $Ac_2O$ (2 mL) was added Zn dust (0.52 g, 8 mmol) and stirred for 12 h at room temperature. Upon completion, the reaction mixture was filtered through celite and volatiles were evaporated. The remaining residue was extracted with ethyl acetate, saturated $NaHCO_3$ and washed with brine. The collected organic layer was dried over $Na_2SO_4$, filtered, concentrated and purified through silica gel column chromatography (ethyl acetate/ hexane= 1/2.5, v/v) to obtain compound **28** in 70

% yield. $^{1}$H NMR (400 MHz, Chloroform-*d*) δ 7.92 – 7.86 (m, 3H), 7.82- 7.81 (m, 2H), 7.78 (d, *J* = 8.5 Hz, 1H), 7.76 – 7.74 (m, 1H), 7.71- 7.70 (m, 2H), 7.69 – 7.68 (m, 3H), 7.68 – 7.66 (m, 2H), 7.65 (d, *J* = 1.3 Hz, 1H), 7.58 (s, 1H), 7.53 (dt, *J* = 6.1, 2.7 Hz, 2H), 7.51 – 7.49 (m, 1H), 7.48 – 7.46 (m, 2H), 7.45 – 7.42 (m, 3H), 7.41 (s, 2H), 7.39 – 7.38 (m, 2H), 7.38 – 7.37 (m, 1H), 7.35- 7.31 (m, 7H), 7.29 (s, 1H), 7.28 – 7.27 (m, 7H), 7.26 – 7.24 (m, 3H), 7.23 – 7.20 (m, 3H), 7.18 – 7.16 (m, 2H), 7.05 (d, *J* = 7.3 Hz, 2H), 5.50 (s, 1H), 5.42 (t, *J* = 5.2 Hz, 1H), 5.16 (d, *J* = 3.6 Hz, 1H), 5.07 – 5.03 (m, 4H), 5.00 (s, 1H), 4.93 – 4.90 (m, 3H), 4.80 (d, *J* = 3.5 Hz, 1H), 4.77 (d, *J* = 2.1 Hz, 1H), 4.73 (d, *J* = 6.9 Hz, 1H), 4.63 (d, *J* = 12.4 Hz, 1H), 4.48 (s, 1H), 4.42 (d, *J* = 3.4 Hz, 1H), 4.37 (s, 1H), 4.33 (d, *J* = 2.5 Hz, 2H), 4.30 (d, *J* = 5.4 Hz, 1H), 4.27 – 4.21 (m, 1H), 4.09 (qd, *J* = 6.2, 4.2, 3.7 Hz, 3H), 4.02 – 3.89 (m, 7H), 3.86 – 3.70 (m, 2H), 3.68 – 3.59 (m, 5H), 3.53 (q, *J* = 10.8, 9.0 Hz, 2H), 3.36 (dt, *J* = 11.3, 6.0 Hz, 1H), 3.27 (dt, *J* = 13.8, 6.7 Hz, 1H), 1.83 – 1.80 (m, 2H), 1.59 (s, 3H), 1.39 (s, 3H), 1.09 (s, 9H), 1.06 (s, 9H). $^{13}$C NMR (101 MHz, Chloroform-*d* ) δ 169.88, 169.77, 167.57, 167.18, 156.46, 138.08, 136.62, 136.59, 135.92, 135.89, 135.78, 135.64, 135.57, 133.55, 133.28, 133.20, 133.08, 133.02, 132.94, 132.85, 132.54, 129.96, 129.83, 129.63, 128.64, 128.50, 128.46, 128.33, 128.29, 128.22, 128.09, 128.04, 127.93, 127.90, 127.78, 127.71, 127.66, 127.52, 127.16, 126.58, 126.44, 126.38, 126.34, 126.28, 126.26, 98.94, 98.73, 98.38, 96.61, 79.70, 79.39, 79.08, 79.00, 78.65, 78.28, 78.04, 77.29, 76.88, 75.09, 74.98, 74.79, 72.84, 72.28, 72.22, 72.13, 71.74, 69.35, 68.57, 66.60, 61.94, 61.70, 52.92, 52.80, 39.16, 29.61, 26.94, 26.87, 23.17, 22.87, 19.26, 19.20. HR-ESI-MS *(m/z)*: $[M+H]^+$ calcd for $C_{114}H_{124}N_3O_{23}Si_2$, 1958.8164; found, 1958.8163.

**General procedure for benzyl ester formation:**

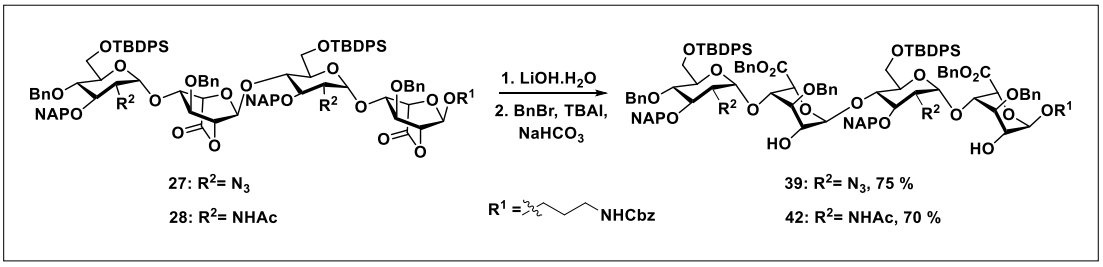


To a solution of starting material (1 mmol) in THF/ $H_2O$ (1/ 1) was added LiOH• $H_2O$ (3 mmol) and stirred at room temperature for 2 h. Upon completion, the reaction mixture was quenched using Amberlite IR 120H$^+$ resin, filtered, evaporated and dried. Next, the residue

was dissolved in DMF and added BnBr (4 mmol), TBAI (1.4 mmol), $NaHCO_3$ (5 mmol) and stirred at 60 $^{o}$C under $N_2$ atmosphere. After 2 h, the reaction mixture was extracted with ethyl acetate and washed with brine. The collected organic layer was dried over $Na_2SO_4$, filtered, concentrated and purified through silica gel column chromatography.

**N-benzyloxycarbonyl-3-aminopropyl-*O*-[(benzyl (2-azido-4-*O*-benzyl-6-*O*-*tert*-butyldiphenylsilyl-3-*O*-(2-naphthylmethyl)-2-deoxy-*α*-D-glucopyranosyl))-(1→4)-*O*-(3-*O*-benzyl-*α*-L-idopyranosyluronate)-(1→4)-*O*-(benzyl (2-azido-6-*O*-*tert*-butyldiphenylsilyl-3-*O*-(2-naphthylmethyl)-2-deoxy-*α*-D-glucopyranosyl))]-(1→4)-*O*-3-*O*-benzyl-*α*-L-idopyranosiduronate (39)**

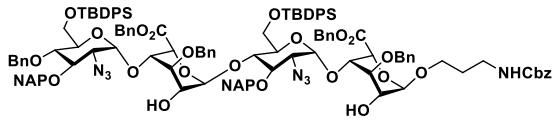

39

$^{1}$H NMR (400 MHz, Chloroform-d) δ 7.74 – 7.66 (m, 3H), 7.65 – 7.41 (m, 13H), 7.38 – 7.35 (m, 2H), 7.33 – 7.11 (m, 37H), 7.07 (ddd, J = 13.9, 6.6, 2.9 Hz, 4H), 6.94 (ddt, J = 8.6, 3.3, 1.7 Hz, 1H), 6.85 (t, J = 7.5 Hz, 2H), 6.77 (d, J = 7.2 Hz, 2H), 5.44 – 5.36 (m, 2H), 5.04 (d, J = 12.4 Hz, 1H), 4.96 (d, J = 3.6 Hz, 1H), 4.93 – 4.88 (m, 4H), 4.77 – 4.73 (m, 4H), 4.70 – 4.67 (m, 2H), 4.61 (dd, J = 12.2, 6.2 Hz, 2H), 4.56 (d, J = 2.7 Hz, 2H), 4.53 (d, J = 4.4 Hz, 1H), 4.51 – 4.39 (m, 3H), 4.08 (t, J = 9.5 Hz, 1H), 3.95 – 3.93 (m, 2H), 3.85 (t, J = 3.9 Hz, 1H), 3.76 (ddd, J = 22.1, 12.9, 7.5 Hz, 5H), 3.68 (d, J = 4.5 Hz, 1H), 3.64 – 3.57 (m, 4H), 3.53 – 3.47 (m, 3H), 3.43 – 3.30 (m, 5H), 3.19 (d, J = 10.6 Hz, 1H), 3.16 – 3.11 (m, 1H), 1.78 – 1.65 (m, 2H), 0.98 (s, 9H), 0.94 (s, 9H). $^{13}$C NMR (101 MHz, Chloroform-*d*) δ 169.02, 168.76, 156.46, 138.24, 137.35, 137.32, 136.57, 135.99, 135.88, 135.86, 135.60, 135.19, 135.18, 134.81, 133.47, 133.34, 133.30, 133.26, 133.15, 133.05, 132.75, 129.74, 129.69, 129.67, 128.68, 128.62, 128.51, 128.41, 128.33, 128.27, 128.24, 128.21, 128.12, 128.01, 127.94, 127.92, 127.81, 127.77, 127.72, 127.65, 127.62, 127.55, 127.53, 127.50, 126.95, 126.30, 126.25, 126.05, 126.02, 125.96, 125.71, 125.51, 101.48, 100.99, 95.43, 80.83, 79.48, 79.46, 77.59, 77.24, 75.79, 75.17, 74.93, 74.29, 73.33, 72.96, 72.55, 72.22, 71.56, 71.39, 71.24, 68.44, 68.22, 68.00, 67.99, 67.21, 67.09, 67.08, 67.00, 66.64, 66.61, 64.15, 63.81, 62.13, 61.68, 39.83, 29.45, 26.94, 26.88. HR-ESI-MS *(m/z)*: $[M+Na]^+$ calcd for $C_{124}H_{131}N_7O_{23}Si_2Na$, 2165.8766; found, 2165.8772.

**N-benzyloxycarbonyl-3-aminopropyl-*O*-[(benzyl (2-acetamido-4-*O*-benzyl-6-*O*-*tert*-butyldiphenylsilyl-3-*O*-(2-naphthylmethyl)-2-deoxy-*α*-D-glucopyranosyl))-(1→4)-*O*-(3-*O*-benzyl-*α*-L-idopyranosyluronate)-(1→4)-*O*-(benzyl (2-acetamido-6-*O*-*tert*-butyldiphenylsilyl-3-*O*-(2-naphthylmethyl)-2-deoxy-*α*-D-glucopyranosyl))]-(1→4)-*O*-3-*O*-benzyl-*α*-L-idopyranosiduronate (42)**

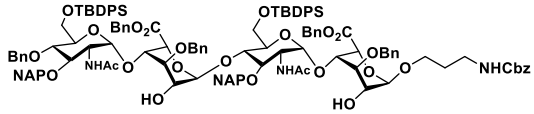

42

$^{1}$H NMR (400 MHz, Chloroform-d) δ 7.82-7.77 (m, 3H), 7.76 – 7.74 (m, 2H), 7.73 – 7.72 (m, 2H), 7.71 (d, J = 1.6 Hz, 1H), 7.70 (d, J = 1.6 Hz, 2H), 7.69 – 7.68 (m, 2H), 7.67 – 7.66 (m, 1H), 7.65 (d, J = 1.3 Hz, 1H), 7.63 (d, J = 1.4 Hz, 1H), 7.55 (s, 1H), 7.45 (dd, J = 6.2, 3.3 Hz, 2H), 7.42 (s, 1H), 7.41 – 7.40 (m, 2H), 7.39 (d, J = 1.5 Hz, 2H), 7.37 (d, J = 2.1 Hz, 2H), 7.36- 7.35 (m, 2H), 7.35 (s, 4H), 7.32 – 7.30 (m, 6H), 7.29 (s, 1H), 7.28 – 7.22 (m, 17H), 7.20- 7.16 (m, 5H), 6.95 (t, J = 7.7 Hz, 2H), 6.86 (d, J = 7.9 Hz, 2H), 5.77 – 5.75 (m, 1H), 5.45 (t, J = 5.3 Hz, 1H), 5.37 (s, 1H), 5.16 (s, 1H), 5.14 – 5.09 (m, 2H), 5.03 – 5.00 (m, 1H), 5.00 – 4.93 (m, 1H), 4.91 (s, 1H), 4.88 (s, 2H), 4.85 (s, 1H), 4.81 (s, 1H), 4.77 – 4.74 (m, 2H), 4.70 (dd, J = 11.7, 3.6 Hz, 2H), 4.62 (d, J = 12.3 Hz, 1H), 4.56 (d, J = 11.4 Hz, 1H), 4.48 (d, J = 5.4 Hz, 1H), 4.46 – 4.42 (m, 2H), 4.30 (td, J = 10.7, 3.0 Hz, 1H), 4.26 – 4.15 (m, 2H), 4.05 (s, 1H), 3.95 (d, J = 9.5 Hz, 1H), 3.92 – 3.84 (m, 3H), 3.84 – 3.81 (m, 1H), 3.78 (d, J = 12.1 Hz, 2H), 3.73 (dd, J = 5.9, 1.8 Hz, 1H), 3.71 – 3.65 (m, 3H), 3.65 – 3.62 (m, 3H), 3.58 – 3.53 (m, 2H), 3.53 – 3.50 (m, 1H), 3.39 (dd, J = 16.5, 7.9 Hz, 2H), 3.30 – 3.21 (m, 1H), 2.90 – 2.86 (m, 1H), 2.74 (s, 1H), 1.80 – 1.79 (m, 2H), 1.67 (s, 3H), 1.29 (s, 3H), 1.07 (s, 9H), 1.04 (s, 9H). $^{13}$C NMR (101 MHz, Chloroform-*d*) δ 170.65, 170.42, 169.27, 168.97, 156.50, 138.43, 137.24, 137.15, 136.47, 135.96, 135.89, 135.70, 135.60, 134.57, 134.36, 133.54, 133.43, 133.27, 133.18, 133.09, 132.91, 132.80, 129.82, 129.62, 129.61, 128.66, 128.63, 128.55, 128.44, 128.33, 128.29, 128.18, 128.09, 128.00, 127.93, 127.87, 127.85, 127.79, 127.70, 127.62, 127.55, 126.73, 126.51, 126.17, 126.12, 125.97, 125.93, 101.13, 100.61, 96.80, 94.89, 79.93, 78.26, 77.73, 75.17, 75.13, 74.48, 74.26, 73.00, 72.73, 72.53, 72.45, 72.08, 71.87, 71.55, 69.35, 68.01, 67.60, 67.33, 67.18, 67.15, 67.07, 66.67, 62.15, 62.05, 52.64,

52.41, 39.54, 29.73, 29.48, 26.93, 26.86, 22.83, 22.56, 19.47, 19.29. HR-ESI-MS *(m/z)*: $[M+Na]^+$ calcd for $C_{128}H_{139}N_3O_{25}Si_2Na$, 2196.9134; found, 2196.9077.

**General procedure for selective NAP deprotection:**

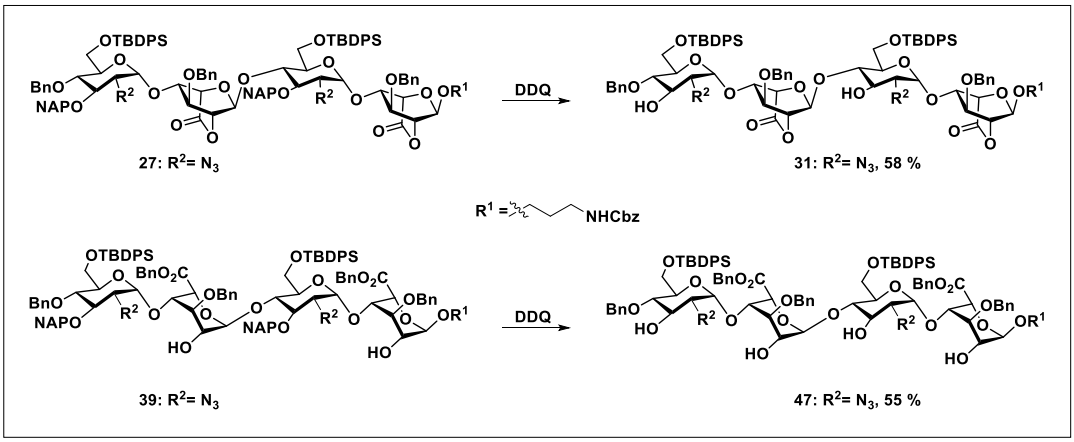


To a solution of starting material (1 mmol) in $CH_2Cl_2$ (6 mL) and $H_2O$ (340 µL) was added DDQ (5 mmol) portion wise over the interval of 20 min. After 1 h, the reaction mixture was quenched using $NaHCO_3$, extracted with $CH_2Cl_2$ and washed with brine. The collected organic layer was dried over $Na_2SO_4$, filtered, concentrated and purified through silica gel column chromatography.

**N-benzyloxycarbonyl-3-aminopropyl-*O*-[(2-azido-4-*O*-benzyl-6-*O*-*tert*-butyldiphenylsilyl-2-deoxy-*α*-D-glucopyranosyl)-(1→4)-*O*-(3-*O*-benzyl-*α*-L-idopyranosylurono-6,2-lactone)-(1→4)-*O*-(2-azido-6-*O*-*tert*-butyldiphenylsilyl-2-deoxy-*α*-D-glucopyranosyl)]-(1→4)-*O*-3-*O*-benzyl-*α*-L-idopyranosidurono-6,2-lactone (31)**

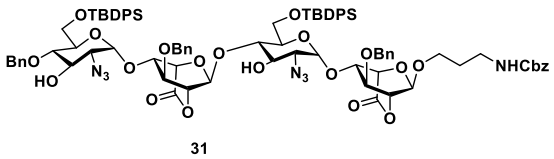

31

$^1$H NMR (400 MHz, Chloroform-d) δ 7.72 (t, J = 1.3 Hz, 1H), 7.70 – 7.67 (m, 3H), 7.63 – 7.61 (m, 4H), 7.46 – 7.42 (m, 3H), 7.41 – 7.34 (m, 12H), 7.33 – 7.29 (m, 13H), 7.26 – 7.23 (m, 4H), 5.82 (t, J = 5.4 Hz, 1H), 5.12 – 5.08 (m, 3H), 5.04 (dd, J = 2.3, 1.0 Hz, 1H), 4.99 (d, J = 3.8 Hz, 1H), 4.91 (d, J = 3.6 Hz, 1H), 4.81 – 4.69 (m, 3H), 4.62 (d, J = 12.4 Hz, 1H), 4.54 (d, J = 11.6 Hz, 1H), 4.45 – 4.42 (m, 2H), 4.36 (dd, J = 5.9, 3.3 Hz, 2H), 4.22 – 4.19 (m, 1H), 4.13 – 4.11 (m, 1H), 4.03 (t, J = 2.6 Hz, 1H), 4.00 – 3.92 (m, 5H), 3.90 (dd, J =

12.0, 1.8 Hz, 1H), 3.81 – 3.79 (m, 2H), 3.77 – 3.75 (m, 2H), 3.72 (s, 1H), 3.70 – 3.68 (m, 2H), 3.65 – 3.59 (m, 2H), 3.49 – 3.41 (m, 1H), 3.35 – 3.28 (m, 1H), 3.24 (dd, J = 10.4, 3.7 Hz, 1H), 3.18 (dd, J = 10.5, 3.7 Hz, 1H), 2.46 (s, 1H), 1.86 (s, 1H), 1.09 (s, 9H), 1.06 (s, 9H). 13C NMR (101 MHz, Chloroform-d) δ 167.28, 166.35, 156.61, 137.96, 136.92, 136.69, 136.53, 135.95, 135.79, 135.67, 135.57, 133.42, 133.02, 132.78, 130.02, 129.89, 129.82, 129.76, 128.69, 128.65, 128.54, 128.48, 128.32, 128.23, 128.18, 128.16, 128.10, 128.09, 128.00, 127.93, 127.86, 127.72, 127.70, 127.60, 100.17, 99.91, 97.84, 96.72, 81.04, 80.48, 79.81, 79.06, 78.70, 78.06, 77.23, 74.89, 72.67, 72.55, 72.27, 71.67, 71.17, 71.04, 70.29, 69.61, 69.46, 69.29, 66.63, 62.68, 62.43, 62.26, 61.72, 39.87, 29.44, 26.94. HR-ESI-MS *(m/z)*: $[M+Na]^+$ calcd for $C_{88}H_{99}N_7O_{21}Si_2Na$, 1668.6330; found, 1668.6327.

**N-benzyloxycarbonyl-3-aminopropyl-*O*-[(benzyl (2-azido-4-*O*-benzyl-6-*O*-*tert*-butyldiphenylsilyl-2-deoxy-*α*-D-glucopyranosyl))-(1→4)-*O*-(3-*O*-benzyl-*α*-L-idopyranosyluronate)-(1→4)-*O*-(benzyl (2-azido-6-*O*-*tert*-butyldiphenylsilyl-2-deoxy-*α*-D-glucopyranosyl))]-(1→4)-*O*-3-*O*-benzyl-*α*-L-idopyranosiduronate (47)**

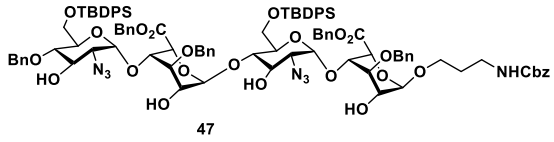

47

$^1$H NMR (400 MHz, Chloroform-d) δ 7.67 (tdd, J = 8.0, 4.1, 1.8 Hz, 8H), 7.42 – 7.28 (m, 19H), 7.25 – 7.20 (m, 15H), 7.19 – 7.15 (m, 6H), 7.10 (dd, J = 7.2, 2.5 Hz, 2H), 5.52 (t, J = 5.2 Hz, 1H), 5.16 (d, J = 3.5 Hz, 1H), 5.11 (d, J = 12.1 Hz, 1H), 5.04 – 4.94 (m, 6H), 4.81 (d, J = 3.3 Hz, 2H), 4.75 – 4.70 (m, 4H), 4.52 (d, J = 8.7 Hz, 3H), 4.30 (d, J = 2.0 Hz, 1H), 4.10 – 4.08 (m, 1H), 4.03 (s, 1H), 3.88 – 3.70 (m, 11H), 3.65 – 3.56 (m, 3H), 3.55 – 3.46 (m, 4H), 3.40 (td, J = 10.9, 10.4, 4.7 Hz, 2H), 3.34 (dd, J = 10.2, 3.7 Hz, 1H), 3.20 (ddt, J = 12.6, 7.0, 4.5 Hz, 1H), 2.95 (d, J = 9.3 Hz, 1H), 2.32 (d, J = 3.3 Hz, 1H), 1.78 (s, 2H), 1.08 (s, 9H), 1.06 (s, 9H). $^{13}$C NMR (101 MHz, Chloroform-d) δ 169.04, 168.53, 156.46, 138.23, 137.34, 137.30, 136.56, 135.84, 135.79, 135.74, 135.64, 134.78, 134.55, 133.41, 133.27, 133.25, 133.12, 129.83, 129.77, 129.74, 129.70, 128.70, 128.64, 128.62, 128.59, 128.51, 128.50, 128.40, 128.27, 128.11, 128.08, 128.05, 128.00, 127.97, 127.78, 127.75, 127.61, 102.91, 101.42, 96.09, 94.99, 80.84, 77.92, 77.24, 74.96, 74.24, 73.00, 72.65, 72.41, 72.19, 71.94, 71.80, 71.25, 71.09, 69.65, 69.53, 68.00, 67.66, 67.24, 67.13, 66.95, 66.59, 63.27, 63.02, 62.19, 61.96, 39.84,

29.41, 26.93. HR-ESI-MS *(m/z)*: $[M+Na]^+$ calcd for $C_{102}H_{115}N_7O_{23}Si_2Na$, 1885.7514; found, 1885.7581.

**General procedure for desilylation pre *O*- sulfation:**

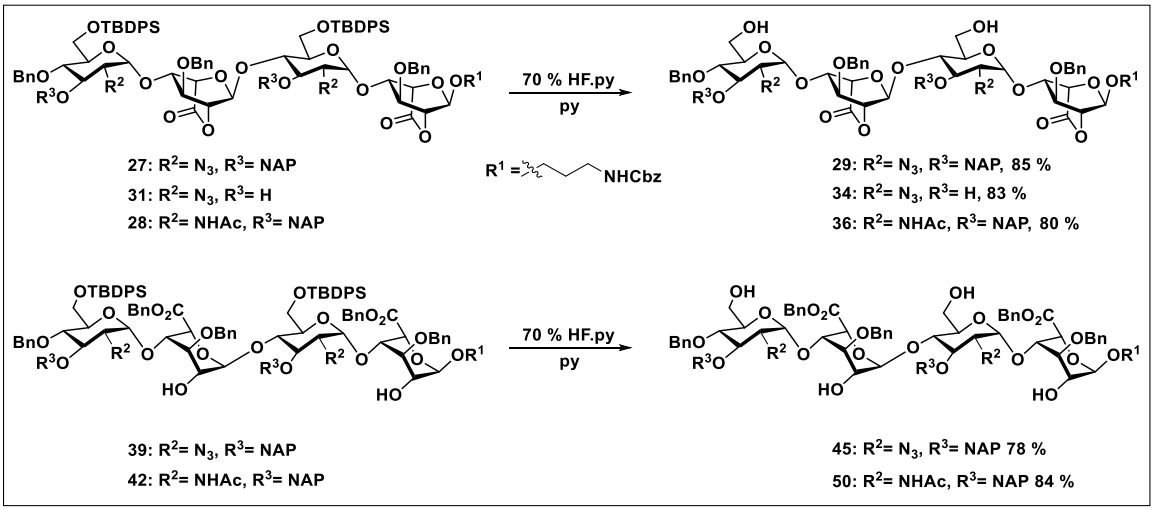


A solution of starting material (1 mmol) in pyridine (1 mL) was stirred at ice cold temperature under $N_2$ atmosphere. After 15 minutes, 70 % HF.py complex (5 mmol) was added drop wise and reaction mixture was stirred for 12 h. Upon completion, the mixture was extracted with ethyl acetate and washed with 1 N HCl and brine. The combined organic layer was dried over $Na_2SO_4$, filtered, concentrated and purified through silica gel column chromatography.

**N-benzyloxycarbonyl-3-aminopropyl-*O*-[(2-azido-4-*O*-benzyl-3-*O*-(2-naphthylmethyl)-2-deoxy-*α*-D-glucopyranosyl)-(1→4)-*O*-(3-*O*-benzyl-*α*-L-idopyranosylurono-6,2-lactone)-(1→4)-*O*-(2-azido-3-*O*-(2-naphthylmethyl)-2-deoxy-*α*-D-glucopyranosyl)]-(1→4)-*O*-3-*O*-benzyl-*α*-L-idopyranosidurono-6,2-lactone (29)**

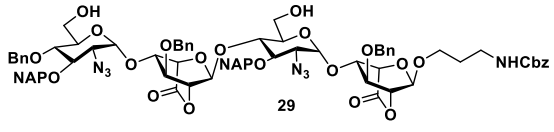


$^1$H NMR (400 MHz, Chloroform-d) δ 7.92 (s, 1H), 7.89 – 7.76 (m, 6H), 7.72 (s, 1H), 7.53 – 7.50 (m, 2H), 7.49 – 7.45 (m, 3H), 7.44 – 7.40 (m, 2H), 7.38 (s, 2H), 7.37 – 7.31 (m 8H), 7.30 – 7.29 (m, 7H), 7.24 (dd, J = 7.5, 1.9 Hz, 2H), 5.75 (t, J = 5.1 Hz, 1H), 5.35 (s, 1H), 5.16 (d, J = 12.1 Hz, 1H), 5.09 – 5.07 (m, 3H),

5.01 (s, 1H), 4.98 – 4.93 (m, 3H), 4.79 – 4.70 (m, 3H), 4.67 – 4.64 (m, 1H), 4.62 – 4.56 (m, 2H), 4.52 (t, J = 3.4 Hz, 2H), 4.46 (t, J = 2.6 Hz, 1H), 4.30 – 4.28 (m, 2H), 3.95 – 3.85 (m, 5H), 3.82 – 3.76 (m, 2H), 3.73 (td, J = 3.1, 1.5 Hz, 1H), 3.71 – 3.68 (m, 3H), 3.66 – 3.61 (m, 2H), 3.57 (d, J = 3.8 Hz, 1H), 3.51 – 3.27 (m, 6H), 2.83 (dd, J = 10.4, 3.7 Hz, 1H), 2.05 (s, 1H), 1.85 (s, 2H). $^{13}$C NMR (101 MHz, Chloroform-d) δ 167.92, 167.82, 156.62, 137.78, 137.02, 136.76, 136.67, 135.98, 135.15, 133.50, 133.28, 133.06, 132.84, 129.71, 128.57, 128.54, 128.48, 128.46, 128.27, 128.24, 128.22, 128.18, 128.11, 128.09, 128.00, 127.99, 127.84, 127.81, 127.69, 127.68, 127.61, 126.87, 126.22, 126.10, 126.00, 125.94, 125.89, 125.04, 124.64, 99.68, 99.50, 97.00, 96.69, 80.78, 80.67, 79.57, 78.47, 78.22, 77.97, 77.67, 77.23, 76.49, 75.54, 74.97, 73.94, 72.66, 72.63, 72.30, 72.26, 72.08, 72.03, 69.47, 69.23, 69.18, 66.63, 63.23, 63.16, 61.09, 39.76, 29.44. HR-ESI-MS *(m/z)*: $[M+Na]^+$ calcd for $C_{78}H_{79}N_7O_{21}Na$, 1472.5227; found, 1472.5231.

**N-benzyloxycarbonyl-3-aminopropyl-*O*-[(2-azido-4-*O*-benzyl-2-deoxy-*α*-D-glucopyranosyl)-(1→4)-*O*-(3-*O*-benzyl-*α*-L-idopyranosylurono-6,2-lactone)-(1→4)-*O*-(2-azido-2-deoxy-*α*-D-glucopyranosyl)]-(1→4)-*O*-3-*O*-benzyl-*α*-L-idopyranosidurono-6,2-lactone (34)**

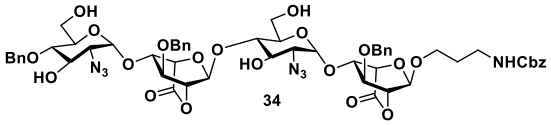


$^1$H NMR (400 MHz, Chloroform-d) δ 7.40 – 7.28 (m, 20H), 5.75 (t, J = 5.2 Hz, 1H), 5.28 (s, 1H), 5.09 (d, J = 3.7 Hz, 1H), 5.06 (s, 3H), 4.94 (d, J = 3.4 Hz, 1H), 4.78 – 4.70 (m, 4H), 4.67 (d, J = 3.3 Hz, 1H), 4.66 – 4.60 (m, 2H), 4.53 (t, J = 2.6 Hz, 1H), 4.50 (d, J = 3.2 Hz, 1H), 4.47 (t, J = 2.6 Hz, 1H), 4.30 – 4.28 (m, 1H), 4.25 – 4.23 (m, 1H), 4.03 – 3.89 (m, 6H), 3.83 – 3.80 (m, 2H), 3.77 – 3.70 (m, 3H), 3.60 (td, J = 9.7, 9.2, 3.9 Hz, 3H), 3.47 – 3.40 (m, 2H), 3.28 (q, J = 5.9 Hz, 1H), 3.24 – 3.19 (m, 2H), 2.73 (s, 1H), 2.21 (s, 2H), 1.83 (s, 2H). $^{13}$C NMR (101 MHz, Chloroform-d) δ 167.99, 167.19, 156.64, 137.73, 136.83, 136.64, 136.50, 128.76, 128.75, 128.55, 128.48, 128.45, 128.27, 128.25, 128.22, 128.18, 128.09, 99.96, 99.64, 97.33, 96.66, 80.70, 80.18, 79.33, 79.20, 78.78, 77.96, 77.24, 75.03, 73.04, 72.60, 72.54, 72.24, 72.20, 71.42, 70.92, 70.26, 69.65, 69.41, 69.11, 66.63, 62.76, 62.32, 61.55, 61.34, 39.73, 29.41. HR-ESI-MS *(m/z)*: $[M+Na]^+$ calcd for $C_{56}H_{63}N_7O_{21}Na$, 1192.3975; found, 1192.3975.

**N-benzyloxycarbonyl-3-aminopropyl-*O*-[(2-acetamido-4-*O*-benzyl-3-*O*-(2-naphthylmethyl)-2-deoxy-*α*-D-glucopyranosyl)-(1→4)-*O*-(3-*O*-benzyl-*α*-L-idopyranosylurono-6,2-lactone)-(1→4)-*O*-(2-acetamido-3-*O*-(2-naphthylmethyl)-2-deoxy-*α*-D-glucopyranosyl)]-(1→4)-*O*-3-*O*-benzyl-*α*-L-idopyranosidurono-6,2-lactone (36)**

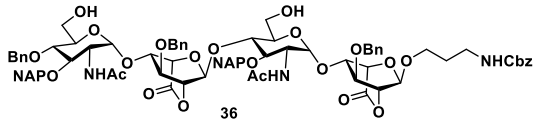

36

$^{1}$H NMR (400 MHz, Chloroform-*d*) δ 7.87 (s, 1H), 7.84 (d, *J* = 10.4 Hz, 5H), 7.77 (s, 1H), 7.67 (s, 1H), 7.51 (dd, *J* = 7.8, 4.9 Hz, 4H), 7.45 (dd, *J* = 8.4, 1.5 Hz, 1H), 7.36 – 7.30 (m, 14H), 7.24 (d, *J* = 8.4 Hz, 3H), 7.20 – 7.17 (m, 2H), 7.08 (d, *J* = 6.7 Hz, 2H), 5.50 (t, *J* = 5.1 Hz, 1H), 5.41 (d, *J* = 0.8 Hz, 1H), 5.11 (d, *J* = 3.7 Hz, 1H), 5.08 – 5.03 (m, 3H), 5.01- 4.88 (m, 4H), 4.85 (d, *J* = 11.0 Hz, 1H), 4.75 – 4.67 (m, 4H), 4.59 (s, 1H), 4.53 – 4.52 (m, 1H), 4.47 (d, *J* = 2.8 Hz, 1H), 4.42 – 4.31 (m, 5H), 4.18 (d, *J* = 3.4 Hz, 1H), 4.13 – 4.07 (m, 2H), 3.95 – 3.87 (m, 3H), 3.78 (dd, *J* = 25.8, 10.9 Hz, 3H), 3.68 – 3.53 (m, 11H), 3.44 – 3.36 (m, 1H), 3.23 (ddd, *J* = 10.4, 9.5, 5.3 Hz, 1H), 1.81 (s, 2H), 1.52 (d, *J* = 9.8 Hz, 6H). $^{13}$C NMR (101 MHz, Chloroform-*d* ) δ 170.00, 169.88, 167.96, 167.82, 156.58, 137.84, 136.61, 136.48, 135.58, 133.28, 133.22, 132.99, 132.95, 128.67, 128.56, 128.51, 128.48, 128.46, 128.39, 128.21, 128.09, 128.04, 128.01, 127.97, 127.74, 127.69, 127.28, 126.70, 126.52, 126.41, 126.35, 126.21, 125.86, 98.80, 98.69, 97.72, 96.52, 79.65, 79.29, 78.94, 78.81, 78.28, 77.97, 77.26, 76.64, 75.08, 74.77, 73.37, 72.48, 72.22, 72.11, 72.02, 71.89, 69.41, 69.34, 68.53, 66.62, 61.28, 61.02, 52.73, 52.32, 39.22, 29.71, 29.52, 23.03, 22.92. HR-ESI-MS *(m/z)*: $[M+Na]^+$ calcd for $C_{82}H_{87}N_3O_{23}Na$, 1504.5628; found, 1504.5608.

**N-benzyloxycarbonyl-3-aminopropyl-*O*-[(benzyl (2-azido-4-*O*-benzyl-3-*O*-(2-naphthylmethyl)-2-deoxy-*α*-D-glucopyranosyl))-(1→4)-*O*-(3-*O*-benzyl-*α*-L-idopyranosyluronate)-(1→4)-*O*-(benzyl (2-azido-3-*O*-(2-naphthylmethyl)-2-deoxy-*α*-D-glucopyranosyl))]-(1→4)-*O*-3-*O*-benzyl-*α*-L-idopyranosiduronate (45)**

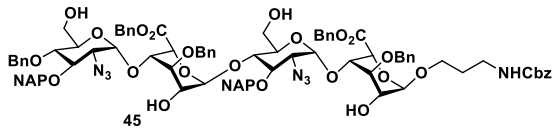

45

$^{1}$H NMR (400 MHz, Chloroform-d) δ 7.82 – 7.78 (m, 2H), 7.75 (dd, J = 6.1, 3.5 Hz, 1H), 7.71 (s, 4H), 7.67 (d, J = 8.5 Hz, 1H), 7.46

(dd, J = 6.2, 3.3 Hz, 2H), 7.42 (dd, J = 8.5, 1.6 Hz, 1H), 7.38 – 7.29 (m, 21H), 7.25 – 7.16 (m, 8H), 7.14 – 7.10 (m, 2H), 7.04 – 7.02 (m, 2H), 5.54 (t, J = 5.0 Hz, 1H), 5.32 – 5.29 (m, 2H), 5.13 (d, J = 12.4 Hz, 1H), 5.03 (s, 2H), 4.99 (s, 1H), 4.97 (d, J = 3.7 Hz, 1H), 4.90 – 4.87 (m, 3H), 4.84 (t, J = 2.6 Hz, 2H), 4.81 (s, 1H), 4.78 (d, J = 3.2 Hz, 1H), 4.74 (s, 1H), 4.72 – 4.59 (m, 5H), 4.48 (d, J = 12.2 Hz, 1H), 4.08 – 4.06 (m, 1H), 4.04 (s, 1H), 3.93 – 3.85 (m, 3H), 3.81 – 3.69 (m, 7H), 3.62 – 3.57 (m, 2H), 3.47 (ddt, J = 22.2, 15.5, 7.5 Hz, 9H), 3.28 – 3.20 (m, 1H), 2.02 (s, 1H), 1.83 (s, 2H), 1.44 (s, 1H). $^{13}$C NMR (101 MHz, Chloroform-d) δ 169.31, 169.21, 156.48, 137.79, 137.23, 137.18, 136.55, 135.22, 135.07, 134.92, 134.70, 133.27, 133.02, 132.85, 128.74, 128.71, 128.65, 128.52, 128.48, 128.43, 128.41, 128.30, 128.26, 128.24, 128.21, 128.13, 128.08, 128.07, 128.04, 127.98, 127.97, 127.92, 127.85, 127.78, 127.66, 127.60, 126.81, 126.34, 126.09, 125.99, 125.89, 125.85, 125.68, 125.63, 101.63, 101.07, 95.96, 95.53, 80.66, 79.37, 77.24, 75.69, 75.26, 75.05, 74.98, 74.48, 73.15, 72.54, 72.38, 72.30, 72.11, 71.54, 69.45, 69.28, 68.07, 67.31, 67.10, 67.03, 66.96, 66.65, 63.99, 63.64, 61.18, 60.98, 39.90, 29.45. HR-ESI-MS *(m/z)*: $[M+Na]^+$ calcd for $C_{92}H_{95}N_7O_{23}Na$, 1689.6411; found, 1689.6372.

**N-benzyloxycarbonyl-3-aminopropyl-*O*-[(benzyl (2-acetamido-4-*O*-benzyl-3-*O*-(2-naphthylmethyl)-2-deoxy-*α*-D-glucopyranosyl))-(1→4)-*O*-(3-*O*-benzyl-*α*-L-idopyranosyluronate)-(1→4)-*O*-(benzyl (2-acetamido-3-*O*-(2-naphthylmethyl)-2-deoxy-*α*-D-glucopyranosyl))]-(1→4)-*O*-3-*O*-benzyl-*α*-L-idopyranosiduronate (50)**

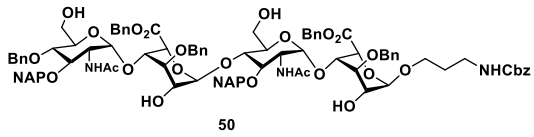

50

$^1$H NMR (400 MHz, Chloroform-d) δ 7.81-7.75 (m, 4H), 7.75 – 7.70 (m, 2H), 7.66 (d, J = 6.9 Hz, 2H), 7.47 (dd, J = 6.2, 3.3 Hz, 2H), 7.44 – 7.39 (m, 3H), 7.39 – 7.36 (m, 2H), 7.35 – 7.33 (m, 4H), 7.32- 7.29 (m, 9H), 7.27- 7.22 (m, 9H), 7.21 – 7.13 (m, 5H), 7.07 (d, J = 7.5 Hz, 2H), 5.48 (t, J = 5.4 Hz, 1H), 5.31 – 5.25 (m, 2H), 5.06- 5.04 (m, 4H), 4.99 – 4.96 (m, 2H), 4.93 – 4.87 (m, 4H), 4.87 – 4.82 (m, 3H), 4.75 (d, J = 11.7 Hz, 1H), 4.65 (dd, J = 11.3, 8.1 Hz, 2H), 4.58 (d, J = 12.2 Hz, 1H), 4.52 (d, J = 11.6 Hz, 2H), 4.43 (t, J = 12.2 Hz, 1H), 4.23 – 4.15 (m, 2H), 4.11 – 4.09 (m, 1H), 4.01 – 3.94 (m, 2H), 3.88 – 3.84 (m, 2H), 3.79 – 3.62 (m, 9H), 3.61 – 3.48 (m, 6H), 3.42 – 3.37 (m, 1H), 3.31- 3.25 (m, 1H), 3.08 (s, 1H), 2.63 (s, 1H), 1.81 (s, 2H), 1.67 (s, 3H), 1.44

(s, 3H). $^{13}$C NMR (101 MHz, Chloroform-d) δ 170.93, 170.65, 169.45, 169.26, 156.53, 138.08, 137.19, 136.45, 135.79, 135.67, 134.75, 134.58, 133.22, 133.20, 132.90, 132.83, 128.75, 128.72, 128.65, 128.52, 128.46, 128.45, 128.42, 128.34, 128.26, 128.22, 128.18, 128.15, 128.10, 128.01, 127.97, 127.84, 127.62, 126.62, 126.17, 126.04, 125.98, 101.15, 96.81, 96.07, 79.79, 77.92, 77.70, 75.51, 75.07, 74.03, 73.70, 72.84, 72.66, 72.44, 72.35, 71.98, 71.32, 69.22, 68.66, 67.92, 67.48, 67.34, 67.30, 67.11, 66.69, 61.31, 61.10, 52.76, 52.55, 39.55, 29.72, 29.47. HR-ESI-MS *(m/z)*: $[M+H]^+$ calcd for $C_{96}H_{104}N_3O_{25}$, 1698.6959; found, 1698.6862.

**General procedure for *O*-sulfation:**

To a solution of starting material (1 mmol) in DMF (2 mL) was added $SO_3.NEt_3$ complex (10 mmol per -OH) under $N_2$ atmosphere and stirred at 60 $^o$C for 3 days. Upon completion of reaction, aqueous $NaHCO_3$ (20 mmol) was added to reaction mixture and stirred for another 16 h. Next, the reaction mixture was concentrated under reduced pressure and the resulting residue was filtered with MeOH through wattman filter paper. The filtrate was concentrated and purified using silica column chromatography.

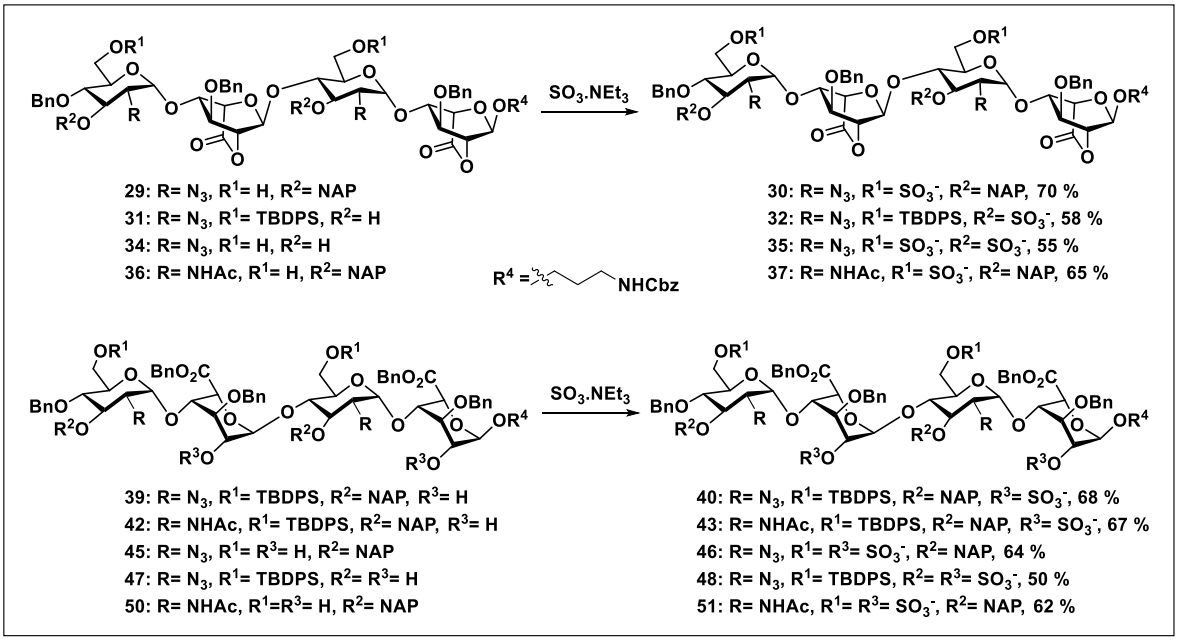


**N-benzyloxycarbonyl-3-aminopropyl-*O*-[(2-azido-4-*O*-benzyl-6-*O*-sulfonato-3-*O*-(2-naphthylmethyl)-2-deoxy-*α*-D-glucopyranosyl)-(1→4)-*O*-(3-*O*-benzyl-*α*-L-idopyranosylurono-6,2-lactone)-(1→4)-*O*-(2-azido-6-*O*-sulfonato-3-*O*-(2-**

**naphthylmethyl)-2-deoxy-*α*-D-glucopyranosyl)]-(1→4)-*O*-3-*O*-benzyl-*α*-L-idopyranosidurono-6,2-lactone (30)**

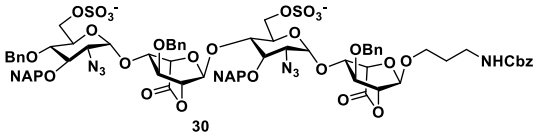

30

$^{1}$H NMR (400 MHz, Methanol-*d*$_4$) δ 7.85 – 7.80 (m, 4H), 7.79 (d, *J* = 2.2 Hz, 1H), 7.76 – 7.74 (m, 2H), 7.70 (d, *J* = 8.4 Hz, 2H), 7.58-7.54 (m, 2H), 7.52 – 7.50 (m, 1H), 7.49 (d, *J* = 2.1 Hz, 1H), 7.48 – 7.39 (m, 8H), 7.38 – 7.26 (m, 13H), 5.29 (s, 1H), 5.18 (d, *J* = 3.2 Hz, 1H), 5.15 (d, *J* = 3.5 Hz, 1H), 5.07 (s, 2H), 4.99 (d, *J* = 2.9 Hz, 1H), 4.93 (s, 2H), 4.82 (d, *J* = 3.1 Hz, 2H), 4.80 – 4.79 (m, 2H), 4.76-4.75 (m, 5H), 4.34 – 4.26 (m, 2H), 4.23 (dt, *J* = 4.9, 2.4 Hz, 1H), 4.20 – 4.18 (m, 1H), 4.12 (d, *J* = 9.4 Hz, 1H), 4.04 (t, *J* = 3.8 Hz, 1H), 3.98- 3.93 (m, 3H), 3.91 – 3.84 (m, 3H), 3.78 – 3.68 (m, 4H), 3.67 – 3.58 (m, 3H), 3.55 (dd, *J* = 9.9, 3.5 Hz, 1H), 3.45 (d, *J* = 9.5 Hz, 1H), 3.26 (tt, *J* = 13.0, 6.5 Hz, 2H), 1.86- 1.79 (m, 2H). $^{13}$C NMR (101 MHz, Methanol-*d*$_4$) δ 170.23, 170.06, 157.43, 138.27, 138.00, 137.89, 136.95, 135.52, 135.13, 133.42, 133.31, 133.05, 133.01, 131.01, 128.47, 128.31, 128.09, 128.04, 128.01, 127.83, 127.76, 127.68, 127.65, 127.60, 127.55, 127.50, 127.48, 127.45, 127.38, 127.30, 127.25, 127.15, 126.35, 126.22, 125.91, 125.65, 125.59, 125.49, 101.46, 100.56, 96.18, 95.58, 80.06, 78.87, 77.24, 74.86, 74.67, 74.40, 74.03, 72.77, 72.58, 72.36, 71.69, 70.72, 70.38, 68.65, 68.51, 68.36, 67.99, 67.71, 66.45, 66.03, 65.64, 65.33, 64.09, 63.48, 51.72, 50.83, 38.77, 38.03, 33.50, 31.67, 30.76, 29.07, 28.70, 23.55, 22.63, 22.34. HR-ESI-MS (m/z): [M-2H]$^{2-}$ calcd for $C_{78}H_{77}N_7O_{27}S_2^{2-}$, 803.7160; found, 803.7170.

**N-benzyloxycarbonyl-3-aminopropyl-*O*-[(2-azido-4-*O*-benzyl-6-*O*-*tert*-butyldiphenylsilyl-3-*O*-sulfonato-2-deoxy-*α*-D-glucopyranosyl)-(1→4)-*O*-(3-*O*-benzyl-*α*-L-idopyranosylurono-6,2-lactone)-(1→4)-*O*-(2-azido-6-*O*-*tert*-butyldiphenylsilyl-3-*O*-sulfonato-2-deoxy-*α*-D-glucopyranosyl)]-(1→4)-*O*-3-*O*-benzyl-*α*-L-idopyranosidurono-6,2-lactone (32)**

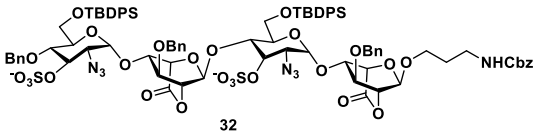

32

$^{1}$H NMR (400 MHz, Methanol-*d*$_4$) δ 7.68 – 7.67 (m, 1H), 7.66 (d, J = 2.0 Hz, 1H), 7.65 – 7.61 (m, 4H), 7.60 (s, 1H), 7.58 (d, J = 1.3 Hz, 1H), 7.41 (d, J = 7.4 Hz, 2H), 7.39 – 7.34 (m, 4H), 7.32 – 7.29 (m, 9H), 7.29 – 7.22 (m, 13H), 7.20 – 7.13 (m, 4H), 5.49 (s, 1H), 5.18 (d, J = 10.6 Hz, 1H), 5.13 (d, J = 3.4 Hz, 1H),

5.06 (s, 1H), 5.02- 5.00 (m, 2H), 4.98 – 4.87 (m, 2H), 4.76 – 4.70 (m, 5H), 4.56 (dd, J = 18.2, 11.0 Hz, 2H), 4.43 – 4.42 (m, 1H), 4.41- 4.39 (m, 2H), 4.35 – 4.32 (m, 1H), 4.07 – 3.94 (m, 3H), 3.87- 3.83 (m, 3H), 3.80- 3.65 (m, 5H), 3.55 (dt, J = 9.3, 5.5 Hz, 1H), 3.26 – 3.16 (m, 3H), 1.78 – 1.74 (m, 2H), 0.99 (s, 9H), 0.96 (s, 9H). $^{13}$C NMR (101 MHz, Methanol-*d*$_4$) δ 168.67, 167.84, 157.33, 138.44, 137.64, 137.34, 136.96, 135.65, 135.56, 135.43, 135.40, 133.36, 133.05, 132.95, 132.75, 129.53, 129.50, 129.39, 128.37, 128.18, 128.13, 128.08, 128.02, 127.98, 127.72, 127.67, 127.62, 127.59, 127.41, 127.38, 127.36, 127.29, 127.07, 100.08, 99.67, 97.02, 94.52, 79.87, 79.56, 79.41, 79.12, 78.50, 78.07, 76.48, 75.53, 74.72, 73.99, 71.92, 71.81, 71.51, 71.32, 69.49, 69.39, 67.63, 66.07, 62.84, 62.52, 62.40, 62.10, 38.36, 29.23, 26.05. HR-ESI-MS (m/z): [M-2H]$^{2-}$ calcd for $C_{88}H_{97}N_7O_{27}S_2Si_2^{2-}$, 901.7711; found 901.7706.

**N-benzyloxycarbonyl-3-aminopropyl-*O*-[(2-azido-4-*O*-benzyl-6-*O*-sulfonato-3-*O*-sulfonato-2-deoxy-*α*-D-glucopyranosyl)-(1→4)-*O*-(3-*O*-benzyl-*α*-L-idopyranosylurono-6,2-lactone)-(1→4)-*O*-(2-azido-6-*O*-sulfonato-3-*O*-sulfonato-2-deoxy-*α*-D-glucopyranosyl)]-(1→4)-*O*-3-*O*-benzyl-*α*-L-idopyranosidurono-6,2-lactone (35)**

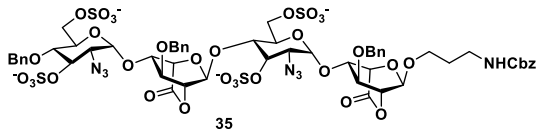

35

$^1$H NMR (400 MHz, Methanol-*d*$_4$) δ 7.53 (d, J = 7.0 Hz, 2H), 7.46 (d, J = 7.4 Hz, 2H), 7.42 – 7.22 (m, 16H), 5.33 (s, 1H), 5.21 – 5.14 (m, 4H), 5.08 – 5.02 (m, 3H), 4.83 (d, J = 11.8 Hz, 2H), 4.78 – 4.76 (m, 1H), 4.70 (d, J = 11.7 Hz, 2H), 4.64 (t, J = 9.1 Hz, 2H), 4.58 – 4.52 (m, 1H), 4.32 (td, J = 10.4, 9.7, 3.0 Hz, 1H), 4.27 (d, J = 3.2 Hz, 1H), 4.24 – 4.18 (m, 3H), 4.11 (t, J= 4.6 Hz, 1H), 3.94 – 3.80 (m, 6H), 3.71 – 3.67 (m, 2H), 3.63 – 3.55 (m, 2H), 3.55 – 3.44 (m, 2H), 3.31 – 3.22 (m, 2H), 1.85 – 1.76 (m, 2H). $^{13}$C NMR (101 MHz, Methanol-*d*$_4$) δ 171.28, 170.46, 157.45, 138.41, 138.10, 137.97, 136.94, 128.91, 128.10, 128.08, 128.00, 127.80, 127.69, 127.59, 127.45, 127.37, 127.11, 126.99, 102.93, 101.09, 96.85, 95.66, 78.94, 78.08, 76.76, 76.60, 75.76, 74.57, 73.85, 72.82, 72.31, 72.23, 72.09, 70.61, 70.20, 69.48, 69.24, 69.04, 67.90, 66.56, 66.02, 65.71, 65.54, 63.01, 62.67, 37.93, 29.35. HR-ESI-MS (m/z): [M-4H]$^{4-}$ calcd for $C_{56}H_{59}N_7O_{35}S_4^{4-}$, 371.3015; found, 371.3012.

**N-benzyloxycarbonyl-3-aminopropyl-*O*-[(2-acetamido-4-*O*-benzyl-6-*O*-sulfonato-3-*O*-(2-naphthylmethyl)-2-deoxy-*α*-D-glucopyranosyl)-(1→4)-*O*-(3-*O*-benzyl-*α*-L-idopyranosylurono-6,2-lactone)-(1→4)-*O*-(2-acetamido-6-*O*-sulfonato-3-*O*-(2-naphthylmethyl)-2-deoxy-*α*-D-glucopyranosyl)]-(1→4)-*O*-3-*O*-benzyl-*α*-L-idopyranosidurono-6,2-lactone (37)**

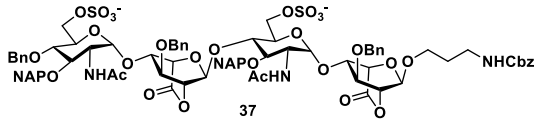

37

$^{1}$H NMR (400 MHz, Methanol-$d_4$) δ 7.91 – 7.70 (m, 9H), 7.51 – 7.37 (m, 14H), 7.33 – 7.22 (m, 11H), 5.54 (s, 1H), 5.13 (d, $J$ = 7.0 Hz, 2H), 5.09 (s, 1H), 5.06 (s, 2H), 4.81 – 4.52 (m, 9H), 4.46 (d, $J$ = 8.9 Hz, 1H), 4.39 (d, $J$ = 8.3 Hz, 2H), 4.32 – 4.27 (m, 3H), 4.25 – 4.16 (m, 3H), 4.10 – 3.89 (m, 8H), 3.83 – 3.54 (m, 6H), 3.26 – 3.15 (m, 2H), 1.84 – 1.75 (m, 8H). $^{13}$C NMR (101 MHz, Methanol-$d_4$ ) δ 171.75, 171.66, 168.63, 168.43, 157.34, 138.24, 137.55, 137.08, 136.22, 136.19, 133.39, 133.35, 133.33, 133.02, 132.99, 132.91, 128.29, 128.26, 128.11, 128.03, 127.90, 127.81, 127.64, 127.60, 127.51, 127.46, 127.43, 127.29, 126.00, 125.76, 125.60, 125.51, 125.46, 125.41, 125.28, 125.04, 99.43, 99.29, 98.51, 96.93, 80.13, 80.10, 79.78, 79.62, 78.24, 78.08, 77.74, 77.66, 74.58, 72.13, 72.10, 71.96, 71.92, 71.87, 70.26, 69.65, 69.62, 66.93, 65.94, 65.52, 52.93, 52.82, 37.71, 29.29, 21.50, 21.42. HR-ESI-MS *(m/z)*: $[M-2H]^{2-}$ calcd for $C_{82}H_{85}N_3O_{29}S_2^{2-}$, 819.7361; found, 819.7369.

**N-benzyloxycarbonyl-3-aminopropyl-*O*-[(benzyl (2-azido-4-*O*-benzyl-6-*O*-*tert*-butyldiphenylsilyl-3-*O*-(2-naphthylmethyl)-2-deoxy-*α*-D-glucopyranosyl))-(1→4)-*O*-(3-*O*-benzyl-2-*O*-sulfonato-*α*-L-idopyranosyluronate)-(1→4)-*O*-(benzyl (2-azido-6-*O*-*tert*-butyldiphenylsilyl-3-*O*-(2-naphthylmethyl)-2-deoxy-*α*-D-glucopyranosyl))]-(1→4)-*O*-3-*O*-benzyl-2-*O*-sulfonato-*α*-L-idopyranosiduronate (40)**

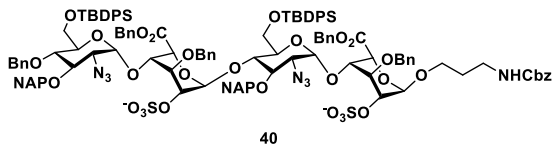

40

$^{1}$H NMR (400 MHz, Methanol-$d_4$) δ 7.79 – 7.76 (m, 7H), 7.74 – 7.70 (m, 3H), 7.61 – 7.41 (m, 13H), 7.38 – 7.30 (m, 14H), 7.29 – 7.15 (m, 23H), 7.04 (t, J = 6.6 Hz, 2H), 6.96 (t, J = 7.5 Hz, 2H), 6.65 (d, J = 7.7 Hz, 1H), 5.71 (s, 1H), 5.37 (d, J = 12.1 Hz, 1H), 5.22 (d, J = 3.5 Hz, 1H), 5.17 (s, 2H), 5.06 (s, 1H), 5.02 – 4.89 (m, 7H), 4.83 (d, J = 5.6 Hz, 1H), 4.77 – 4.69 (m, 4H), 4.63 – 4.51 (m, 3H), 4.48 (s,

1H), 4.38 (d, J = 11.7 Hz, 1H), 4.33 – 4.26 (m, 2H), 4.22 – 4.19 (m, 2H), 4.04 – 3.98 (m, 3H), 3.86 (d, J = 10.4 Hz, 2H), 3.82 – 3.70 (m, 4H), 3.65 – 3.54 (m, 4H), 3.29 – 3.12 (m, 3H), 1.81 – 1.73 (m, 2H), 0.99 (d, J = 6.8 Hz, 18H). $^{13}$C NMR (101 MHz, Methanol-$d_4$) δ 169.75, 169.00, 157.34, 138.43, 137.89, 137.83, 136.89, 135.91, 135.79, 135.69, 135.41, 134.97, 133.67, 133.35, 133.25, 133.03, 132.78, 129.45, 129.20, 128.45, 128.15, 128.09, 128.04, 127.83, 127.47, 127.38, 127.22, 126.97, 126.45, 125.95, 125.56, 125.41, 125.36, 125.22, 125.07, 99.44, 98.67, 96.01, 94.54, 79.41, 78.57, 77.75, 74.81, 74.28, 74.15, 73.06, 72.48, 72.31, 72.03, 71.88, 71.38, 70.72, 69.27, 67.89, 67.22, 66.95, 66.35, 65.94, 63.89, 63.75, 62.39, 62.06, 37.92, 29.35, 29.16, 26.31, 26.05. HR-ESI-MS (m/z): $[M-2H]^{2-}$ calcd for $C_{124}H_{129}N_7O_{29}S_2Si_2^{2-}$, 1150.3930; found, 1150.3950.

**N-benzyloxycarbonyl-3-aminopropyl-*O*-[(benzyl (2-acetamido-4-*O*-benzyl-6-*O*-*tert*-butyldiphenylsilyl-3-*O*-(2-naphthylmethyl)-2-deoxy-*α*-D-glucopyranosyl))-(1→4)-*O*-(3-*O*-benzyl-2-*O*-sulfonato-*α*-L-idopyranosyluronate)-(1→4)-*O*-(benzyl (2-acetamido-6-*O*-*tert*-butyldiphenylsilyl-3-*O*-(2-naphthylmethyl)-2-deoxy-*α*-D-glucopyranosyl))]-(1→4)-*O*-3-*O*-benzyl-2-*O*-sulfonato-*α*-L-idopyranosiduronate (43)**

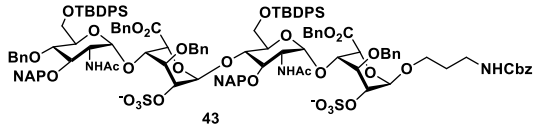

43

$^1$H NMR (400 MHz, Methanol-$d_4$) δ 7.83 (s, 1H), 7.82 – 7.80 (m, 2H), 7.79 (s, 2H), 7.76 – 7.73 (m, 3H), 7.71 (s, 1H), 7.68 (d, J = 7.6 Hz, 3H), 7.63 (s, 1H), 7.61 (d, J = 5.1 Hz, 2H), 7.58 (d, J = 6.1 Hz, 3H), 7.48 (dd, J = 16.8, 8.0 Hz, 4H), 7.43- 7.38 (m, 9H), 7.36- 7.30 (m, 16H), 7.25 – 7.20 (m, 7H), 7.19- 7.15 (m, 7H), 6.98 (d, J = 7.4 Hz, 2H), 5.71 (s, 1H), 5.20 (s, 4H), 4.98 (s, 3H), 4.83 (s, 1H), 4.81 – 4.75 (m, 3H), 4.69 (d, J = 12.0 Hz, 2H), 4.57 – 4.50 (m, 5H), 4.41 – 4.34 (m, 5H), 4.24 – 4.03 (m, 5H), 3.90 (d, J = 15.9 Hz, 2H), 3.81- 3.74 (m, 6H), 3.65 – 3.56 (m, 5H), 3.29 – 3.25 (m, 1H), 3.20- 3.13 (m, 1H), 2.01 (s, 3H), 1.84 – 1.75 (m, 5H), 1.07 (s, 9H), 0.98 (s, 9H). $^{13}$C NMR (101 MHz, Methanol-$d_4$) δ 169.56, 169.49, 169.38, 157.31, 137.61, 137.59, 136.82, 136.31, 135.95, 135.79, 135.75, 135.66, 135.38, 135.15, 134.79, 134.55, 134.31, 134.25, 133.42, 133.33, 133.32, 133.29, 133.20, 133.01, 132.93, 132.63, 129.45, 129.28, 129.24, 128.45, 128.33, 128.28, 128.23, 128.21, 128.18, 128.10, 128.05, 127.97, 127.92, 127.83, 127.74, 127.71, 127.67, 127.63, 127.61, 127.57, 127.45, 127.35, 127.28, 127.26, 127.23, 127.21, 127.18, 126.98, 126.38, 125.90, 125.63, 125.58, 125.47, 125.41, 99.99,

99.54, 98.82, 80.73, 79.13, 78.20, 77.87, 77.70, 77.67, 77.55, 75.38, 75.34, 74.51, 73.19, 72.75, 72.48, 72.13, 72.07, 72.03, 70.76, 70.49, 70.36, 67.09, 66.53, 66.31, 66.01, 62.40, 62.09, 53.23, 38.23, 34.06, 31.66, 30.78, 29.33, 26.37, 26.05. HR-ESI-MS (m/z): [M-2H] $^{2-}$ calcd for $C_{128}H_{137}N_3O_{31}S_2Si_2^{2-}$, 1166.4130; found, 1166.4142.

**N-benzyloxycarbonyl-3-aminopropyl-*O*-[(benzyl (2-azido-4-*O*-benzyl-6-*O*-sulfonato-3-*O*-(2-naphthylmethyl)-2-deoxy-*α*-D-glucopyranosyl))-(1→4)-*O*-(3-*O*-benzyl-2-*O*-sulfonato-*α*-L-idopyranosyluronate)-(1→4)-*O*-(benzyl (2-azido-6-*O*-sulfonato-3-*O*-(2-naphthylmethyl)-2-deoxy-*α*-D-glucopyranosyl))]-(1→4)-*O*-3-*O*-benzyl-2-*O*-sulfonato-*α*-L-idopyranosiduronate (46)**

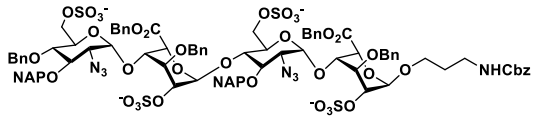

46

$^1$H NMR (400 MHz, Methanol-*d*$_4$) δ 7.84 – 7.75 (m, 4H), 7.71- 7.68 (m, 3H), 7.62 (d, *J* = 8.5 Hz, 1H), 7.55 – 7.42 (m, 9H), 7.40 (d, *J* = 8.5 Hz, 5H), 7.36- 7.31 (m, 10H), 7.28 – 7.23 (m, 7H), 7.15 – 7.09 (m, 1H), 7.02 (t, *J* = 7.3 Hz, 2H), 6.59 (d, *J* = 7.5 Hz, 2H), 5.53 (s, 1H), 5.44 (d, *J* = 12.1 Hz, 1H), 5.22 – 5.15 (m, 3H), 5.11 (s, 1H), 5.07 – 5.02 (m, 3H), 5.01 – 4.94 (m, 3H), 4.82- 4.74 (m, 4H), 4.72- 4.65 (m, 4H), 4.62 – 4.57 (m, 2H), 4.53- 4.50 (m, 2H), 4.40 – 4.34 (m, 4H), 4.17- 4.07 (m, 4H), 4.01 – 3.80 (m, 6H), 3.67- 3.58 (m, 3H), 3.41 – 3.36 (m, 1H), 3.31 – 3.16 (m, 2H), 1.87-1.75 (m, 2H). $^{13}$C NMR (101 MHz, Methanol-*d*$_4$) δ 170.01, 169.88, 157.39, 138.37, 137.81, 137.42, 136.92, 135.91, 135.57, 135.31, 134.50, 133.35, 133.33, 133.03, 132.92, 128.59, 128.49, 128.40, 128.36, 128.29, 128.16, 128.15, 128.08, 127.99, 127.83, 127.57, 127.44, 127.34, 127.26, 127.15, 126.22, 125.75, 125.65, 125.63, 125.60, 125.46, 125.35, 99.56, 97.94, 96.62, 80.01, 78.48, 77.41, 74.92, 74.68, 74.57, 72.35, 72.08, 71.84, 70.68, 70.48, 67.73, 67.28, 67.04, 66.95, 66.40, 66.01, 65.38, 64.16, 63.91, 63.89, 38.09, 31.67, 30.77, 29.33, 29.19, 29.06, 28.72. HR-ESI-MS (m/z): [M-4H] $^{4-}$ calcd for $C_{92}H_{91}N_7O_{35}S_4^{4-}$, 495.3615; found, 495.3588.

**N-benzyloxycarbonyl-3-aminopropyl-*O*-[(benzyl (2-azido-4-*O*-benzyl-6-*O*-*tert*-butyldiphenylsilyl-3-*O*-sulfonato-2-deoxy-*α*-D-glucopyranosyl))-(1→4)-*O*-(3-*O*-benzyl-2-*O*-sulfonato-*α*-L-idopyranosyluronate)-(1→4)-*O*-(benzyl (2-azido-6-*O*-*tert*-butyldiphenylsilyl-3-*O*-sulfonato-2-deoxy-*α*-D-glucopyranosyl))]-(1→4)-*O*-3-*O*-benzyl-2-*O*-sulfonato-*α*-L-idopyranosiduronate (48)**

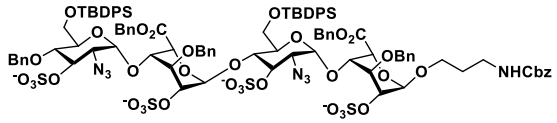

48

$^1$H NMR (400 MHz, Methanol-*d*$_4$) δ 7.61 (dd, *J* = 6.4, 3.0 Hz, 3H), 7.58 (dd, *J* = 3.0, 1.4 Hz, 2H), 7.56 (d, *J* = 1.6 Hz, 1H), 7.53 (d, *J* = 1.3 Hz, 1H), 7.51 (d, *J* = 1.4 Hz, 1H), 7.31 (t, *J* = 2.1 Hz, 1H), 7.29 (dd, *J* = 2.6, 1.2 Hz, 1H), 7.27 (s, 2H), 7.25 (s, 2H), 7.24 (s, 2H), 7.22- 7.20 (m, 7H), 7.18 – 7.15 (m, 7H), 7.13 – 7.11 (m, 5H), 7.07 (d, *J* = 1.5 Hz, 2H), 7.05 – 7.03 (m, 6H), 7.02 (s, 4H), 7.01 – 6.99 (m, 3H), 5.35 (s, 2H), 5.09 (d, *J* = 10.1 Hz, 1H), 5.04 (d, *J* = 2.6 Hz, 1H), 5.03- 4.99 (m, 3H), 4.96 (s, 1H), 4.90 (d, *J* = 12.1 Hz, 2H), 4.84 (s, 2H), 4.61 (d, *J* = 9.4 Hz, 2H), 4.55 (d, *J* = 12.3 Hz, 2H), 4.44 (d, *J* = 6.3 Hz, 1H), 4.33 (s, 1H), 4.28 (d, *J* = 12.2 Hz, 2H), 4.16 (d, *J* = 11.7 Hz, 2H), 3.94 (s, 1H), 3.90 (s, 1H), 3.84 (d, *J* = 8.2 Hz, 2H), 3.77 (dd, *J* = 19.4, 9.5 Hz, 3H), 3.71- 3.69 (m, 3H), 3.56- 3.50 (m, 3H), 3.44 – 3.41 (m, 2H), 3.29 (dd, *J* = 10.2, 3.3 Hz, 1H), 3.10 (d, *J* = 6.4 Hz, 1H), 3.05- 3.00 (m, 1H), 2.92 (dd, *J* = 9.7, 3.5 Hz, 1H), 1.66- 1.60 (m, 2H), 0.91 (s, 9H), 0.87 (s, 9H). $^{13}$C NMR (151 MHz, Methanol-*d*$_4$) δ 170.11, 169.28, 157.33, 138.09, 137.94, 137.46, 136.89, 135.80, 135.65, 135.62, 135.45, 134.95, 134.76, 133.52, 133.39, 133.16, 132.94, 129.54, 129.50, 129.30, 129.20, 128.54, 128.43, 128.28, 128.11, 128.08, 128.03, 127.80, 127.77, 127.49, 127.43, 127.41, 127.36, 127.31, 127.25, 127.15, 99.53, 99.36, 94.65, 79.20, 76.45, 75.07, 72.15, 72.10, 72.06, 71.95, 71.55, 70.56, 69.92, 69.39, 67.90, 67.23, 67.21, 66.91, 66.21, 65.90, 63.61, 63.16, 62.32, 62.05, 37.89, 29.37, 29.08, 26.26, 26.06. HR-ESI-MS (m/z): $[M-4H]^{4-}$ calcd for $C_{102}H_{111}N_7O_{35}S_4Si_2^{4-}$, 544.6399; found, 544.6364.

**N-benzyloxycarbonyl-3-aminopropyl-*O*-[(benzyl (2-acetamido-4-*O*-benzyl-6-*O*-sulfonato-3-*O*-(2-naphthylmethyl)-2-deoxy-*α*-D-glucopyranosyl))-(1→4)-*O*-(3-*O*-benzyl-2-*O*-sulfonato-*α*-L-idopyranosyluronate)-(1→4)-*O*-(benzyl (2-acetamido-6-*O*-sulfonato-3-*O*-(2-naphthylmethyl)-2-deoxy-*α*-D-glucopyranosyl))]-(1→4)-*O*-3-*O*-benzyl-2-*O*-sulfonato-*α*-L-idopyranosiduronate (51)**

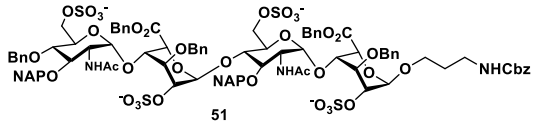

51

$^1$H NMR (400 MHz, Methanol-*d*$_4$) δ 7.78 – 7.62 (m, 8H), 7.53 (d, J = 8.5 Hz, 1H), 7.43 – 7.25 (m, 20H), 7.25 – 7.13 (m, 11H), 7.11- 7.07

(m, 1H), 6.98 (t, J = 7.6 Hz, 2H), 6.60 (d, J = 7.5 Hz, 1H), 5.47 (s, 1H), 5.35 (d, J = 12.1 Hz, 1H), 5.16 (d, J = 12.9 Hz, 3H), 5.03- 4.94 (m, 4H), 4.83 – 4.76 (m, 2H), 4.74- 4.68 (m, 4H), 4.67 – 4.46 (m, 8H), 4.36 (d, J = 11.0 Hz, 1H), 4.28 (d, J = 14.2 Hz, 2H), 4.23 – 4.17 (m, 2H), 4.13- 4.11 (m, 2H), 4.07- 4.02 (m, 2H), 3.89- 3.87 (m, 2H), 3.83- 3.72 (m, 5H), 3.63 – 3.55 (m, 2H), 3.19- 3.12 (m, 1H), 1.92 (s, 3H), 1.83- 1.74 (m, 2H), 1.69 (s, 3H). $^{13}$C NMR (126 MHz, Methanol-$d_4$) δ 173.34, 170.81, 170.57, 158.07, 139.19, 138.14, 138.04, 137.53, 137.05, 137.02, 135.96, 135.16, 134.06, 133.67, 133.47, 129.10, 129.07, 129.05, 128.98, 128.81, 128.77, 128.65, 128.55, 128.50, 128.45, 128.32, 128.29, 128.26, 128.24, 128.17, 128.13, 127.94, 127.89, 127.76, 126.73, 126.44, 126.23, 126.03, 125.89, 125.80, 125.73, 100.33, 99.07, 80.98, 79.68, 78.24, 75.91, 75.42, 75.31, 73.50, 72.95, 72.47, 71.73, 71.46, 71.40, 71.31, 71.18, 68.13, 67.81, 67.34, 67.29, 66.78, 66.38, 66.11, 54.01, 53.95, 39.07, 29.98, 29.87. HR-ESI-MS (m/z): $[M-4H]^{4-}$ calcd for $C_{96}H_{99}N_3O_{37}S_4^{4-}$, 503.6224; found, 503.6204.

**General procedure for *O*-phophorylation:**

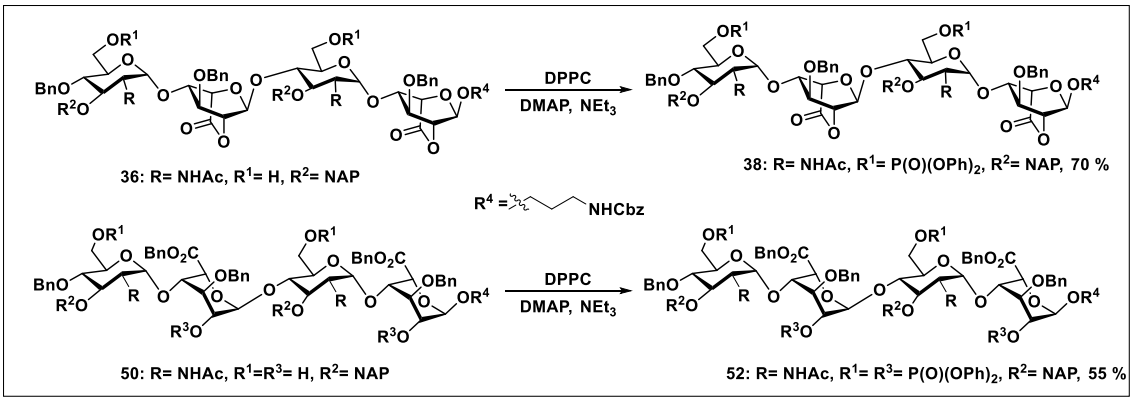


To a solution of starting material (1 mmol) in $CH_2Cl_2$ (1 mL) and pyridine (1 mL) was added $NEt_3$ (10 mmol), DMAP (0.3 mmol) and Diphenyl phosphoryl chloride (5 mmol for **38** and 10 mmol for **52**) at 0 $^{o}$ C. After 12 h, the reaction mixture was diluted with $CH_2Cl_2$ and extracted with 1 N HCl and brine. The combined organic layer was dried over $Na_2SO_4$, filtered, concentrated and purified through silica gel column chromatography.

**N-benzyloxycarbonyl-3-aminopropyl-*O*-[(2-acetamido-4-*O*-benzyl-6-*O*-diphenylphosphoryl-3-*O*-(2-naphthylmethyl)-2-deoxy-*α*-D-glucopyranosyl)-(1→4)-**

***O*-(3-*O*-benzyl-*α*-L-idopyranosylurono-6,2-lactone)-(1→4)-*O*-(2-acetamido-6-*O*-diphenylphosphoryl-3-*O*-(2-naphthylmethyl)-2-deoxy-*α*-D-glucopyranosyl)]-(1→4)-*O*-3-*O*-benzyl-*α*-L-idopyranosidurono-6,2-lactone (38)**

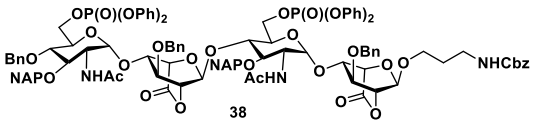

38

$^{1}$H NMR (400 MHz, Chloroform-*d*) δ 7.84 (dd, *J* = 12.9, 8.5 Hz, 6H), 7.73 (d, *J* = 20.7 Hz, 2H), 7.54 – 7.46 (m, 4H), 7.44 – 7.31 (m, 16H), 7.28 – 7.21 (m, 19H), 7.19 – 7.08 (m, 7H), 5.35 – 5.29 (m, 2H), 5.05 (s, 3H), 5.01 – 4.97 (m, 3H), 4.89 (d, *J* = 11.6 Hz, 2H), 4.78 – 4.69 (m, 3H), 4.63 (t, *J* = 2.6 Hz, 1H), 4.56 (dd, *J* = 15.6, 7.7 Hz, 3H), 4.52 – 4.42 (m, 4H), 4.41 – 4.33 (m, 4H), 4.31 – 4.27 (m, 2H), 4.21 (dd, *J* = 4.9, 3.3 Hz, 1H), 4.11 – 4.07 (m, 1H), 4.06 – 3.88 (m, 3H), 3.76 – 3.69 (m, 2H), 3.66 – 3.52 (m, 7H), 3.39 – 3.30 (m, 1H), 3.23 (dt, *J* = 12.9, 5.5 Hz, 1H), 1.81 (s, 2H), 1.51 (s, 3H), 1.42 (s, 3H). 13C NMR (101 MHz, Chloroform-*d* ) δ 169.99, 169.79, 167.70, 167.68, 156.42, 150.55, 150.49, 150.43, 150.36, 150.21, 150.14, 137.59, 136.71, 136.63, 136.45, 135.57, 135.34, 133.21, 133.00, 132.96, 130.06, 129.92, 129.84, 129.81, 128.68, 128.51, 128.46, 128.40, 128.33, 128.29, 128.16, 128.07, 128.02, 127.95, 127.85, 127.70, 127.28, 127.00, 126.59, 126.46, 126.41, 126.25, 126.22, 125.93, 125.62, 125.54, 125.48, 120.34, 120.29, 120.09, 120.07, 120.05, 120.03, 99.12, 98.65, 98.28, 96.58, 80.09, 79.95, 79.02, 78.28, 77.92, 77.70, 77.24, 75.06, 74.82, 73.61, 72.65, 72.25, 72.20, 71.59, 70.70, 70.62, 69.99, 69.92, 69.48, 69.26, 68.38, 66.56, 52.50, 52.21, 39.01, 29.59, 23.02, 22.73. $^{31}$P NMR (162 MHz, Chloroform-*d*) δ -10.59, -11.46. HR-ESI-MS *(m/z)*: $[M+H]^+$ calcd for $C_{106}H_{106}N_3O_{29}P_2$, 1947.6421; found, 1947.5958.

**N-benzyloxycarbonyl-3-aminopropyl-*O*-[(benzyl (2-acetamido-4-*O*-benzyl-6-*O*-diphenylphosphoryl-3-*O*-(2-naphthylmethyl)-2-deoxy-*α*-D-glucopyranosyl))-(1→4)-*O*-(3-*O*-benzyl-2-*O*-diphenylphosphoryl-*α*-L-idopyranosyluronate)-(1→4)-*O*-(benzyl (2-acetamido-6-*O*-diphenylphosphoryl-3-*O*-(2-naphthylmethyl)-2-deoxy-*α*-D-glucopyranosyl))]-(1→4)-*O*-3-*O*-benzyl-2-*O*-diphenylphosphoryl-*α*-L-idopyranosiduronate (52)**

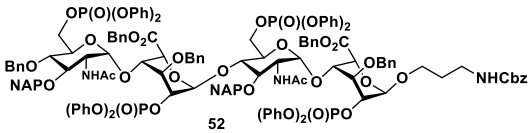

52

$^{1}$H NMR (400 MHz, Chloroform-d) δ 7.78 – 7.74 (m, 1H), 7.67 (t, J = 7.7 Hz, 3H), 7.65 – 7.60 (m, 4H), 7.51 (s, 1H), 7.43 – 7.39 (m, 2H),

7.36 (s, 1H), 7.35 – 7.34 (m, 1H), 7.33 – 7.32 (m, 3H), 7.31 (dd, J = 3.2, 1.1 Hz, 2H), 7.29 (d, J = 1.9 Hz, 1H), 7.27 (s, 2H), 7.26- 7.25 (m, 2H), 7.23 (t, J = 2.3 Hz, 3H), 7.22- 7.21 (m, 3H), 7.20 (d, J = 2.1 Hz, 2H), 7.19 (s, 6H), 7.17 – 7.16 (m, 5H), 7.15- 7.14 (m, 10H), 7.13 (s, 5H), 7.12 (s, 6H), 7.10 (d, J = 4.1 Hz, 3H), 7.08 (s, 3H), 7.05 (s, 3H), 7.04 (s, 2H), 7.02 (s, 1H), 7.00- 6.95 (m, 3H), 6.91- 6.87 (m, 4H), 6.80 (d, J = 7.3 Hz, 2H), 5.49 (t, J = 5.4 Hz, 1H), 5.46 (s, 1H), 5.27 (d, J = 12.0 Hz, 1H), 5.06 (d, J = 12.0 Hz, 1H), 4.99 (s, 2H), 4.92 (s, 2H), 4.84 (dd, J = 23.1, 11.8 Hz, 3H), 4.78 – 4.74 (m, 1H), 4.71 (s, 1H), 4.69 – 4.64 (m, 2H), 4.64 – 4.61 (m, 2H), 4.61 – 4.57 (m, 4H), 4.56- 4.49 (m, 4H), 4.44 (s, 2H), 4.41- 4.40 (m, 3H), 4.37 (d, J = 2.0 Hz, 1H), 4.24 – 4.13 (m, 4H), 4.01 (d, J = 8.8 Hz, 1H), 3.94 – 3.81 (m, 6H), 3.78 – 3.71 (m, 1H), 3.59 (d, J = 9.5 Hz, 1H), 3.56 – 3.50 (m, 1H), 3.46- 3.40 (m, 1H), 3.25 – 3.17 (m, 1H), 1.80 (m, 2H), 1.75 (s, 3H), 1.68 (s, 3H). $^{13}$C NMR (101 MHz, Chloroform-d) δ 171.23, 170.89, 168.76, 168.18, 156.40, 150.52, 150.52, 150.45, 150.44, 150.42, 150.34, 150.26, 150.24, 150.20, 150.17, 150.03, 149.95, 138.27, 136.47, 136.39, 136.35, 136.32, 136.28, 134.92, 134.82, 133.29, 133.22, 132.77, 132.74, 130.10, 130.07, 130.02, 129.80, 129.77, 129.72, 128.97, 128.70, 128.65, 128.60, 128.42, 128.37, 128.31, 128.20, 128.10, 128.07, 127.99, 127.92, 127.90, 127.78, 127.72, 127.60, 127.57, 127.49, 127.43, 126.14, 125.99, 125.83, 125.77, 125.64, 125.58, 125.54, 125.44, 125.38, 125.35, 125.32, 102.44, 100.52, 99.12, 98.97, 98.77, 98.64, 80.34, 78.62, 74.77, 74.72, 73.43, 72.75, 72.64, 72.54, 72.42, 72.29, 72.22, 72.16, 70.67, 70.65, 70.61, 70.57, 68.21, 67.98, 67.13, 66.96, 66.73, 66.55, 53.12, 52.41, 39.83, 29.38, 22.65. $^{31}$P NMR (162 MHz, Chloroform-d) δ -10.81, -11.15, -14.13, -14.74. HR-ESI-MS *(m/z)*: $[M+Na]^+$ calcd for $C_{144}H_{139}N_3O_{37}P_4Na$, 2649.7969; found, 2649.4785.

**General procedure for desilylation post *O*- sulfation:**

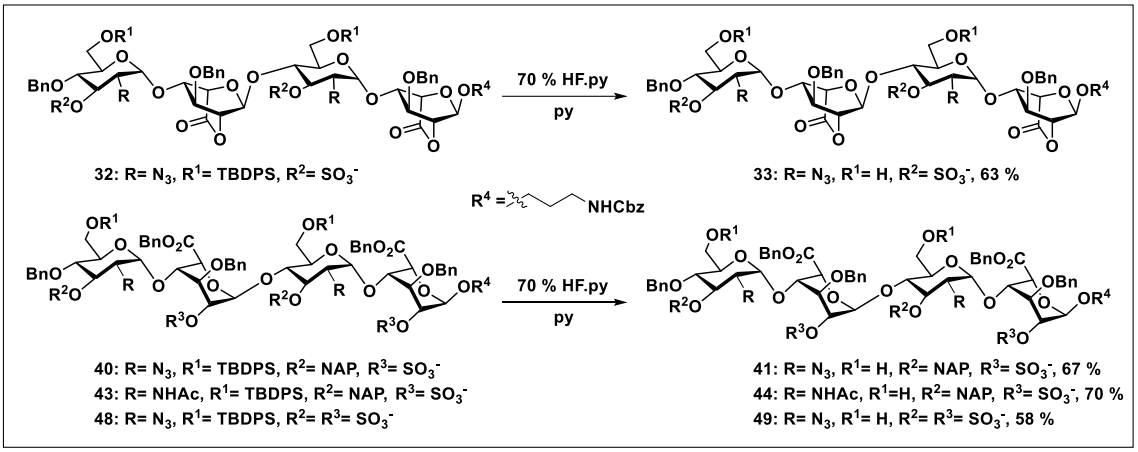


To a solution of starting material (1 mmol) in pyridine (1 mL) was added HF.py (5 mmol) at ice cold temperature. After stirring for 12 h the volatiles were evaporated and the residue was purified using Sephadex LH 20 column using MeOH as an eluent.

**N-benzyloxycarbonyl-3-aminopropyl-*O*-[(2-azido-4-*O*-benzyl-3-*O*-sulfonato-2-deoxy-*α*-D-glucopyranosyl)-(1→4)-*O*-(3-*O*-benzyl-*α*-L-idopyranosylurono-6,2-lactone)-(1→4)-*O*-(2-azido-3-*O*-sulfonato-2-deoxy-*α*-D-glucopyranosyl)]-(1→4)-*O*-3-*O*-benzyl-*α*-L-idopyranosidurono-6,2-lactone (33)**

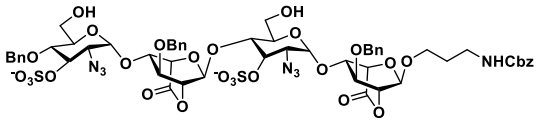
33

1H NMR (400 MHz, Methanol-$d_4$) δ 7.50 – 7.41 (m, 7H), 7.38- 7.37 (m, 3H), 7.34 – 7.25 (m, 10H), 5.40 (dd, J = 7.5, 2.8 Hz, 2H), 5.24 – 5.13 (m, 4H), 5.07 (s, 2H), 4.94 (dd, J = 5.1, 3.0 Hz, 1H), 4.83 – 4.78 (m, 3H), 4.76 (d, J = 3.7 Hz, 4H), 4.61 (d, J = 3.0 Hz, 1H), 4.57 (d, J = 10.5 Hz, 1H), 4.50 (d, J = 3.2 Hz, 1H), 4.41 – 4.37 (m, 1H), 3.95 – 3.88 (m, 3H), 3.88 – 3.83 (m, 4H), 3.83 – 3.57 (m, 2H), 3.26 (dt, J = 12.8, 6.1 Hz, 2H), 1.82 – 1.79 (m, 2H). 13C NMR (101 MHz, Methanol-$d_4$) δ 169.02, 168.19, 157.38, 138.44, 137.74, 137.37, 137.00, 128.48, 128.29, 128.10, 128.06, 128.01, 127.73, 127.63, 127.57, 127.53, 127.39, 127.19, 100.09, 100.02, 97.04, 96.02, 80.05, 79.93, 79.30, 78.82, 78.46, 78.07, 76.40, 76.10, 75.34, 74.56, 72.12, 72.08, 71.82, 71.77, 71.57, 69.71, 69.54, 67.44, 66.02, 62.71, 62.32, 60.35, 60.02, 38.16.HR-ESI-MS (m/z): $[M-2H]^{2-}$ calcd for $C_{56}H_{61}N_7O_{27}S_2^{2-}$, 663.6534; found 663.6534.

**N-benzyloxycarbonyl-3-aminopropyl-*O*-[(benzyl (2-azido-4-*O*-benzyl-3-*O*-(2-naphthylmethyl)-2-deoxy-*α*-D-glucopyranosyl))-(1→4)-*O*-(3-*O*-benzyl-2-*O*-sulfonato-*α*-L-idopyranosyluronate)-(1→4)-*O*-(benzyl (2-azido-3-*O*-(2-naphthylmethyl)-2-deoxy-*α*-D-glucopyranosyl))]-(1→4)-*O*-3-*O*-benzyl-2-*O*-sulfonato-*α*-L-idopyranosiduronate (41)**

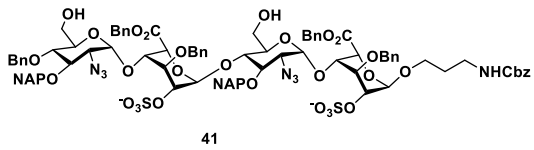

41

$^{1}$H NMR (400 MHz, Methanol-*d*$_4$) δ 7.82 – 7.78 (m, 1H), 7.76- 7.74 (m, 2H), 7.72- 7.70 (m, 2H), 7.63 (dd, *J* = 16.5, 8.2 Hz, 2H), 7.47-7.39 (m, 10H), 7.36- 7.34 (m, 5H), 7.32- 7.27 (m, 10H), 7.26 – 7.24 (m, 5H), 7.17 – 7.10 (m, 3H), 7.02 (t, *J* = 7.5 Hz, 2H), 6.62 (d, *J* = 7.5 Hz, 2H), 5.51 (s, 1H), 5.41 (d, *J* = 12.1 Hz, 1H), 5.27 – 5.26 (m, 1H), 5.20 (s, 1H), 5.15 (d, *J* = 3.0 Hz, 1H), 5.09 – 5.06 (m, 2H), 5.02 – 4.97 (m, 4H), 4.94 – 4.89 (m, 2H), 4.79 – 4.69 (m, 3H), 4.64 – 4.62 (m, 1H), 4.62 – 4.50 (m, 4H), 4.39- 4.35 (m, 3H), 4.18 – 4.14 (m, 1H), 4.12 – 4.03 (m, 2H), 3.99 – 3.73 (m, 7H), 3.61- 3.51 (m, 3H), 3.48 – 3.38 (m, 3H), 3.31 – 3.13 (m, 4H), 1.84- 1.76 (m, 2H). $^{13}$C NMR (101 MHz, Methanol-*d*$_4$) δ 174.15, 169.81, 157.39, 138.37, 137.87, 137.71, 136.94, 135.77, 135.69, 135.07, 134.51, 133.33, 133.31, 133.04, 132.85, 128.51, 128.41, 128.27, 128.25, 128.20, 128.13, 128.06, 127.95, 127.89, 127.82, 127.75, 127.68, 127.60, 127.58, 127.55, 127.54, 127.39, 127.37, 127.31, 127.24, 127.18, 126.39, 125.86, 125.62, 125.49, 125.45, 125.22, 125.09, 99.55, 98.87, 95.46, 95.27, 79.55, 78.42, 77.42, 74.73, 74.36, 74.06, 73.69, 72.81, 72.32, 72.19, 72.08, 71.28, 71.25, 70.76, 70.26, 69.98, 69.74, 68.03, 67.49, 67.26, 66.50, 66.39, 65.96, 65.07, 63.71, 62.66, 59.83, 59.72, 37.99, 33.56, 31.67, 29.37, 29.35, 29.31, 29.20, 29.07, 29.01, 28.81, 24.60, 22.34, 13.07, 7.89. HR-ESI-MS (m/z): $[M-2H]^{2-}$ calcd for $C_{92}H_{93}N_7O_{29}S_2^{2-}$, 911.7735; found, 911.7748.

**N-benzyloxycarbonyl-3-aminopropyl-*O*-[(benzyl (2-acetamido-4-*O*-benzyl-3-*O*-(2-naphthylmethyl)-2-deoxy-*α*-D-glucopyranosyl))-(1→4)-*O*-(3-*O*-benzyl-2-*O*-sulfonato-*α*-L-idopyranosyluronate)-(1→4)-*O*-(benzyl (2-acetamido-3-*O*-(2-naphthylmethyl)-2-deoxy-*α*-D-glucopyranosyl))]-(1→4)-*O*-3-*O*-benzyl-2-*O*-sulfonato-*α*-L-idopyranosiduronate (44)**

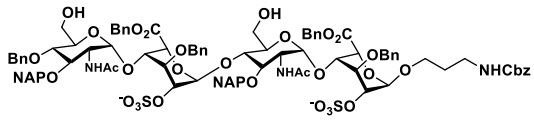

44

$^{1}$H NMR (400 MHz, Methanol-$d_4$) δ 7.68 – 7.65 (m, 2H), 7.63- 7.60 (m, 3H), 7.53 – 7.45 (m, 4H), 7.34 (d, $J$ = 3.3 Hz, 2H), 7.32 – 7.31 (m, 4H), 7.28- 7.25 (m, 7H), 7.20- 7.18 (m, 7H), 7.16 – 7.12 (m, 5H), 7.08 (dd, $J$ = 5.0, 1.9 Hz, 3H), 7.05 (dd, $J$ = 8.5, 1.5 Hz, 2H), 6.99 (dd, $J$ = 6.6, 3.1 Hz, 2H), 6.95 (d, $J$ = 7.4 Hz, 1H), 6.81 (t, $J$ = 7.7 Hz, 2H), 5.43 (s, 1H), 5.21 (d, $J$ = 12.0 Hz, 1H), 5.07 (d, $J$ = 9.6 Hz, 2H), 4.97- 4.94 (m, 2H), 4.87 (d, $J$ = 2.9 Hz, 1H), 4.68 – 4.66 (m, 2H), 4.61 (dd, $J$ = 11.1, 4.7 Hz, 3H), 4.48 (d, $J$ = 5.3 Hz, 3H), 4.44 (dd, $J$ = 9.1, 3.0 Hz, 3H), 4.39 (d, $J$ = 9.3 Hz, 2H), 4.16 (s, 3H), 4.04 – 3.98 (m, 4H), 3.85 (t, $J$ = 12.0 Hz, 4H), 3.67- 3.60 (m, 4H), 3.55 – 3.41 (m, 5H), 3.30- 3.26 (m, 2H), 3.11 – 3.05 (m, 2H), 1.93 (s, 3H), 1.74 – 1.68 (m, 2H), 1.61 (s, 3H). $^{13}$C NMR (151 MHz, Methanol-$d_4$) δ 169.82, 169.70, 157.37, 138.45, 137.52, 137.49, 136.90, 136.37, 136.00, 134.89, 134.19, 133.34, 133.01, 132.71, 128.57, 128.46, 128.33, 128.08, 128.06, 128.04, 127.83, 127.75, 127.70, 127.61, 127.55, 127.54, 127.48, 127.45, 127.36, 127.29, 127.28, 127.21, 127.10, 126.34, 126.13, 125.89, 125.59, 125.51, 125.43, 125.10, 124.47, 99.56, 98.88, 80.32, 78.98, 77.33, 75.18, 74.47, 73.33, 72.75, 72.09, 71.64, 70.55, 70.13, 67.37, 66.78, 66.68, 66.51, 66.00, 59.78, 59.45, 53.23, 53.14, 38.22, 29.19, 22.04, 21.76. HR-ESI-MS (m/z): [M-2H] $^{2-}$ calcd for $C_{96}H_{101}N_3O_{31}S_2^{2-}$, 928.2952; found, 928.2969.

**Global Deprotection:**

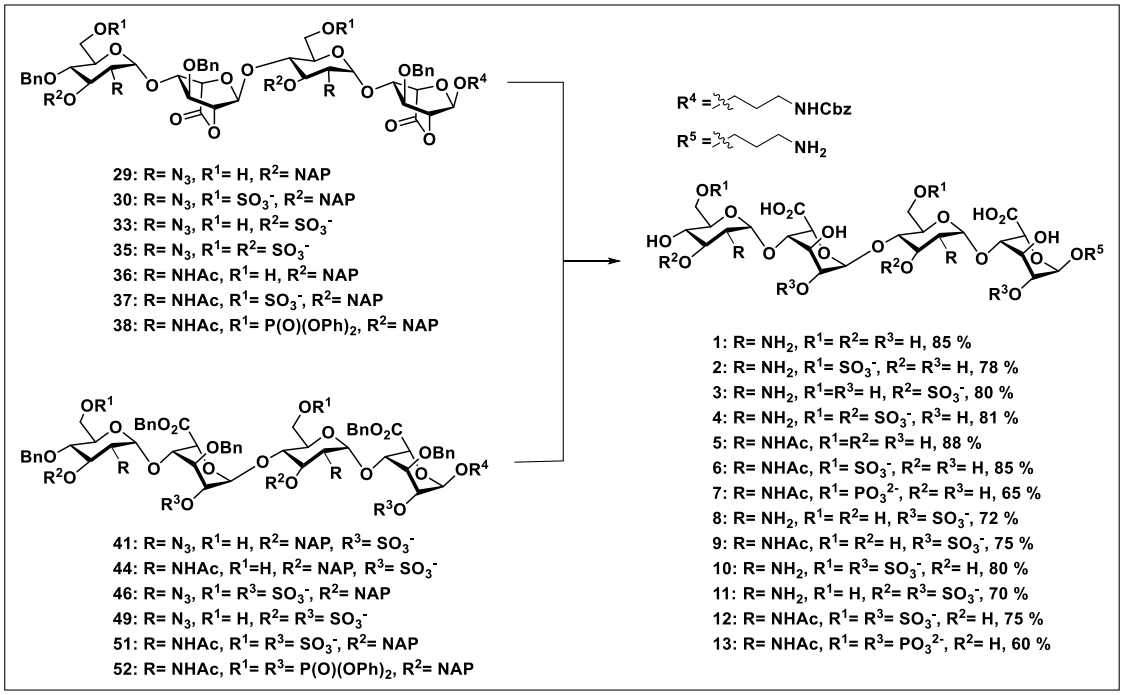


To a solution of starting material (1 mmol for **1-7**) in THF (1 mL) and $H_2O$ (1 mL) was added LiOH.$H_2O$ (10 mmol) and stirred at room temperature for 2 h. Upon completion, the reaction mixture was diluted with MeOH and quenched using Dowex 50WX8 $H^+$ resin. The mixture was filtered, concentrated and eluted through Bond Elute C-18 column ($H_2O$/ ACN= 1/5, v/v). The combined fraction was concentrated under reduced pressure and dissolved in MeOH for hydrogenolysis. The reaction mixture along with $Pd(OH)_2$ was stirred under $H_2$ atm. After 36 h, the mixture was filtered, concentrated and eluted through Bond Elute C-18 column using $H_2O$ as eluent. The combined $H_2O$ fraction were pooled and lyophilized to yield fully deprotected *O*- sulfated tetrasaccharides. For **7 & 13** after $Pd(OH)_2$ hydrogenolysis the as obtained product was again kept for hydrogenolysis using $PtO_2$ as a catalyst under $H_2$ atm for 24 h. Finally, the reaction mixture was filtered, concentrated under reduced pressure and eluted through Bond Elute C-18 column using $H_2O$ as eluent. The combined $H_2O$ fraction were pooled and lyophilized to yield fully deprotected 6-*O*- phosphorylated tetrasaccharides **7 & 13.** For **8-12** hydrogenation was carried out by the above-described method.

**3-aminopropyl-*O*-[(2-amino-2-deoxy-*α*-D-glucopyranosyl)-(1→4)-*O*-(*α*-L-idopyranosyluronate)-(1→4)-*O*-(2-amino-2-deoxy-*α*-D-glucopyranosyl)]-(1→4)-*O*-*α*-L-idopyranosiduronate (1)**

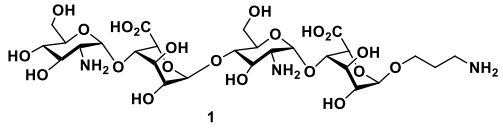

1

$^{1}$H NMR (400 MHz, Deuterium Oxide) δ 5.37 (d, J = 3.6 Hz, 1H), 5.29 (d, J = 3.7 Hz, 1H), 4.72 (d, J = 4.2 Hz, 1H), 4.59 (d, J = 3.2 Hz, 1H), 4.36 (d, J = 2.7 Hz, 1H), 4.03 – 4.01 (m, 1H), 3.96 (t, J = 3.1 Hz, 1H), 3.91 – 3.88 (m, 1H), 3.79 (dd, J = 7.0, 3.8 Hz, 1H), 3.76- 3.72 (m, 2H), 3.70 (s, 3H), 3.68- 3.66 (m, 3H), 3.65 – 3.63 (m, 1H), 3.61 (d, J = 9.4 Hz, 1H), 3.57- 3.56 (m, 1H), 3.55- 3.51 (m, 3H), 3.32 (t, J = 9.4 Hz, 1H), 3.19 (ddd, J = 12.6, 10.6, 3.6 Hz, 2H), 2.97 (t, J = 6.7 Hz, 2H), 1.87- 1.78 (m, 2H). $^{13}$C NMR (101 MHz, Deuterium Oxide) δ 174.73, 174.51, 101.85, 100.65, 92.25, 92.22, 75.58, 74.41, 73.27, 72.32, 71.49, 70.12, 70.10, 69.42, 69.23, 68.69, 68.41, 68.12, 67.59, 66.35, 59.88, 59.30, 54.23, 53.97, 38.03, 26.36. HR-ESI-MS (m/z): $[M+H]^+$ calcd for $C_{27}H_{47}N_3O_{21}^+$, 750.2775; found, 750.2780.

**3-aminopropyl-*O*-[(2-amino-6-*O*-sulfonato-2-deoxy-*α*-D-glucopyranosyl)-(1→4)-*O*-(*α*-L-idopyranosyluronate)-(1→4)-*O*-(2-amino-6-*O*-sulfonato-2-deoxy-*α*-D-glucopyranosyl)]-(1→4)-*O*-*α*-L-idopyranosiduronate (2)**

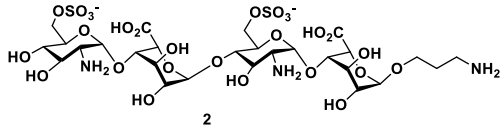

2

$^{1}$H NMR (600 MHz, Deuterium Oxide) δ 5.41 (d, J = 3.7 Hz, 1H), 5.39 (d, J = 3.6 Hz, 1H), 5.04 – 5.03 (m, 3H), 4.15 – 4.11 (m, 1H), 4.07 – 3.97 (m, 1H), 3.85 – 3.81 (m, 2H), 3.80- 3.72 (m, 5H), 3.70 – 3.59 (m, 5H), 3.50 – 3.39 (m, 2H), 3.30 (td, J = 10.7, 10.0, 3.6 Hz, 1H), 3.08- 3.05 (m, 2H), 2.76 (d, J = 5.2 Hz, 1H), 1.96-1.88 (m, 2H). $^{13}$C NMR (151 MHz, Deuterium Oxide) δ 171.27, 101.97, 100.86, 93.16, 92.70, 76.71, 73.37, 73.00, 72.55, 71.93, 69.35, 69.02, 68.46, 68.01, 67.80, 67.35, 66.81, 65.95, 60.01, 59.35, 54.03, 53.83, 38.01, 26.26. HR-ESI-MS (m/z): $[M-2H]^{2-}$ calcd for $C_{27}H_{45}N_3O_{27}S_2^{2-}$, 453.5846; found, 453.5981.

**3-aminopropyl-*O*-[(2-amino-3-*O*-sulfonato-2-deoxy-*α*-D-glucopyranosyl)-(1→4)-*O*-(*α*-L-idopyranosyluronate)-(1→4)-*O*-(2-amino-3-*O*-sulfonato-2-deoxy-*α*-D-glucopyranosyl)]-(1→4)-*O*-*α*-L-idopyranosiduronate (3)**

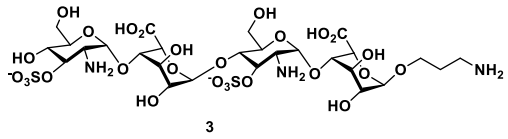

3

$^{1}$H NMR (600 MHz, Deuterium Oxide) δ 5.51 (d, J = 3.5 Hz, 1H), 5.41 – 5.39 (m, 1H), 4.95 (d, J = 2.8 Hz, 1H), 4.87 (d, J = 4.0 Hz, 1H), 4.56 – 4.50 (m, 1H), 4.48 – 4.42 (m, 2H), 4.19 (t, J = 3.6 Hz, 1H), 4.08 – 4.05 (m, 1H), 3.99 (t, J = 3.8 Hz, 1H), 3.93 (t, J = 9.6 Hz, 1H), 3.89 (s, 1H), 3.88 – 3.84 (m, 2H), 3.82 – 3.77 (m, 6H), 3.69- 3.67 (m, 1H), 3.64 – 3.59 (m, 4H), 3.55 (dd, J = 10.4, 3.6 Hz, 1H), 3.06 – 3.04 (m, 2H), 1.96 – 1.87 (m, 2H). $^{13}$C NMR (151 MHz, Deuterium Oxide) δ 174.57, 100.92, 100.59, 92.63, 92.42, 77.31, 74.86, 74.78, 73.72, 72.07, 71.46, 71.42, 69.98, 69.80, 69.50, 68.57, 68.15, 67.39, 67.29, 66.43, 59.78, 59.17, 53.63, 53.12, 38.06. HR-ESI-MS (m/z): $[M-2H]^{2-}$ calcd for $C_{27}H_{45}N_3O_{27}S_2^{2-}$, 453.5846; found, 453.5826.

**3-aminopropyl-*O*-[(2-amino-6-*O*-sulfonato-3-*O*-sulfonato-2-deoxy-*α*-D-glucopyranosyl)-(1→4)-*O*-(*α*-L-idopyranosyluronate)-(1→4)-*O*-(2-amino-6-*O*-sulfonato-3-*O*-sulfonato-2-deoxy-*α*-D-glucopyranosyl)]-(1→4)-*O*-*α*-L-idopyranosiduronate (4)**

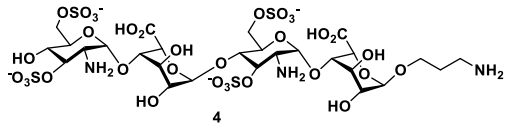

4

$^{1}$H NMR (600 MHz, Deuterium Oxide) δ 5.26 (d, J = 3.2 Hz, 1H), 5.09 (d, J = 3.5 Hz, 1H), 4.87 (d, J = 4.2 Hz, 1H), 4.80- 4.78 (m, 2H), 4.42 (d, J = 2.7 Hz, 1H), 4.31 – 4.24 (m, 4H), 4.20 – 4.17 (m, 1H), 4.13 – 4.08 (m, 2H), 4.02 – 3.99 (m, 3H), 3.96 – 3.95 (m, 2H), 3.88 (t, J = 9.7 Hz, 1H), 3.84- 3.79 (m, 2H), 3.67 – 3.55 (m, 4H), 3.08- 3.04 (m, 4H), 2.99 (dd, J = 10.2, 3.5 Hz, 1H), 1.94- 1.87 (m, 2H). $^{13}$C NMR (151 MHz, Deuterium Oxide) δ 174.98, 171.04, 100.49, 100.43, 96.66, 95.49, 79.53, 75.67, 74.77, 71.37, 70.91, 70.40, 70.14, 70.03, 69.95, 68.98, 68.79, 68.40, 67.47, 66.48, 66.29, 66.13, 54.46, 53.86, 38.14, 26.39. HR-ESI-MS (m/z): $[M+H]^{+}$ calcd for $C_{27}H_{48}N_3O_{33}S_4^{+}$, 1070.1048; found, 1070.1050.

**3-aminopropyl-*O*-[(2-acetamido-2-deoxy-*α*-D-glucopyranosyl)-(1→4)-*O*-(*α*-L-idopyranosyluronate)-(1→4)-*O*-(2-acetamido-2-deoxy-*α*-D-glucopyranosyl)]-(1→4)-*O*-*α*-L-idopyranosiduronate (5)**

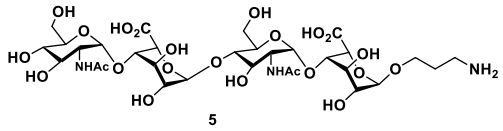
5

$^{1}$H NMR (400 MHz, Deuterium Oxide) δ 5.08 (d, J = 3.7 Hz, 1H), 5.05 (d, J = 3.8 Hz, 1H), 5.00 (d, J = 2.7 Hz, 1H), 4.90 (d, J = 2.7 Hz, 1H), 4.84 (d, J = 1.8 Hz, 1H), 4.67 (d, J = 2.4 Hz, 1H), 4.02 (t, J = 3.1 Hz, 1H), 3.99 (t, J = 2.6 Hz, 1H), 3.94 (t, J = 3.6 Hz, 1H), 3.91 – 3.79 (m, 4H), 3.75- 3.71 (m, 4H), 3.67 – 3.65 (m, 3H), 3.64 – 3.58 (m, 3H), 3.58 – 3.52 (m, 2H), 3.45 (d, J = 9.3 Hz, 1H), 3.06 (t, J = 6.6 Hz, 2H), 1.95 – 1.88 (m, 8H). $^{13}$C NMR (101 MHz, Deuterium Oxide) δ 174.43, 174.40, 173.41, 173.02, 101.63, 100.57, 95.15, 95.00, 76.85, 73.76, 73.26, 72.45, 71.49, 71.08, 69.77, 69.29, 69.03, 68.07, 68.04, 67.96, 67.16, 66.63, 60.03, 59.55, 53.64, 53.39, 38.13, 26.24, 21.93. HR-ESI-MS (m/z): $[M-H]^-$ calcd for $C_{31}H_{50}N_3O_{23}^-$, 832.2840; found, 832.2835.

**3-aminopropyl-*O*-[(2-acetamido-6-*O*-sulfonato-2-deoxy-*α*-D-glucopyranosyl)-(1→4)-*O*-(*α*-L-idopyranosyluronate)-(1→4)-*O*-(2-acetamido-6-*O*-sulfonato-2-deoxy-*α*-D-glucopyranosyl)]-(1→4)-*O*-*α*-L-idopyranosiduronate (6)**

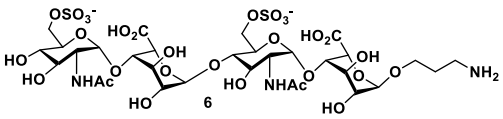
6

$^{1}$H NMR (400 MHz, Deuterium Oxide) δ 4.99 (t, *J* = 4.2 Hz, 2H), 4.95 (d, *J* = 2.4 Hz, 1H), 4.87 (s, 1H), 4.77 (s, 1H), 4.60 (d, *J* = 1.9 Hz, 1H), 4.16 (ddd, *J* = 11.0, 8.0, 3.3 Hz, 2H), 4.06 (ddd, *J* = 10.9, 6.7, 1.8 Hz, 2H), 3.94 (dt, *J* = 4.8, 2.8 Hz, 2H), 3.89 – 3.72 (m, 6H), 3.64- 3.62 (m, 2H), 3.60 – 3.53 (m, 4H), 3.50 (d, *J* = 10.4 Hz, 1H), 3.42 (d, *J* = 9.7 Hz, 1H), 2.99 (t, *J* = 6.6 Hz, 2H), 1.88- 1.80 (m, 8H). $^{13}$C NMR (101 MHz, Deuterium Oxide ) δ 174.43, 174.33, 173.41, 101.86, 100.50, 95.24, 94.96, 77.25, 73.66, 73.34, 71.03, 70.60, 69.91, 69.54, 68.99, 68.58, 68.06, 67.55, 67.42, 67.15, 66.67, 66.58, 66.53, 66.13, 53.49, 53.22, 38.18, 26.21, 21.96. HR-ESI-MS *(m/z)*: $[M-2H]^{2-}$ calcd for $C_{31}H_{49}N_3O_{29}S_2^{2-}$, 495.5952; found, 495.5974.

**3-aminopropyl-*O*-[(2-acetamido-6-*O*-phosphonato-2-deoxy-*α*-D-glucopyranosyl)-(1→4)-*O*-(*α*-L-idopyranosyluronate)-(1→4)-*O*-(2-acetamido-6-*O*-phosphonato-2-deoxy-*α*-D-glucopyranosyl)]-(1→4)-*O*-*α*-L-idopyranosiduronate (7)**

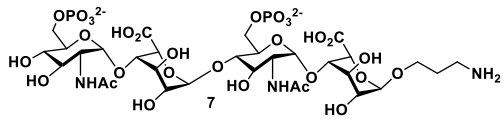

7

$^{1}$H NMR (400 MHz, Deuterium Oxide ) δ 4.98 (d, *J* = 3.1 Hz, 2H), 4.89 (s, 1H), 4.78 (s, 1H), 3.99- 3.70 (m, 6H), 3.85 (ddd, *J* = 14.1, 8.1, 3.2 Hz, 4H), 3.80 – 3.73 (m, 1H), 3.69 – 3.49 (m, 9H), 3.48 – 3.40 (m, 1H), 2.99 (t, *J* = 6.4 Hz, 2H), 1.92- 1.82 (m, 8H). $^{13}$C NMR (151 MHz, Deuterium Oxide ) δ 174.65, 174.46, 174.34, 101.85, 100.44, 95.06, 94.58, 81.76, 77.10, 74.05, 73.37, 71.07, 70.33, 70.28, 69.87, 69.15, 68.97, 68.52, 68.46, 68.13, 67.97, 67.11, 63.64, 63.30, 53.64, 53.43, 38.24, 26.31, 21.97. $^{31}$P NMR (162 MHz, $D_2O$) δ 1.35, 0.85. HR-ESI-MS *(m/z)*: $[M-2H]^{2-}$ calcd for $C_{31}H_{53}N_3O_{29}P_2^{2-}$, 495.6047; found, 495.6060.

**3-aminopropyl-*O*-[(2-amino-2-deoxy-*α*-D-glucopyranosyl)-(1→4)-*O*-(2-*O*-sulfonato-*α*-L-idopyranosyluronate)-(1→4)-*O*-(2-amino-2-deoxy-*α*-D-glucopyranosyl)]-(1→4)-*O*-2-*O*-sulfonato-*α*-L-idopyranosiduronate (8)**

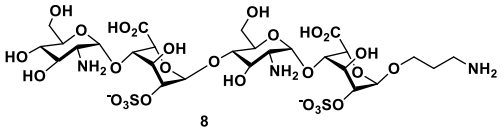

8

$^{1}$H NMR (600 MHz, Deuterium Oxide) δ 5.33 (s, 1H), 5.15 (s, 1H), 5.05 (s, 1H), 4.84 (s, 1H), 4.46 (s, 1H), 4.28 – 4.25 (m, 3H), 4.17 (s, 1H), 4.06 (d, *J* = 14.2 Hz, 2H), 3.88 (t, *J* = 9.9 Hz, 1H), 3.81 – 3.77 (m, 5H), 3.73 (s, 2H), 3.68- 3.67 (m, 2H), 3.64 – 3.62 (m, 1H), 3.40 (t, *J* = 9.6 Hz, 1H), 3.29 (d, *J* = 10.7 Hz, 1H), 3.26 – 3.24 (m, 1H), 3.09- 3.05 (m, 2H), 1.96- 1.87 (m, 2H). $^{13}$C NMR (151 MHz, Deuterium Oxide) δ 175.38, 174.85, 98.74, 97.78, 91.06, 90.96, 76.07, 72.53, 72.42, 72.01, 71.44, 70.06, 69.95, 69.33, 69.06, 67.99, 66.87, 66.59, 66.43, 62.40, 62.37, 59.71, 59.27, 54.50, 54.14, 38.32, 26.06. HR-ESI-MS (m/z): $[M-2H]^{2-}$ calcd for $C_{27}H_{45}N_3O_{27}S_2^{2-}$, 453.5846; found, 453.5911.

**3-aminopropyl-*O*-[(2-acetamido-2-deoxy-*α*-D-glucopyranosyl)-(1→4)-*O*-(2-*O*-sulfonato-*α*-L-idopyranosyluronate)-(1→4)-*O*-(2-acetamido-2-deoxy-*α*-D-glucopyranosyl)]-(1→4)-*O*-2-*O*-sulfonato-*α*-L-idopyranosiduronate (9)**

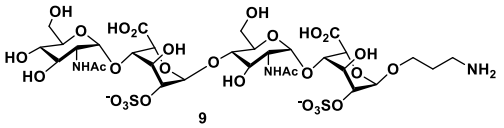

9

$^{1}$H NMR (600 MHz, Deuterium Oxide) δ 5.12 (s, 2H), 5.06 (s, 1H), 5.03 (d, *J* = 3.4 Hz, 1H), 5.01 (d, *J* = 3.4 Hz, 1H), 4.76 (d, *J* = 1.8 Hz, 1H), 4.21

(d, *J* = 6.5 Hz, 2H), 4.17 (d, *J* = 13.4 Hz, 2H), 3.97 (d, *J* = 11.1 Hz, 2H), 3.90 (ddd, *J* = 18.5, 10.5, 3.4 Hz, 2H), 3.85 – 3.81 (m, 1H), 3.76 (s, 2H), 3.71 (d, *J* = 2.8 Hz, 2H), 3.65 – 3.59 (m, 4H), 3.56 – 3.50 (m, 2H), 3.42 (d, *J* = 9.2 Hz, 1H), 3.06 (t, *J* = 6.3 Hz, 2H), 1.98 (s, 3H), 1.96 (s, 3H), 1.93 – 1.88 (m, 2H). $^{13}$C NMR (151 MHz, Deuterium Oxide) δ 174.80, 173.03, 172.79, 99.17, 98.34, 94.86, 94.32, 76.95, 73.19, 73.15, 72.36, 71.60, 71.36, 71.05, 70.94, 69.70, 69.34, 66.72, 66.19, 63.97, 63.42, 60.02, 59.47, 53.51, 53.22, 38.15, 26.02, 22.14. HR-ESI-MS *(m/z)*: $[M-2H]^{2-}$ calcd for $C_{31}H_{49}N_3O_{29}S_2^{2-}$, 495.5952; found, 495.5922.

**3-aminopropyl-*O*-[(2-amino-6-*O*-sulfonato-2-deoxy-*α*-D-glucopyranosyl)-(1→4)-*O*-(2-*O*-sulfonato-*α*-L-idopyranosyluronate)-(1→4)-*O*-(2-amino-6-*O*-sulfonato-2-deoxy-*α*-D-glucopyranosyl)]-(1→4)-*O*-2-*O*-sulfonato-*α*-L-idopyranosiduronate (10)**

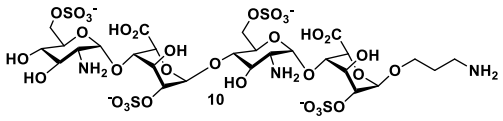


$^1$H NMR (400 MHz, Deuterium Oxide) δ 5.29 (dd, *J* = 7.0, 3.7 Hz, 2H), 5.10 (s, 1H), 5.01 (s, 1H), 4.83 (s, 1H), 4.47 (s, 1H), 4.25 – 4.23 (m, 2H), 4.22 (d, *J* = 2.0 Hz, 1H), 4.19 (d, *J* = 3.0 Hz, 1H), 4.17 – 4.14 (m, 2H), 4.13 – 4.11 (m, 1H), 4.09 (s, 1H), 4.06 (s, 1H), 4.04 (s, 1H), 3.87 (d, *J* = 9.6 Hz, 1H), 3.82 (d, *J* = 10.4 Hz, 1H), 3.80 – 3.75 (m, 2H), 3.74 – 3.69 (m, 1H), 3.66 (d, *J* = 9.7 Hz, 1H), 3.61- 3.55 (m, 1H), 3.43 (t, *J* = 9.7 Hz, 1H), 3.31 – 3.22 (m, 2H), 3.02 (q, *J* = 6.7, 5.6 Hz, 2H), 1.91- 1.82 (m, 2H). $^{13}$C NMR (151 MHz, Deuterium Oxide) δ 174.95, 98.71, 97.82, 91.30, 90.92, 75.55, 72.67, 72.48, 70.32, 70.14, 69.59, 69.23, 68.64, 68.10, 67.05, 66.76, 66.38, 66.13, 62.72, 62.30, 54.27, 53.99, 38.43, 26.08. HR-ESI-MS (m/z): $[M+H]^+$ calcd for $C_{27}H_{48}N_3O_{33}S_4^+$, 1070.1048; found, 1070.1051.

**3-aminopropyl-*O*-[(2-amino-3-*O*-sulfonato-2-deoxy-*α*-D-glucopyranosyl)-(1→4)-*O*-(2-*O*-sulfonato-*α*-L-idopyranosyluronate)-(1→4)-*O*-(2-amino-3-*O*-sulfonato-2-deoxy-*α*-D-glucopyranosyl)]-(1→4)-*O*-2-*O*-sulfonato-*α*-L-idopyranosiduronate (11)**

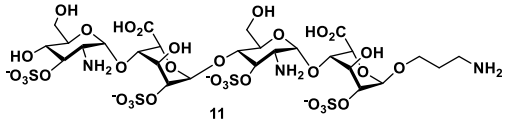


$^1$H NMR (600 MHz, Deuterium Oxide) δ 5.44 (d, J = 3.6 Hz, 1H), 5.37 (d, J = 3.7 Hz, 1H), 4.83 (d, J = 3.7 Hz, 1H), 4.80 (d, J = 2.4 Hz, 1H), 4.77 (d, J = 3.1 Hz, 1H), 4.52 (d, J = 2.6 Hz, 1H), 4.12 – 4.11 (m, 1H), 4.06 – 4.05 (m, 1H), 4.00 –

3.97 (m, 1H), 3.90 (dd, J = 6.8, 4.1 Hz, 1H), 3.85- 3.81 (m, 2H), 3.77- 3.72 (m, 6H), 3.70 – 3.67 (m, 2H), 3.66 – 3.62 (m, 3H), 3.41 (t, J = 9.6 Hz, 1H), 3.31 – 3.26 (m, 2H), 3.07 – 3.05 (m, 2H), 1.94 – 1.87 (m, 2H). $^{13}$C NMR (151 MHz, Deuterium Oxide) δ 174.23, 173.94, 101.86, 100.69, 92.45, 92.34, 75.87, 74.15, 73.16, 72.48, 69.81, 69.45, 69.40, 69.17, 68.49, 68.09, 68.03, 67.22, 66.45, 59.90, 59.32, 54.23, 53.96, 38.06, 26.35 HR-ESI-MS (m/z): $[M+H]^+$ calcd for $C_{27}H_{48}N_3O_{33}S_4^+$, 1070.1048; found, 1070.1052.

**3-aminopropyl-*O*-[(2-acetamido-6-*O*-sulfonato-2-deoxy-*α*-D-glucopyranosyl)-(1→4)-*O*-(2-*O*-sulfonato-*α*-L-idopyranosyluronate)-(1→4)-*O*-(2-acetamido-6-*O*-sulfonato-2-deoxy-*α*-D-glucopyranosyl)]-(1→4)-*O*-2-*O*-sulfonato-*α*-L-idopyranosiduronate (12)**

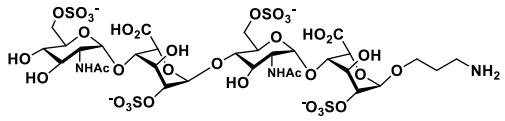

12

1H NMR (400 MHz, Deuterium Oxide) δ 5.14 (s, 1H), 5.10 (d, J = 1.7 Hz, 1H), 5.07 (d, J = 3.7 Hz, 3H), 4.76 (d, J = 2.0 Hz, 1H), 4.28 – 4.13 (m, 8H), 4.04 – 4.03 (m, 2H), 3.96 (ddd, J = 16.3, 10.3, 3.5 Hz, 2H), 3.91- 3.83 (m, 2H), 3.77 – 3.62 (m, 4H), 3.61 – 3.55 (m, 1H), 3.50 (d, J = 9.6 Hz, 1H), 3.09 (t, J = 6.4 Hz, 2H), 2.00 (s, 3H), 1.98 (s, 3H), 1.96- 1.91 (m, 2H). $^{13}$C NMR (101 MHz, Deuterium Oxide) δ 174.82, 173.03, 99.15, 98.35, 95.05, 93.90, 76.67, 73.68, 73.24, 72.06, 70.91, 70.83, 70.52, 69.88, 69.62, 69.12, 66.82, 66.56, 66.50, 64.65, 63.24, 53.30, 53.15, 38.30, 26.05, 22.19. HR-ESI-MS (m/z): $[M-3H]^{3-}$ calcd for $C31H_{48}N_3O_{35}S_4^{3-}$, 383.3656; found, 383.3639.

**3-aminopropyl-*O*-[(2-acetamido-6-*O*-phosphonato-2-deoxy-*α*-D-glucopyranosyl)-(1→4)-*O*-(2-*O*-phosphonato-*α*-L-idopyranosyluronate)-(1→4)-*O*-(2-acetamido-6-*O*-phosphonato-2-deoxy-*α*-D-glucopyranosyl)]-(1→4)-*O*-2-*O*-phosphonato-*α*-L-idopyranosiduronate (13)**

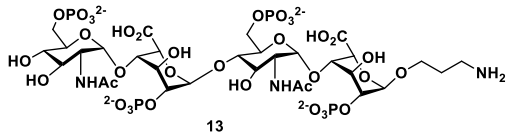

13

$^1$H NMR (400 MHz, Deuterium Oxide) δ 5.13 (d, J = 10.1 Hz, 1H), 5.05 (dd, J = 10.2, 6.5 Hz, 2H), 4.79 (s, 1H), 4.15 – 4.02 (m, 10H), 3.94 (td, J = 10.5, 3.4 Hz, 2H), 3.88 – 3.75 (m, 4H), 3.72 – 3.62 (m, 4H), 3.59 – 3.57 (m, 1H), 3.51 (d, J = 9.2 Hz, 1H), 3.08 (t, J = 6.4 Hz, 1H), 2.02 – 1.90 (m, 8H). $^{13}$C NMR (151 MHz, Deuterium Oxide) δ 174.81, 172.75, 172.64, 100.08, 99.35, 95.88, 95.61, 77.05, 73.30,

73.24, 71.62, 71.33, 70.66, 69.65, 69.12, 66.86, 66.79, 66.61, 63.79, 53.58, 53.34, 38.27, 26.07, 22.21, 22.15. $^{31}$P NMR (162 MHz, Deuterium Oxide) δ 0.75, 0.15, -0.10, -0.27. HR-ESI-MS *(m/z)*: $[M-2H]^{2-}$ calcd for $C_{31}H_{53}N_3O_{35}P_4^2$, 575.5710; found, 575.5759.

### 2.4.3 Glycan microarray

**Materials**. PBSx10 was purchased from Hy-labs, ethanolamine from Fisher, ovalbumin (Grade V), sodium phosphate monobasic monohydrate, sodium phosphate dibasic heptahydrate, Tween-20 and Tris/HCl were purchased from Sigma-Aldrich. Antibodies were purchased from Peprotech: Human SD1α CXCL12, human IL8 CXCL8 72 aa, human exodus-2 CCL21, human MCP-3 CCL7, human MCP-4 CCL13, human IP-10 CXCL10, human MEC CCL28, human RANTES CCL5, human MCP-1/MCAF CCL2, biotinylated antigen affinity-purified goat-anti-murine SDF-1α, biotinylated-rabbit-anti-human IL8 CXCL8, biotinylated-rabbit-anti-human Exodus-2 CCL21, biotinylated goat-anti-human MCP-3, biotinylated anti-H-MCP-4, biotinylated rabbit-anti-human IP-10, biotinylated anti-human MEC, biotinylated-rabbit-anti-human MCAF/MCP-1. Biotinylated anti-Rantes was purchased from R&D. Cy3-sterptavidin (Cy3-SA) was purchased from Jackson ImmunoResearch. IVIG GammaGard 10% (Baxter, USA) were a kind gift from Adriana Tremolot, Childrens hospital UCSD.

**Heparin tetrasaccharide microarray fabrication.** Arrays were fabricated with NanoPrint LM-60 Microarray Printer (Arrayit) on epoxide-derivatized slides (PolyAn 2D) with 16 sub-array blocks on each slide. Glycoconjugates were distributed into 384-well source plates using 4 replicate wells per sample and 7 µl per well. Each glycoconjugate diluted into 50 and 100 µM in an optimized printing buffer (300 mM phosphate buffer, pH 8.4 Version VrHI.01. To monitor printing Alexaflour-555-hydraside (Invitrogen, at 1 ng/µl in 178 mM phosphate buffer, pH 5.5) was used for each printing run. The arrays were printed with four 946MP3 pins (5 µm tip, 0.25 µl sample channel, ~100 µm spot diameter; Arrayit). The humidity level in the arraying chamber was maintained at about 70% during printing. Printed slides were left on arrayer deck over-night, allowing humidity to drop to ambient levels (40-45%). Next, slides were packed, vacuum-sealed and stored at room temperature (RT) until used.

**HS tetrasaccharide microarray binding assay.** Slides were developed and analyzed as previously described[33, 34] with some modifications. Slides were rehydrated with $dH_2O$ and incubated for 30 min in a staining dish with 50°C pre-warmed ethanolamine (0.05 M) in Tris-HCl (0.1 M, pH 9.0) to block the remaining reactive epoxy groups on the slide surface, then washed with 50 °C pre-warmed $dH_2O$. Slides were centrifuged at 200×*g* for three min then fitted with ProPlate™ Multi-Array 16-well slide module (Grace Bio-lab P37001) to divide into the sub-arrays (blocks). Slides were washed with PBST (0.1% Tween 20), aspirated and blocked with 200 µl/sub-array of blocking buffer (PBS pH 7.3 + 1% w/v ovalbumin) for 1 hour at RT with gentle shaking. Next, the blocking solution was aspirated and 100 µl/block of primary detection proteins (for each detection, 3 serially decreasing concentrations were used, see Table 1) diluted in PBS pH 7.3 + 1% w/v ovalbumin, were incubated with gentle shaking for 2 hours at RT. Slides were washed 4 times with PBST, then with PBS (without Tween-20) for 2 min. Bound antibodies were detected by incubating with biotinylated secondary detections (1 ng/µl, see Table 1) diluted in PBS, 200 µl/block at RT for 1 hour. Slides were washed 4 times with PBST, then with PBS (without Tween-20) for 2 min and biotinylated antibodies were detected with Cy3-SA (1.2µg/ml). Slides were washed 4 times with PBST, then with PBS for 10 min followed by removal from ProPlate™ Multi-Array slide module and immediately dipping in a staining dish with $dH_2O$ for 10 min with shaking. Slide then were centrifuged at 200×*g* for 3 min. and the dry slides immediately scanned.

**Array slide processing.** Processed slides were scanned and analyzed as described at 10 µm resolution with a Genepix 4000B microarray scanner (Molecular Devices) using 350 gain. Image analysis was carried out with Genepix Pro 4.0 analysis software (Molecular Devices). Spots were defined as circular features with a variable radius as determined by the Genepix scanning software. Local background subtraction was performed. RFU from each spot was calculated and Ranking (per printed glycan per concentration, per each chemokine dilution, per printed block) was used to compare the data between detections; since each glycans was printed at 2 concentration, 100% binding was set separately for each concentration. Then, binding to all the other glycans at the same concentration was ranked in comparison to the maximal binding, and the average rank binding and SEM for

each glycan across the two glycan concentrations and three examined dilutions of each chemokine was calculated (n=6, 2 glycan concentrations across 3 chemokine dilutions).

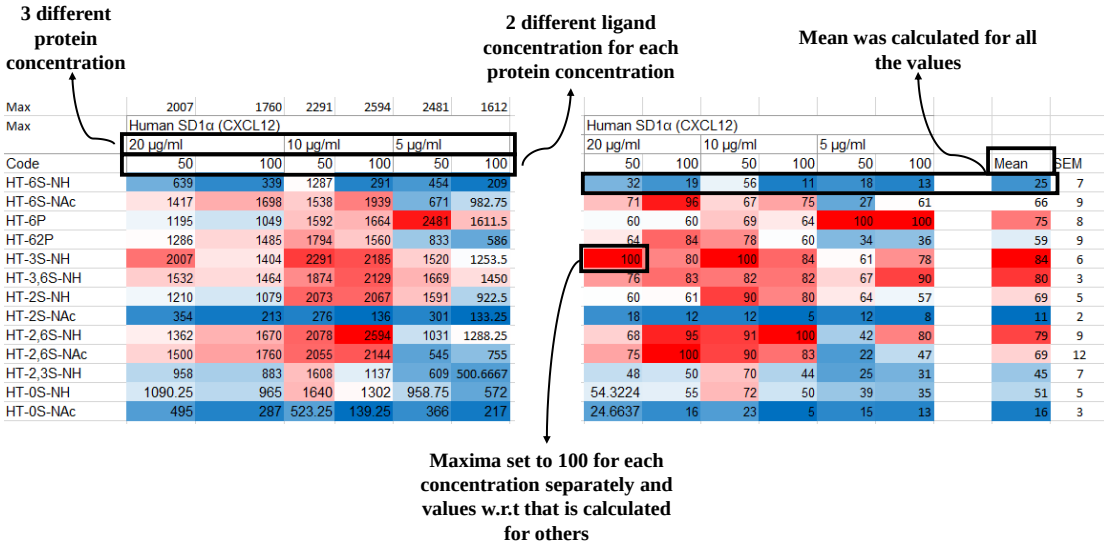


| Max | 2007 | 1760 | 2291 | 2594 | 2481 | 1612 |
|---|---|---|---|---|---|---|
| Max | Human SD1α (CXCL12) | | | | | |
| | 20 µg/ml | | 10 µg/ml | | 5 µg/ml | |
| Code | 50 | 100 | 50 | 100 | 50 | 100 |
| HT-6S-NH | 639 | 339 | 1287 | 291 | 454 | 209 |
| HT-6S-NAc | 1417 | 1698 | 1538 | 1939 | 671 | 982.75 |
| HT-6P | 1195 | 1049 | 1592 | 1664 | 2481 | 1611.5 |
| HT-62P | 1286 | 1485 | 1794 | 1560 | 833 | 586 |
| HT-3S-NH | 2007 | 1404 | 2291 | 2185 | 1520 | 1253.5 |
| HT-3,6S-NH | 1532 | 1464 | 1874 | 2129 | 1669 | 1450 |
| HT-2S-NH | 1210 | 1079 | 2073 | 2067 | 1591 | 922.5 |
| HT-2S-NAc | 354 | 213 | 276 | 136 | 301 | 133.25 |
| HT-2,6S-NH | 1362 | 1670 | 2078 | 2594 | 1031 | 1288.25 |
| HT-2,6S-NAc | 1500 | 1760 | 2055 | 2144 | 545 | 755 |
| HT-2,3S-NH | 958 | 883 | 1608 | 1137 | 609 | 500.6667 |
| HT-0S-NH | 1090.25 | 965 | 1640 | 1302 | 958.75 | 572 |
| HT-0S-NAc | 495 | 287 | 523.25 | 139.25 | 366 | 217 |

| Human SD1α (CXCL12) | | | | | | | |
|---|---|---|---|---|---|---|---|
| 20 µg/ml | | 10 µg/ml | | 5 µg/ml | | | |
| 50 | 100 | 50 | 100 | 50 | 100 | Mean | SEM |
| 32 | 19 | 56 | 11 | 18 | 13 | 25 | 7 |
| 71 | 96 | 67 | 75 | 27 | 61 | 66 | 9 |
| 60 | 60 | 69 | 64 | 100 | 100 | 75 | 8 |
| 64 | 84 | 78 | 60 | 34 | 36 | 59 | 9 |
| 100 | 80 | 100 | 84 | 61 | 78 | 84 | 6 |
| 76 | 83 | 82 | 82 | 67 | 90 | 80 | 3 |
| 60 | 61 | 90 | 80 | 64 | 57 | 69 | 5 |
| 18 | 12 | 12 | 5 | 12 | 8 | 11 | 2 |
| 68 | 95 | 91 | 100 | 42 | 80 | 79 | 9 |
| 75 | 100 | 90 | 83 | 22 | 47 | 69 | 12 |
| 48 | 50 | 70 | 44 | 25 | 31 | 45 | 7 |
| 54.3224 | 55 | 72 | 50 | 39 | 35 | 51 | 5 |
| 24.6637 | 16 | 23 | 5 | 15 | 13 | 16 | 3 |

**Figure R1:** Representative image for the ranking calculation

**Table 1. Primary detection concentrations used on the array and Secondary Biotinylated antibodies.**

| Primary Detection | Concentrations used (ng/µl) | Secondary Detection |
|---|---|---|
| Human SD1α (CXCL12) | 20, 10, 5 | Biotinylated antigen affinity-purified goat-anti-murine SDF-1α |
| Human IL8 (CXCL8) 72 aa | 20, 10, 5 | Biotinylated-rabbit-anti-human IL8 (CXCL8) |
| Human Exodus-2 (CCL21) | 20, 10, 5 | Biotinylated-rabbit-anti-human Exodus-2 (CCL21) |
| Human MCP-3 (CCL7) | 20, 10, 5 | Biotinylated-goat-anti-human MCP-3 |

| | | |
|---|---|---|
| Human MCP-4 (CCL13) | 20, 10, 5 | Biotinylated anti-human MCP-4 |
| Human IP-10 (CXCL10) | 10, 5, 2.5 | Biotinylated-rabbit-anti-human IP-10 |
| Human BCA-1 (CXCL13) | 10, 5, 2.5 | Biotinylated-rabbit-anti-human BCA-1 |
| Human MEC (CCL28) | 10, 5, 2.5 | Biotinylated-anti-human MEC |
| Human RANTES (CCL5) | 2, 1, 0.5 | Biotinylated anti-Rantes |
| Human MCP-1/MCAF (CCL2) | 2, 1, 0.5 | Biotinylated-rabbit-anti-human MCAF/MCP-1 |

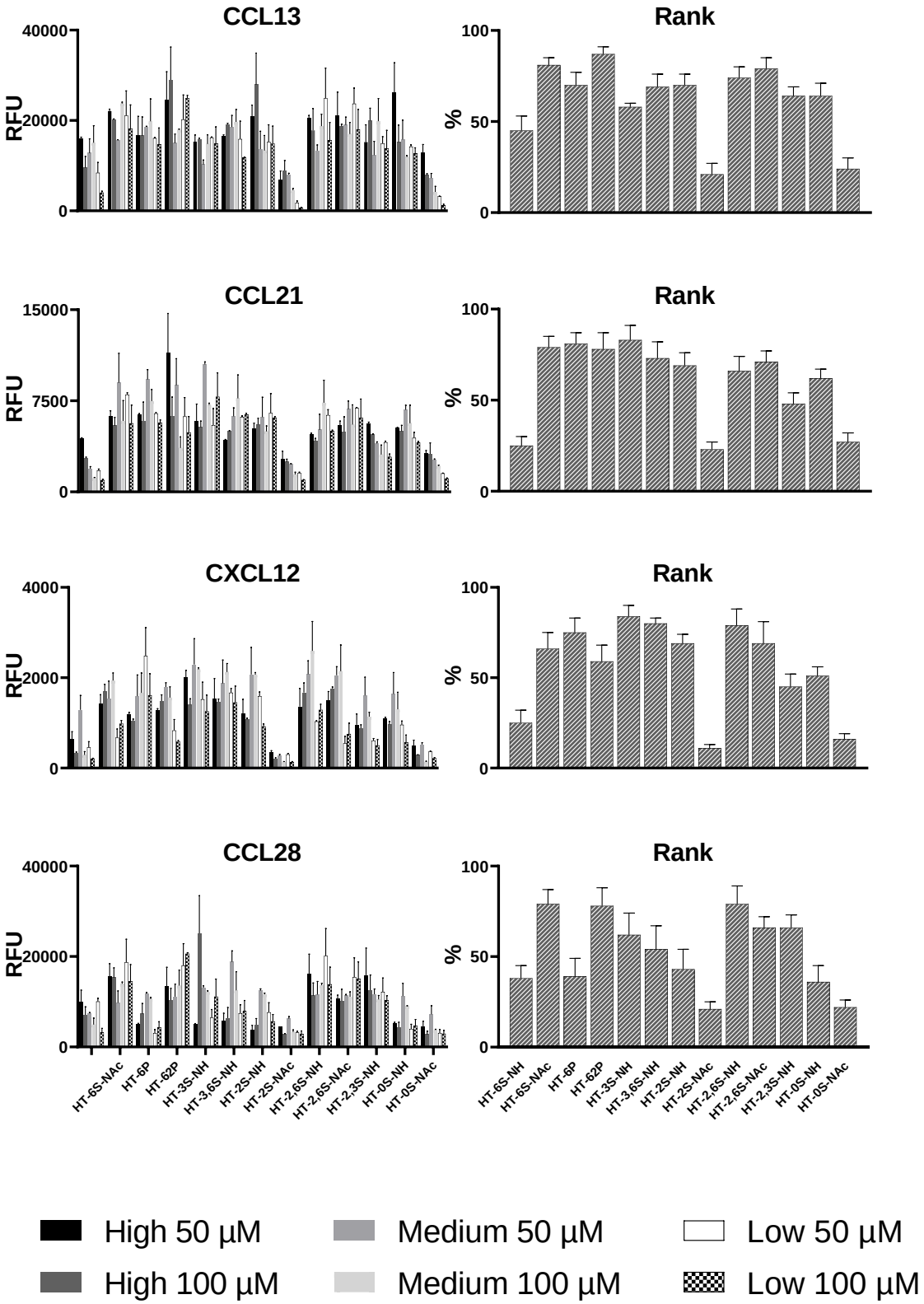
CCL13
RFU
40000
20000
0
Rank
%
100
50
0
CCL21
RFU
15000
7500
0
Rank
%
100
50
0
CXCL12
RFU
4000
2000
0
Rank
%
100
50
0
CCL28
RFU
40000
20000
0
Rank
%
100
50
0
HT-6S-NAc
HT-6P
HT-6?P
HT-3S-NH
HT-3,6S-NH
HT-2S-NH
HT-2S-NAc
HT-2,6S-NH
HT-2,6S-NAc
HT-2,3S-NH
HT-0S-NH
HT-0S-NAc
HT-6S-NH
High 50 µM
Medium 50 µM
Low 50 µM
High 100 µM
Medium 100 µM
Low 100 µM

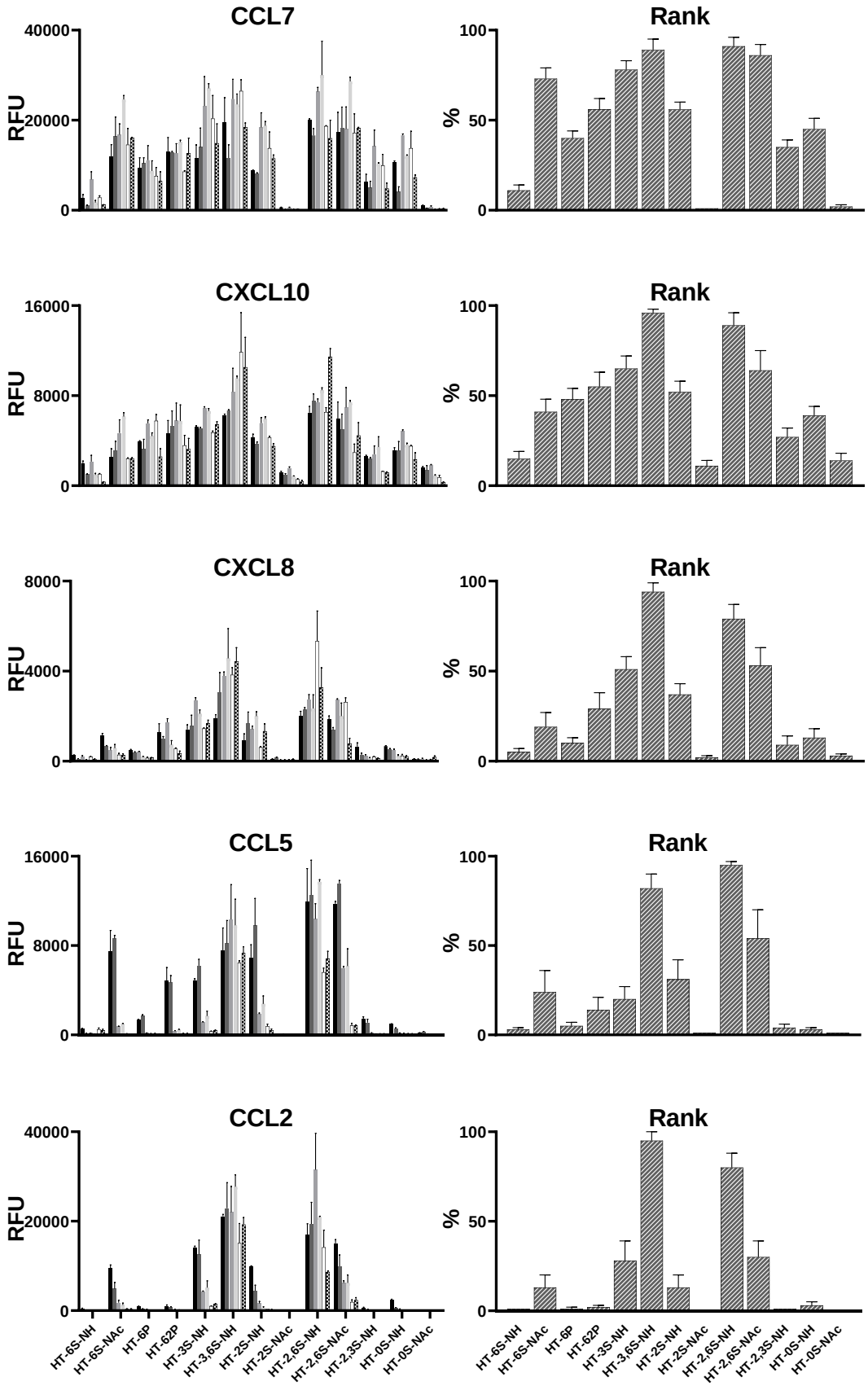
CCL7
RFU
40000
20000
0
Rank
%
100
50
0
CXCL10
16000
8000
CXCL8
4000
CCL5
CCL2
HT-6S-NH
HT-6S-NAc
HT-6P
HT-62P
HT-3S-NH
HT-3,6S-NH
HT-2S-NH
HT-2S-NAc
HT-2,6S-NH
HT-2,6S-NAc
HT-2,3S-NH
HT-0S-NH
HT-0S-NAc

**Figure 4.** Chemokine glycan microarray binding assay. Binding was tested at 3 serial dilutions across 2 glycan concentrations (High, medium and low chemokine concentration at 50µM and 100µM glycan concentration on the array), then detected with the relevant biotinylated secondary antibody (1 µg/ml) followed by Cy3-Strepavidin (1.5 µg/ml) (**Table 1**). Arrays were scanned, relative fluorescent units (RFU) obtained, and maximum RFU determined and set as 100% binding. Then rank binding (per printed glycan per concentration, per each chemokine dilution, per printed block) was determined. Since each glycans was printed at 2 concentration, 100% binding was set separately for each concentration. Then, binding to all the other glycans at the same concentration was ranked in comparison to the maximal binding, and the average rank binding and SEM for each glycan across the two glycan concentrations and three examined dilutions of each chemokine was calculated (n=6, 2 glycan concentrations across 3 chemokine dilutions). This analysis allowed to compare the glycan binding profiles of the different chemokines and dissect their binding preferences. The mean rank is shown as a heatmap of all the examined binding assays together (red highest, blue lowest and white 50$^{th}$ percentile of ranking).

## 2.4.4 Surface Plasmon Resonance binding kinetics.

HS tetrasaccharides (**HT-2,6S-NH** or **HT-3,6S-NH**) were immobilized on CM5 sensor surface using a coupling reaction. A known concentration of chemokines were injected in HBS-EP buffer at a flow rate of 50 µl/min at 25 º C for 200 sec followed by followed by running buffer (HBS-EP without chemokine) was then flowed for another 100 sec to enable dissociation. The CM5 chip was regenerated by washing with 0.1% SDS and 0.085% $H_3PO_4$ injected for 3 min at a flow rate of 100 µL/min. Kinetic analysis was executed using the BIAevaluation software for T100. $K_{off}$ and $K_{on}$ phase was globally fitted to a simple 1:1 interaction model.

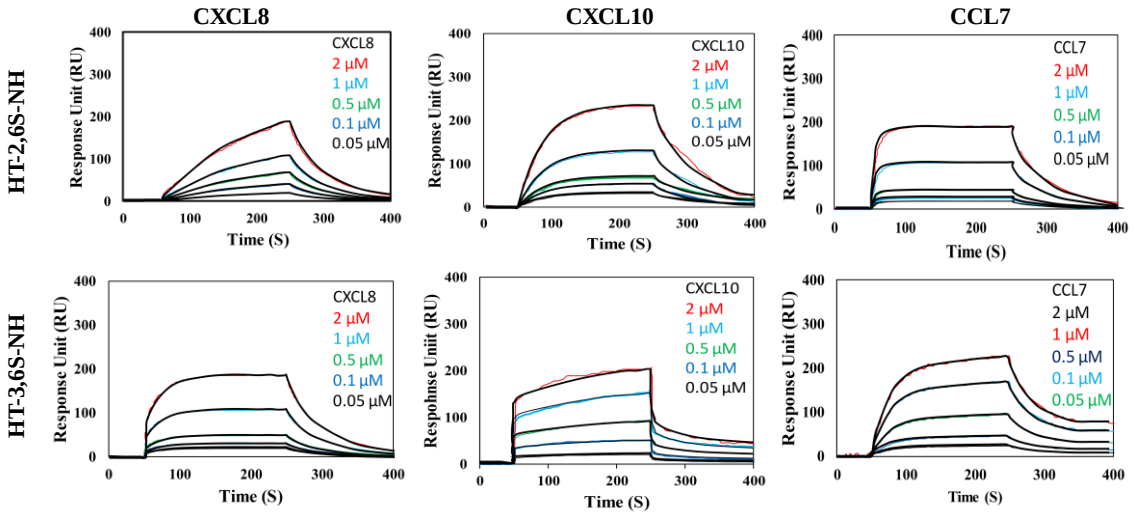

**Figure 5.** SPR analysis of chemokine binding profile on sensor chip having HT-2,6S-NH and HT-3,6S-NH ligands: (a) (b) & (c) SPR binding analysis of the interaction between HT-2,6S-NH with CXCL8, CXCL10 and CCL7 respectively. Concentrations of chemokine were 0.05–2 µM. A global fit according to a 1:1 binding model was applied (black curves); (d), (e) & (f) SPR binding analysis of the interaction between HT-3,6S-NH with CXCL8, CXCL10 and CCL7 respectively.

**Table 2: SPR analysis of kinetic rate constants and equilibrium affinities for HS lligands binding to chemokines**.

| Substrate | Chemokines | $K_D$ (µM) | $K_{on}$ ($M^{-1}S^{-1}$) | $K_{off}$ ($s^{-1}$) |
|---|---|---|---|---|
| HT-2,6S-NH | CXCL8 | 15.93 ± 0.23 | $1.23 \pm 0.17 \times 10^4$ | $1.96 \pm 0.29 \times 10^{-1}$ |
| | CXCL10 | 10.7 ± 0.37 | $2.07 \pm 0.26 \times 10^4$ | $2.24 \pm 0.35 \times 10^{-1}$ |
| | CCL7 | 11.51 ± 0.17 | $1.96 \pm 0.22 \times 10^4$ | $2.25 \pm 0.29 \times 10^{-1}$ |
| | CCL5 | 2.34 ± 0.44 | $9.15 \pm 0.34 \times 10^4$ | $2.14 \pm 0.48 \times 10^{-1}$ |
| | CCL2 | 9.82 ± 0.18 | $2.07 \pm 0.13 \times 10^4$ | $2.03 \pm 0.17 \times 10^{-1}$ |
| HT-3,6S-NH | CXCL8 | 11.67 ± 0.17 | $1.87 \pm 0.22 \times 10^4$ | $2.18 \pm 0.28 \times 10^{-1}$ |
| | CXCL10 | 11.02 ± 0.37 | $1.53 \pm 0.26 \times 10^4$ | $1,69 \pm 0.33 \times 10^{-1}$ |
| | CCL7 | 11.3 ± 0.18 | $2.53 \pm 0.15 \times 10^4$ | $2.86 \pm 0.21 \times 10^{-1}$ |
| | CCL5 | 6.81 ± 0.33 | $4.37 \pm 0.31 \times 10^4$ | $2.98 \pm 0.31 \times 10^{-1}$ |
| | CCL2 | 1.89 ± 0.24 | $11.17 \pm 0.32 \times 10^4$ | $2.11 \pm 0.34 \times 10^{-1}$ |

### 2.4.5 CCR2 expression level.

MCF-7 cells were seeded on 6 well plate in RPMI-1640 medium in 1% FBS. Approximately $10^4$ cells were transferred to FACS tubes and incubated with primary murine Anti-CCR2 antibody (2 µl) for half hour, followed by FITC tagged secondary antibody. The fluorescent channel FL-2 was used to quantify CCR2 expression level on MCF-7 cells.

### 2.4.6 Cell proliferation assay.

Approximately $10^4$ MCF-7 were feeded on 96-well plates in a RPMI-1640 medium in 1% FBS. Then, HS tetrasaccharide (**HT-3,6S-NH**, 10 or 50 µg/ml) and native heparin (10 or 50 µg/ml) were mixed with CCL2 (50 ng) and added to the cells. After 72 h of incubation, cell were fixed with paraformaldehyde and stained with 4% sulforhodamine B in 1% acetic

acid for 30 min. Cell proliferation was quantified with 2-(4-iodophenyl)-3-(4-nitrophenyl)-5-(2,4-disulfophenyl)- 2H-tetrazolium monosodium salt at 450 nm.

### 2.4.7 Cell-division cycle analysis.

Chemokines and **HT-3,6S-NH** treated MCF-7 cells were harvested and fixed with 70 % ethanol at -20 °C for 12 h. The fixed cells were incubated with propidium iodide (5 µg/mL) and RNase (10 µg/mL) for 30 min at RT. Using flow cytometer stained cells were quantified. The DNA content in the cell phases was quantified by using ModFitLT version 3.0 software.

### 2.4.8 Wound healing assay

MCF-7 cells were seeded on 24-well plat and cell monolayer was generated, Then, by using 1000 µl pipette tip wound was created. Cells were treated with native heparin and **HT-3,6S-NH** (50 µg/ml) with CCL2 (50 ng). It was observed that CCL2 treated monolayer showed complete wound healing after 8 h. At that point, percentage of cell migration distance of **HT-3,6S-NH,** heparin and control cells were quantified.

### 2.4.9 Cell invasion assay.

Boyden chamber cell invasion assay was performed in as reported in the protocol. Briefly, the upper chamber of transwell inserts were coated with Matrigel and the bottom chamber contained RPMI-1640 medium supplemented with 1 % FBS and CCL2 (50 ng/ml) with **HT-3,6S-NH** (50 µg/ml) and heparin. MCF-7 cells were feeded to the upper chamber. After 24 h of incubation, non-invading cells were removed and lower chamber cells were fixed and stained with 0.5 % crystal violet for 30 min and cell invasion was quantified by bright field imaging

### 2.4.10 Western Blot Analysis.

MCF-7 cells were seeded on Petri dishes and CCL2 (50 ng) was added with or without **HT-3,6S-NH** (50 µg./ml) for half hr. The cells were transferred into folcon tube and pelleted. Then cell pellet was treasted with lysis buffer containing 150 mM NaCl, 1% NP-40, 0.25% sodium dodecyl sulfate (SDS), 1 mM ethylenediamine tetraacetic acid (EDTA)

and protease inhibitor, and 1 mM phenylmethane sulfonyl fluoride (PMSF) in 50 mM Tris-Cl (pH 7.4). After 1 h, mixture was centrifuge and supernatant was collected. Using Brandford method, the protein concentration was determined. Approximately 35 μg of protein was loaded on SDS-polyacrylamide gel electrophoresis (10%) and transferred onto a polyvinylidene fluoride (PVDF) membrane. Using specific antibodies corresponding to MAPK blot was developed. Finally, The membrane was incubated with horse radish peroxidase (HRP)-conjugated secondary antibody and visualization by using an Immobilon Western Chemiluminescent HRP substrate kit (Millipore Corporation, MA, USA) with GAPDH as internal standard.

## 2.5 References:


1. Mantovani, A.; Bonecchi, R.; Locati, M., Tuning inflammation and immunity by chemokine sequestration: decoys and more. *Nat. Rev. Immunol.* **2006,** *6* (12), 907-918.
2. Mackay, C. R., Chemokines: immunology's high impact factors. *Nat. Immunol.* **2001,** *2* (2), 95-101.
3. Nibbs, R. J.; Graham, G. J., Immune regulation by atypical chemokine receptors. *Nature Rev. Immunol.* **2013,** *13* (11), 815-829.
4. Moser, B.; Loetscher, P., Lymphocyte traffic control by chemokines. *Nat. Immunol.* **2001,** *2* (2), 123-128.
5. Mortier, A.; Van Damme, J.; Proost, P., Overview of the mechanisms regulating chemokine activity and availability. *Immunol. Lett.* **2012,** *145* (1-2), 2-9.
6. Jöhrer, K.; Pleyer, L.; Olivier, A.; Maizner, E.; Zelle-Rieser, C.; Greil, R., Tumour-immune cell interactions modulated by chemokines. *Expert Opin. Biol. Th.* **2008,** *8* (3), 269-290.
7. Liang, W. G.; Triandafillou, C. G.; Huang, T.-Y.; Zulueta, M. M. L.; Banerjee, S.; Dinner, A. R.; Hung, S.-C.; Tang, W.-J., Structural basis for oligomerization and glycosaminoglycan binding of CCL5 and CCL3. *Proc. Natl. Acad. Sci.* **2016,** *113* (18), 5000-5005.

8. Dyer, D. P.; Salanga, C. L.; Volkman, B. F.; Kawamura, T.; Handel, T. M., The dependence of chemokine–glycosaminoglycan interactions on chemokine oligomerization. *Glycobiology* **2016,** *26* (3), 312-326.
9. Wang, L.; Fuster, M.; Sriramarao, P.; Esko, J. D., Endothelial heparan sulfate deficiency impairs L-selectin-and chemokine-mediated neutrophil trafficking during inflammatory responses. *Nat. Immunol.* **2005,** *6* (9), 902-910.
10. Parish, C. R., The role of heparan sulphate in inflammation. *Nature Rev. Immunol.* **2006,** *6* (9), 633-643.
11. Proudfoot, A. E.; Handel, T. M.; Johnson, Z.; Lau, E. K.; LiWang, P.; Clark-Lewis, I.; Borlat, F.; Wells, T. N.; Kosco-Vilbois, M. H., Glycosaminoglycan binding and oligomerization are essential for the in vivo activity of certain chemokines. *Proc. Natl. Acad. Sci. USA.* **2003,** *100* (4), 1885-1890.
12. Johnson, Z.; Proudfoot, A.; Handel, T., Interaction of chemokines and glycosaminoglycans: a new twist in the regulation of chemokine function with opportunities for therapeutic intervention. *Cytokine Growth Factor Rev.* **2005,** *16* (6), 625-636.
13. Sepuru, K. M.; Rajarathnam, K., Structural basis of chemokine interactions with heparan sulfate, chondroitin sulfate, and dermatan sulfate. *J. Biol. Chem.* **2019,** *294* (43), 15650-15661.
14. Stringer, S. E.; Gallagher, J. T., Specific binding of the chemokine platelet factor 4 to heparan sulfate. *J. Biol. Chem.* **1997,** *272* (33), 20508-20514.
15. Spillmann, D.; Witt, D.; Lindahl, U., Defining the interleukin-8-binding domain of heparan sulfate. *J. Biol. Chem.* **1998,** *273* (25), 15487-15493.
16. Jayson, G. C.; Hansen, S. U.; Miller, G. J.; Cole, C. L.; Rushton, G.; Avizienyte, E.; Gardiner, J. M., Synthetic heparan sulfate dodecasaccharides reveal single sulfation site interconverts CXCL8 and CXCL12 chemokine biology. *Chem. Comm.* **2015,** *51* (72), 13846-13849.
17. Sheng, G. J.; Oh, Y. I.; Chang, S.-K.; Hsieh-Wilson, L. C., Tunable heparan sulfate mimetics for modulating chemokine activity. *J. Am. Chem. Soc.* **2013,** *135* (30), 10898-10901.

18. de Paz, J. L.; Moseman, E. A.; Noti, C.; Polito, L.; von Andrian, U. H.; Seeberger, P. H., Profiling heparin–chemokine interactions using synthetic tools. *ACS Chem. Biol.* **2007,** *2* (11), 735-744.
19. Zong, C.; Venot, A.; Li, X.; Lu, W.; Xiao, W.; Wilkes, J.-S. L.; Salanga, C. L.; Handel, T. M.; Wang, L.; Wolfert, M. A., Boons, G. J., Heparan sulfate microarray reveals that heparan sulfate–protein binding exhibits different ligand requirements. *J. Am. Chem.Soc.* **2017,** *139* (28), 9534-9543.
20. Toida, T.; Yoshida, H.; Toyoda, H.; Koshiishi, I.; Imanari, T.; Hileman, R. E.; Fromm, J. R.; Linhardt, R. J., Structural differences and the presence of unsubstituted amino groups in heparan sulphates from different tissues and species. *Biochem. J.* **1997,** *322* (2), 499-506.
21. Westling, C.; Lindahl, U., Location of N-unsubstituted glucosamine residues in heparan sulfate. *J. Biol. Chem.* **2002,** *277* (51), 49247-49255.
22. Vanpouille, C.; Deligny, A.; Delehedde, M.; Denys, A.; Melchior, A.; Liénard, X.; Lyon, M.; Mazurier, J.; Fernig, D. G.; Allain, F., The heparin/heparan sulfate sequence that interacts with cyclophilin B contains a 3-O-sulfated N-unsubstituted glucosamine residue. *J. Biol. Chem.* **2007,** *282* (33), 24416-24429.
23. Wei, Z.; Lyon, M.; Gallagher, J. T., Distinct substrate specificities of bacterial heparinases against N-unsubstituted glucosamine residues in heparan sulfate. *J. Biol. Chem.* **2005,** *280* (16), 15742-15748.
24. Wei, Z.; Deakin, J. A.; Blaum, B. S.; Uhrín, D.; Gallagher, J. T.; Lyon, M., Preparation of heparin/heparan sulfate oligosaccharides with internal N-unsubstituted glucosamine residues for functional studies. *Glycoconj. J.* **2011,** *28* (8-9), 525-535.
25. Koenig, A.; Norgard-Sumnicht, K.; Linhardt, R.; Varki, A., Differential interactions of heparin and heparan sulfate glycosaminoglycans with the selectins. Implications for the use of unfractionated and low molecular weight heparins as therapeutic agents. *J. Clin. Invest.* **1998,** *101* (4), 877-889.
26. Norgard-Sumnicht, K.; Varki, A., Endothelial heparan sulfate proteoglycans that bind to L-selectin have glucosamine residues with unsubstituted amino groups. *J. Biol. Chem.* **1995,** *270* (20), 12012-12024.

27. Mende, M.; Bednarek, C.; Wawryszyn, M.; Sauter, P.; Biskup, M. B.; Schepers, U.; Bräse, S., Chemical synthesis of glycosaminoglycans. *Chem. Rev.* **2016,** *116* (14), 8193-8255.
28. Hu, Y.-P.; Zhong, Y.-Q.; Chen, Z.-G.; Chen, C.-Y.; Shi, Z.; Zulueta, M. M. L.; Ku, C.-C.; Lee, P.-Y.; Wang, C.-C.; Hung, S.-C., Divergent synthesis of 48 heparan sulfate-based disaccharides and probing the specific sugar–fibroblast growth factor-1 interaction. *J. Am. Chem. Soc.* **2012,** *134* (51), 20722-20727.
29. Hansen, S. U.; Miller, G. J.; Jayson, G. C.; Gardiner, J. M., First gram-scale synthesis of a heparin-related dodecasaccharide. *Org. Lett.* **2013,** *15* (1), 88-91.
30. Arungundram, S.; Al-Mafraji, K.; Asong, J.; Leach III, F. E.; Amster, I. J.; Venot, A.; Turnbull, J. E.; Boons, G.-J., Modular synthesis of heparan sulfate oligosaccharides for structure− activity relationship studies. *J. Am. Chem. Soc.* **2009,** *131* (47), 17394-17405.
31. Noti, C.; de Paz, J. L.; Polito, L.; Seeberger, P. H., Preparation and use of microarrays containing synthetic heparin oligosaccharides for the rapid analysis of heparin–protein interactions. *Chem. Eur. J.* **2006,** *12* (34), 8664-8686.
32. Shanthamurthy, C. D.; Kikkeri, R., Linear Synthesis of De novo Oligo-Iduronic Acid. *Eur. J. Org. Chem.* **2019,** *2019* (18), 2950-2953.
33. Padler-Karavani, V.; Song, X.; Yu, H.; Hurtado-Ziola, N.; Huang, S.; Muthana, S.; Chokhawala, H. A.; Cheng, J.; Verhagen, A.; Langereis, M. A., Cross-comparison of protein recognition of sialic acid diversity on two novel sialoglycan microarrays. *J. Biol. Chem.* **2012,** *287* (27), 22593-22608.
34. Ben-Arye, S. L.; Yu, H.; Chen, X.; Padler-Karavani, V., Profiling anti-Neu5Gc IgG in human sera with a sialoglycan microarray assay. *J. Vis. Exp.* **2017,** (125), e56094.
35. Pettersen, E. F.; Goddard, T. D.; Huang, C. C.; Couch, G. S.; Greenblatt, D. M.; Meng, E. C.; Ferrin, T. E., UCSF Chimera—a visualization system for exploratory research and analysis. *J. Comput. Chem.* **2004,** *25* (13), 1605-1612.
36. Singh, A.; Kett, W. C.; Severin, I. C.; Agyekum, I.; Duan, J.; Amster, I. J.; Proudfoot, A. E.; Coombe, D. R.; Woods, R. J., The interaction of heparin

tetrasaccharides with chemokine CCL5 is modulated by sulfation pattern and pH. *J. Biol. Chem.* **2015,** *290* (25), 15421-15436.

37. Lu, Y.; Cai, Z.; Xiao, G.; Liu, Y.; Keller, E. T.; Yao, Z.; Zhang, J., CCR2 expression correlates with prostate cancer progression. *J. Cellular Biochem.,* **2007,** *101* (3), 676-685.
38. Dutta, P.; Sarkissyan, M.; Paico, K.; Wu, Y.; Vadgama, J. V., MCP-1 is overexpressed in triple-negative breast cancers and drives cancer invasiveness and metastasis. *Breast Cancer Res. Treat.,* **2018,** *170* (3), 477-486.

# 2.6 NMR Spectra

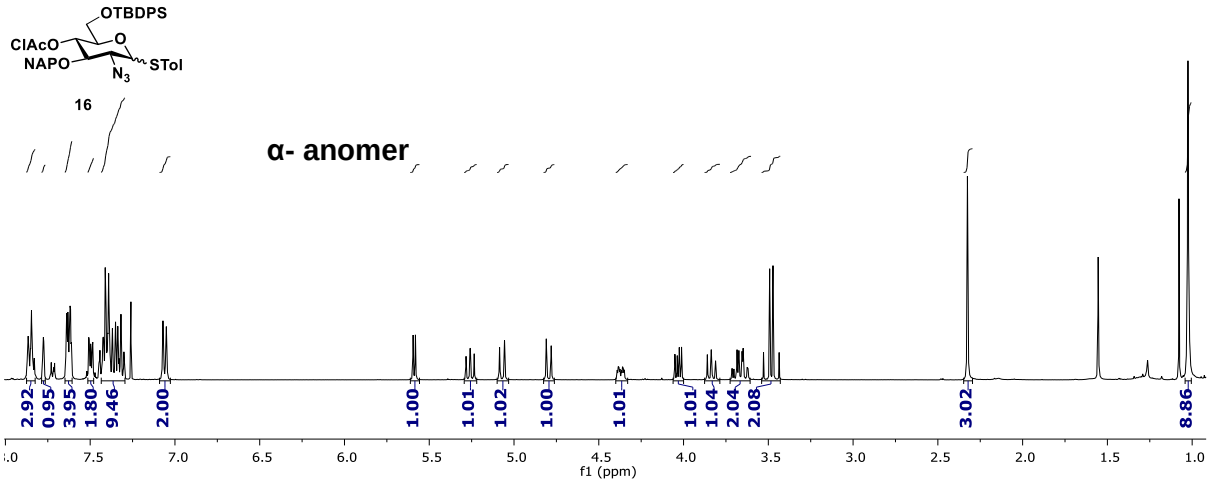


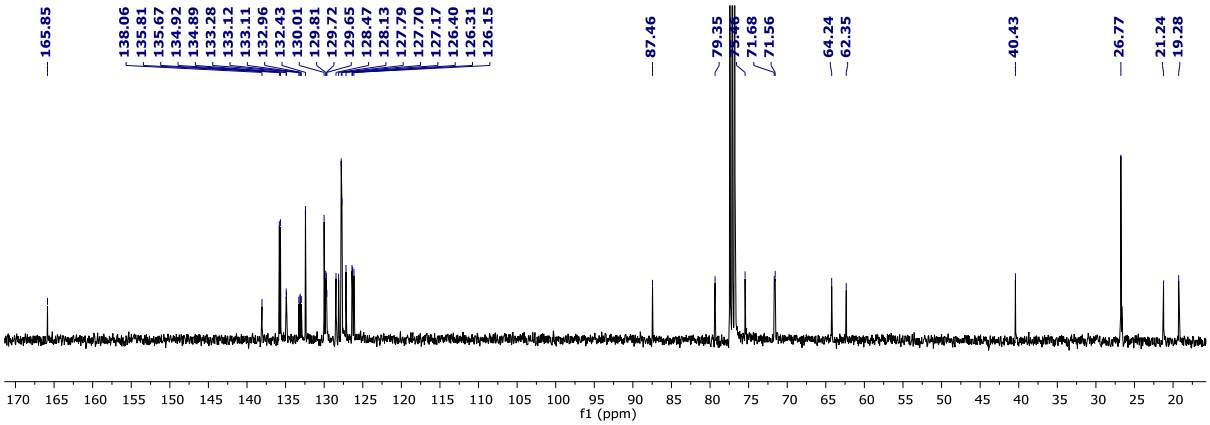


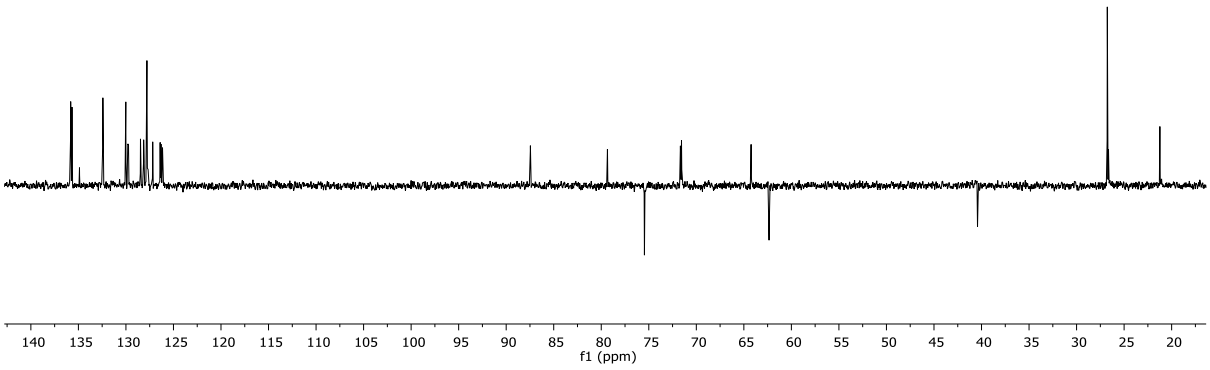

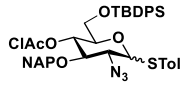
OTBDPS
ClAcO
O
NAPO
N3
STol

16

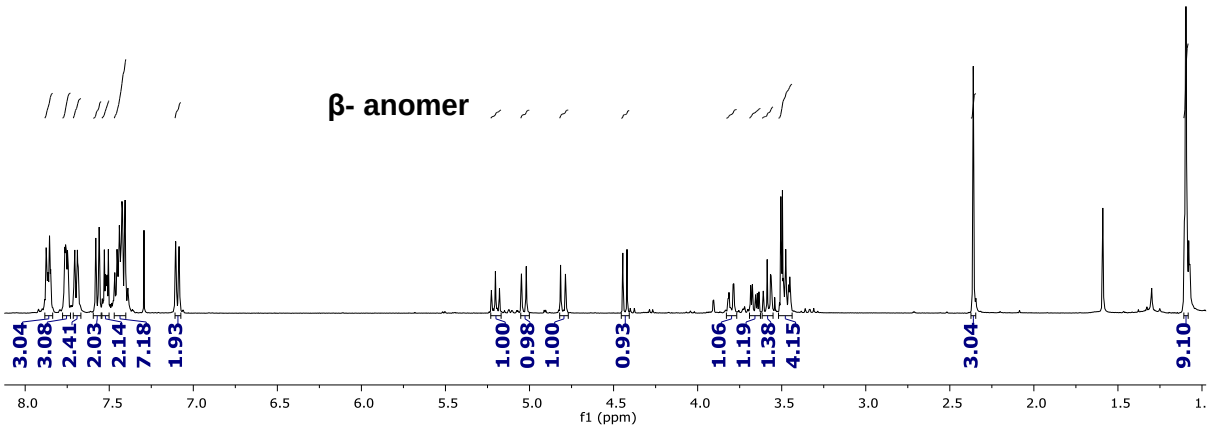
β- anomer
3.04
3.08
2.41
2.03
2.14
7.18
1.93
1.00
0.98
1.00
0.93
1.06
1.19
1.38
4.15
3.04
9.10
f1 (ppm)

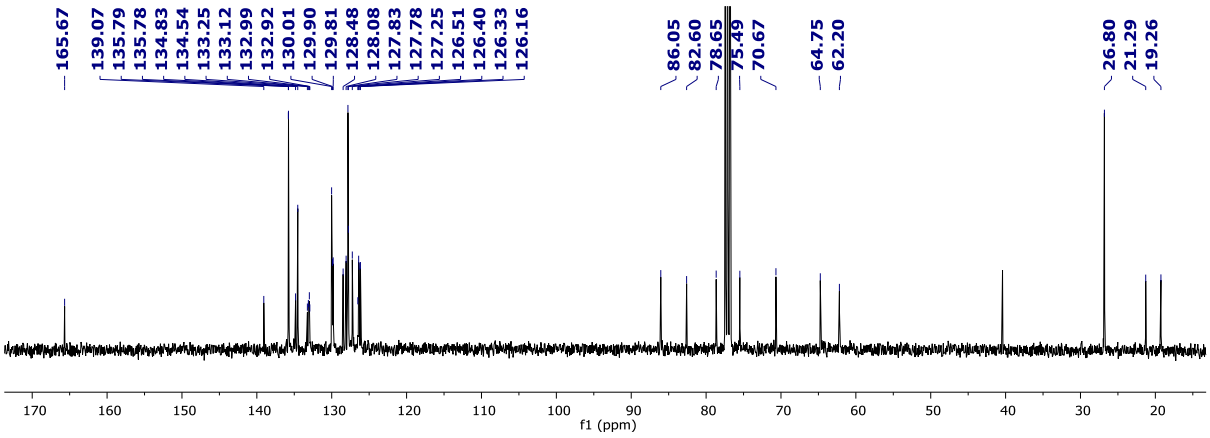
165.67
139.07
135.79
135.78
134.83
134.54
133.25
133.12
132.99
132.92
130.01
129.90
129.81
128.48
128.08
127.83
127.78
127.25
126.51
126.40
126.33
126.16
86.05
82.60
78.65
75.49
70.67
64.75
62.20
26.80
21.29
19.26
f1 (ppm)

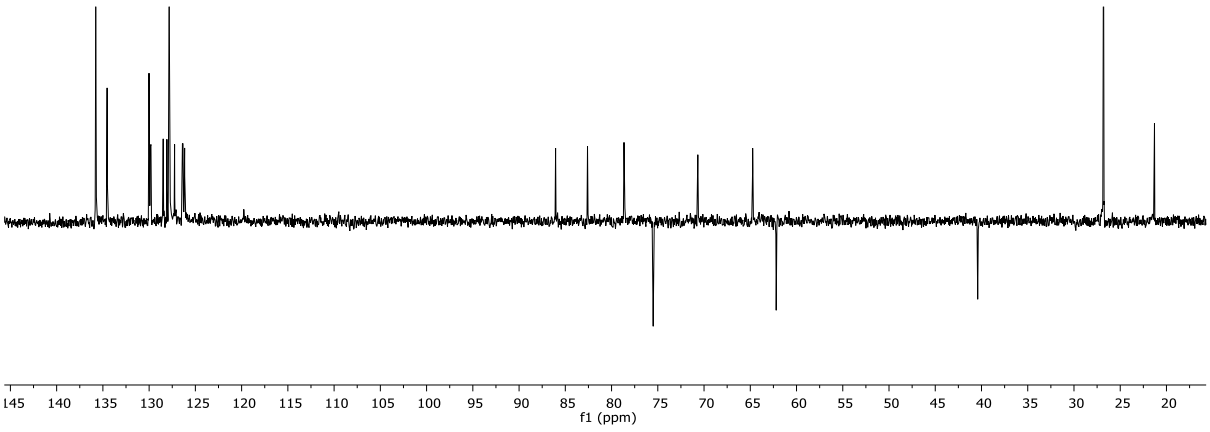
f1 (ppm)

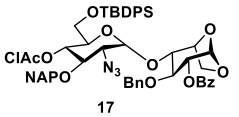
OTBDPS
O
ClAcO
NAPO
N3
O
BnO
O
OBz
O

17

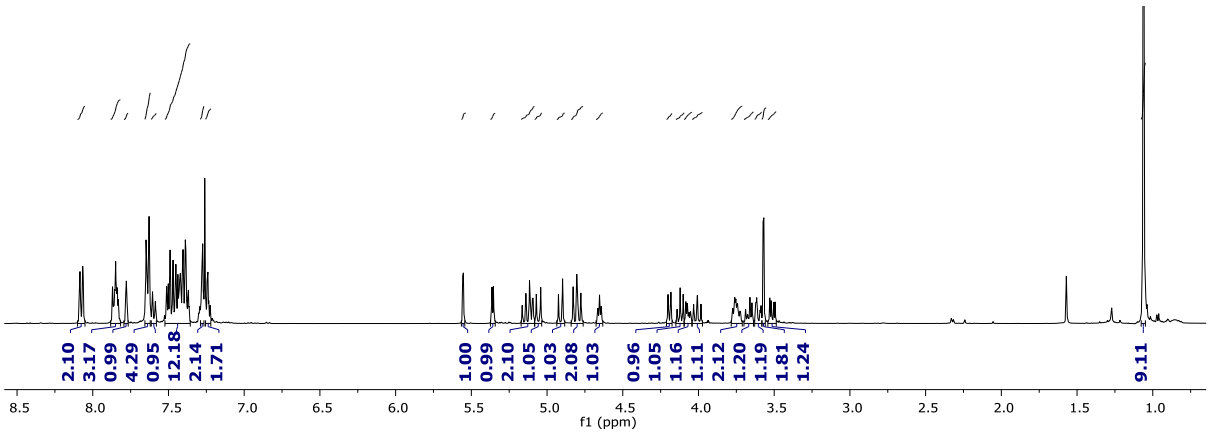
2.10 3.17 0.99 4.29 0.95 12.18 2.14 1.71
1.00 0.99 2.10 1.05 1.03 2.08 1.03
0.96 1.05 1.16 1.11 2.12 1.20 1.19 1.81 1.24
9.11
f1 (ppm)

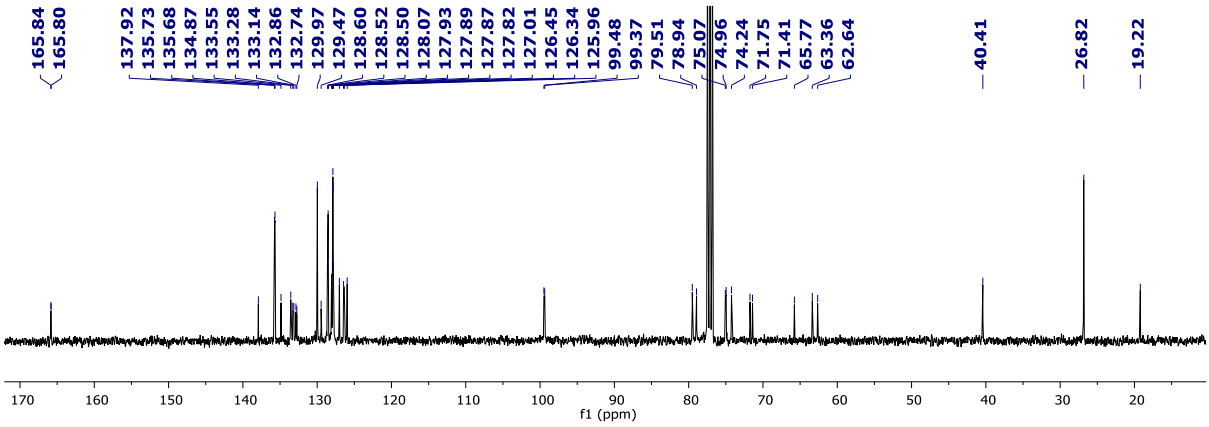
165.84 165.80
137.92 135.73 135.68 134.87 133.55 133.28 133.14 132.86 132.74 129.97 129.47 128.60 128.52 128.50 128.07 127.93 127.89 127.87 127.82 127.01 126.45 126.34 125.96 99.48 99.37 79.51 78.94 75.07 74.96 74.24 71.75 71.41 65.77 63.36 62.64
40.41
26.82
19.22
f1 (ppm)

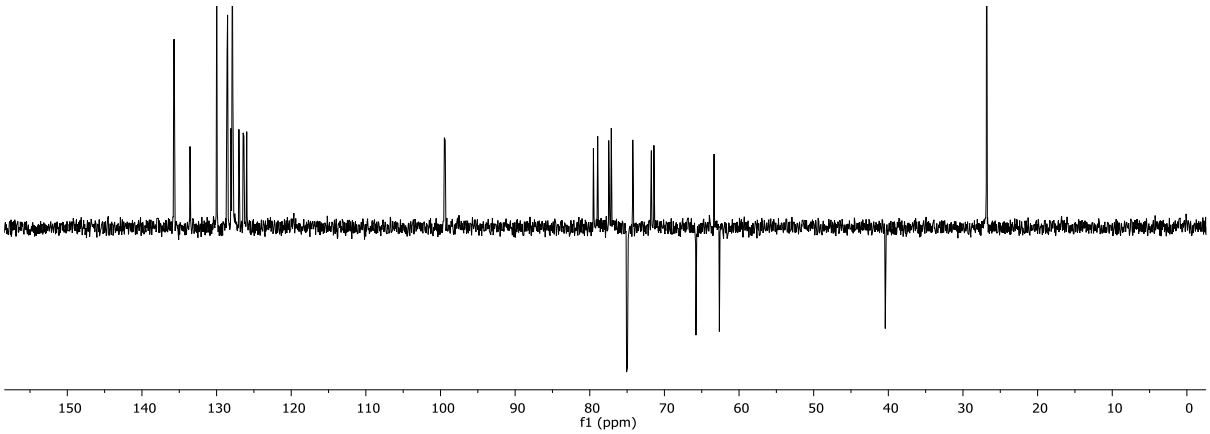
f1 (ppm)

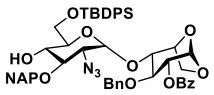
OTBDPS
HO
NAPO
N3
BnO
OBz

18

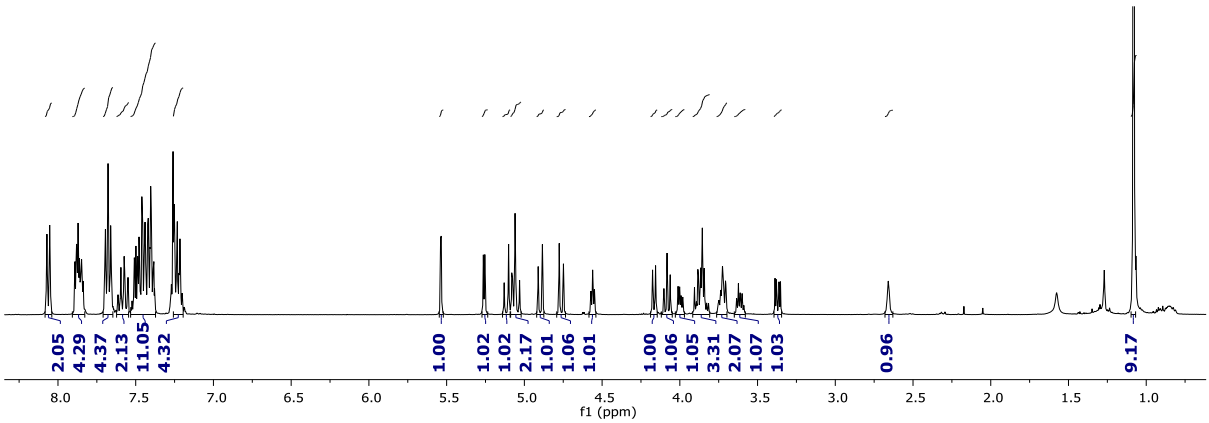
2.05
4.29
4.37
2.13
11.05
4.32
1.00
1.02
1.02
2.17
1.01
1.06
1.01
1.00
1.06
1.05
3.31
2.07
1.07
1.03
0.96
9.17
f1 (ppm)

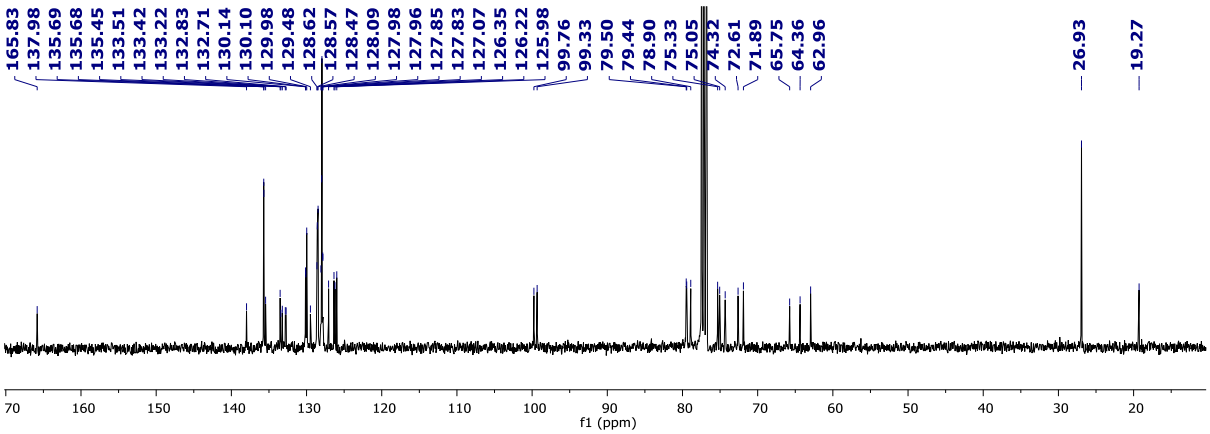
165.83
137.98
135.69
135.68
135.45
133.51
133.42
133.22
132.83
132.71
130.14
130.10
129.98
129.48
128.62
128.57
128.47
128.09
127.98
127.96
127.85
127.83
127.07
126.35
126.22
125.98
99.76
99.33
79.50
79.44
78.90
75.33
75.05
74.32
72.61
71.89
65.75
64.36
62.96
26.93
19.27
f1 (ppm)

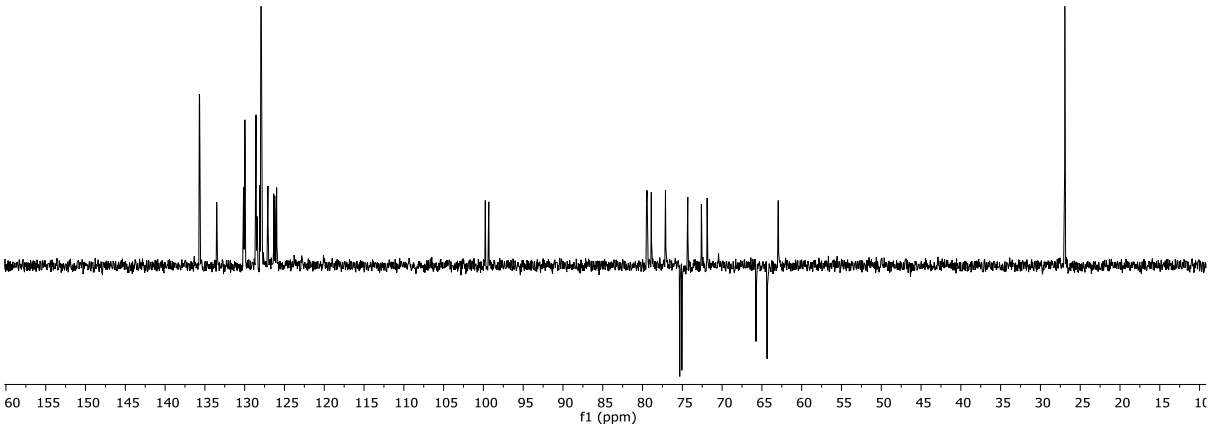
f1 (ppm)

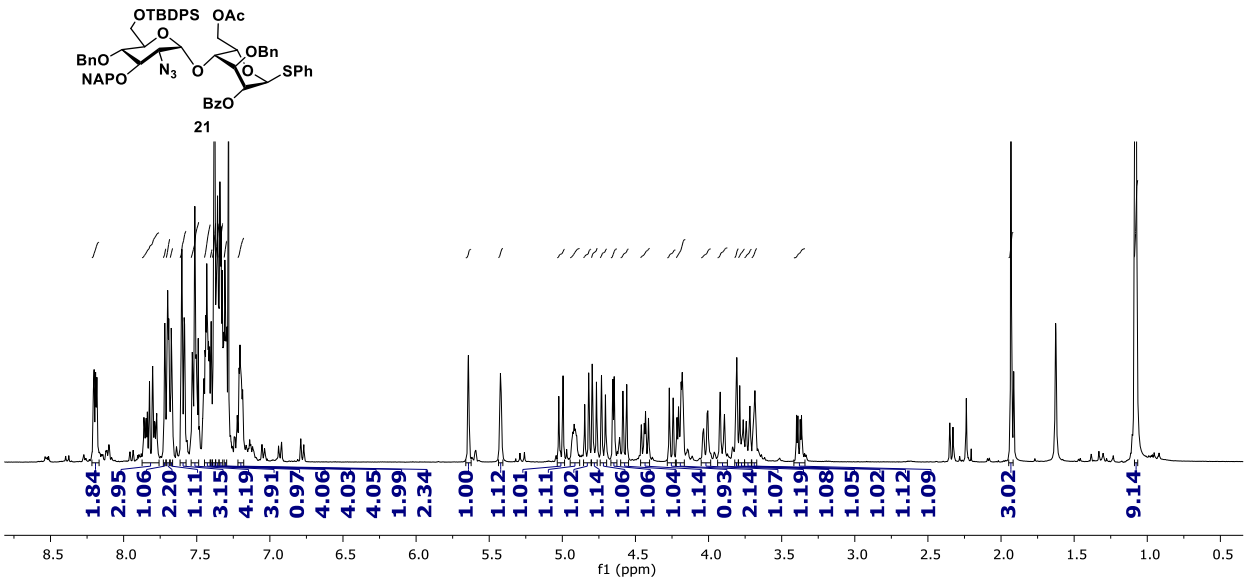
OTBDPS
OAc
BnO
NAPO
N3
O
OBn
O
SPh
BzO
21
1.84 2.95 1.06 2.20 1.11 3.15 4.19 3.91 0.97 4.06 4.03 4.05 1.99 2.34 1.00 1.12 1.01 1.11 1.02 1.14 1.06 1.06 1.04 1.14 0.93 2.14 1.07 1.19 1.08 1.05 1.02 1.12 1.09 3.02 9.14
8.5 8.0 7.5 7.0 6.5 6.0 5.5 5.0 4.5 4.0 3.5 3.0 2.5 2.0 1.5 1.0 0.5
f1 (ppm)

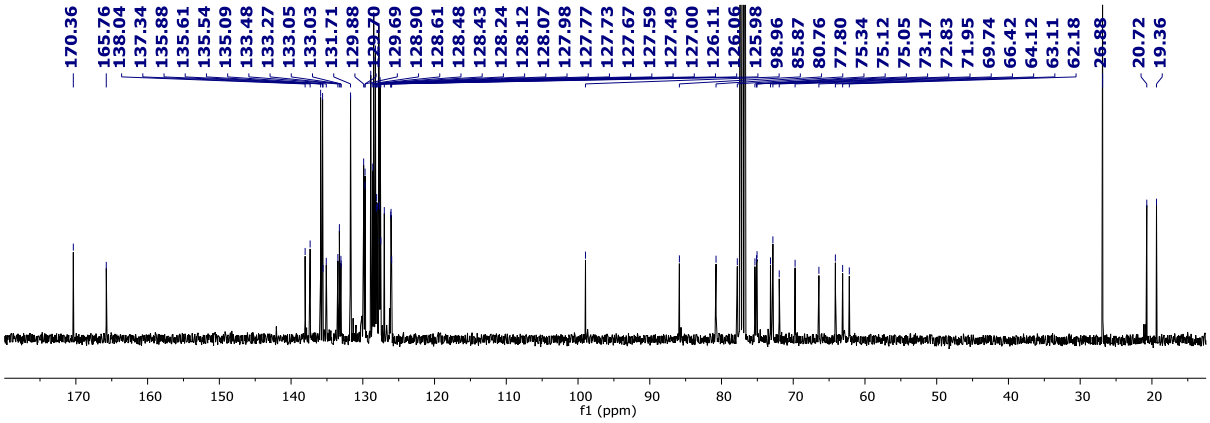
170.36 165.76 138.04 137.34 135.88 135.61 135.54 135.09 133.48 133.27 133.05 133.03 131.71 129.88 129.70 129.69 128.90 128.61 128.48 128.43 128.24 128.12 128.07 127.98 127.77 127.73 127.67 127.59 127.49 127.00 126.11 126.06 125.98 98.96 85.87 80.76 77.80 75.34 75.12 75.05 73.17 72.83 71.95 69.74 66.42 64.12 63.11 62.18 26.88 20.72 19.36
170 160 150 140 130 120 110 100 90 80 70 60 50 40 30 20
f1 (ppm)

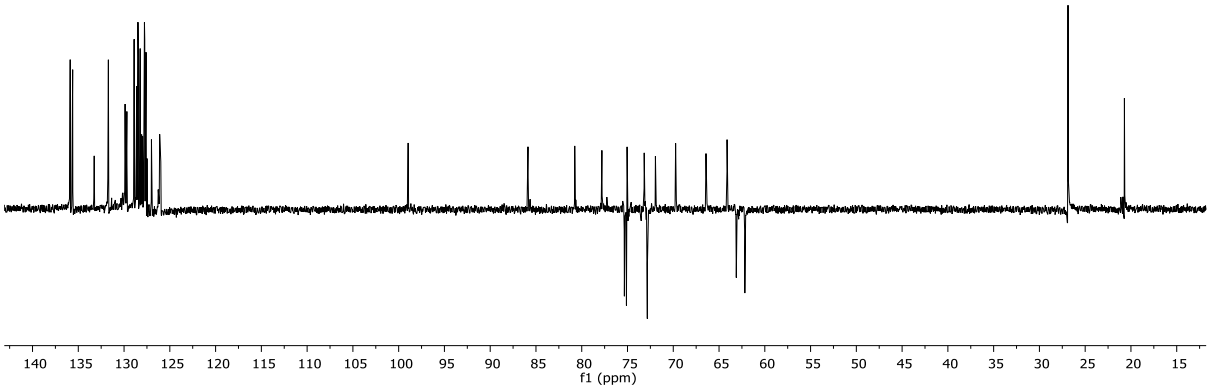
140 135 130 125 120 115 110 105 100 95 90 85 80 75 70 65 60 55 50 45 40 35 30 25 20 15
f1 (ppm)

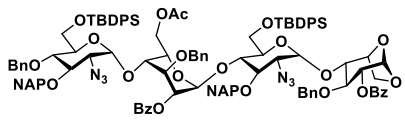
OTBDPS
OAc
OTBDPS
BnO
NAPO
OBn
NAPO
BnO
OBz
BzO

22

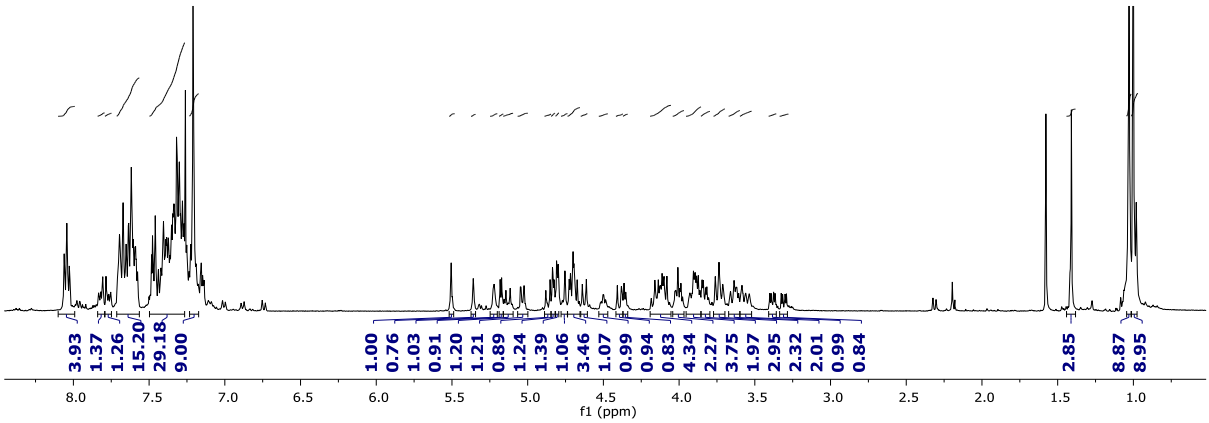
3.93 1.37 1.26 15.20 29.18 9.00 1.00 0.76 1.03 0.91 1.20 1.21 0.89 1.24 1.39 1.06 3.46 1.07 0.99 0.94 0.83 4.34 2.27 3.75 1.97 2.95 2.32 2.01 0.99 0.84 2.85 8.87 8.95
f1 (ppm)

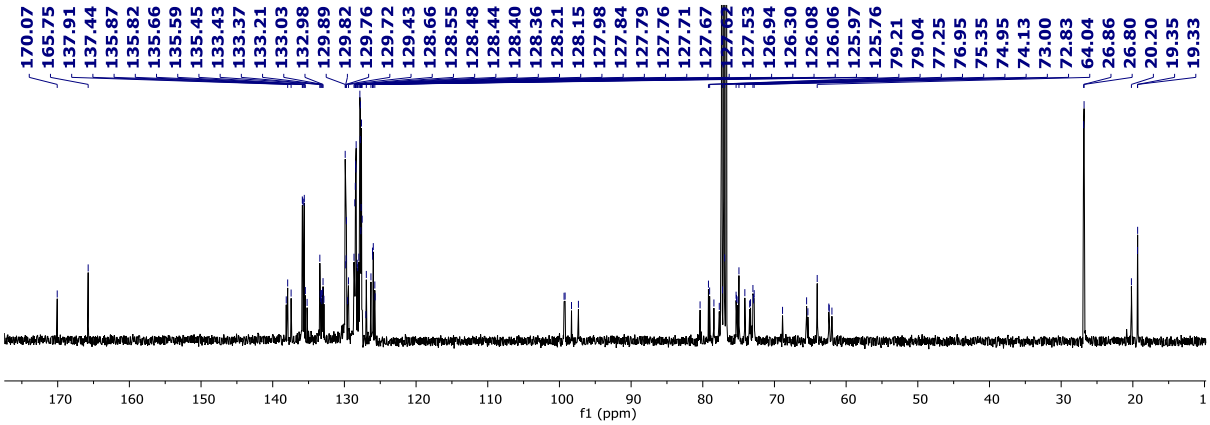
170.07 165.75 137.91 137.44 135.87 135.82 135.66 135.59 135.45 133.43 133.37 133.21 133.03 132.98 129.89 129.82 129.76 129.72 129.43 128.66 128.55 128.48 128.44 128.40 128.36 128.21 128.15 127.98 127.84 127.79 127.76 127.71 127.67 127.07 127.53 126.94 126.30 126.08 126.06 125.97 125.76 79.21 79.04 77.25 76.95 75.35 74.95 74.13 73.00 72.83 64.04 26.86 26.80 20.20 19.35 19.33
f1 (ppm)

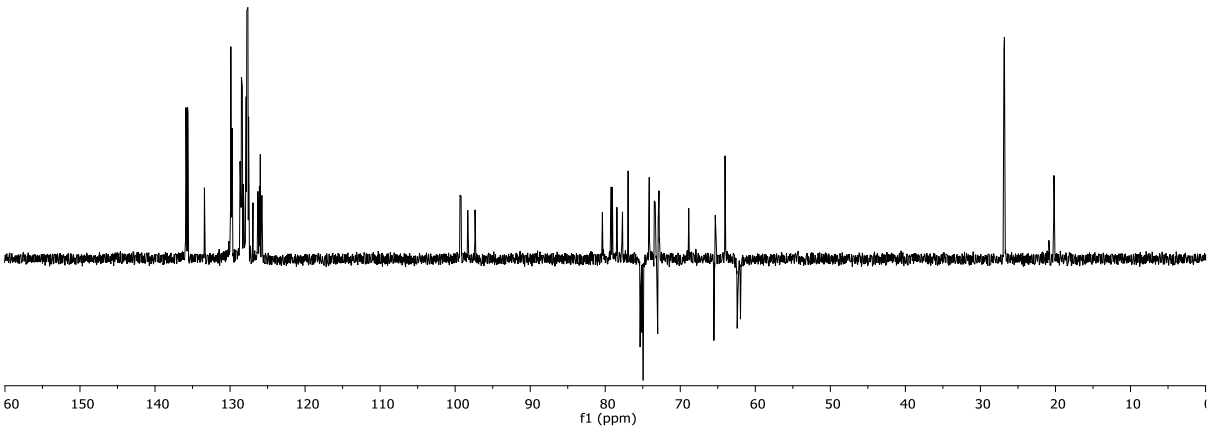
f1 (ppm)

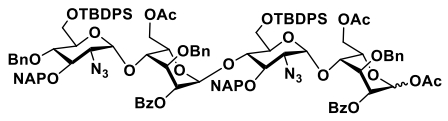
OTBDPS
OAc
BnO
NAPO
N3
O
OBn
BzO
OTBDPS
OAc
NAPO
N3
OBn
OAc
BzO

23

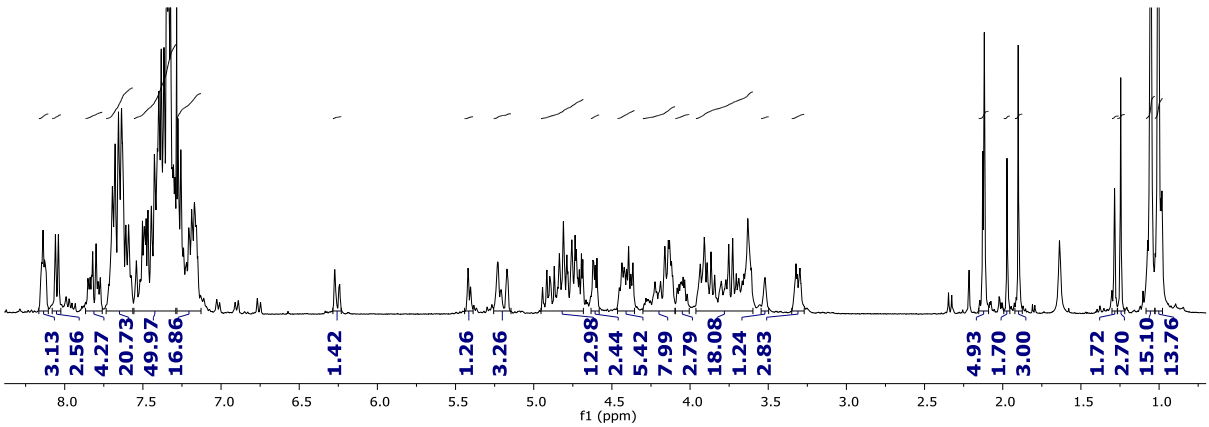
3.13
2.56
4.27
20.73
49.97
16.86
1.42
1.26
3.26
12.98
2.44
5.42
7.99
2.79
18.08
1.24
2.83
4.93
1.70
3.00
1.72
2.70
15.10
13.76
8.0
7.5
7.0
6.5
6.0
5.5
5.0
4.5
4.0
3.5
3.0
2.5
2.0
1.5
1.0
f1 (ppm)

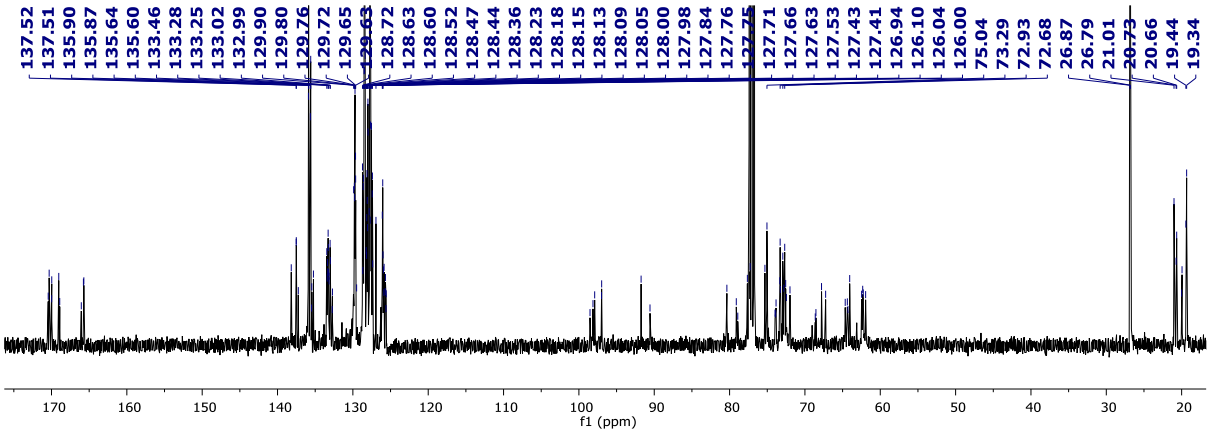
137.52
137.51
135.90
135.87
135.64
135.60
133.46
133.28
133.25
133.02
132.99
129.90
129.80
129.76
129.72
129.65
129.63
128.72
128.63
128.60
128.52
128.47
128.44
128.36
128.23
128.18
128.15
128.13
128.09
128.05
128.00
127.98
127.84
127.76
127.75
127.71
127.66
127.63
127.53
127.43
127.41
126.94
126.10
126.04
126.00
75.04
73.29
72.93
72.68
26.87
26.79
21.01
20.73
20.66
19.44
19.34
170
160
150
140
130
120
110
100
90
80
70
60
50
40
30
20
f1 (ppm)

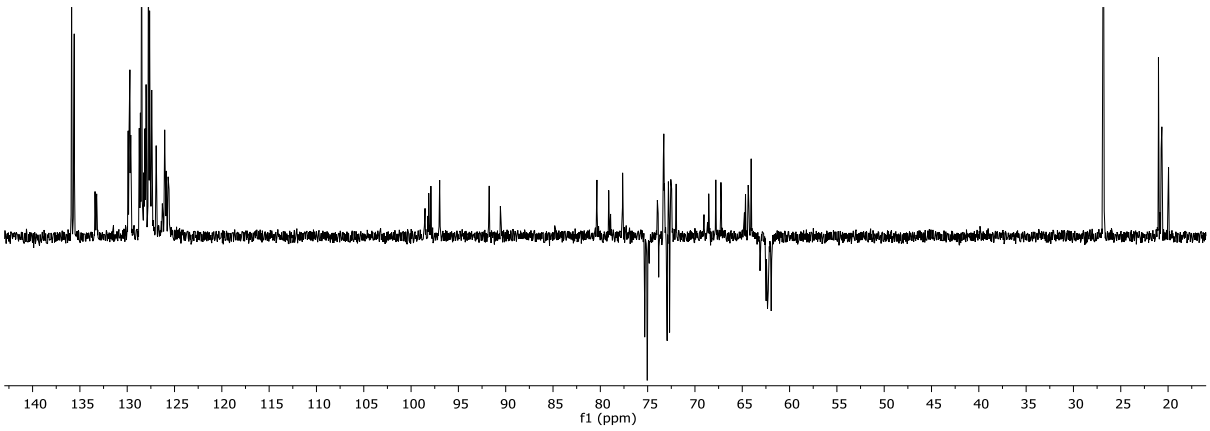
140
135
130
125
120
115
110
105
100
95
90
85
80
75
70
65
60
55
50
45
40
35
30
25
20
f1 (ppm)

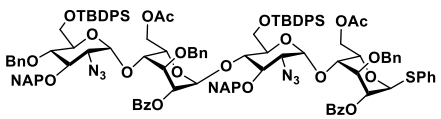
OTBDPS
OAc
BnO
NAPO
OBn
BzO
OTBDPS
OAc
NAPO
OBn
SPh
BzO

24

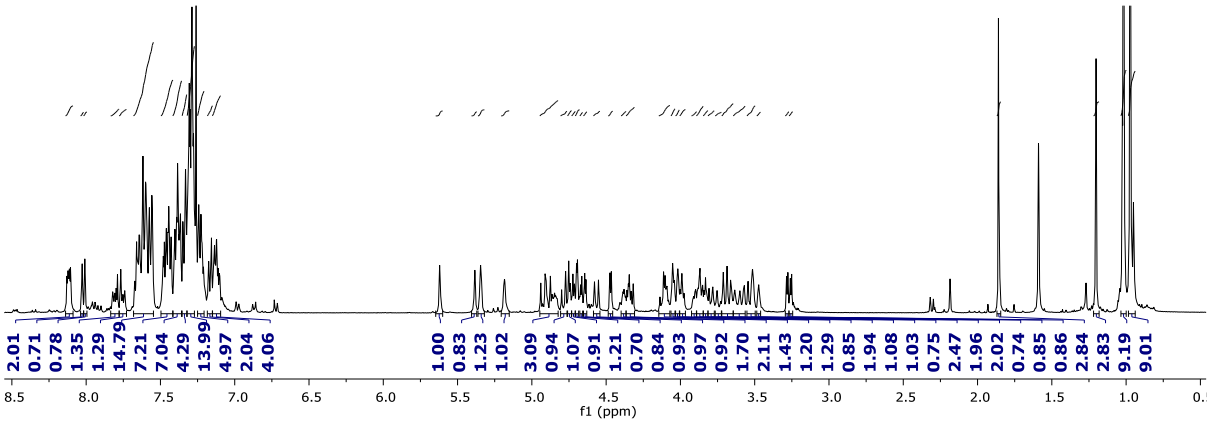
2.01 0.71 0.78 1.35 1.29 14.79 7.21 7.04 4.29 13.99 4.97 2.04 4.06
1.00 0.83 1.23 1.02 3.09 0.94 1.07 0.91 1.21 0.70 0.84 0.93 0.97 0.92 1.70 2.11 1.43 1.20 1.29 0.85 1.94 1.08 1.03 0.75 2.47 1.96 2.02 0.74 0.85 0.86 2.84 2.83 9.19 9.01
f1 (ppm)

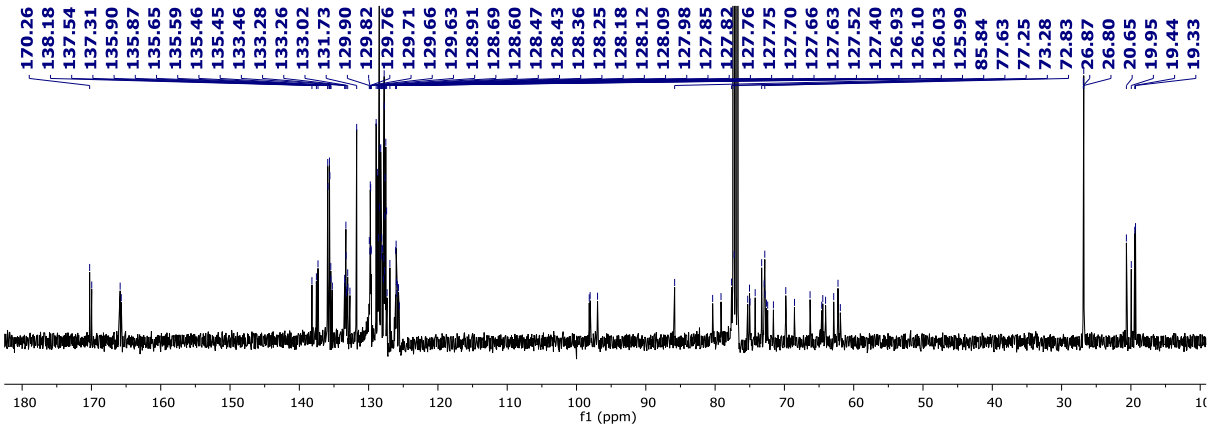
170.26 138.18 137.54 137.31 135.90 135.87 135.65 135.59 135.46 135.45 133.46 133.28 133.26 133.02 131.73 129.90 129.82 129.76 129.71 129.66 129.63 128.91 128.69 128.60 128.47 128.43 128.36 128.25 128.18 128.12 128.09 127.98 127.85 127.82 127.76 127.75 127.70 127.66 127.63 127.52 127.40 126.93 126.10 126.03 125.99 85.84 77.63 77.25 73.28 72.83 26.87 26.80 20.65 19.95 19.44 19.33
f1 (ppm)

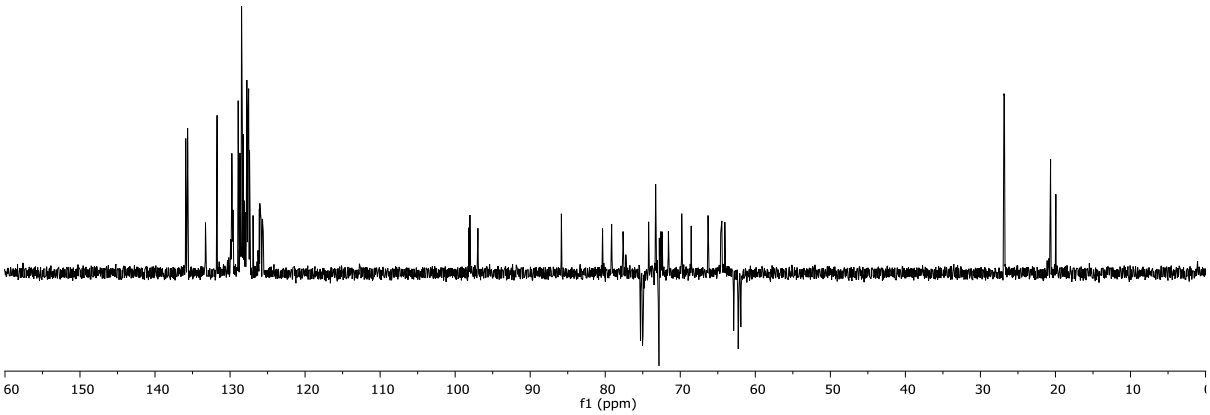
f1 (ppm)

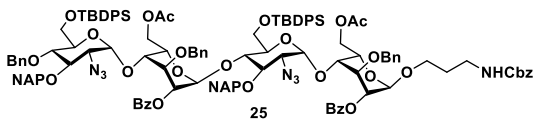
OTBDPS
OAc
BnO
NAPO
N3
OBn
BzO
NAPO
OTBDPS
OAc
N3
OBn
BzO
NHCbz

25

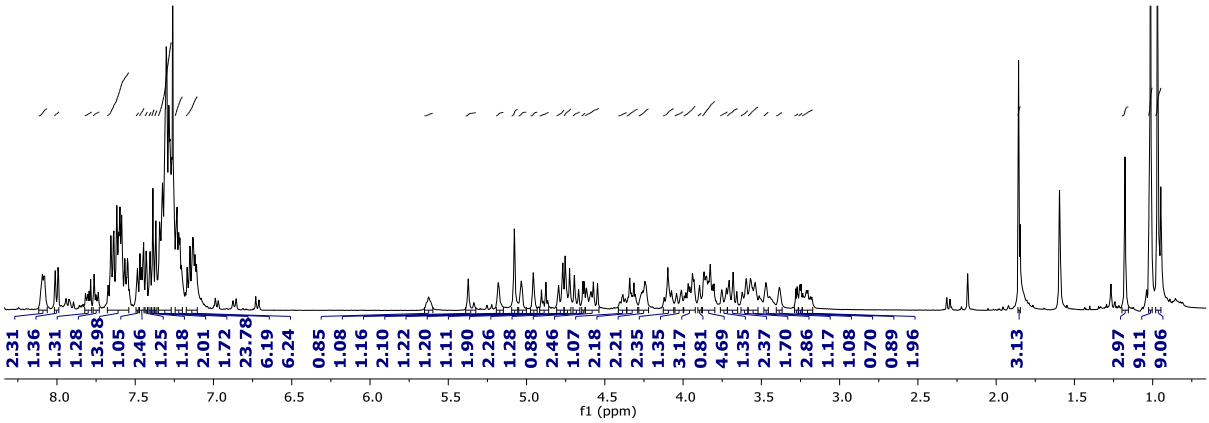
2.31 1.36 1.31 1.28 13.98 1.05 2.46 1.25 1.18 2.01 1.72 23.78 6.19 6.24 0.85 1.08 1.16 2.10 1.22 1.20 1.11 1.90 2.26 1.28 0.88 2.46 1.07 2.18 2.21 2.35 1.35 3.17 0.81 4.69 1.35 2.37 1.70 2.86 1.17 1.08 0.70 0.89 1.96 3.13 2.97 9.11 9.06
8.0 7.5 7.0 6.5 6.0 5.5 5.0 4.5 4.0 3.5 3.0 2.5 2.0 1.5 1.0
f1 (ppm)

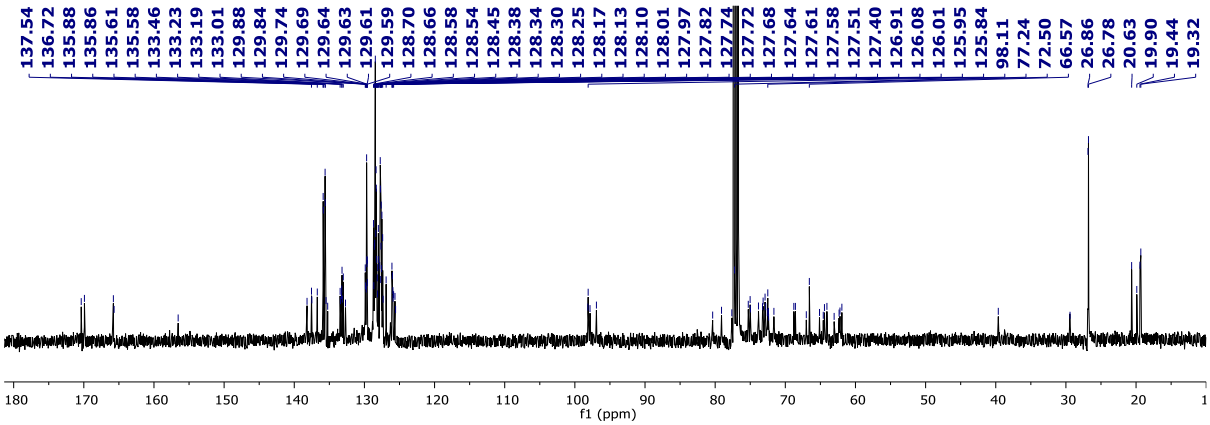
137.54 136.72 135.88 135.86 135.61 135.58 133.46 133.23 133.19 133.01 129.88 129.84 129.74 129.69 129.64 129.63 129.61 129.59 128.70 128.66 128.58 128.54 128.45 128.38 128.34 128.30 128.25 128.17 128.13 128.10 128.01 127.97 127.82 127.74 127.72 127.68 127.64 127.61 127.58 127.51 127.40 126.91 126.08 126.01 125.95 125.84 98.11 77.24 72.50 66.57 26.86 26.78 20.63 19.90 19.44 19.32
180 170 160 150 140 130 120 110 100 90 80 70 60 50 40 30 20
f1 (ppm)

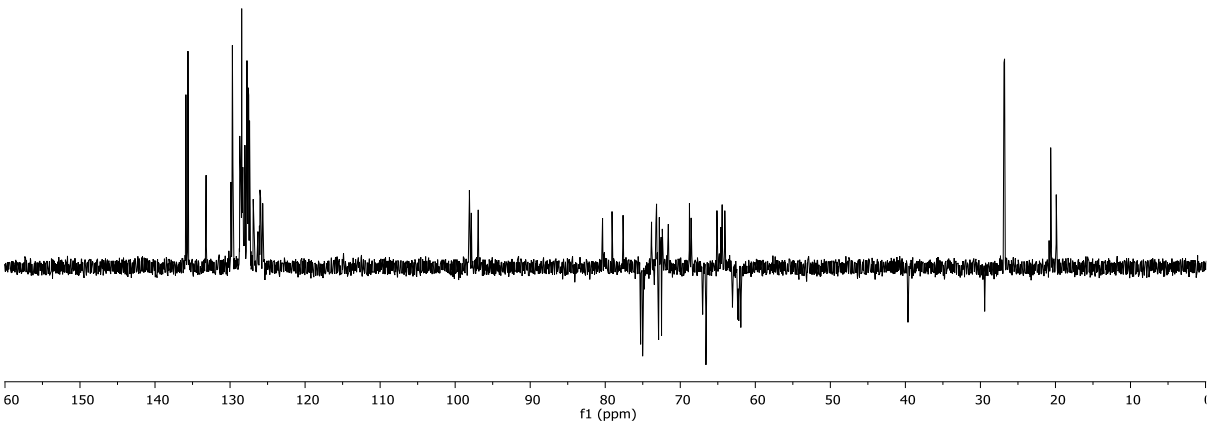
60 150 140 130 120 110 100 90 80 70 60 50 40 30 20 10
f1 (ppm)

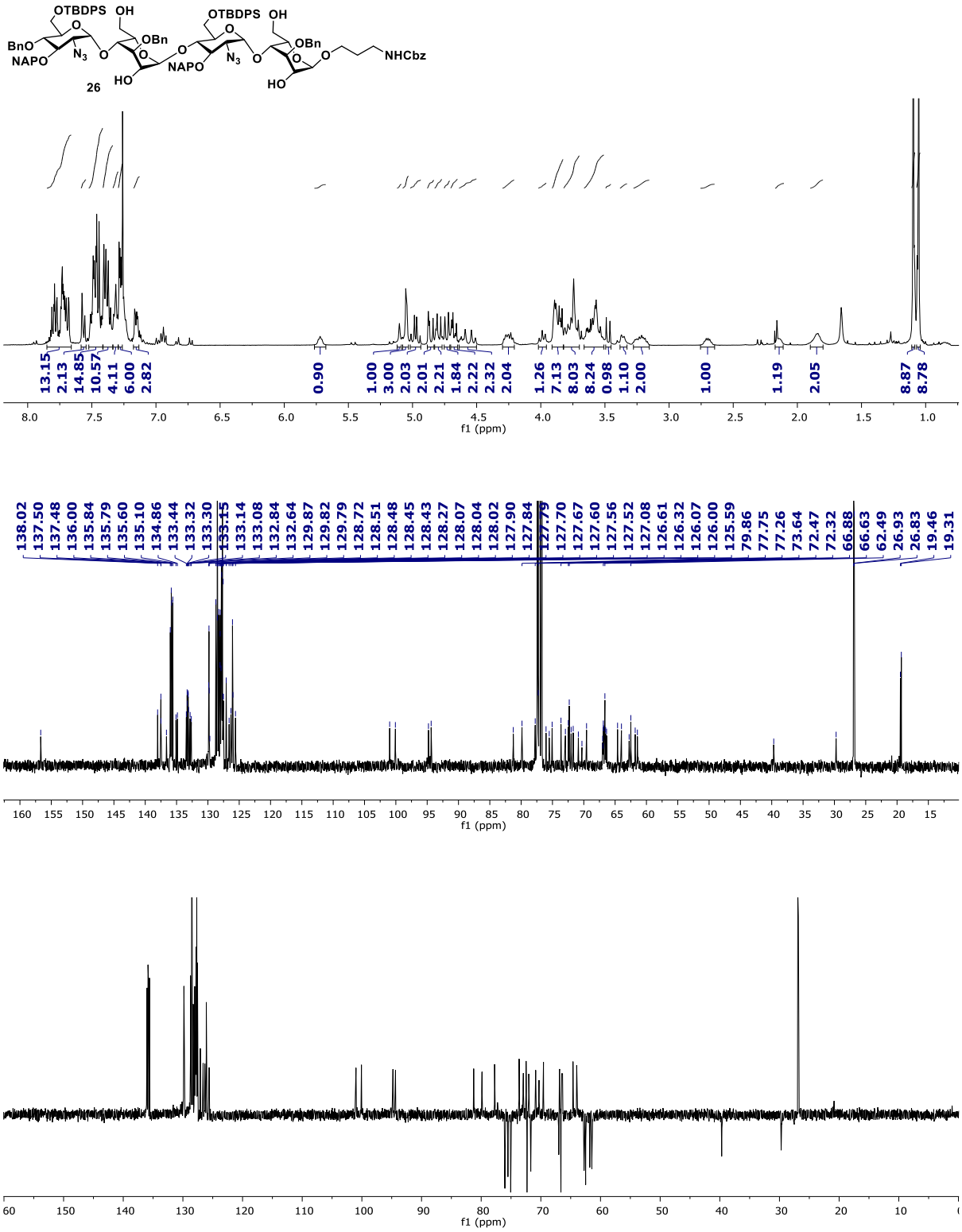
OTBDPS
OH
BnO
NAPO
N3
OBn
HO
NHCbz
26
13.15
2.13
14.85
10.57
4.11
6.00
2.82
0.90
1.00
3.00
2.03
2.01
2.21
1.84
2.22
2.32
2.04
1.26
7.13
8.03
8.24
0.98
1.10
2.00
1.00
1.19
2.05
8.87
8.78
f1 (ppm)
138.02
137.50
137.48
136.00
135.84
135.79
135.60
135.10
134.86
133.44
133.32
133.30
133.15
133.14
133.08
132.84
132.64
129.87
129.82
129.79
128.72
128.51
128.48
128.45
128.43
128.27
128.07
128.04
128.02
127.90
127.84
127.76
127.70
127.67
127.60
127.56
127.52
127.08
126.61
126.32
126.07
126.00
125.59
79.86
77.75
77.26
73.64
72.47
72.32
66.88
66.63
62.49
26.93
26.83
19.46
19.31
f1 (ppm)
f1 (ppm)

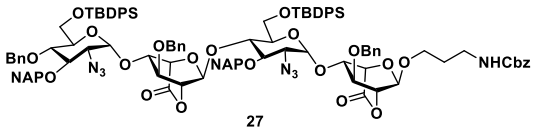
OTBDPS
OTBDPS
BnO
NAPO
N3
OBn
NAPO
N3
OBn
NHCbz

27

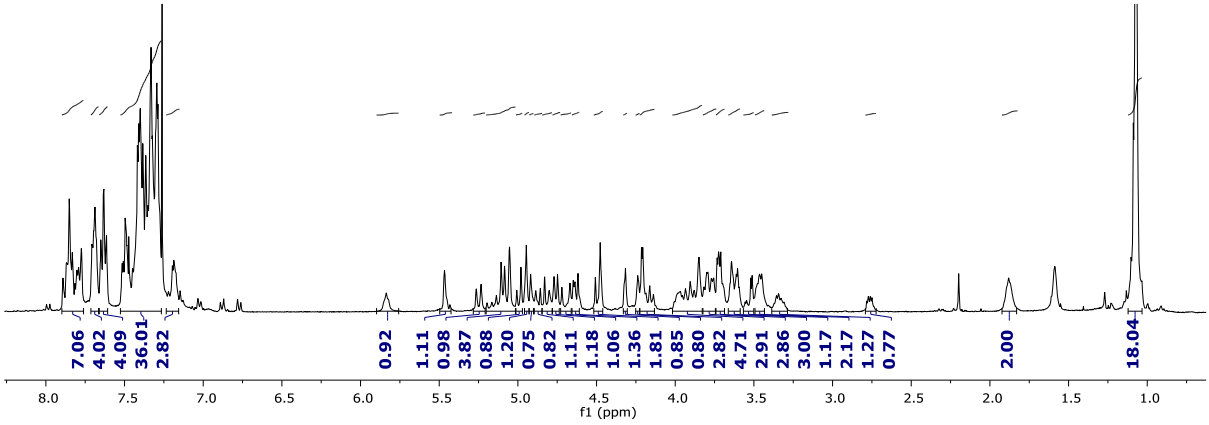
7.06
4.02
4.09
36.01
2.82
0.92
1.11
0.98
3.87
0.88
1.20
0.75
0.82
1.11
1.18
1.06
1.36
1.81
0.85
0.80
2.82
4.71
2.91
2.86
3.00
1.17
2.17
1.27
0.77
2.00
18.04
f1 (ppm)

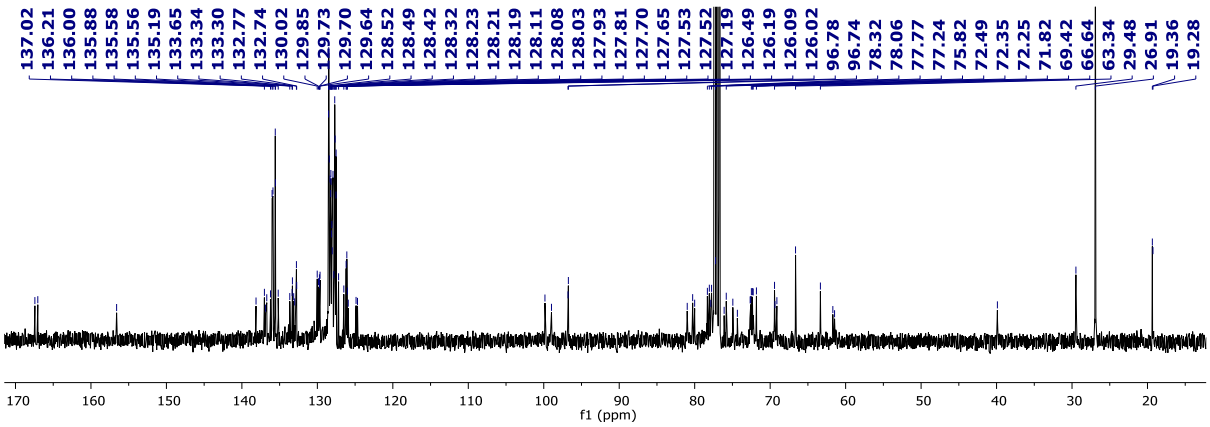
137.02
136.21
136.00
135.88
135.58
135.56
135.19
133.65
133.34
133.30
132.77
132.74
130.02
129.85
129.73
129.70
129.64
128.52
128.49
128.42
128.32
128.23
128.21
128.19
128.11
128.08
128.03
127.93
127.81
127.70
127.65
127.53
127.52
127.19
126.49
126.19
126.09
126.02
96.78
96.74
78.32
78.06
77.77
77.24
75.82
72.49
72.35
72.25
71.82
69.42
66.64
63.34
29.48
26.91
19.36
19.28
f1 (ppm)

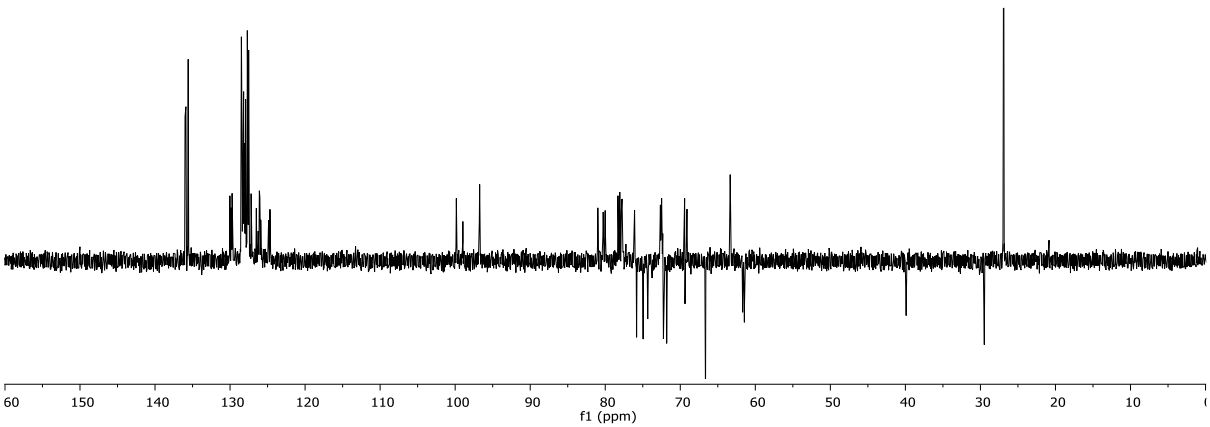
f1 (ppm)

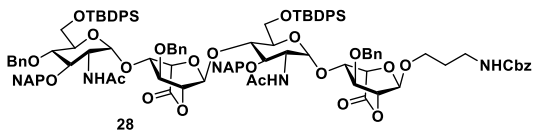
OTBDPS
BnO
NAPO
NHAc
OBn
OTBDPS
NAPO
AcHN
OBn
NHCbz

28

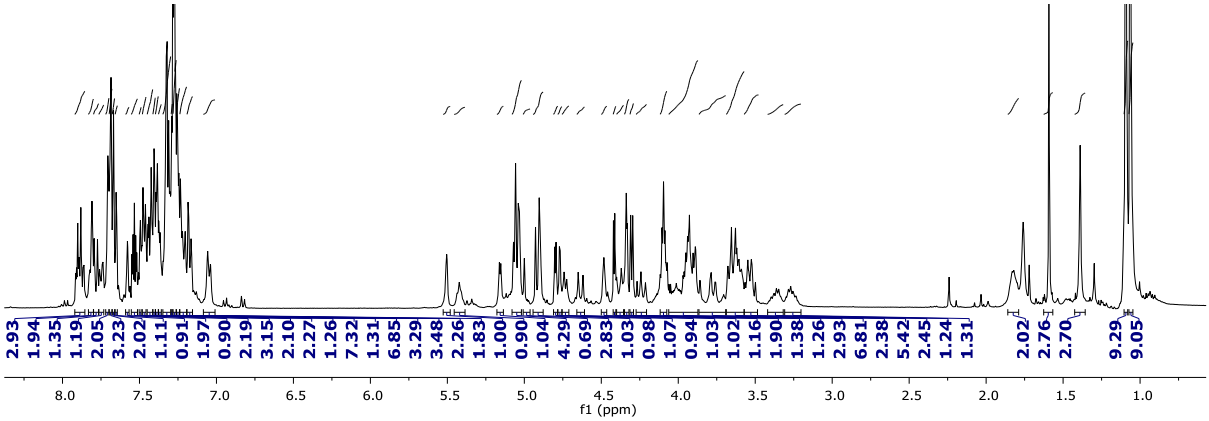
2.93 1.94 1.35 1.19 2.05 3.23 2.02 1.11 0.91 1.97 0.90 2.19 3.15 2.10 2.27 1.26 7.32 1.31 6.85 3.29 3.48 2.26 1.83 1.00 0.90 1.04 4.29 0.69 2.83 1.03 0.98 1.07 0.94 1.03 1.02 1.16 1.90 1.38 1.26 2.93 6.81 2.38 5.42 2.45 1.24 1.31 2.02 2.76 2.70 9.29 9.05
8.0 7.5 7.0 6.5 6.0 5.5 5.0 4.5 4.0 3.5 3.0 2.5 2.0 1.5 1.0
f1 (ppm)

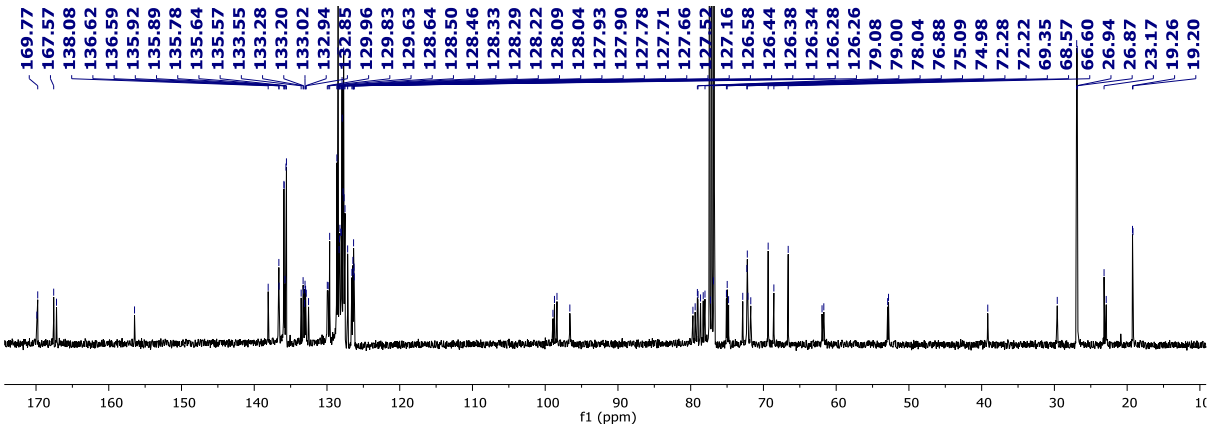
169.77 167.57 138.08 136.62 136.59 135.92 135.89 135.78 135.64 135.57 133.55 133.28 133.20 133.02 132.94 132.85 129.96 129.83 129.63 128.64 128.50 128.46 128.33 128.29 128.22 128.09 128.04 127.93 127.90 127.78 127.71 127.66 127.52 127.16 126.58 126.44 126.38 126.34 126.28 126.26 79.08 79.00 78.04 76.88 75.09 74.98 72.28 72.22 69.35 68.57 66.60 26.94 26.87 23.17 19.26 19.20
170 160 150 140 130 120 110 100 90 80 70 60 50 40 30 20
f1 (ppm)

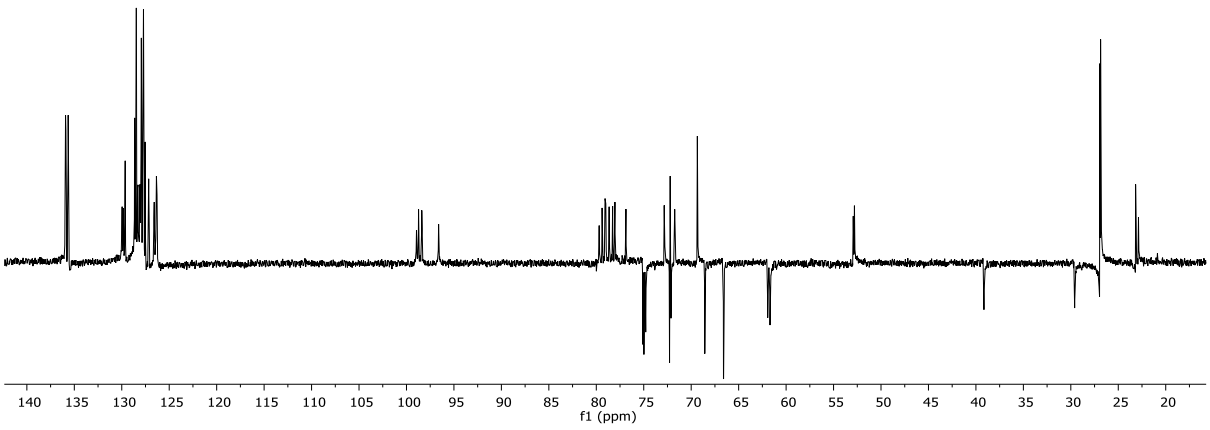
140 135 130 125 120 115 110 105 100 95 90 85 80 75 70 65 60 55 50 45 40 35 30 25 20
f1 (ppm)

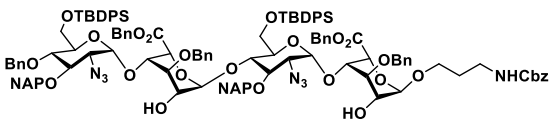
OTBDPS
BnO2C
OBn
BnO
NAPO
N3
O
HO
NHCbz

39

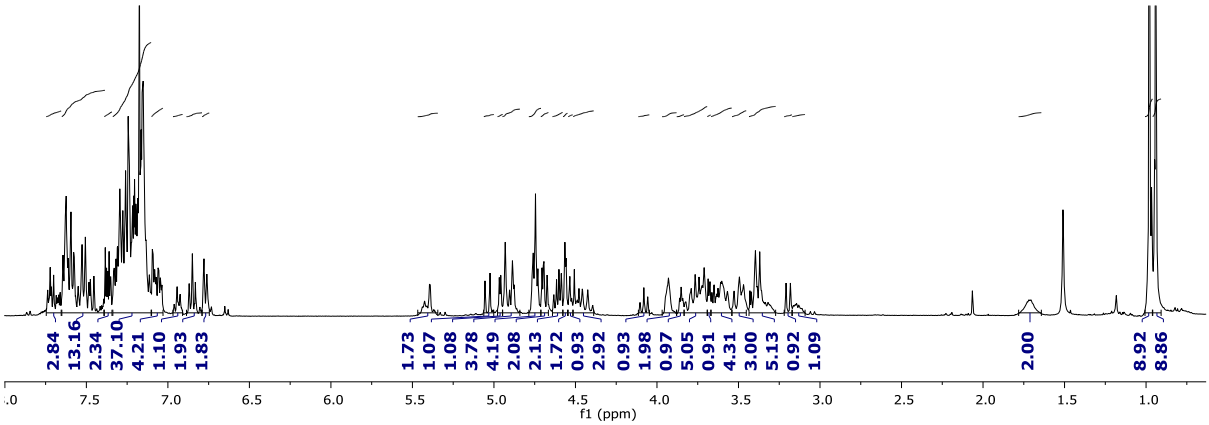
2.84 13.16 2.34 37.10 4.21 1.10 1.93 1.83 1.73 1.07 1.08 3.78 4.19 2.08 2.13 1.72 0.93 2.92 0.93 1.98 0.97 5.05 0.91 4.31 3.00 5.13 0.92 1.09 2.00 8.92 8.86
f1 (ppm)

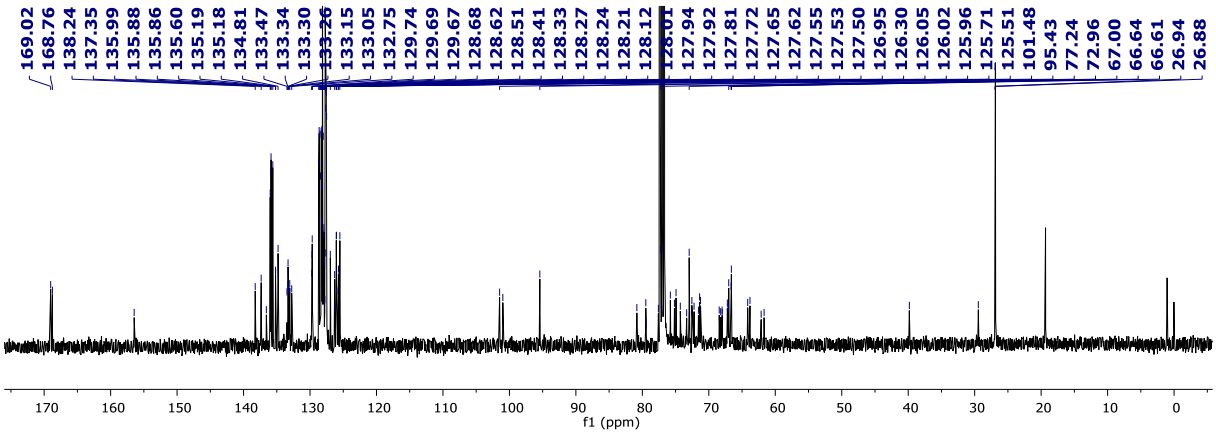
169.02 168.76 138.24 137.35 135.99 135.88 135.86 135.60 135.19 135.18 134.81 133.47 133.34 133.30 133.26 133.15 133.05 132.75 129.74 129.69 129.67 128.68 128.62 128.51 128.41 128.33 128.27 128.24 128.21 128.12 128.01 127.94 127.92 127.81 127.72 127.65 127.62 127.55 127.53 127.50 126.95 126.30 126.05 126.02 125.96 125.71 125.51 101.48 95.43 77.24 72.96 67.00 66.64 66.61 26.94 26.88
f1 (ppm)

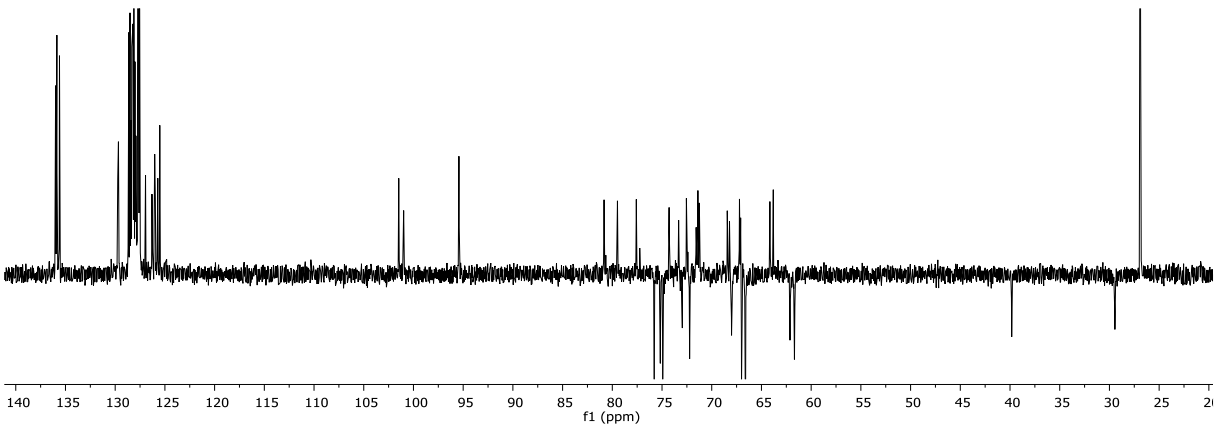
f1 (ppm)

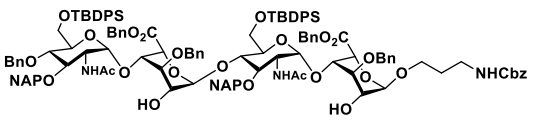
OTBDPS
BnO2C
BnO
NAPO
NHAc
OBn
HO
NHCbz

42

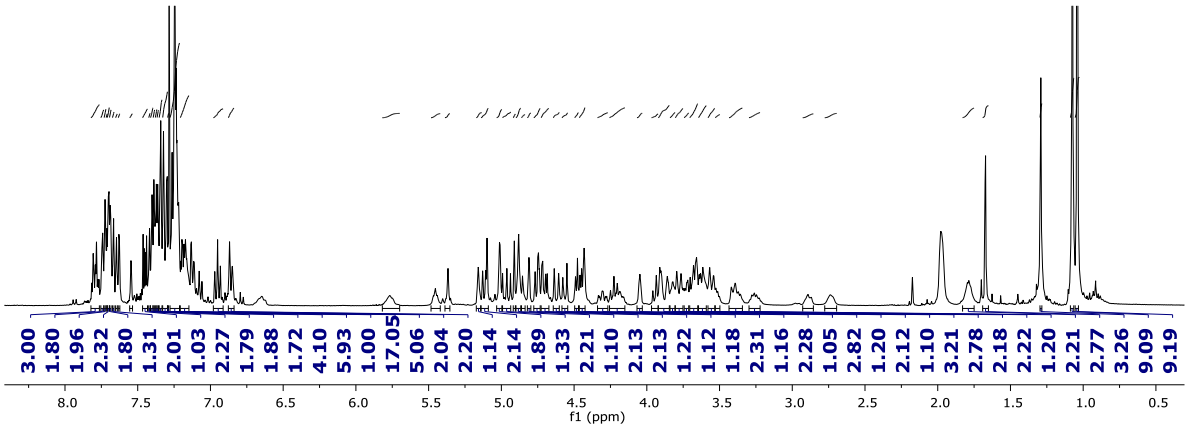
3.00 1.80 1.96 2.32 1.80 1.31 2.01 1.03 2.27 1.79 1.88 1.72 4.10 5.93 1.00 17.05 5.06 2.04 2.20 1.14 2.14 1.89 1.33 2.21 1.10 2.13 2.13 1.22 1.12 1.18 2.31 1.16 2.28 1.05 2.82 1.20 2.12 1.10 3.21 2.78 2.18 2.22 1.20 2.21 2.77 3.26 9.09 9.19
f1 (ppm)

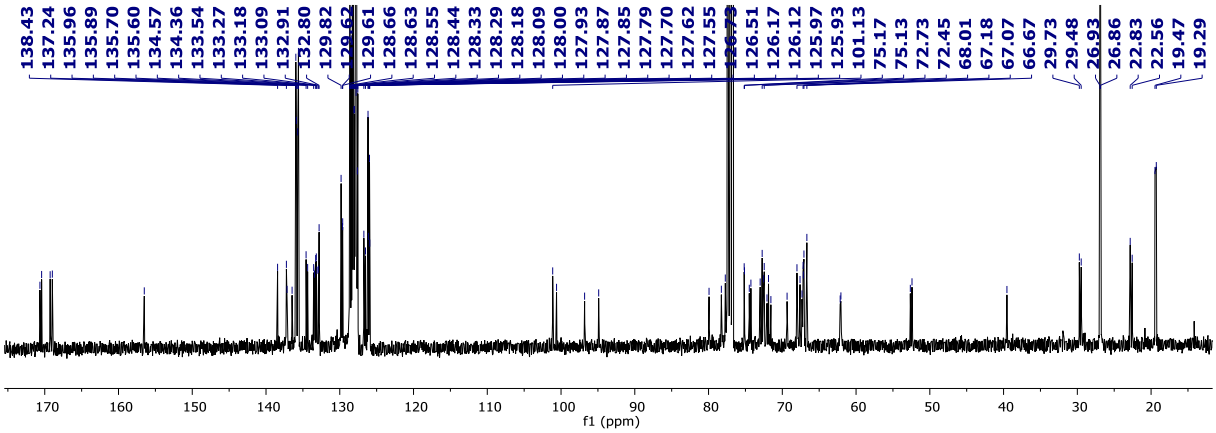
138.43 137.24 135.96 135.89 135.70 135.60 134.57 134.36 133.54 133.27 133.18 133.09 132.91 132.80 129.82 129.62 129.61 128.66 128.63 128.55 128.44 128.33 128.29 128.18 128.09 128.00 127.93 127.87 127.85 127.79 127.70 127.62 127.55 126.73 126.51 126.17 126.12 125.97 125.93 101.13 75.17 75.13 72.73 72.45 68.01 67.18 67.07 66.67 29.73 29.48 26.93 26.86 22.83 22.56 19.47 19.29
f1 (ppm)

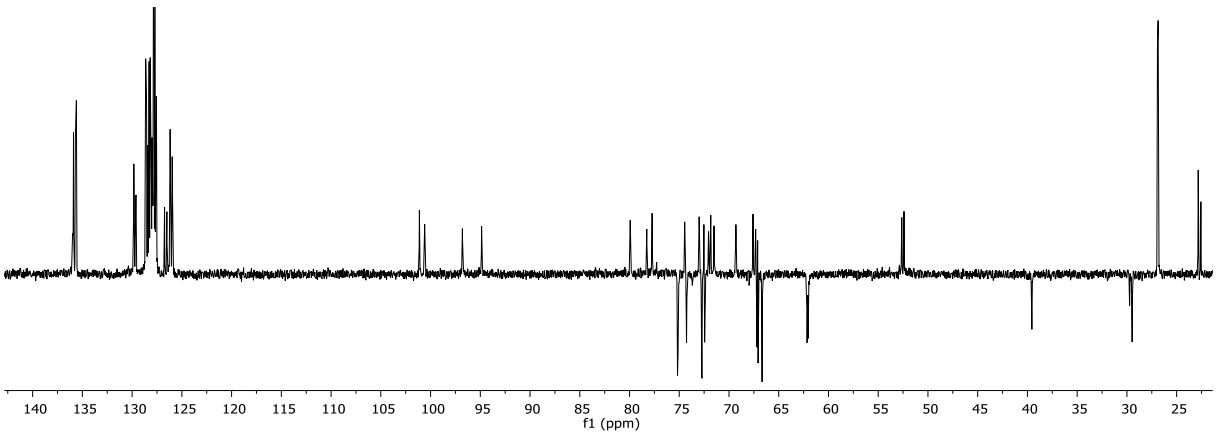
f1 (ppm)

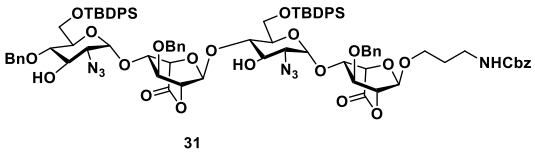
OTBDPS
OTBDPS
BnO
HO
N3
OBn
HO
N3
OBn
NHCbz

31

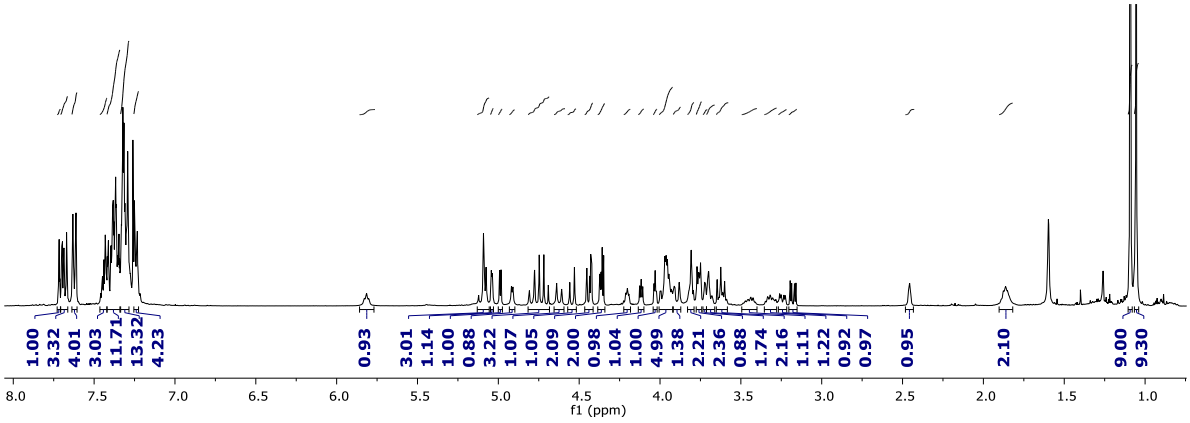
1.00 3.32 4.01 3.03 11.71 13.32 4.23 0.93 3.01 1.14 1.00 0.88 3.22 1.07 1.05 2.09 2.00 0.98 1.04 1.00 4.99 1.38 2.21 2.36 0.88 1.74 2.16 1.11 1.22 0.92 0.97 0.95 2.10 9.00 9.30
f1 (ppm)

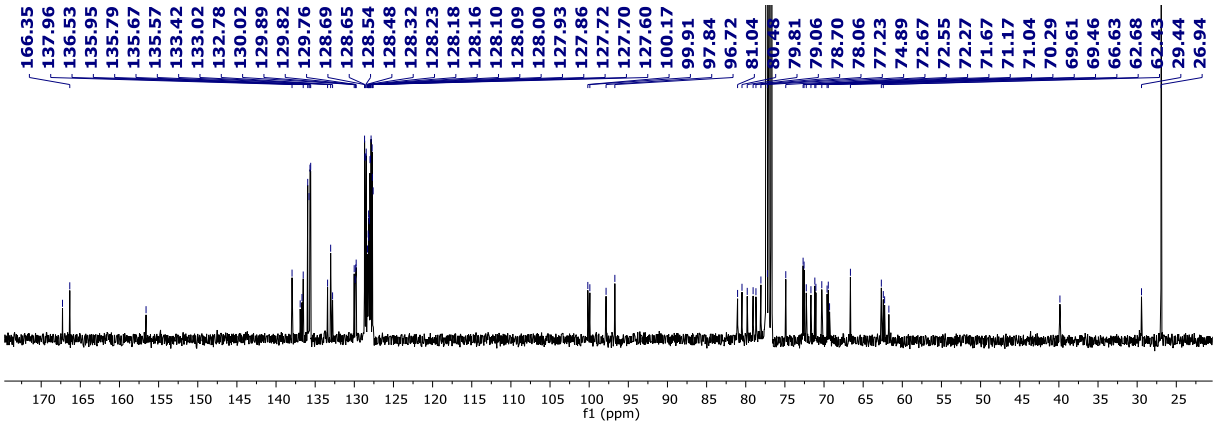
166.35 137.96 136.53 135.95 135.79 135.67 135.57 133.42 133.02 132.78 130.02 129.89 129.82 129.76 128.69 128.65 128.54 128.48 128.32 128.23 128.18 128.16 128.10 128.09 128.00 127.93 127.86 127.72 127.70 127.60 100.17 99.91 97.84 96.72 81.04 80.48 79.81 79.06 78.70 78.06 77.23 74.89 72.67 72.55 72.27 71.67 71.17 71.04 70.29 69.61 69.46 66.63 62.68 62.43 29.44 26.94
f1 (ppm)

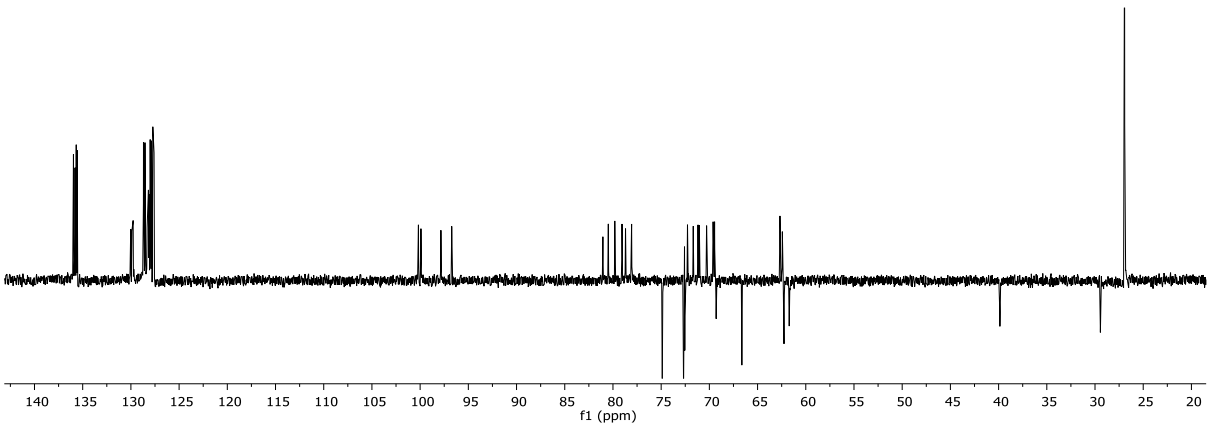
f1 (ppm)

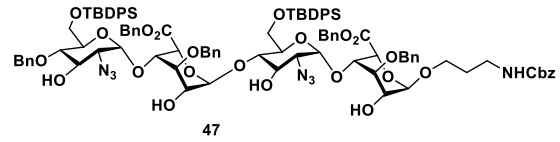
OTBDPS
BnO2C
OBn
BnO
HO
N3
O
NHCbz

47

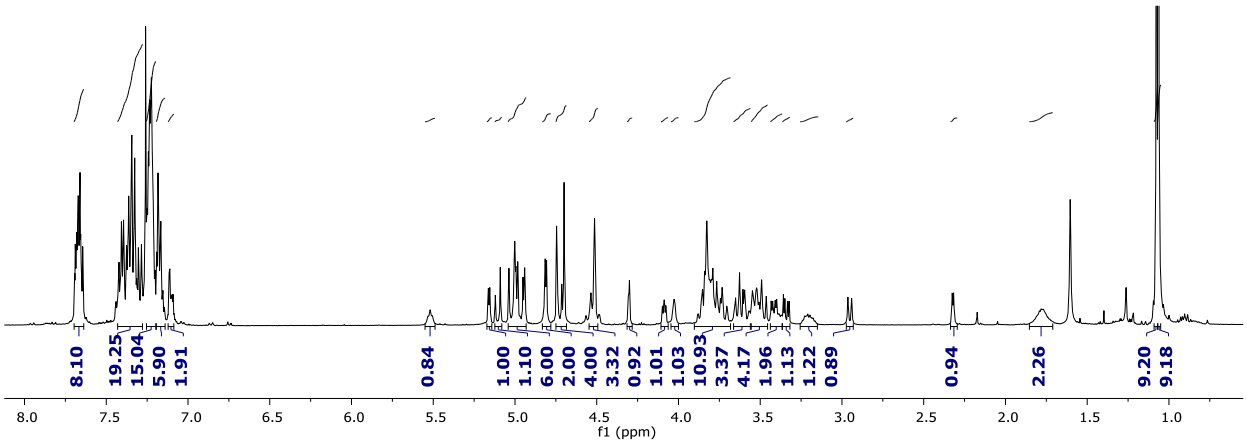
8.10
19.25
15.04
5.90
1.91
0.84
1.00
1.10
6.00
2.00
4.00
3.32
0.92
1.01
1.03
10.93
3.37
4.17
1.96
1.13
1.22
0.89
0.94
2.26
9.20
9.18
f1 (ppm)

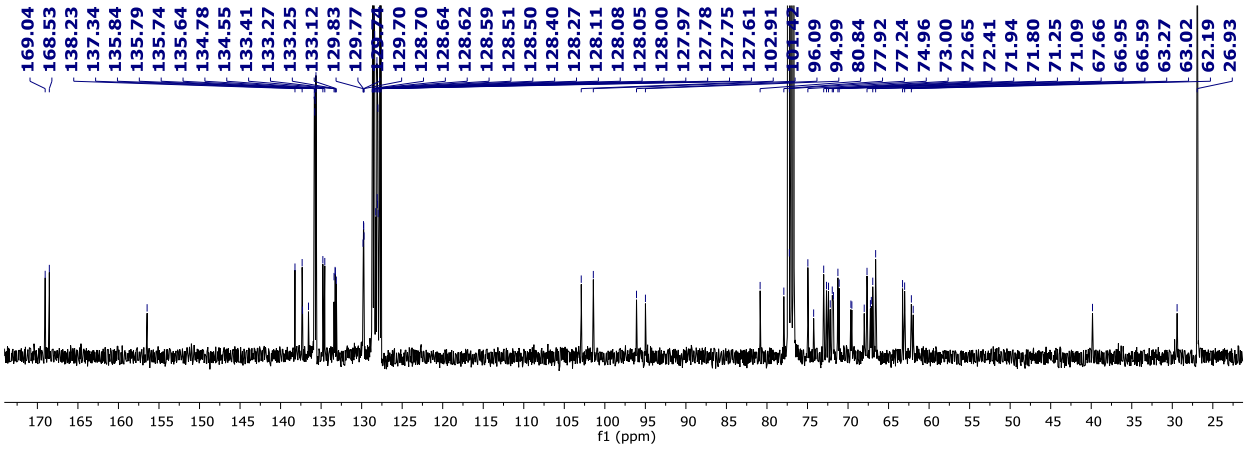
169.04
168.53
138.23
137.34
135.84
135.79
135.74
135.64
134.78
134.55
133.41
133.27
133.25
133.12
129.83
129.77
129.70
128.70
128.64
128.62
128.59
128.51
128.50
128.40
128.27
128.11
128.08
128.05
128.00
127.97
127.78
127.75
127.61
102.91
96.09
94.99
80.84
77.92
77.24
74.96
73.00
72.65
72.41
71.94
71.80
71.25
71.09
67.66
66.95
66.59
63.27
63.02
62.19
26.93
f1 (ppm)

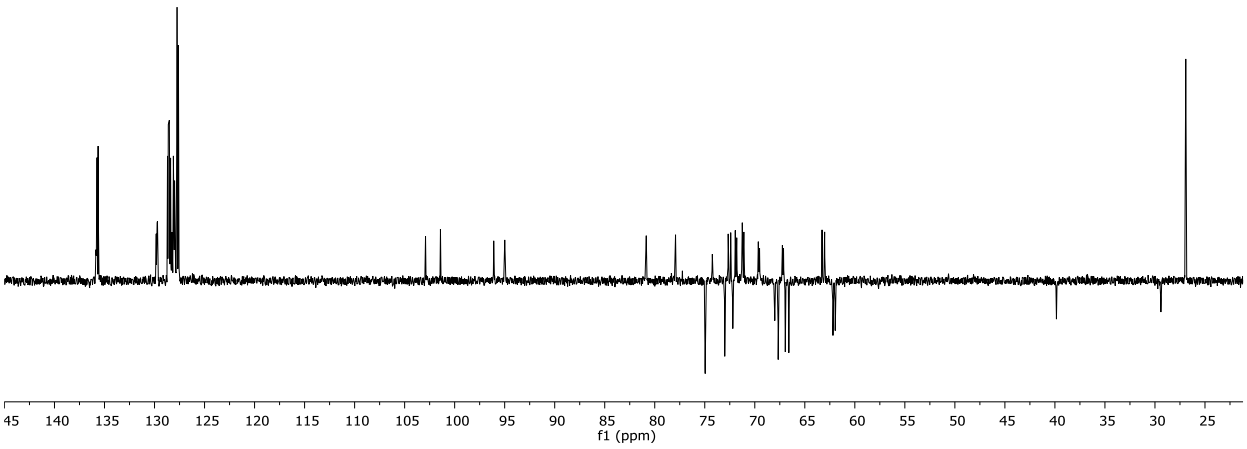
f1 (ppm)

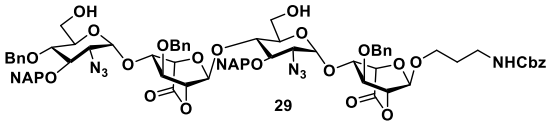
OH
BnO
NAPO
N3
OBn
NAPO
N3
OBn
NHCbz
29

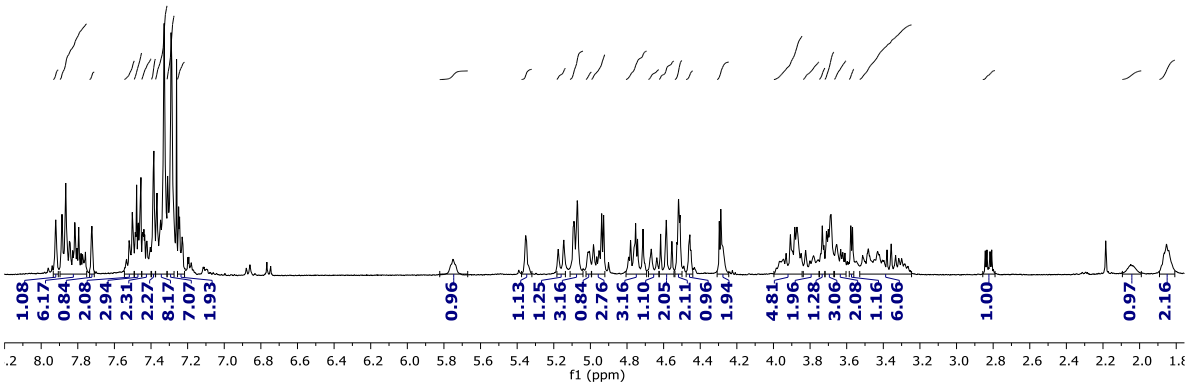
1.08 6.17 0.84 2.08 2.94 2.31 2.27 8.17 7.07 1.93 0.96 1.13 1.25 3.16 0.84 2.76 3.16 1.10 2.05 2.11 0.96 1.94 4.81 1.96 1.28 3.06 2.08 1.16 6.06 1.00 0.97 2.16
f1 (ppm)

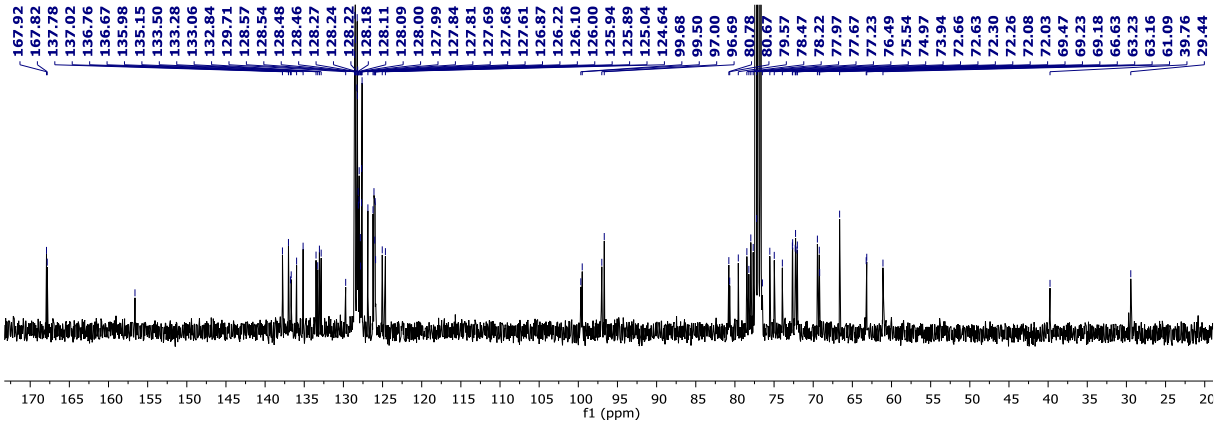
167.92 167.82 137.78 137.02 136.76 136.67 135.98 135.15 133.50 133.28 133.06 132.84 129.71 128.57 128.54 128.48 128.46 128.27 128.24 128.22 128.18 128.11 128.09 128.00 127.99 127.84 127.81 127.69 127.68 127.61 126.87 126.22 126.10 126.00 125.94 125.89 125.04 124.64 99.68 99.50 97.00 96.69 80.78 80.67 79.57 78.47 78.22 77.97 77.67 77.23 76.49 75.54 74.97 73.94 72.66 72.63 72.30 72.26 72.08 72.03 69.47 69.23 69.18 66.63 63.23 63.16 61.09 39.76 29.44
f1 (ppm)

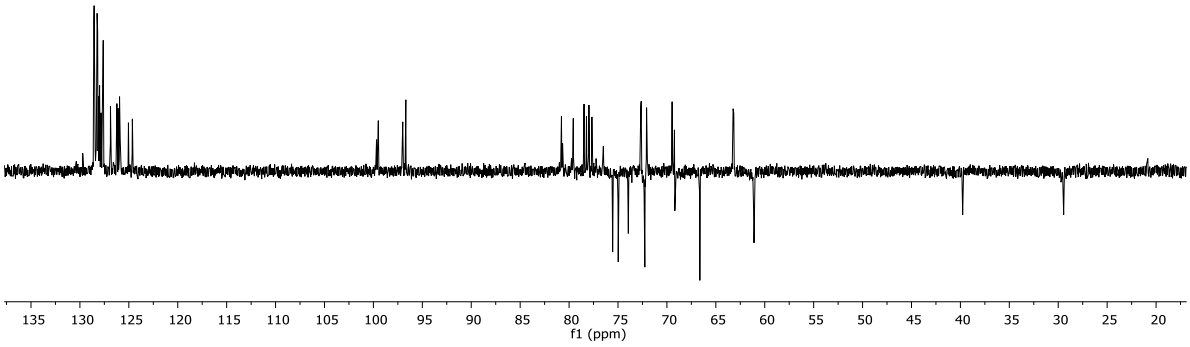
f1 (ppm)

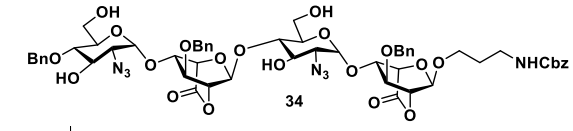
OH
BnO
HO
N3
OBn
O
NHCbz

34

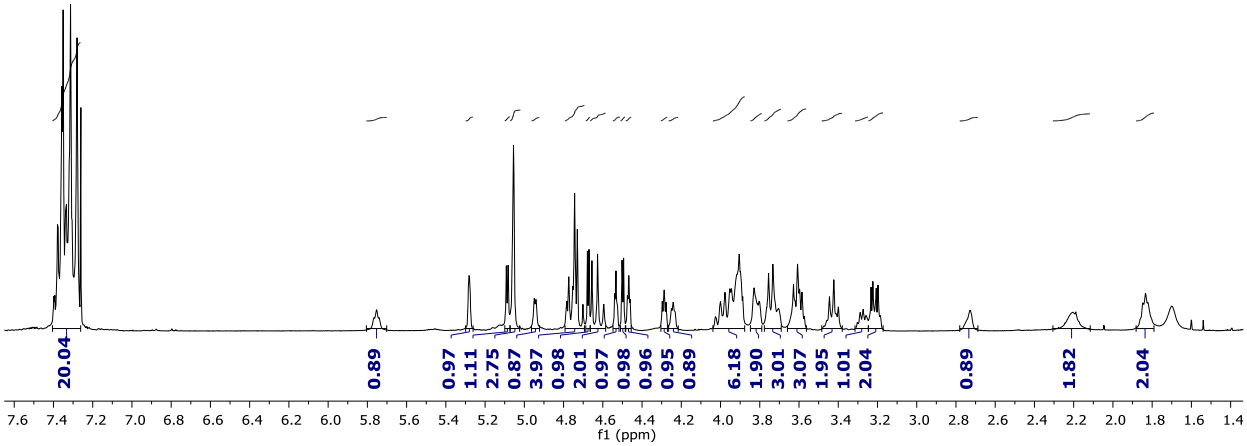
20.04
0.89
0.97
1.11
2.75
0.87
3.97
0.98
2.01
0.97
0.98
0.96
0.95
0.89
6.18
1.90
3.01
3.07
1.95
1.01
2.04
0.89
1.82
2.04
f1 (ppm)

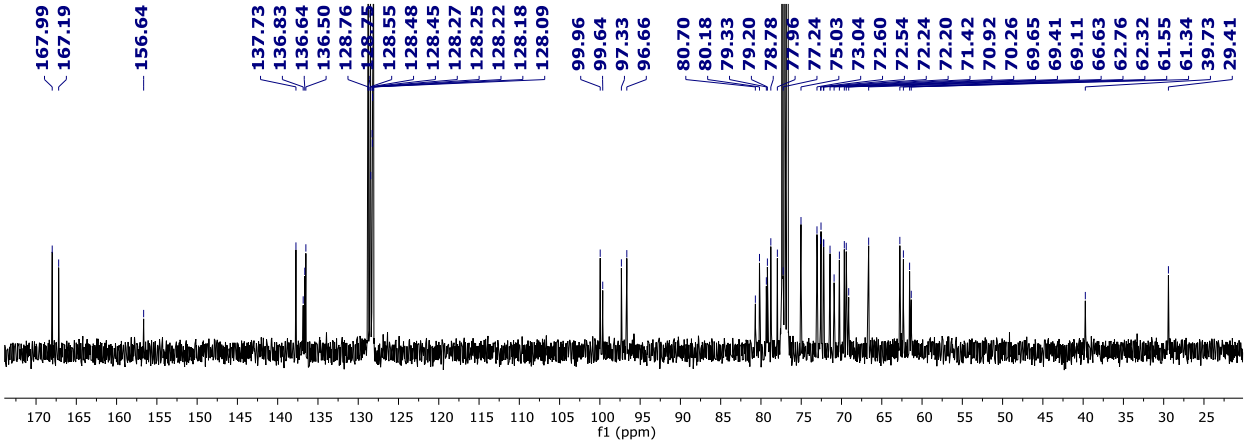
167.99
167.19
156.64
137.73
136.83
136.64
136.50
128.76
128.55
128.48
128.45
128.27
128.25
128.22
128.18
128.09
99.96
99.64
97.33
96.66
80.70
80.18
79.33
79.20
78.78
77.96
77.24
75.03
73.04
72.60
72.54
72.24
72.20
71.42
70.92
70.26
69.65
69.41
69.11
66.63
62.76
62.32
61.55
61.34
39.73
29.41
f1 (ppm)

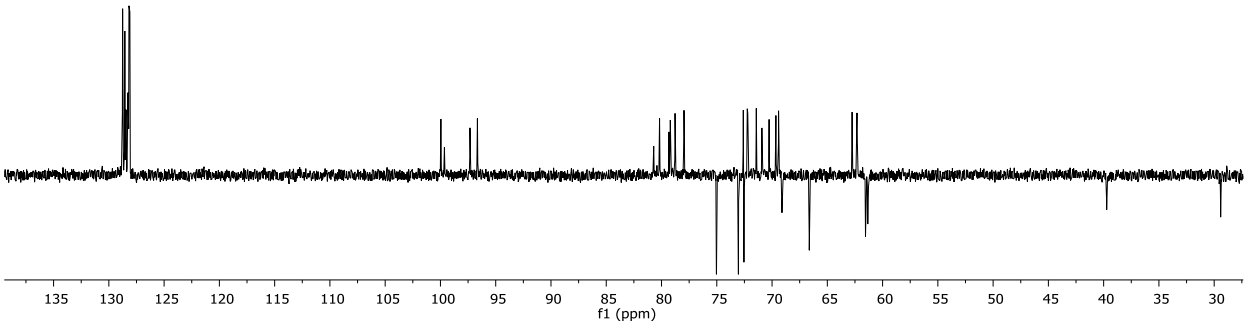
f1 (ppm)

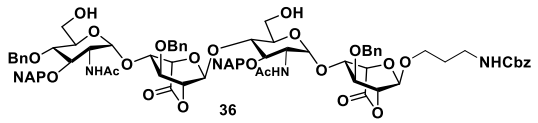
OH
BnO
NAPO
NHAc
OBn
NAPO
AcHN
OBn
NHCbz

36

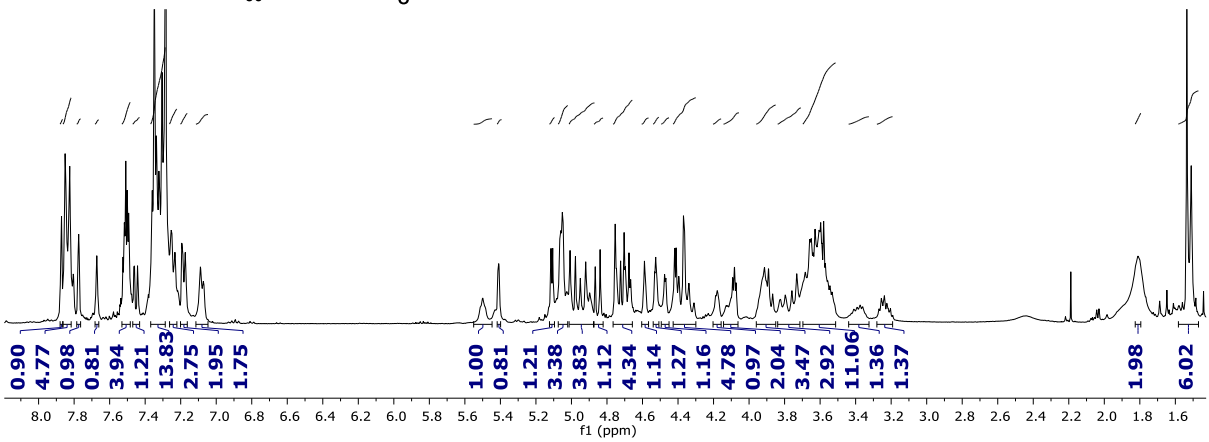
0.90 4.77 0.98 0.81 3.94 1.21 13.83 2.75 1.95 1.75 1.00 0.81 1.21 3.38 3.83 1.12 4.34 1.14 1.27 1.16 4.78 0.97 2.04 3.47 2.92 11.06 1.36 1.37 1.98 6.02
f1 (ppm)

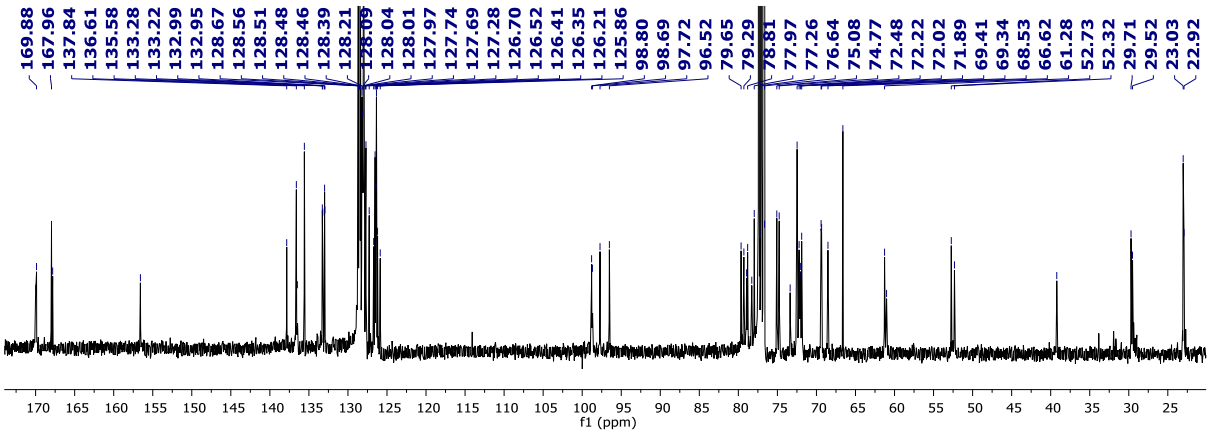
169.88 167.96 137.84 136.61 135.58 133.28 133.22 132.99 132.95 128.67 128.56 128.51 128.48 128.46 128.39 128.21 128.09 128.04 128.01 127.97 127.74 127.69 127.28 126.70 126.52 126.41 126.35 126.21 125.86 98.80 98.69 97.72 96.52 79.65 79.29 78.81 77.97 77.26 76.64 75.08 74.77 72.48 72.22 72.02 71.89 69.41 69.34 68.53 66.62 61.28 52.73 52.32 29.71 29.52 23.03 22.92
f1 (ppm)

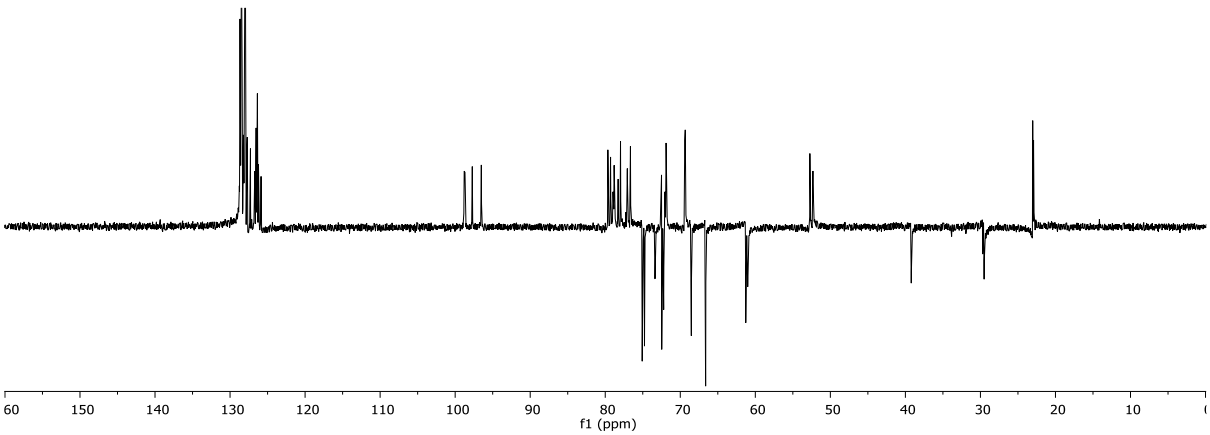
f1 (ppm)

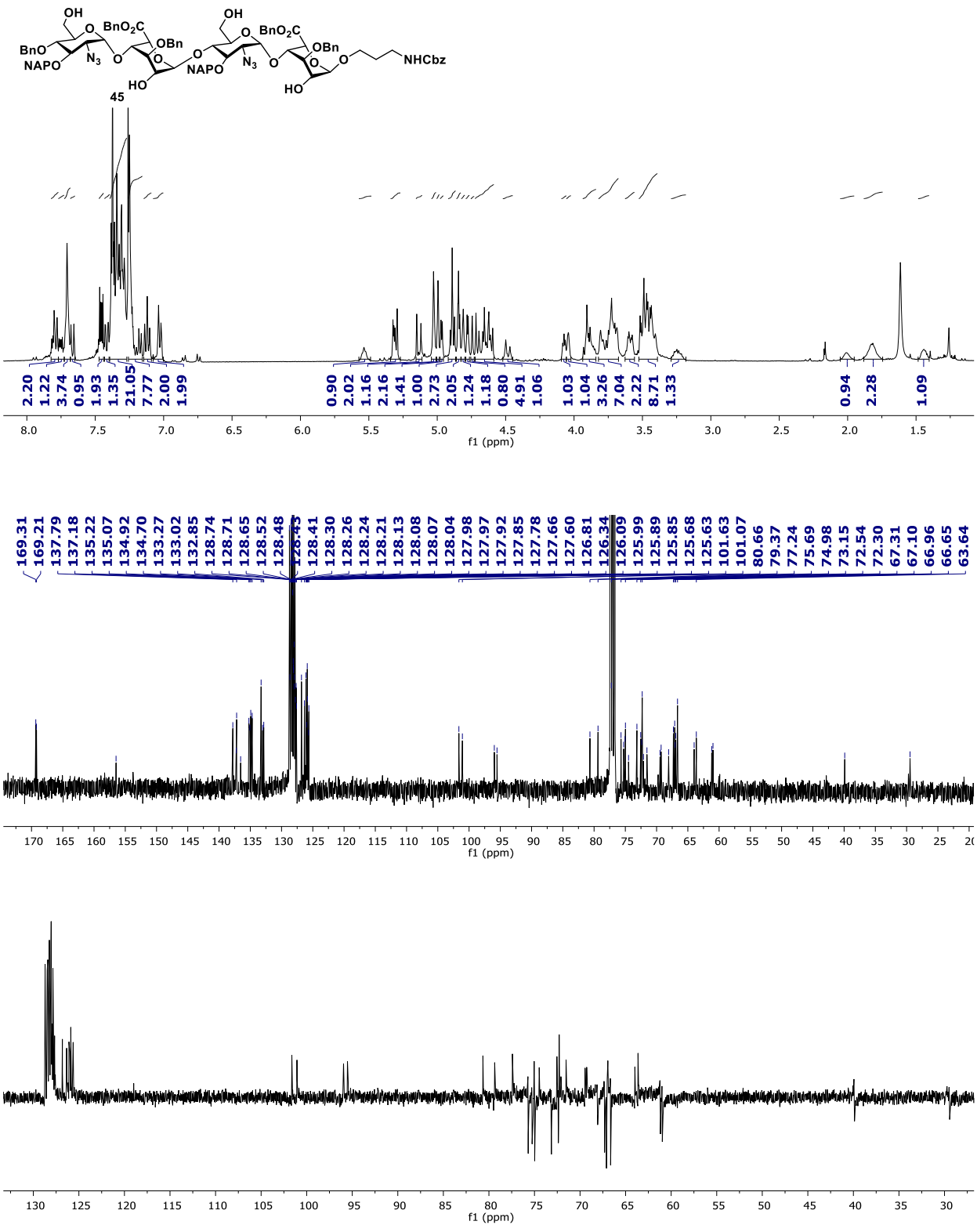
45
2.20 1.22 3.74 0.95 1.93 1.35 21.05 7.77 2.00 1.99 0.90 2.02 1.16 2.16 1.41 1.00 2.73 2.05 1.24 1.18 0.80 4.91 1.06 1.03 1.04 3.26 7.04 2.22 8.71 1.33 0.94 2.28 1.09
f1 (ppm)
169.31 169.21 137.79 137.18 135.22 135.07 134.92 134.70 133.27 133.02 132.85 128.74 128.71 128.65 128.52 128.48 128.43 128.41 128.30 128.26 128.24 128.21 128.13 128.08 128.07 128.04 127.98 127.97 127.92 127.85 127.78 127.66 127.60 126.81 126.34 126.09 125.99 125.89 125.85 125.68 125.63 101.63 101.07 80.66 79.37 77.24 75.69 74.98 73.15 72.54 72.30 67.31 67.10 66.96 66.65 63.64
f1 (ppm)
f1 (ppm)

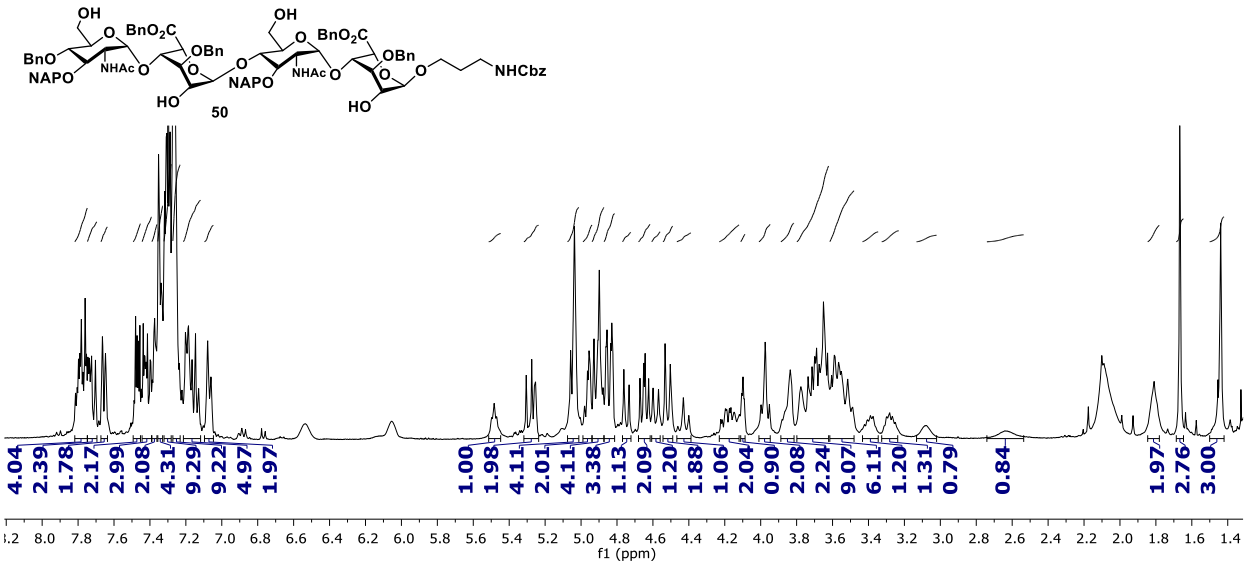
OH
BnO2C
OBn
BnO
NAPO
NHAc
O
HO
NHCbz
50
4.04 2.39 1.78 2.17 2.99 2.08 4.31 9.29 9.22 4.97 1.97 1.00 1.98 4.11 2.01 4.11 3.38 1.13 2.09 1.20 1.88 1.06 2.04 0.90 2.08 2.24 9.07 6.11 1.20 1.31 0.79 0.84 1.97 2.76 3.00
f1 (ppm)

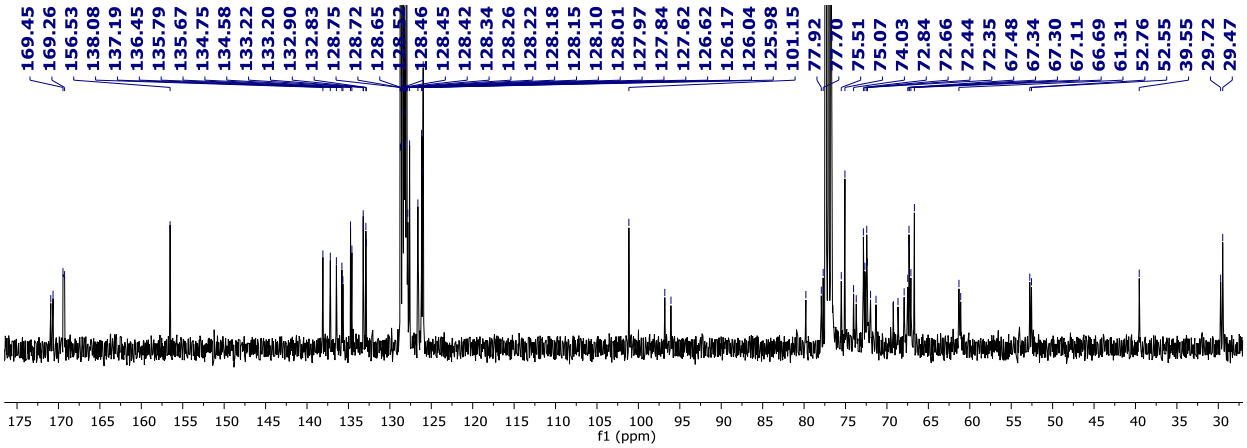
169.45 169.26 156.53 138.08 137.19 136.45 135.79 135.67 134.75 134.58 133.22 133.20 132.90 132.83 128.75 128.72 128.65 128.52 128.46 128.45 128.42 128.34 128.26 128.22 128.18 128.15 128.10 128.01 127.97 127.84 127.62 126.62 126.17 126.04 125.98 101.15 77.92 77.70 75.51 75.07 74.03 72.84 72.66 72.44 72.35 67.48 67.34 67.30 67.11 66.69 61.31 52.76 52.55 39.55 29.72 29.47
f1 (ppm)

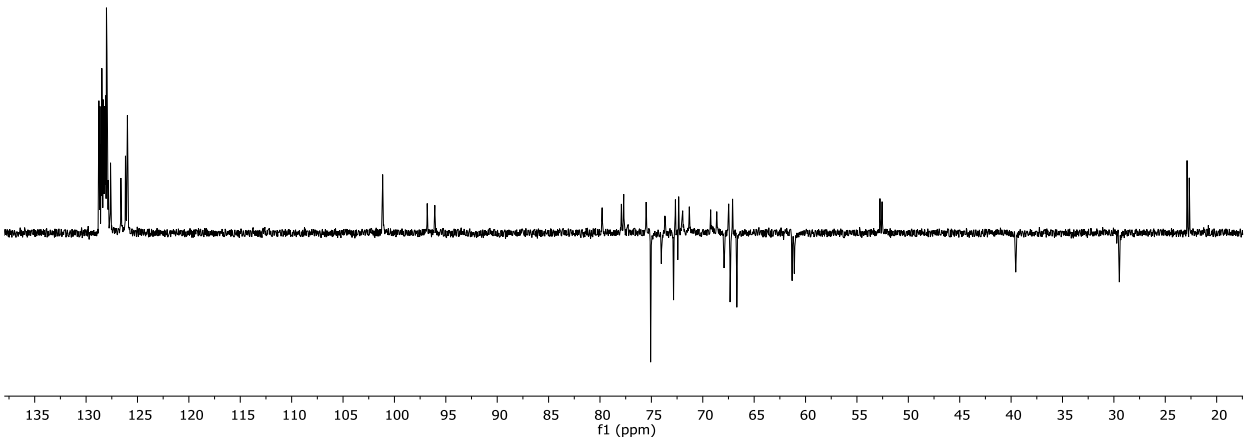
f1 (ppm)

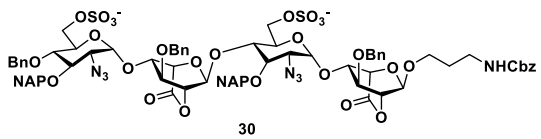
OSO3-
BnO
NAPO
N3
OBn
O
NHCbz

30

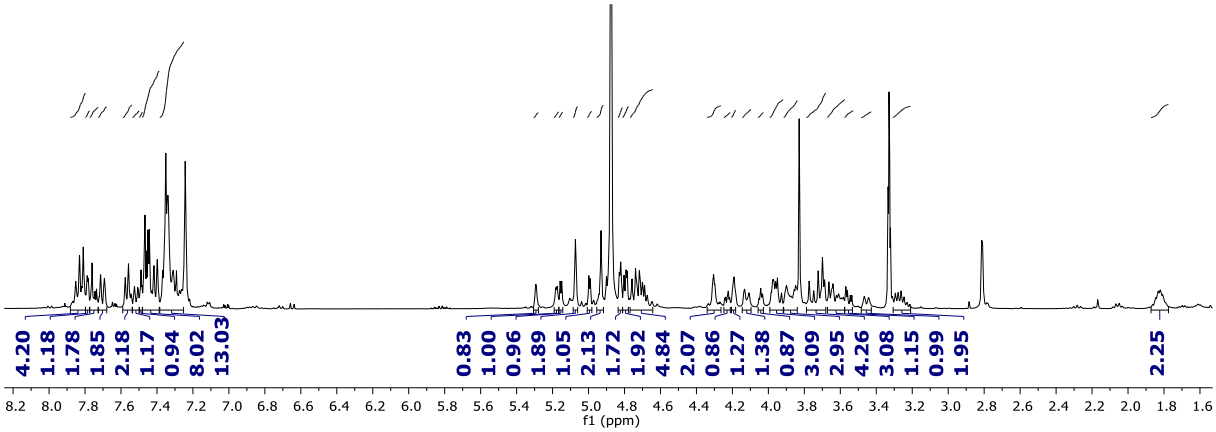
4.20 1.18 1.78 1.85 2.18 1.17 0.94 8.02 13.03
0.83 1.00 0.96 1.89 1.05 2.13 1.72 1.92 4.84 2.07 0.86 1.27 1.38 0.87 3.09 2.95 4.26 3.08 1.15 0.99 1.95
2.25
f1 (ppm)

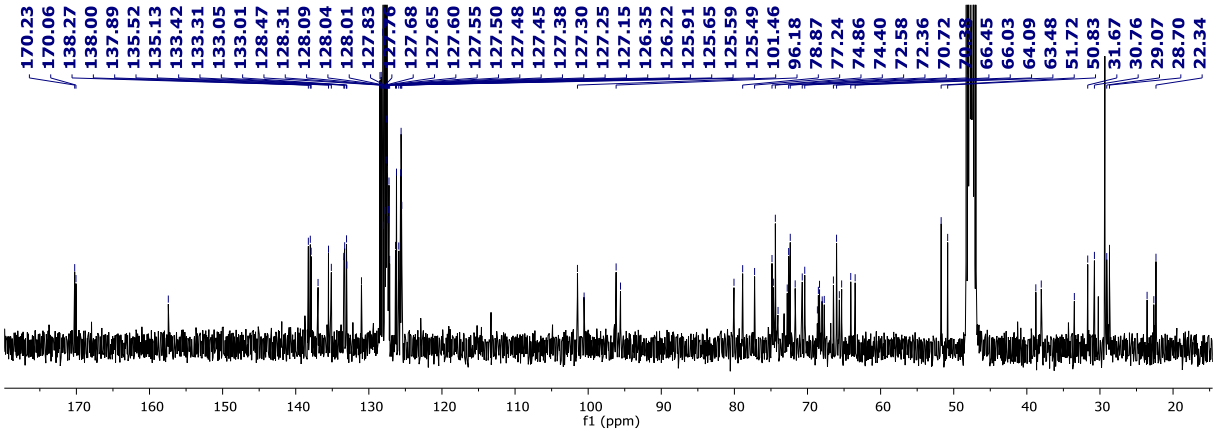
170.23 170.06 138.27 138.00 137.89 135.52 135.13 133.42 133.31 133.05 133.01 128.47 128.31 128.09 128.04 128.01 127.83 127.76 127.68 127.65 127.60 127.55 127.50 127.48 127.45 127.38 127.30 127.25 127.15 126.35 126.22 125.91 125.65 125.59 125.49 101.46 96.18 78.87 77.24 74.86 74.40 72.58 72.36 70.72 70.38 66.45 66.03 64.09 63.48 51.72 50.83 31.67 30.76 29.07 28.70 22.34
f1 (ppm)

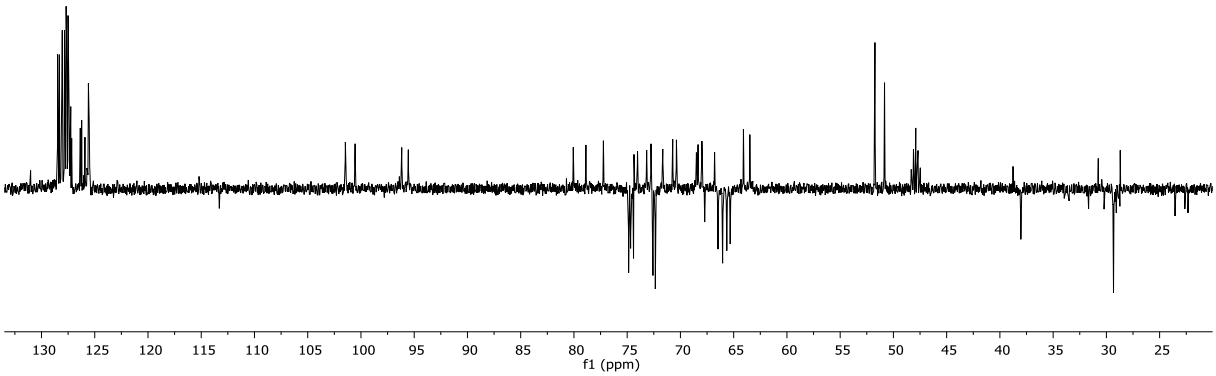
f1 (ppm)

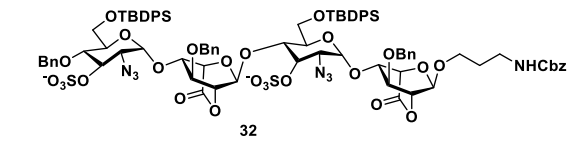
OTBDPS
OTBDPS
BnO
$^{-}O_3SO$
$N_3$
OBn
$^{-}O_3SO$
$N_3$
OBn
NHCbz

32

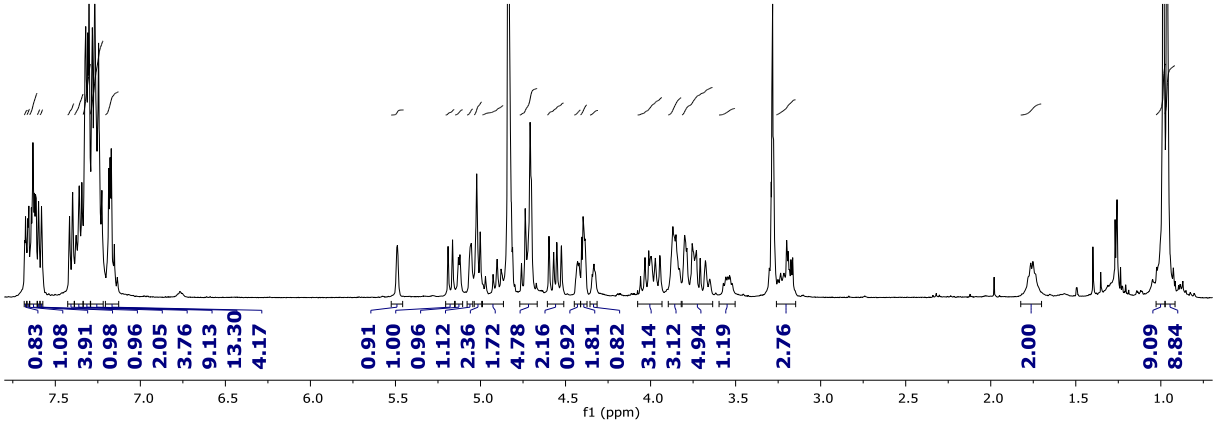
0.83 1.08 3.91 0.98 0.96 2.05 3.76 9.13 13.30 4.17
0.91 1.00 0.96 1.12 2.36 1.72 4.78 2.16 0.92 1.81 0.82 3.14 3.12 4.94 1.19
2.76
2.00
9.09 8.84
f1 (ppm)

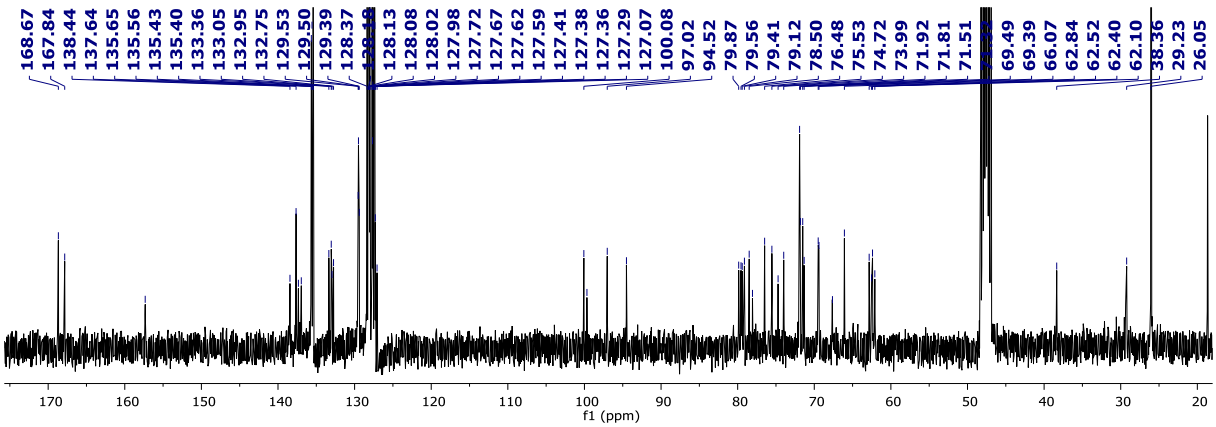
168.67 167.84 138.44 137.64 135.65 135.56 135.43 135.40 133.36 133.05 132.95 132.75 129.53 129.50 129.39 128.37
128.13 128.08 128.02 127.98 127.72 127.67 127.62 127.59 127.41 127.38 127.36 127.29 127.07 100.08 97.02 94.52
79.87 79.56 79.41 79.12 78.50 76.48 75.53 74.72 73.99 71.92 71.81 71.51
69.49 69.39 66.07 62.84 62.52 62.40 62.10 38.36 29.23 26.05
f1 (ppm)

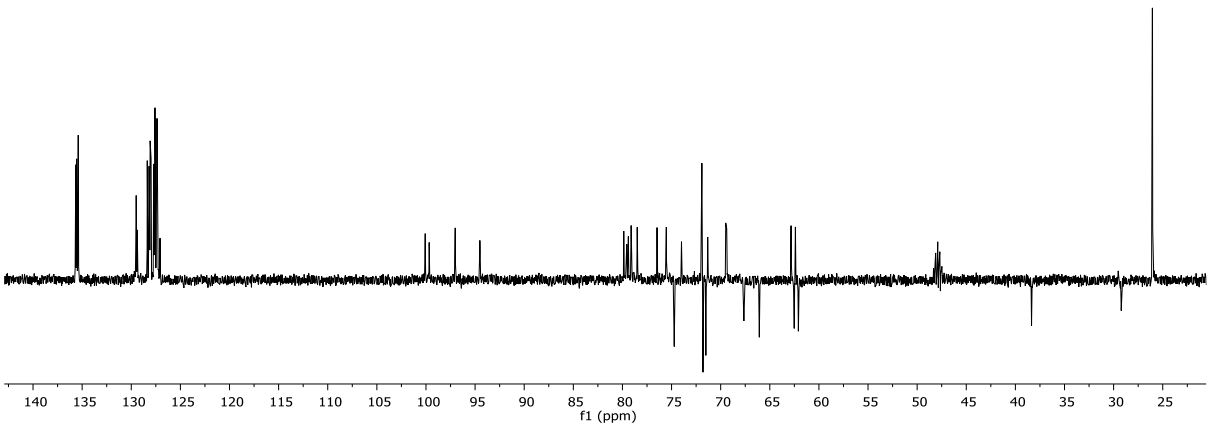
f1 (ppm)

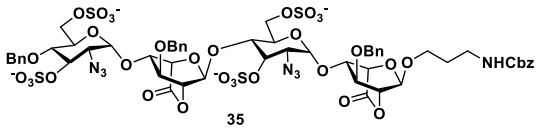
OSO3-
BnO
-O3SO
N3
OBn
NHCbz

35

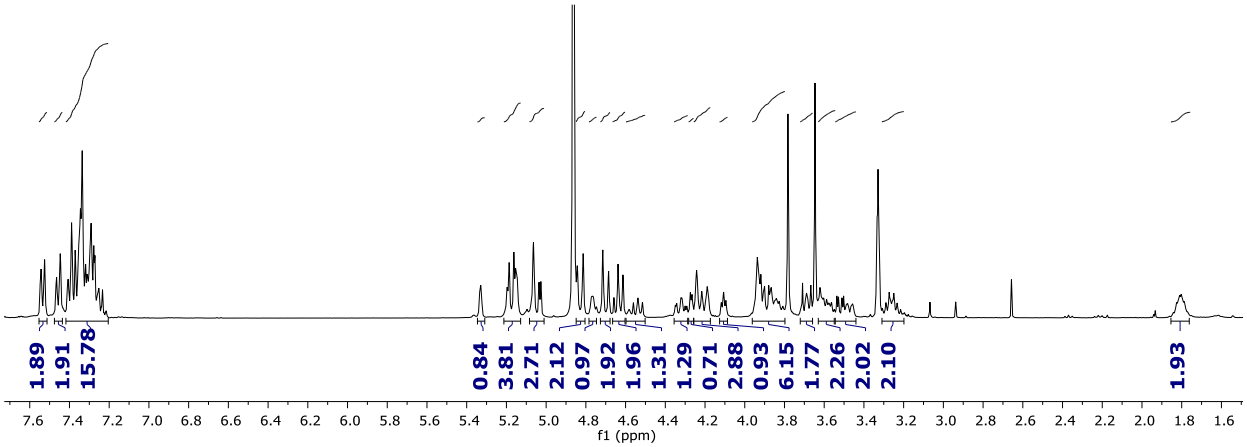
1.89
1.91
15.78
0.84
3.81
2.71
2.12
0.97
1.92
1.96
1.31
1.29
0.71
2.88
0.93
6.15
1.77
2.26
2.02
2.10
1.93
f1 (ppm)

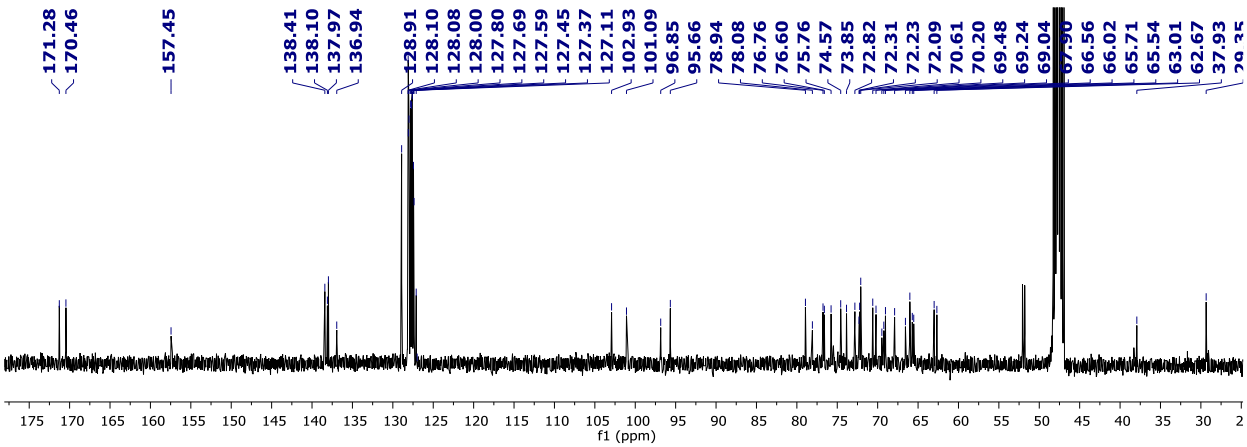
171.28
170.46
157.45
138.41
138.10
137.97
136.94
128.91
128.10
128.08
128.00
127.80
127.69
127.59
127.45
127.37
127.11
102.93
101.09
96.85
95.66
78.94
78.08
76.76
76.60
75.76
74.57
73.85
72.82
72.31
72.23
72.09
70.61
70.20
69.48
69.24
69.04
66.56
66.02
65.71
65.54
63.01
62.67
37.93
f1 (ppm)

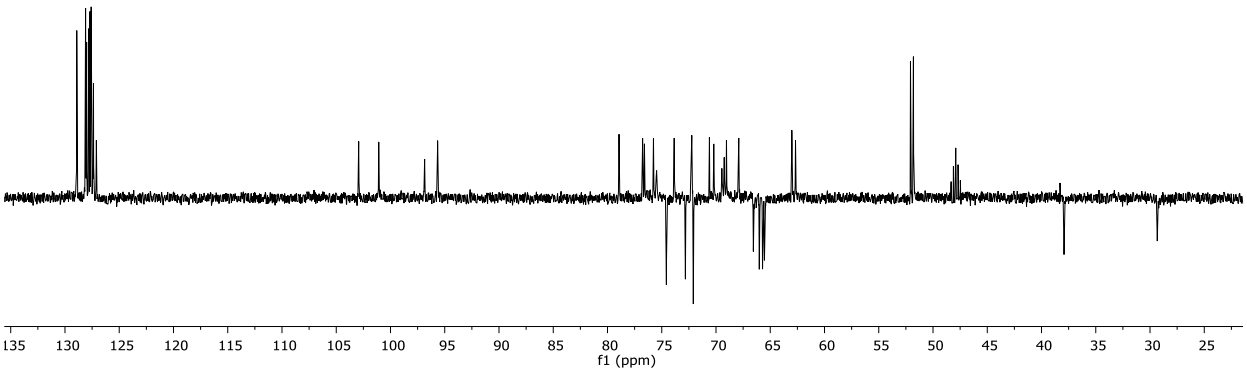
f1 (ppm)

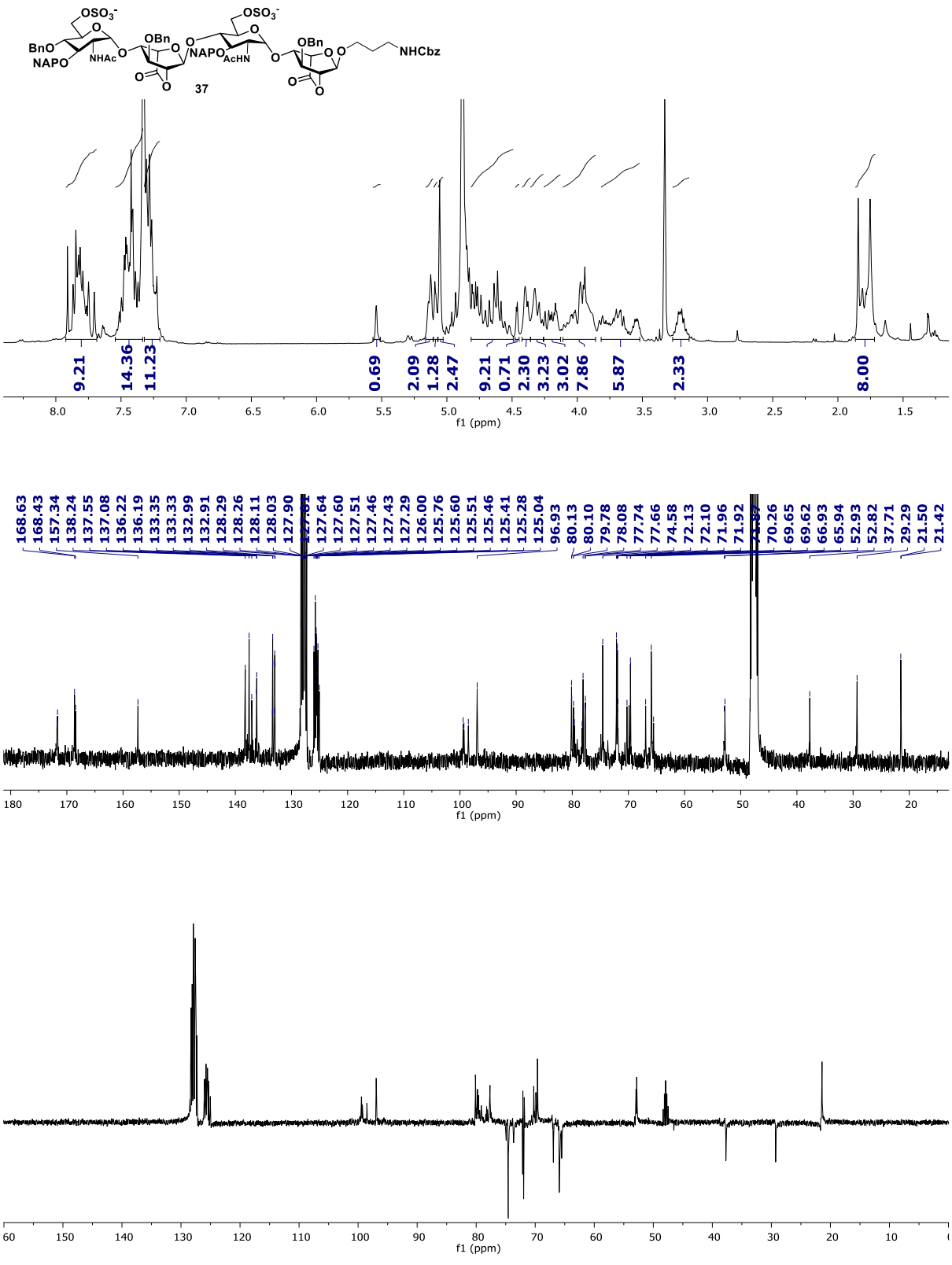
OSO3-
BnO
NAPO
NHAc
OBn
NAPO
AcHN
OBn
NHCbz
37
9.21
14.36
11.23
0.69
2.09
1.28
2.47
9.21
0.71
2.30
3.23
3.02
7.86
5.87
2.33
8.00
f1 (ppm)
168.63
168.43
157.34
138.24
137.55
137.08
136.22
136.19
133.35
133.33
132.99
132.91
128.29
128.26
128.11
128.03
127.90
127.64
127.60
127.51
127.46
127.43
127.29
126.00
125.76
125.60
125.51
125.46
125.41
125.28
125.04
96.93
80.13
80.10
79.78
78.08
77.74
77.66
74.58
72.13
72.10
71.96
71.92
70.26
69.65
69.62
66.93
65.94
52.93
52.82
37.71
29.29
21.50
21.42
f1 (ppm)
f1 (ppm)

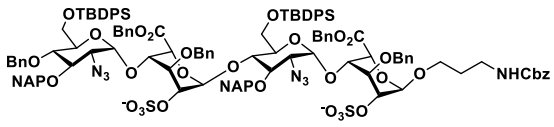
OTBDPS
BnO2C
OBn
BnO
NAPO
N3
O
-O3SO
NHCbz

40

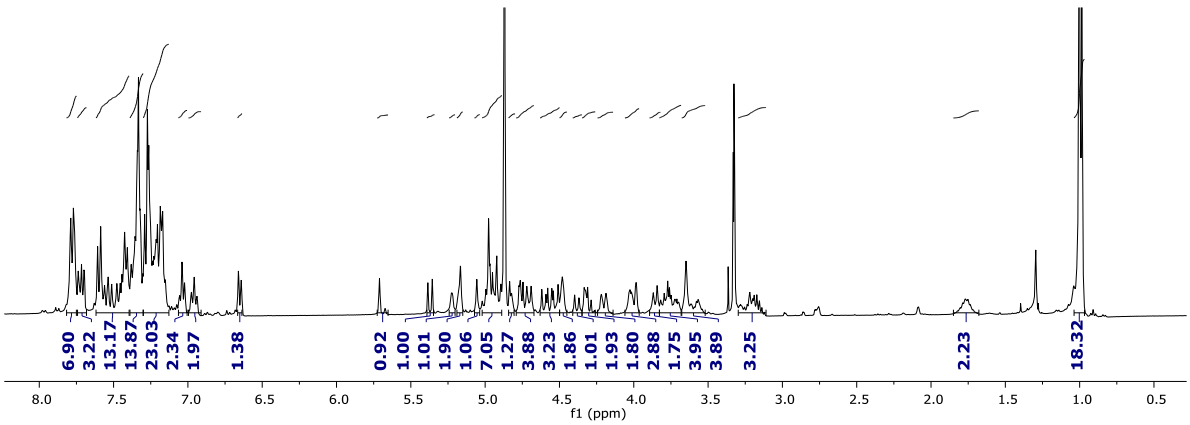
6.90
3.22
13.17
13.87
23.03
2.34
1.97
1.38
0.92
1.00
1.01
1.90
1.06
7.05
1.27
3.88
3.23
1.86
1.01
1.93
1.80
2.88
1.75
3.95
3.89
3.25
2.23
18.32
f1 (ppm)

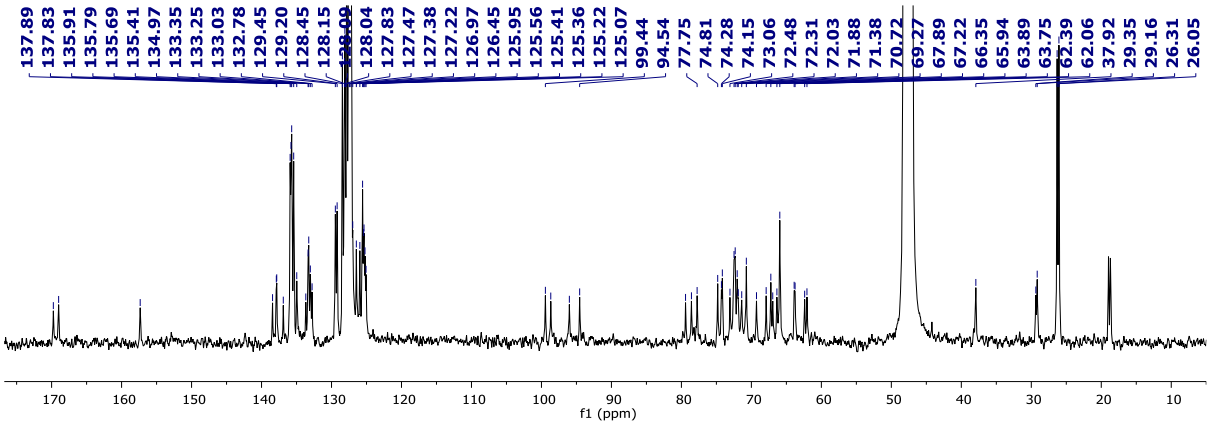
137.89
137.83
135.91
135.79
135.69
135.41
134.97
133.35
133.25
133.03
132.78
129.45
129.20
128.45
128.15
128.09
128.04
127.83
127.47
127.38
127.22
126.97
126.45
125.95
125.56
125.41
125.36
125.22
125.07
99.44
94.54
77.75
74.81
74.28
74.15
73.06
72.48
72.31
72.03
71.88
71.38
70.72
69.27
67.89
67.22
66.35
65.94
63.89
63.75
62.39
62.06
37.92
29.35
29.16
26.31
26.05
f1 (ppm)

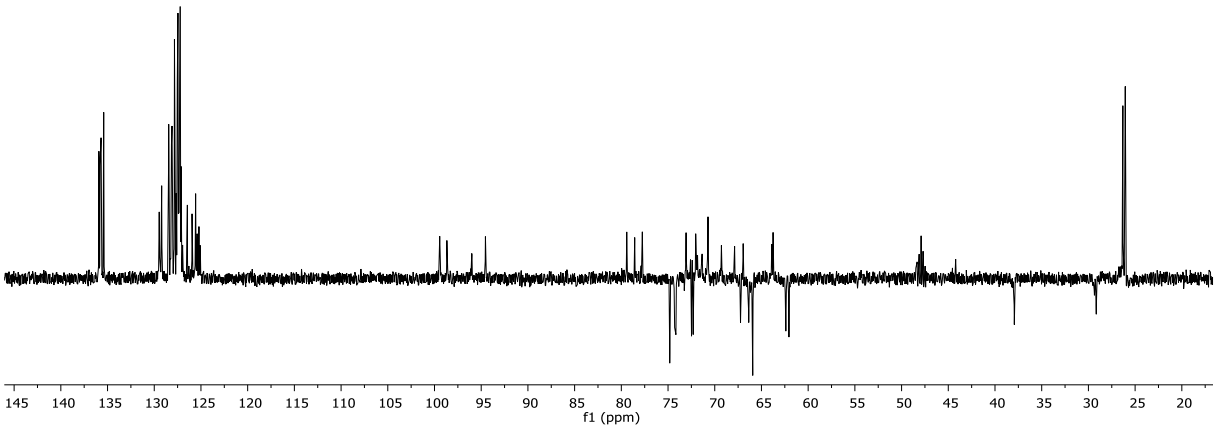
f1 (ppm)

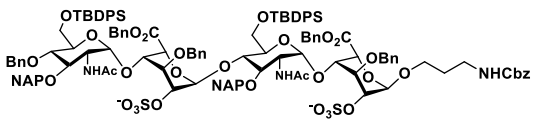
OTBDPS
BnO2C
OBn
BnO
NAPO
NHAc
O
-O3SO
NHCbz

43

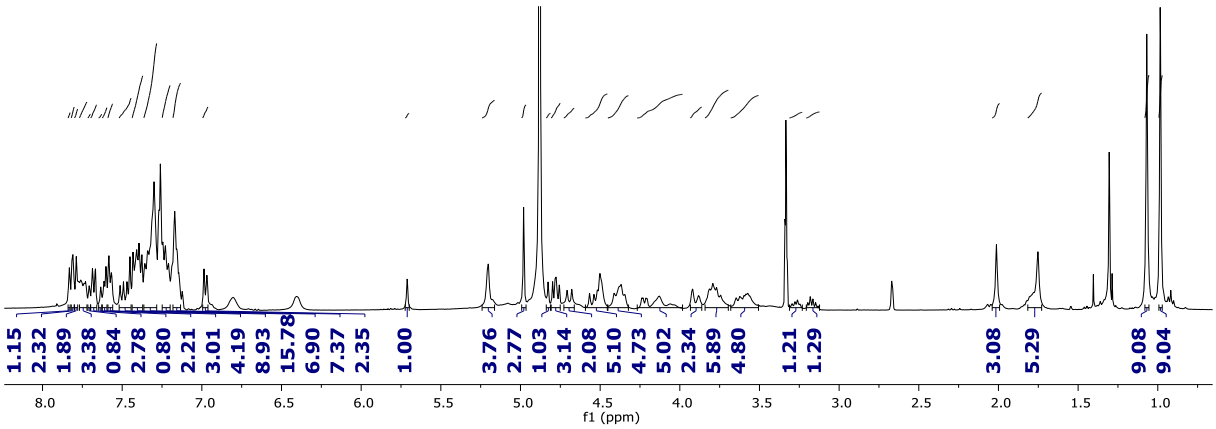
1.15 2.32 1.89 3.38 0.84 2.78 0.80 2.21 3.01 4.19 8.93 15.78 6.90 7.37 2.35 1.00 3.76 2.77 1.03 3.14 2.08 5.10 4.73 5.02 2.34 5.89 4.80 1.21 1.29 3.08 5.29 9.08 9.04
f1 (ppm)

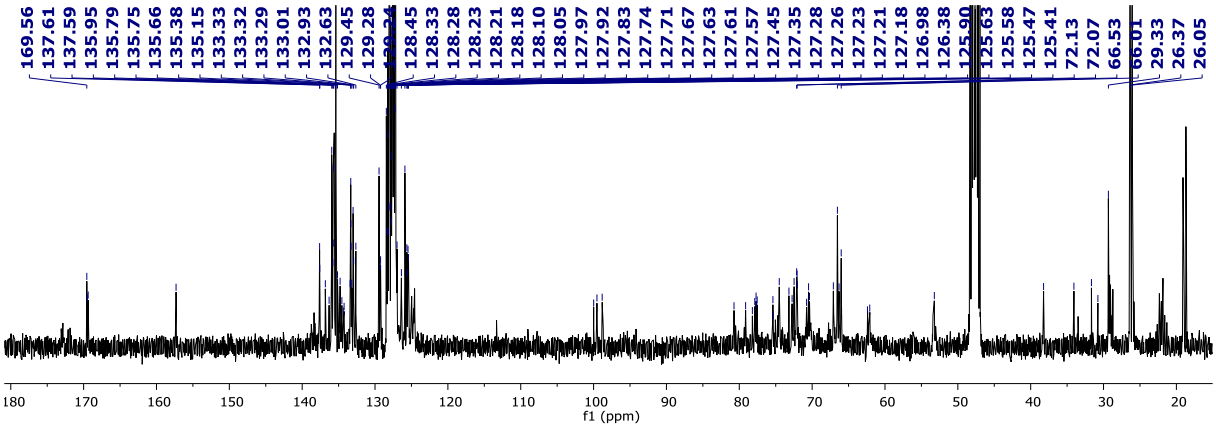
169.56 137.61 137.59 135.95 135.79 135.75 135.66 135.38 135.15 133.33 133.32 133.29 133.01 132.93 132.63 129.45 129.28 128.45 128.33 128.28 128.23 128.21 128.18 128.10 128.05 127.97 127.92 127.83 127.74 127.71 127.67 127.63 127.61 127.57 127.45 127.35 127.28 127.26 127.23 127.21 127.18 126.98 126.38 125.90 125.63 125.58 125.47 125.41 72.13 72.07 66.53 66.01 29.33 26.37 26.05
f1 (ppm)

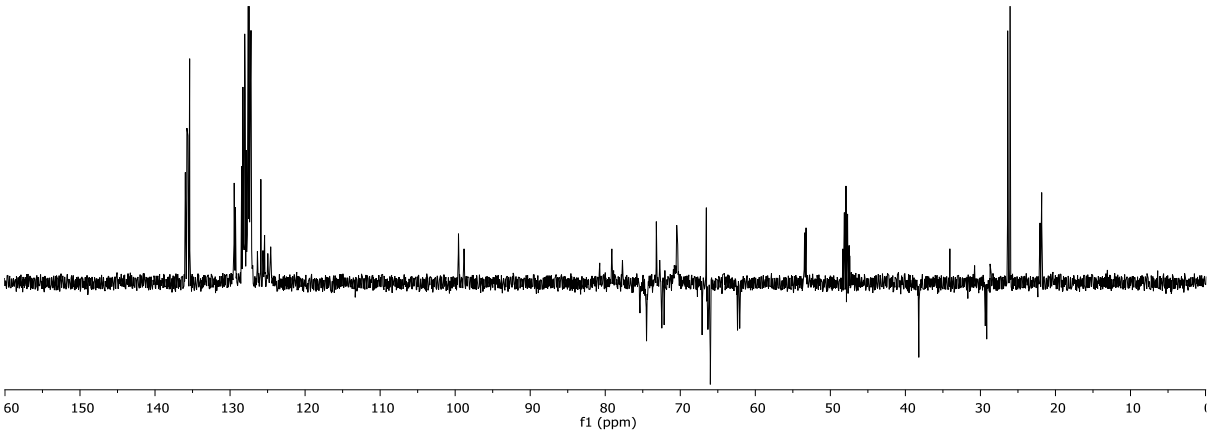
f1 (ppm)

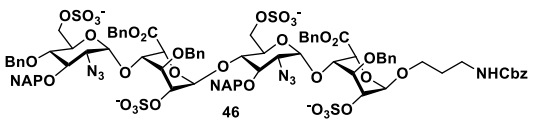
OSO3-
BnO2C
OBn
BnO
NAPO
N3
O
-O3SO
NHCbz

46

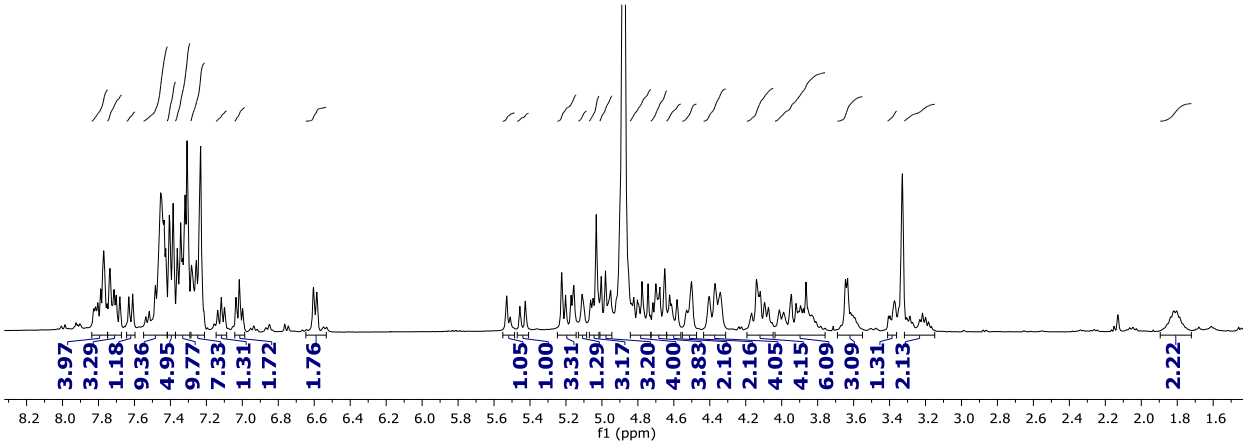
3.97 3.29 1.18 9.36 4.95 9.77 7.33 1.31 1.72 1.76 1.05 1.00 3.31 1.29 3.17 3.20 4.00 3.83 2.16 2.16 4.05 4.15 6.09 3.09 1.31 2.13 2.22
f1 (ppm)

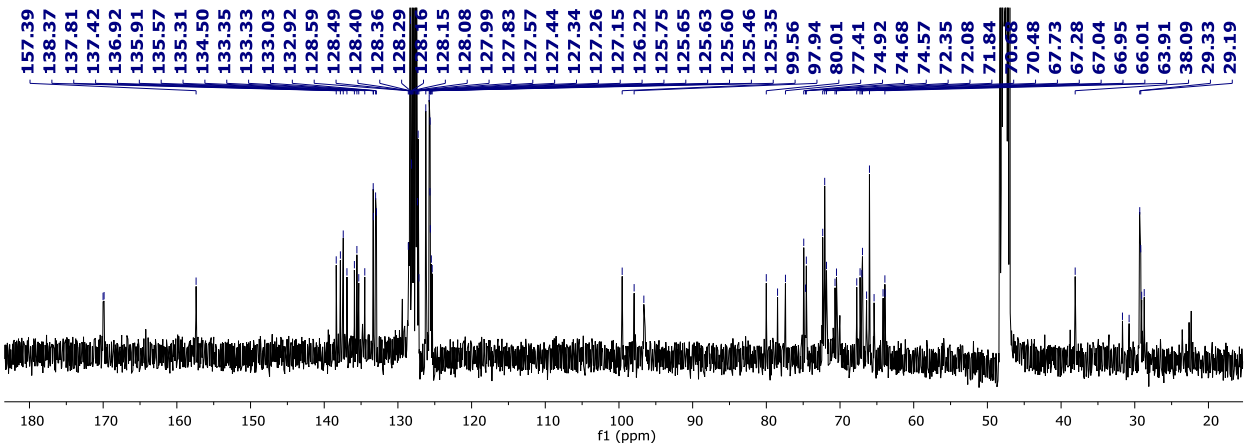
157.39 138.37 137.81 137.42 136.92 135.91 135.57 135.31 134.50 133.35 133.33 133.03 132.92 128.59 128.49 128.40 128.36 128.29 128.16 128.15 128.08 127.99 127.83 127.57 127.44 127.34 127.26 127.15 126.22 125.75 125.65 125.63 125.60 125.46 125.35 99.56 97.94 80.01 77.41 74.92 74.68 74.57 72.35 72.08 71.84 70.68 70.48 67.73 67.28 67.04 66.95 66.01 63.91 38.09 29.33 29.19
f1 (ppm)

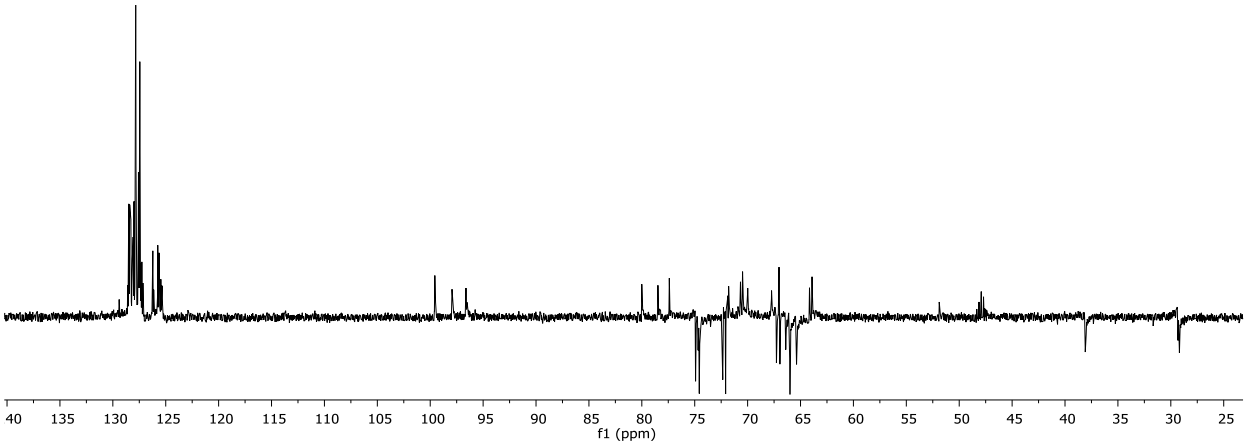
f1 (ppm)

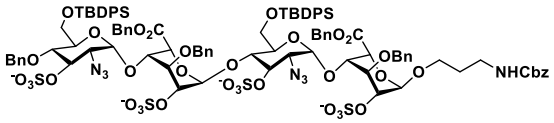
OTBDPS
BnO2C
OBn
BnO
-O3SO
N3
O
NHCbz

48

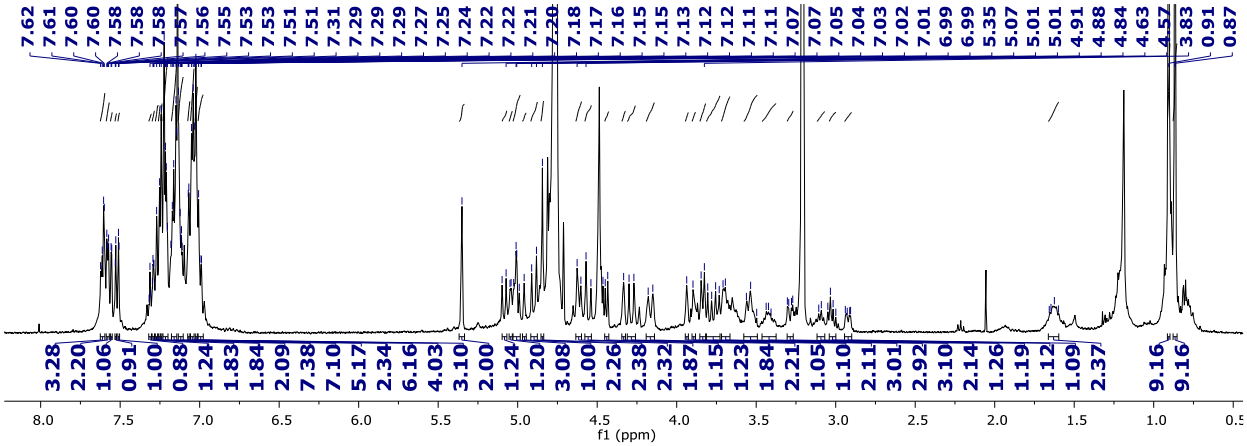
7.62 7.61 7.60 7.60 7.58 7.58 7.57 7.56 7.55 7.53 7.51 7.51 7.31 7.29 7.29 7.27 7.25 7.24 7.22 7.22 7.21 7.20 7.18 7.17 7.16 7.15 7.15 7.13 7.12 7.12 7.11 7.11 7.07 7.07 7.05 7.04 7.03 7.02 7.01 6.99 6.99 5.35 5.07 5.01 5.01 4.91 4.88 4.84 4.63 4.57 3.83 0.91 0.87
3.28 2.20 1.06 0.91 1.00 0.88 1.24 1.83 1.84 2.09 7.38 7.10 5.17 2.34 6.16 4.03 3.10 2.00 1.24 1.20 3.08 1.00 2.26 2.38 2.32 1.87 1.15 1.23 1.84 2.21 1.05 1.10 2.11 3.01 2.92 3.10 2.14 1.26 1.19 1.12 1.09 2.37 9.16 9.16
f1 (ppm)

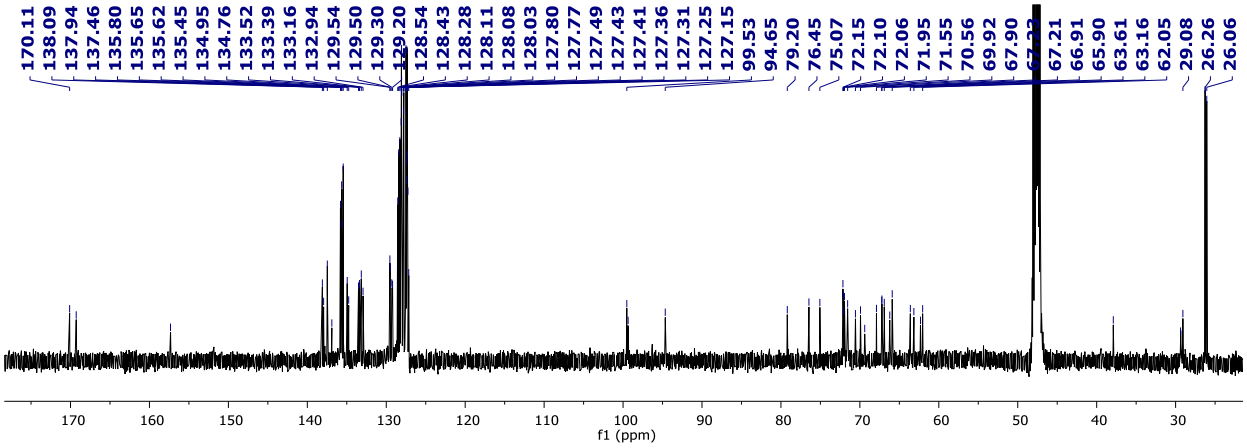
170.11 138.09 137.94 137.46 135.80 135.65 135.62 135.45 134.95 134.76 133.52 133.39 133.16 132.94 129.54 129.50 129.30 129.20 128.54 128.43 128.28 128.11 128.08 128.03 127.80 127.77 127.49 127.43 127.41 127.36 127.31 127.25 127.15 99.53 94.65 79.20 76.45 75.07 72.15 72.10 72.06 71.95 71.55 70.56 69.92 67.90 67.22 67.21 66.91 65.90 63.61 63.16 62.05 29.08 26.26 26.06
f1 (ppm)

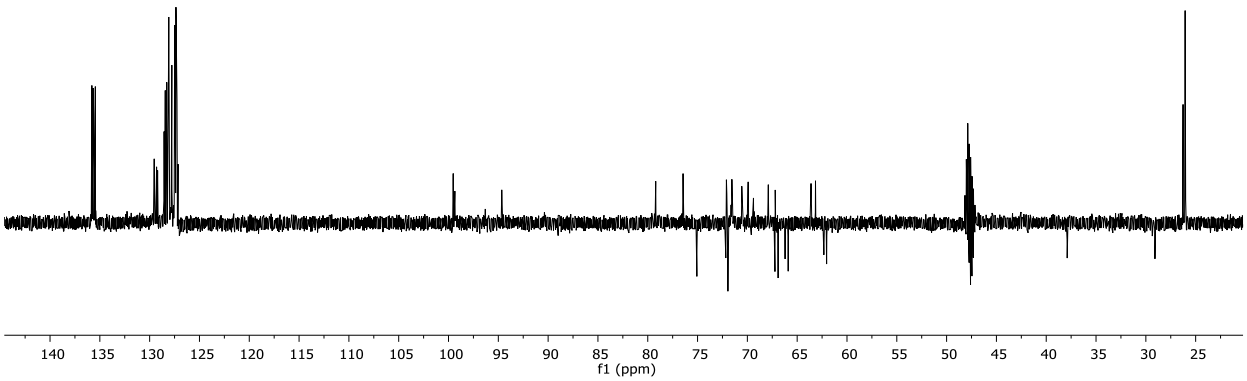
f1 (ppm)

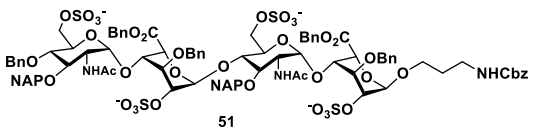
OSO3-
BnO2C
OBn
BnO
NAPO
NHAc
O
-O3SO
NHCbz

51

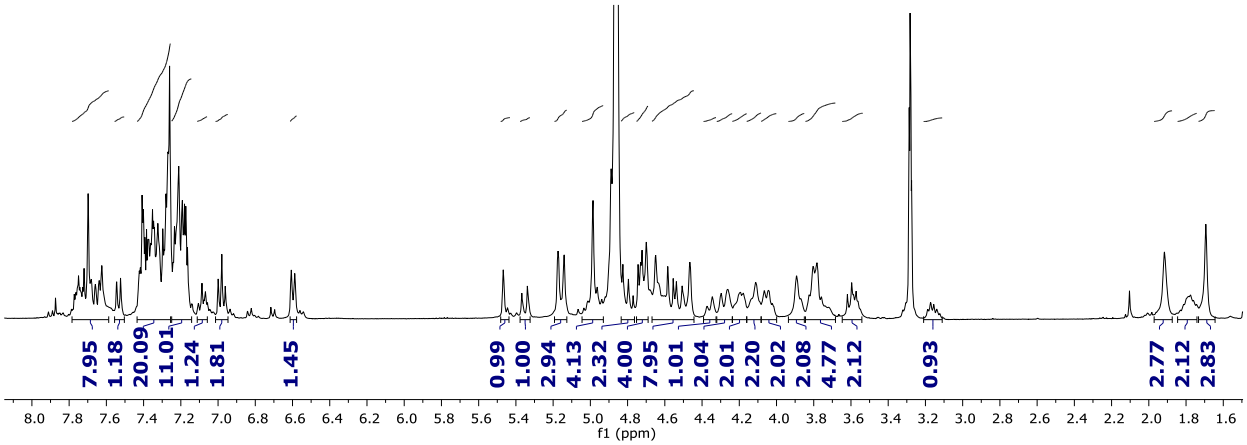
7.95 1.18 20.09 11.01 1.24 1.81 1.45 0.99 1.00 2.94 4.13 2.32 4.00 7.95 1.01 2.04 2.01 2.20 2.02 2.08 4.77 2.12 0.93 2.77 2.12 2.83
f1 (ppm)

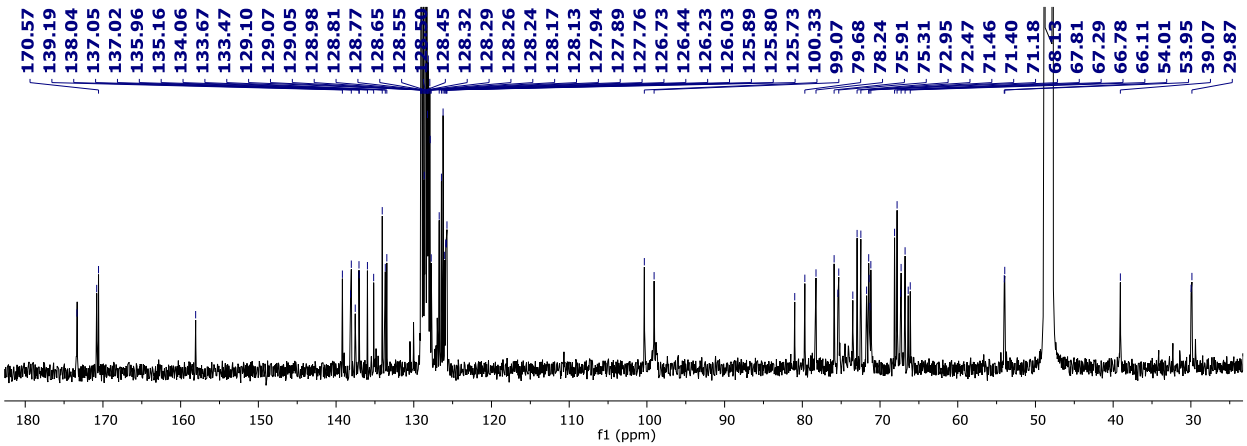
170.57 139.19 138.04 137.05 137.02 135.96 135.16 134.06 133.67 133.47 129.10 129.07 129.05 128.98 128.81 128.77 128.65 128.55 128.45 128.32 128.29 128.26 128.24 128.17 128.13 127.94 127.89 127.76 126.73 126.44 126.23 126.03 125.89 125.80 125.73 100.33 99.07 79.68 78.24 75.91 75.31 72.95 72.47 71.46 71.40 71.18 68.13 67.81 67.29 66.78 66.11 54.01 53.95 39.07 29.87
f1 (ppm)

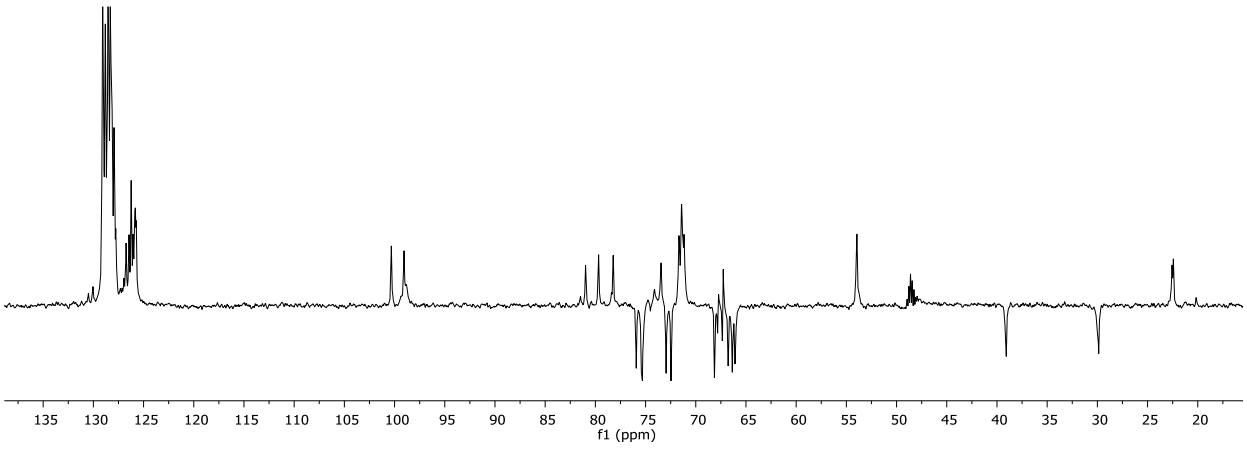
f1 (ppm)

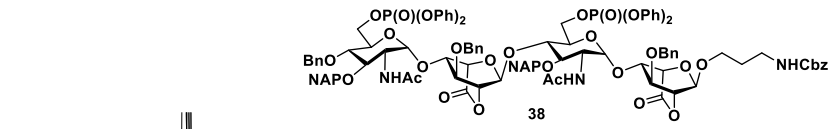
OP(O)(OPh)2
OP(O)(OPh)2
BnO
NAPO
NHAc
OBn
NAPO
AcHN
OBn
NHCbz
38

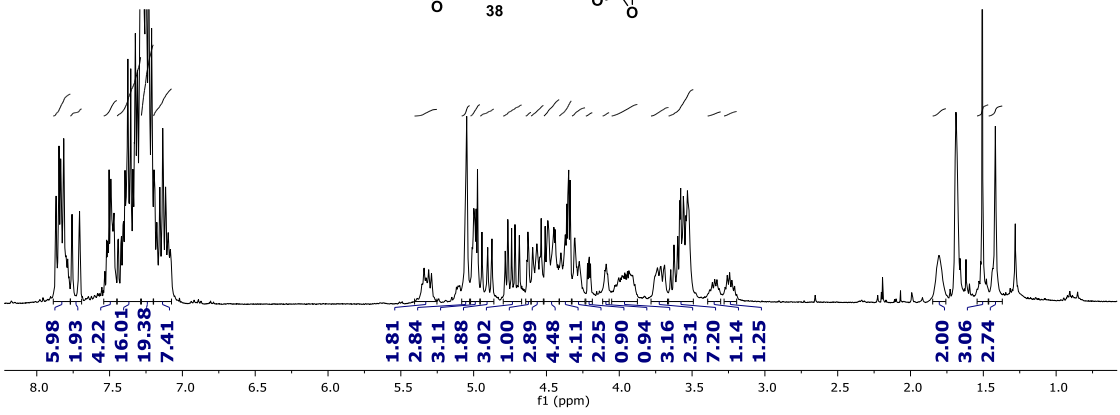
5.98
1.93
4.22
16.01
19.38
7.41
1.81
2.84
3.11
1.88
3.02
1.00
2.89
4.48
4.11
2.25
0.90
0.94
3.16
2.31
7.20
1.14
1.25
2.00
3.06
2.74
f1 (ppm)

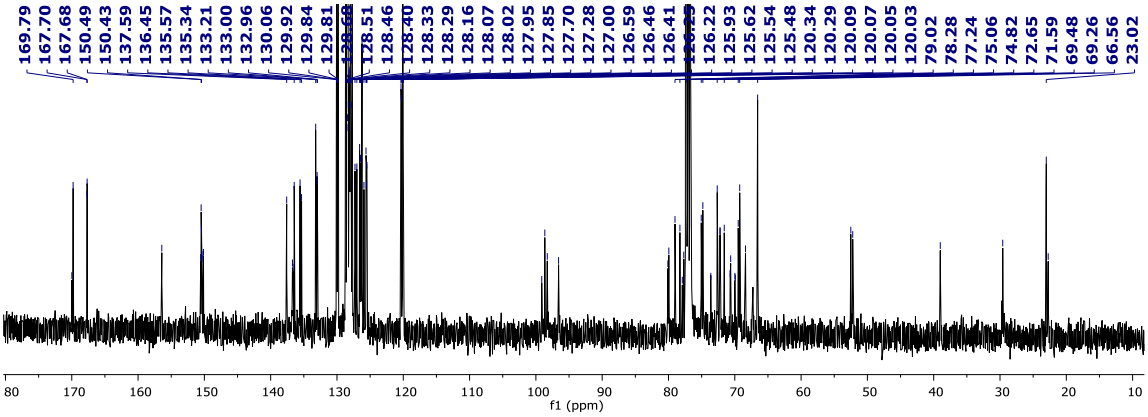
169.79
167.70
167.68
150.49
150.43
137.59
136.45
135.57
135.34
133.21
133.00
132.96
130.06
129.92
129.84
129.81
128.51
128.46
128.40
128.33
128.29
128.16
128.07
128.02
127.95
127.85
127.70
127.28
127.00
126.59
126.46
126.41
126.22
125.93
125.62
125.54
125.48
120.34
120.29
120.09
120.07
120.05
120.03
79.02
78.28
77.24
75.06
74.82
72.65
71.59
69.48
69.26
66.56
23.02
f1 (ppm)

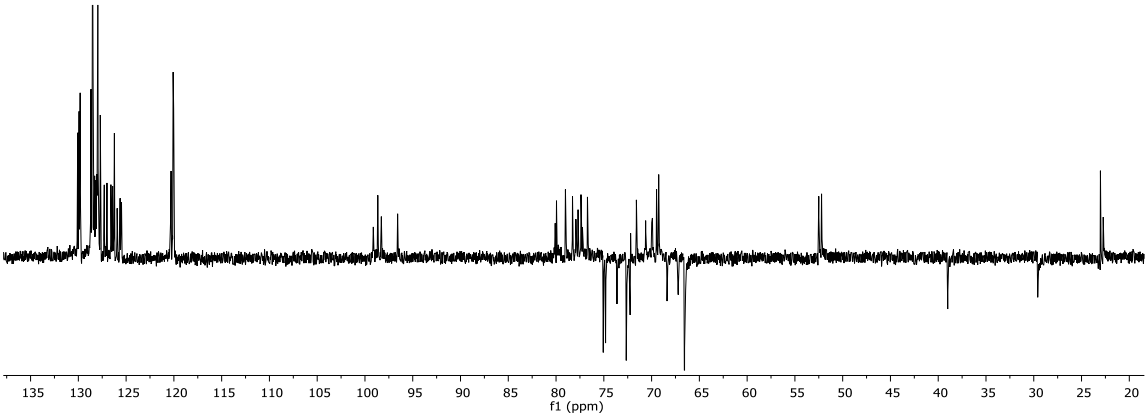
f1 (ppm)

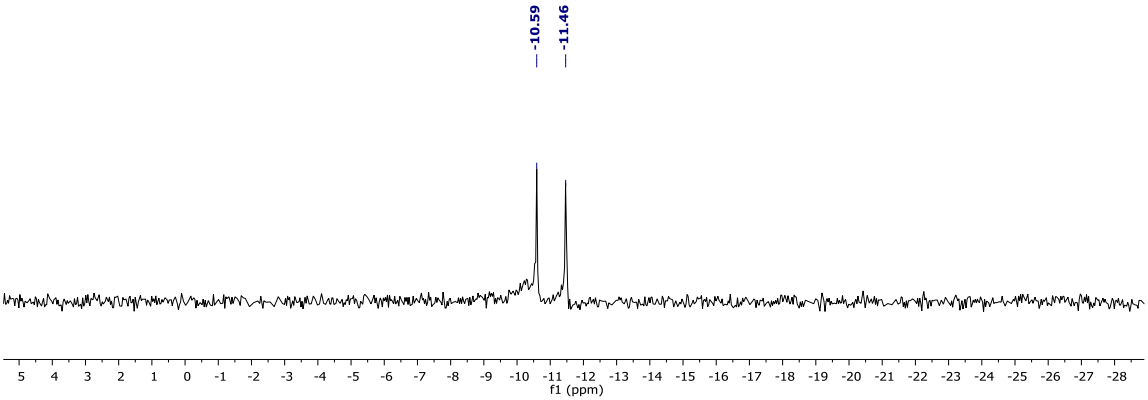
-10.59
-11.46
f1 (ppm)

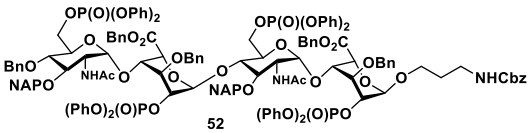
OP(O)(OPh)2
BnO2C
OBn
BnO
NAPO
NHAc
O
(PhO)2(O)PO
NHCbz

52

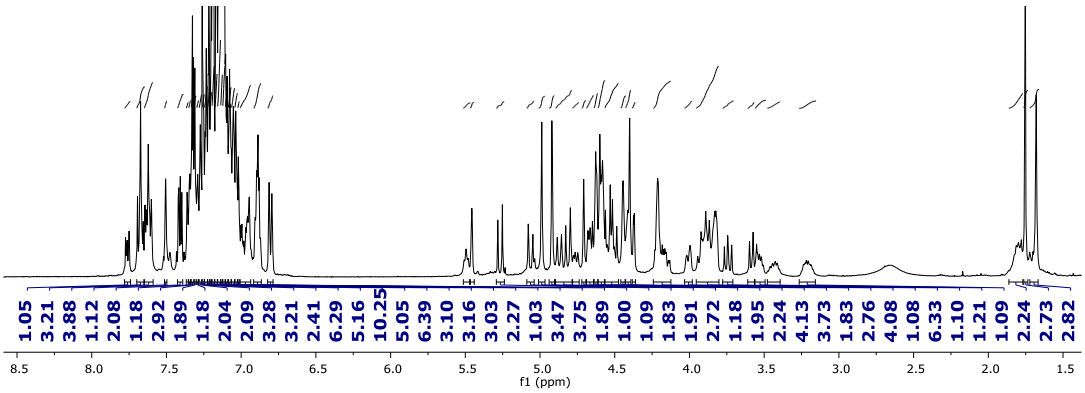
1.05 3.21 3.88 1.12 2.08 1.18 2.92 1.89 1.18 2.04 2.09 3.28 3.21 2.41 6.29 5.16 10.25 5.05 6.39 3.10 3.16 3.03 2.27 1.03 3.47 3.75 1.89 1.00 1.09 1.83 1.91 2.72 1.18 1.95 2.24 4.13 3.73 1.83 2.76 4.08 1.08 6.33 1.10 1.21 1.09 2.24 2.73 2.82
8.5 8.0 7.5 7.0 6.5 6.0 5.5 5.0 4.5 4.0 3.5 3.0 2.5 2.0 1.5
f1 (ppm)

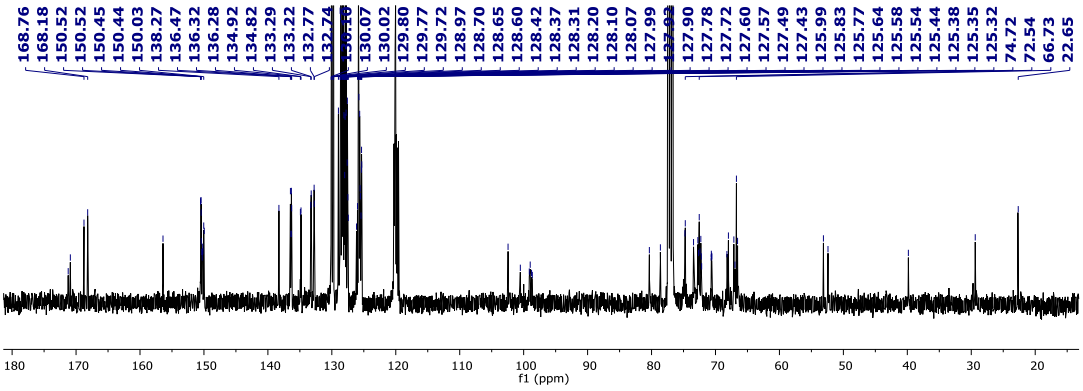
168.76 168.18 150.52 150.52 150.45 150.44 150.03 138.27 136.47 136.32 136.28 134.92 134.82 133.29 133.22 132.77 132.74 130.30 130.07 130.02 129.80 129.77 129.72 128.97 128.70 128.65 128.60 128.42 128.37 128.31 128.20 128.10 128.07 127.99 127.93 127.90 127.78 127.72 127.60 127.57 127.49 127.43 125.99 125.83 125.77 125.64 125.58 125.54 125.44 125.38 125.35 125.32 74.72 72.54 66.73 22.65
180 170 160 150 140 130 120 110 100 90 80 70 60 50 40 30 20
f1 (ppm)

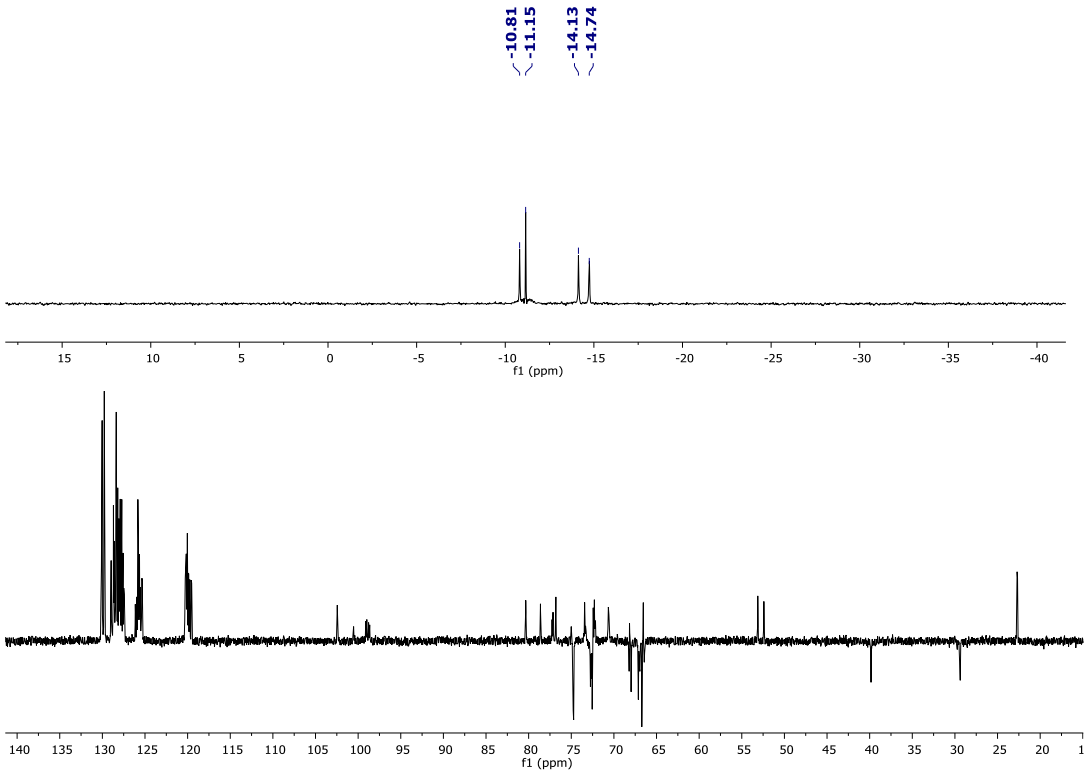
-10.81
-11.15
-14.13
-14.74
15
10
5
0
-5
-10
-15
-20
-25
-30
-35
-40
f1 (ppm)
140
135
130
125
120
115
110
105
100
95
90
85
80
75
70
65
60
55
50
45
40
35
30
25
20
f1 (ppm)

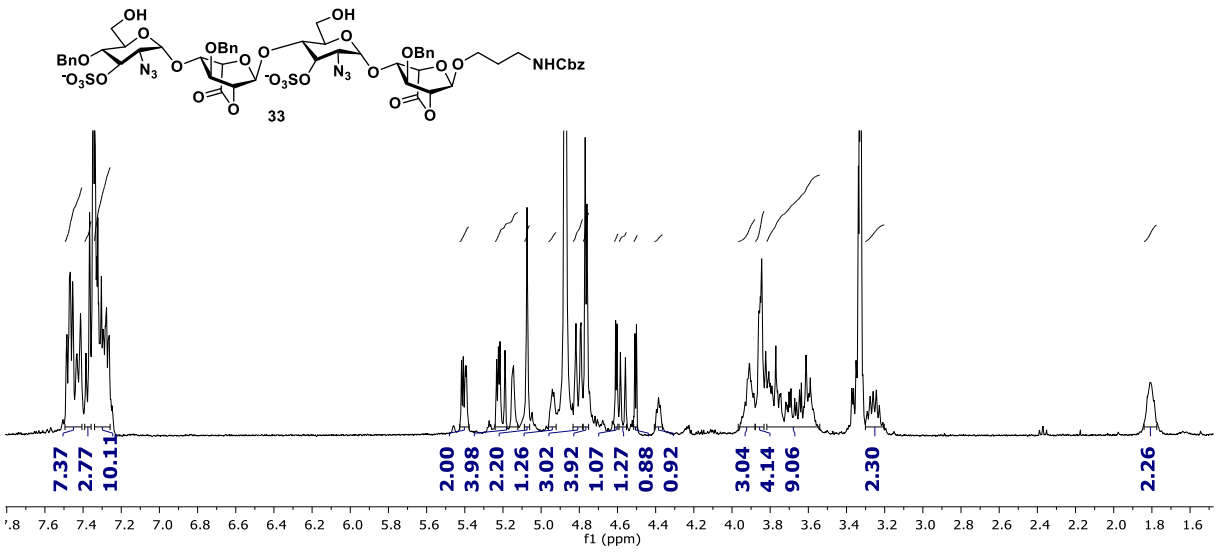
OH
BnO
OBn
$^{-}O_3SO$
$N_3$
NHCbz
33
7.37
2.77
10.11
2.00
3.98
2.20
1.26
3.02
3.92
1.07
1.27
0.88
0.92
3.04
4.14
9.06
2.30
2.26
f1 (ppm)

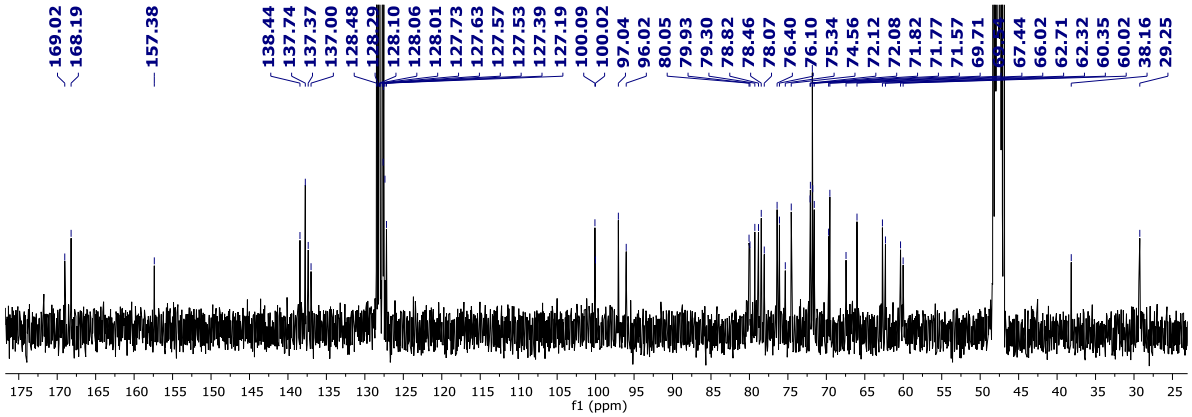
169.02
168.19
157.38
138.44
137.74
137.37
137.00
128.48
128.29
128.10
128.06
128.01
127.73
127.63
127.57
127.53
127.39
127.19
100.09
100.02
97.04
96.02
80.05
79.93
79.30
78.82
78.46
78.07
76.40
76.10
75.34
74.56
72.12
72.08
71.82
71.77
71.57
69.71
67.44
66.02
62.71
62.32
60.35
60.02
38.16
29.25
f1 (ppm)

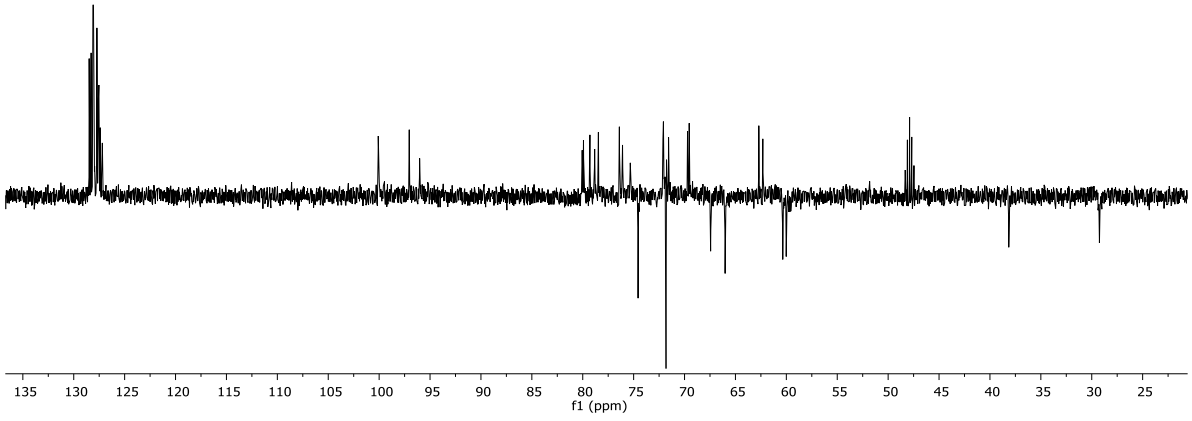
f1 (ppm)

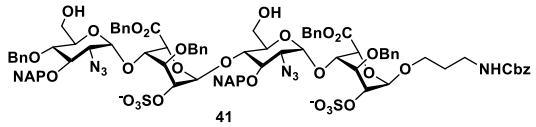
OH
BnO
NAPO
$N_3$
$BnO_2C$
OBn
$^-O_3SO$
NHCbz

41

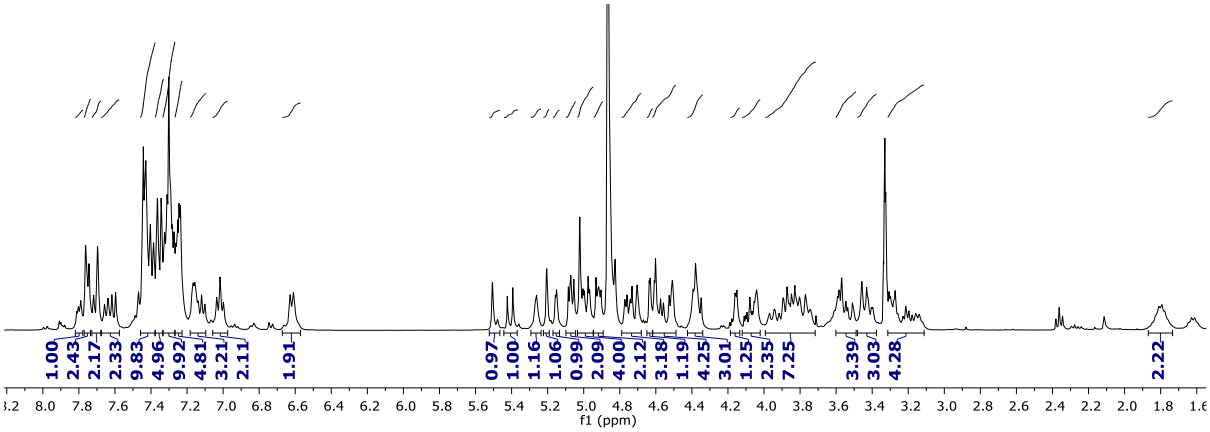
1.00 2.43 2.17 2.33 9.83 4.96 9.92 4.81 3.21 2.11 1.91 0.97 1.00 1.16 1.06 0.99 2.09 4.00 2.12 3.18 1.19 4.25 3.01 1.25 2.35 7.25 3.39 3.03 4.28 2.22
f1 (ppm)

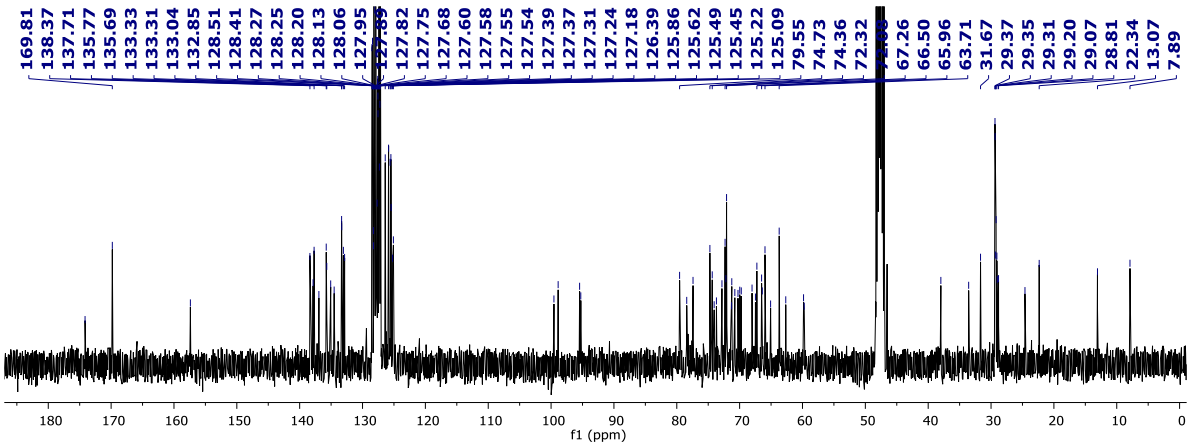
169.81 138.37 137.71 135.77 135.69 133.33 133.31 133.04 132.85 128.51 128.41 128.27 128.25 128.20 128.13 128.06 127.95 127.89 127.82 127.75 127.68 127.60 127.58 127.55 127.54 127.39 127.37 127.31 127.24 127.18 126.39 125.86 125.62 125.49 125.45 125.22 125.09 79.55 74.73 74.36 72.32 67.26 66.50 65.96 63.71 31.67 29.37 29.35 29.31 29.20 29.07 28.81 22.34 13.07 7.89
f1 (ppm)

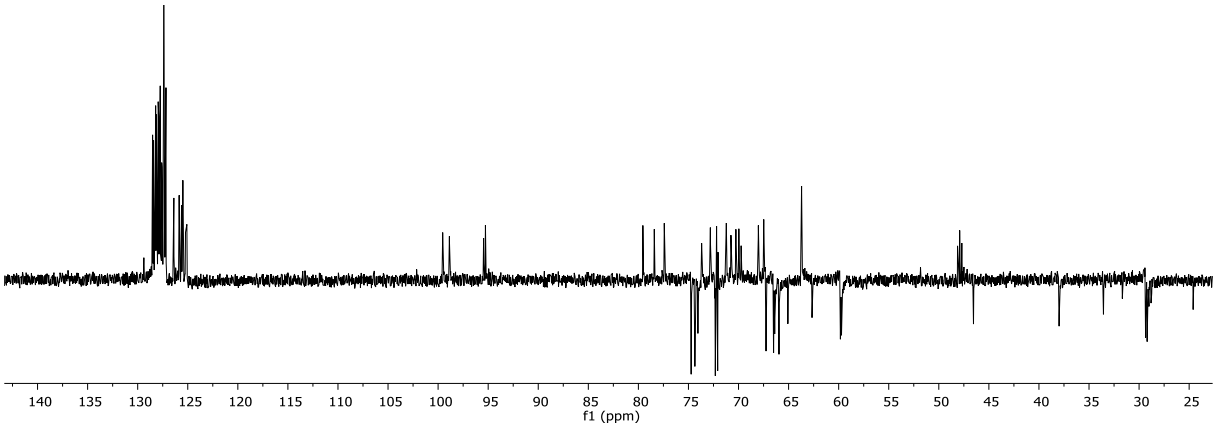
f1 (ppm)

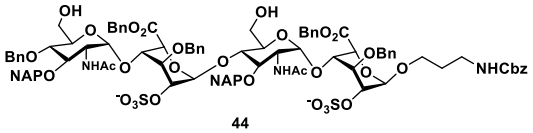
OH
BnO
NAPO
NHAc
BnO2C
OBn
O
-O3SO
NHCbz

44

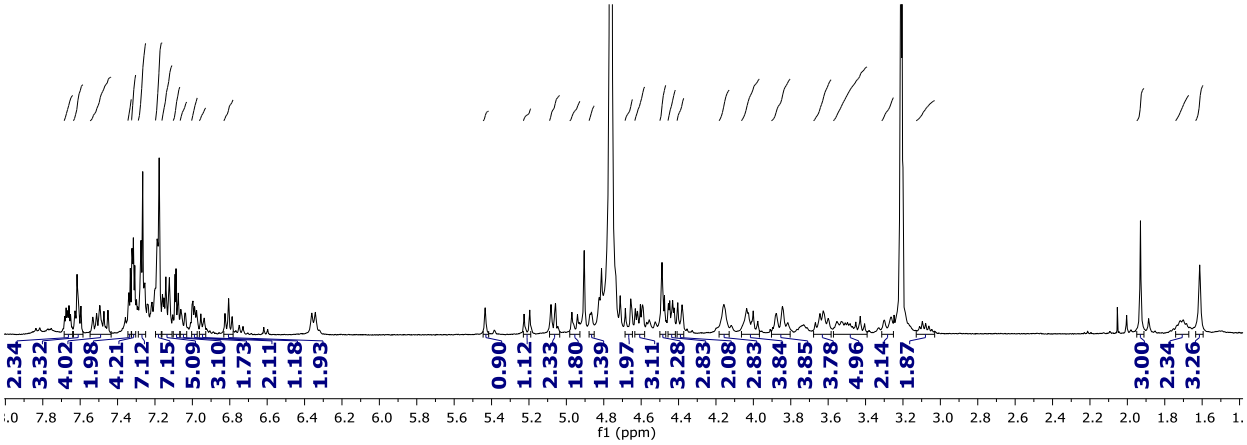
2.34 3.32 4.02 1.98 4.21 7.12 7.15 5.09 3.10 1.73 2.11 1.18 1.93
0.90 1.12 2.33 1.80 1.39 1.97 3.11 3.28 2.83 2.08 2.83 3.84 3.85 3.78 4.96 2.14 1.87
3.00 2.34 3.26
f1 (ppm)

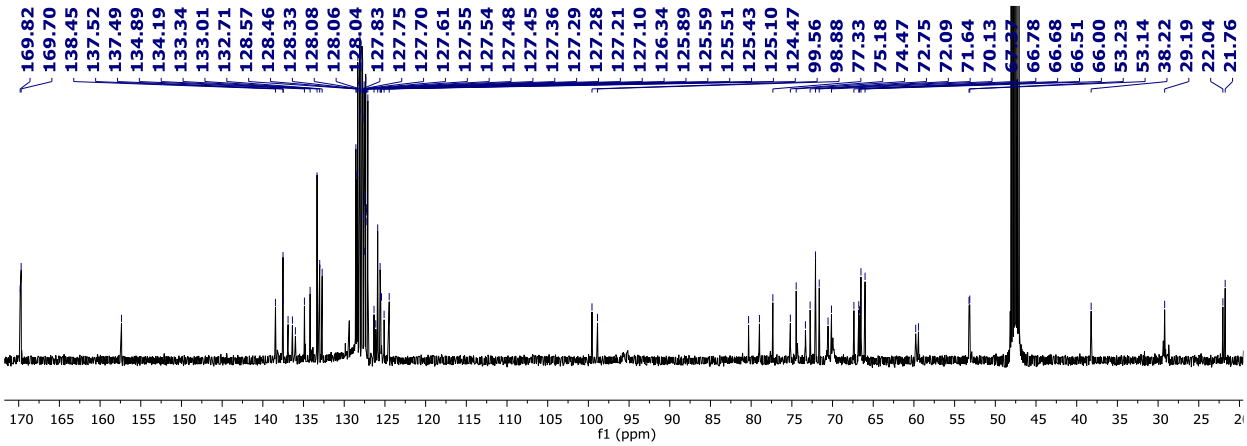
169.82 169.70 138.45 137.52 137.49 134.89 134.19 133.34 133.01 132.71 128.57 128.46 128.33 128.08 128.06 128.04 127.83 127.75 127.70 127.61 127.55 127.54 127.48 127.45 127.36 127.29 127.28 127.21 127.10 126.34 125.89 125.59 125.51 125.43 125.10 124.47 99.56 98.88 77.33 75.18 74.47 72.75 72.09 71.64 70.13 67.37 66.78 66.68 66.51 66.00 53.23 53.14 38.22 29.19 22.04 21.76
f1 (ppm)

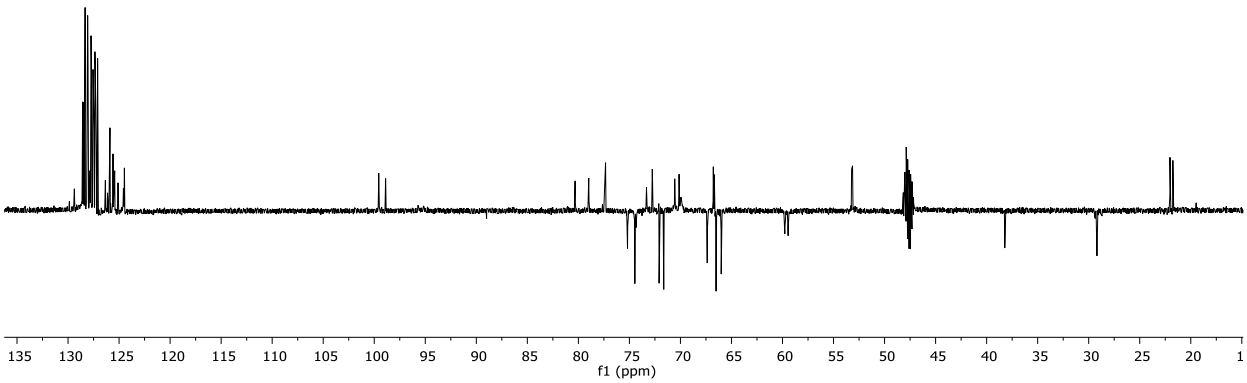
f1 (ppm)

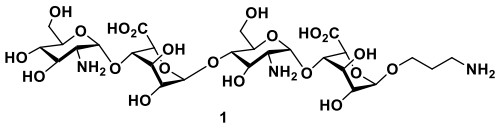

1

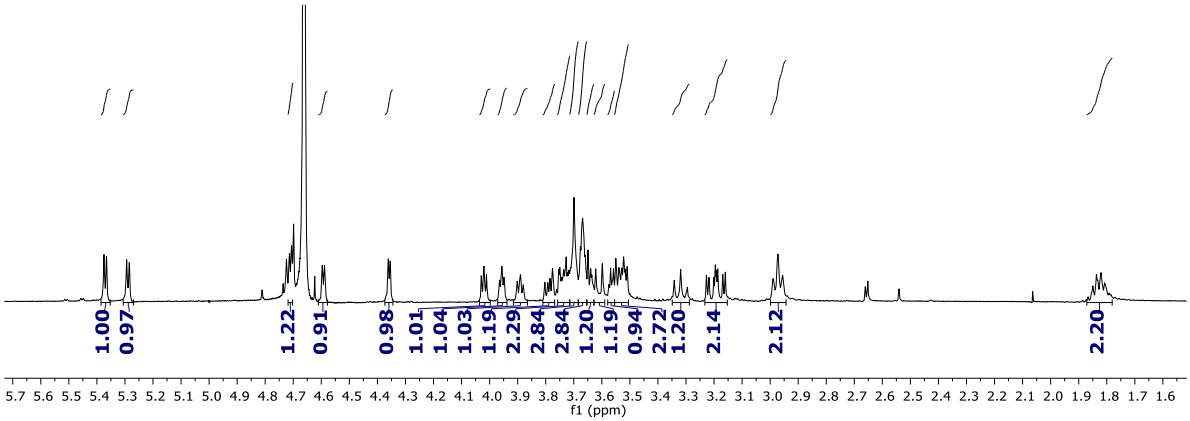
1.00
0.97
1.22
0.91
0.98
1.01
1.04
1.03
1.19
2.29
2.84
2.84
1.20
1.19
0.94
2.72
1.20
2.14
2.12
2.20
f1 (ppm)

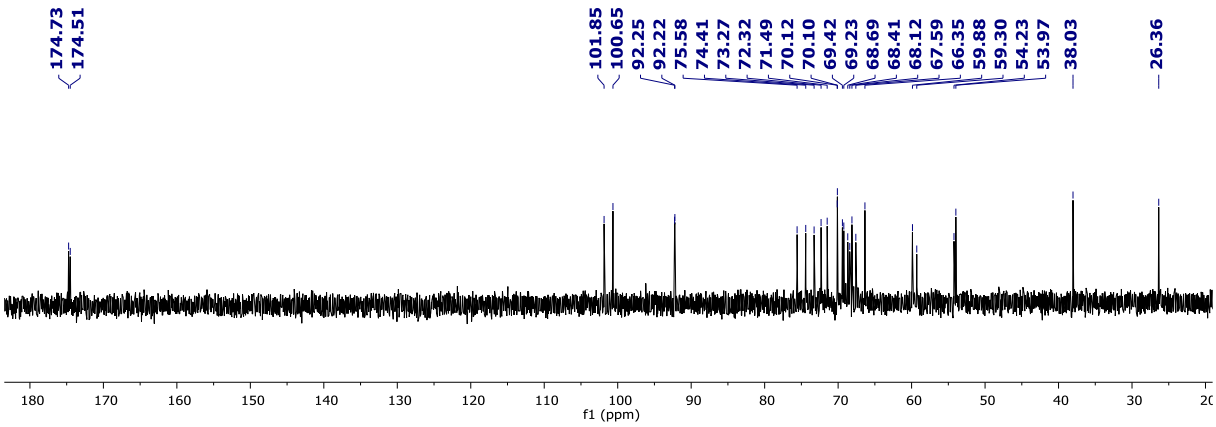
174.73
174.51
101.85
100.65
92.25
92.22
75.58
74.41
73.27
72.32
71.49
70.12
70.10
69.42
69.23
68.69
68.41
68.12
67.59
66.35
59.88
59.30
54.23
53.97
38.03
26.36
f1 (ppm)

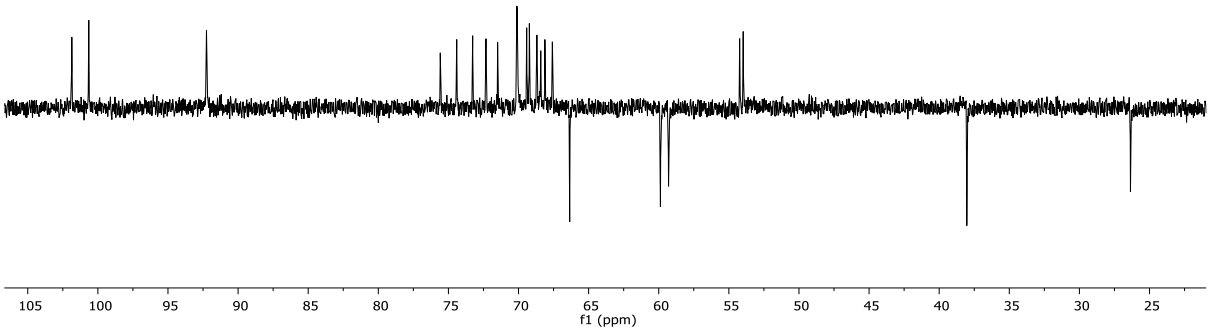
f1 (ppm)

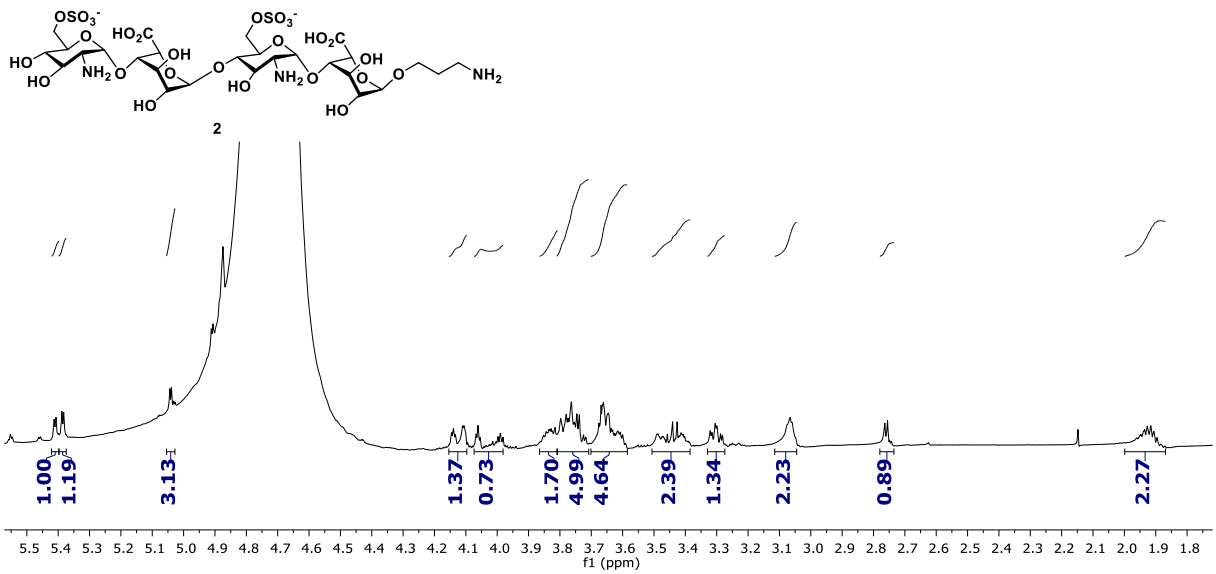
2
1.00
1.19
3.13
1.37
0.73
1.70
4.99
4.64
2.39
1.34
2.23
0.89
2.27
f1 (ppm)

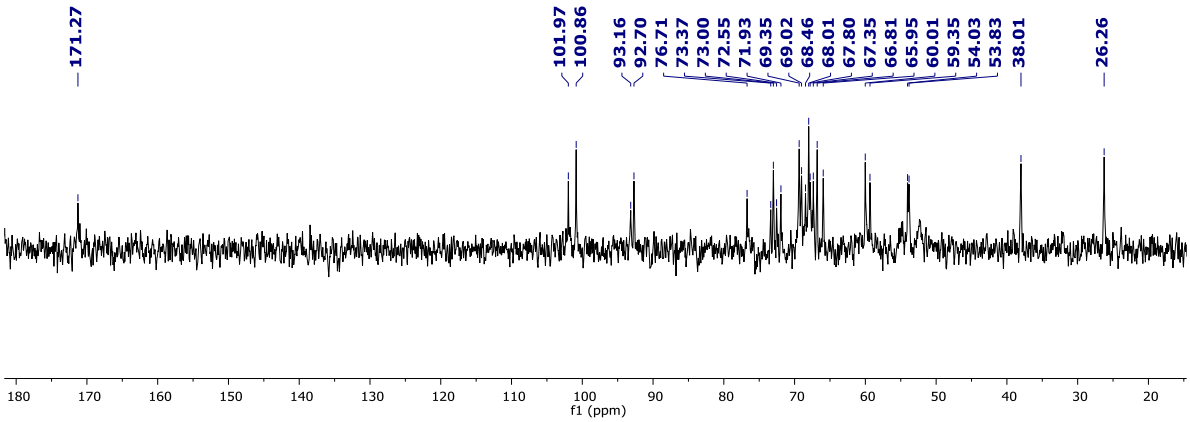
171.27
101.97
100.86
93.16
92.70
76.71
73.37
73.00
72.55
71.93
69.35
69.02
68.46
68.01
67.80
67.35
66.81
65.95
60.01
59.35
54.03
53.83
38.01
26.26
f1 (ppm)

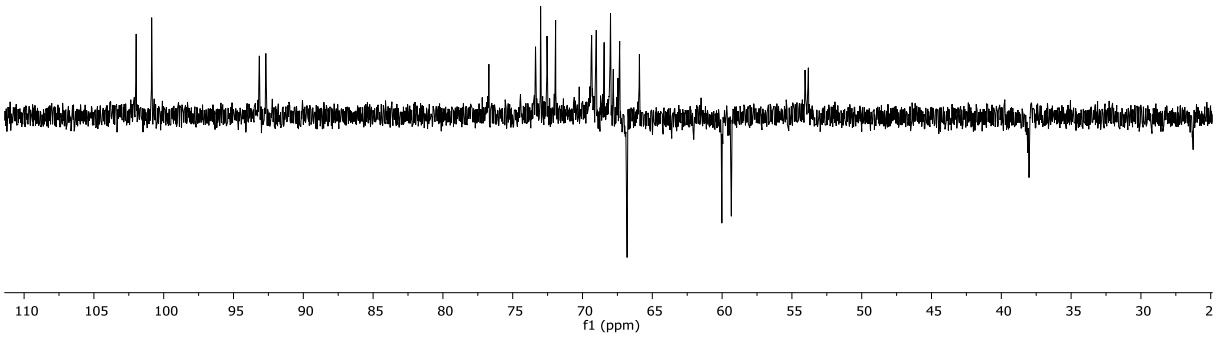
f1 (ppm)

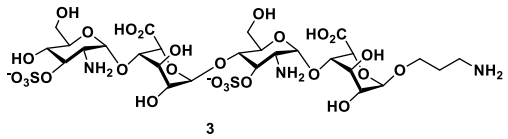

3

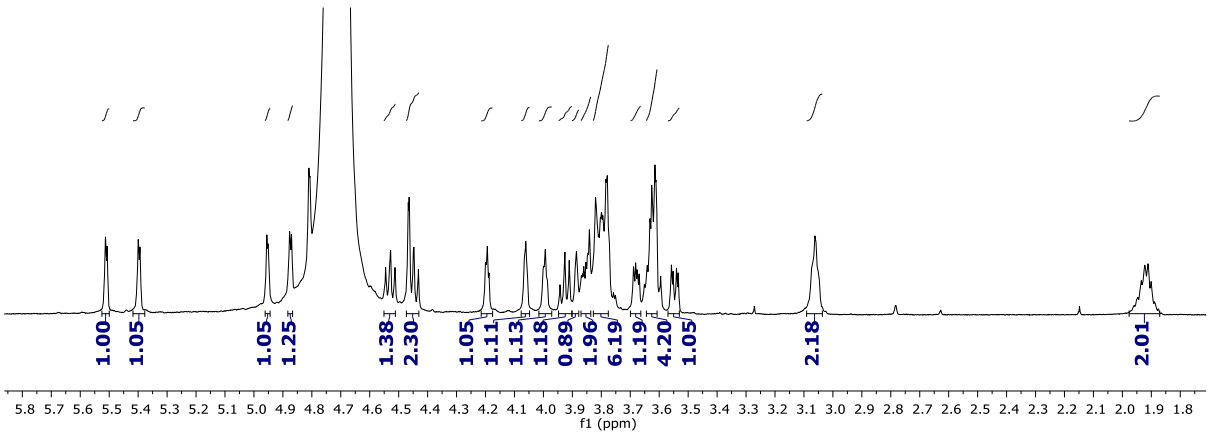
1.00
1.05
1.05
1.25
1.38
2.30
1.05
1.11
1.13
1.18
0.89
1.96
6.19
1.19
4.20
1.05
2.18
2.01
f1 (ppm)

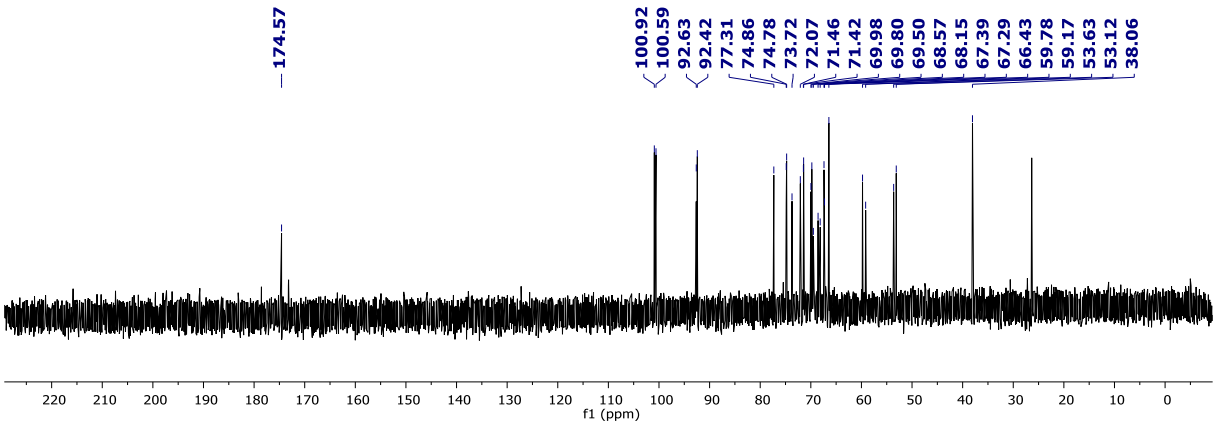
174.57
100.92
100.59
92.63
92.42
77.31
74.86
74.78
73.72
72.07
71.46
71.42
69.98
69.80
69.50
68.57
68.15
67.39
67.29
66.43
59.78
59.17
53.63
53.12
38.06
f1 (ppm)

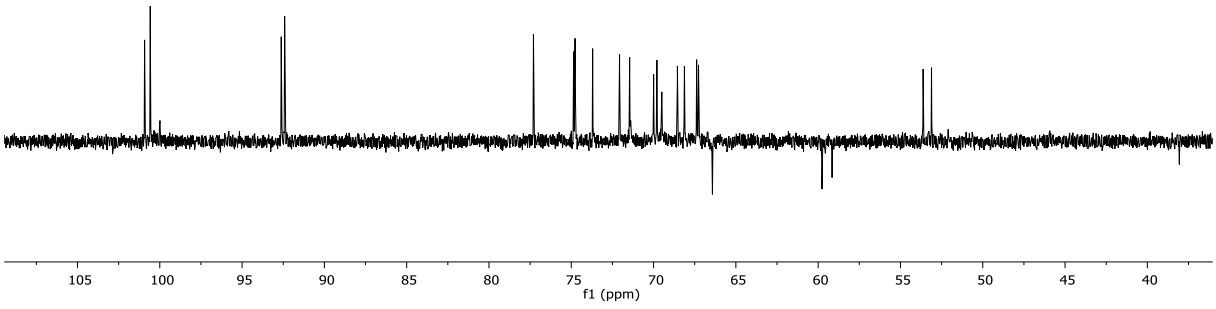
f1 (ppm)

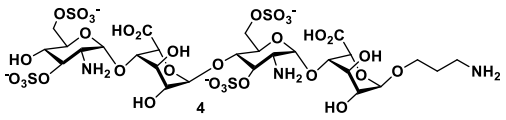

4

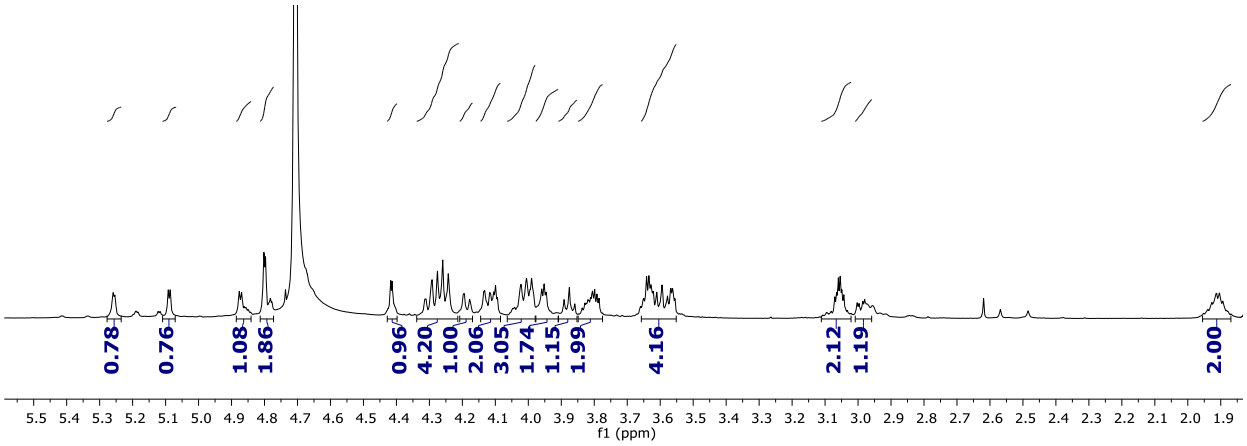
0.78
0.76
1.08
1.86
0.96
4.20
1.00
2.06
3.05
1.74
1.15
1.99
4.16
2.12
1.19
2.00
f1 (ppm)

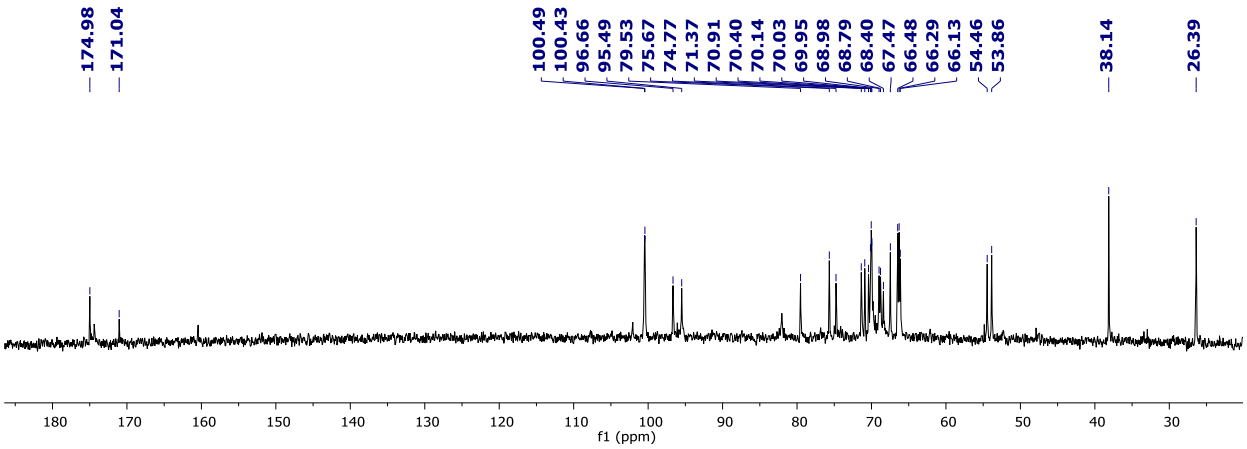
174.98
171.04
100.49
100.43
96.66
95.49
79.53
75.67
74.77
71.37
70.91
70.40
70.14
70.03
69.95
68.98
68.79
68.40
67.47
66.48
66.29
66.13
54.46
53.86
38.14
26.39
f1 (ppm)

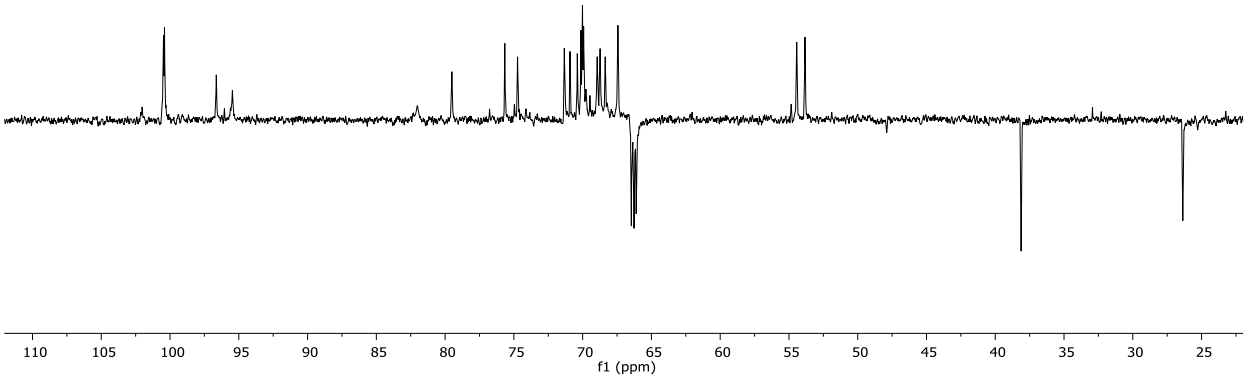
f1 (ppm)

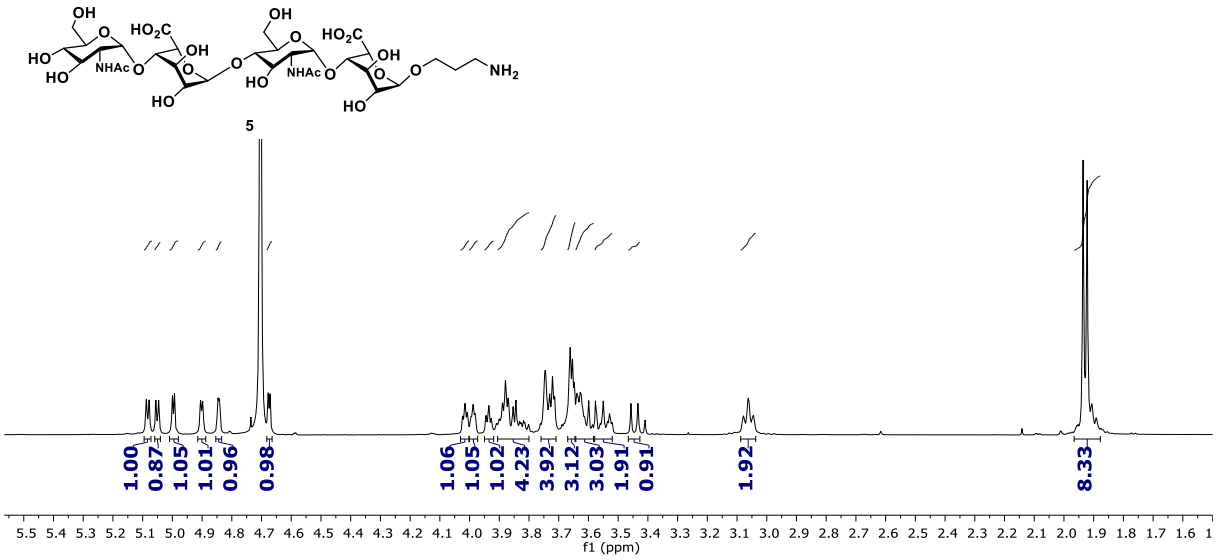
5
1.00
0.87
1.05
1.01
0.96
0.98
1.06
1.05
1.02
4.23
3.92
3.12
3.03
1.91
0.91
1.92
8.33
f1 (ppm)

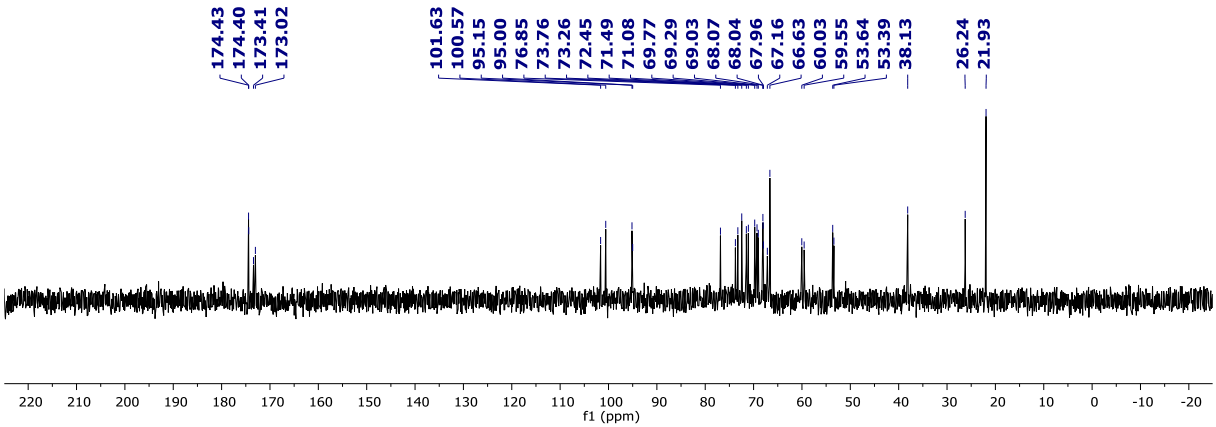
174.43
174.40
173.41
173.02
101.63
100.57
95.15
95.00
76.85
73.76
73.26
72.45
71.49
71.08
69.77
69.29
69.03
68.07
68.04
67.96
67.16
66.63
60.03
59.55
53.64
53.39
38.13
26.24
21.93
f1 (ppm)

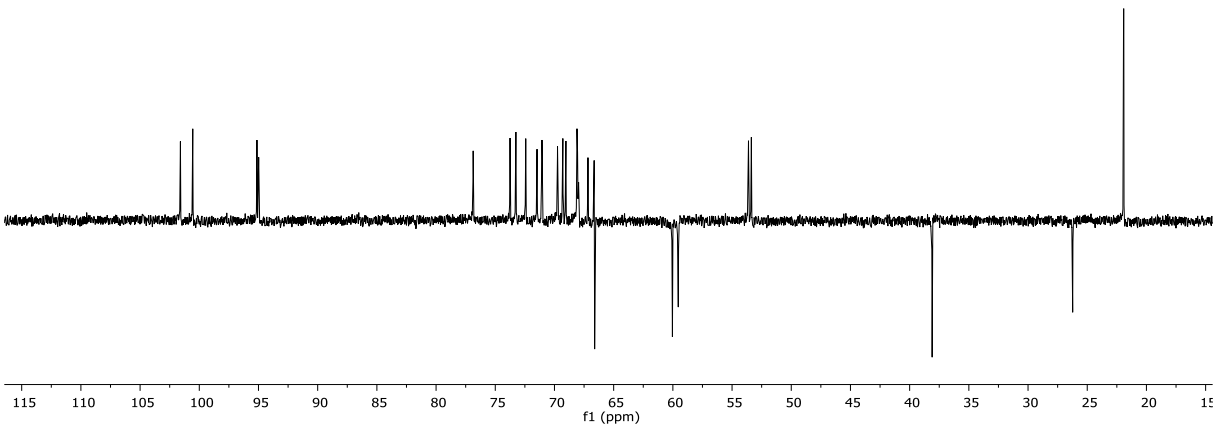
f1 (ppm)

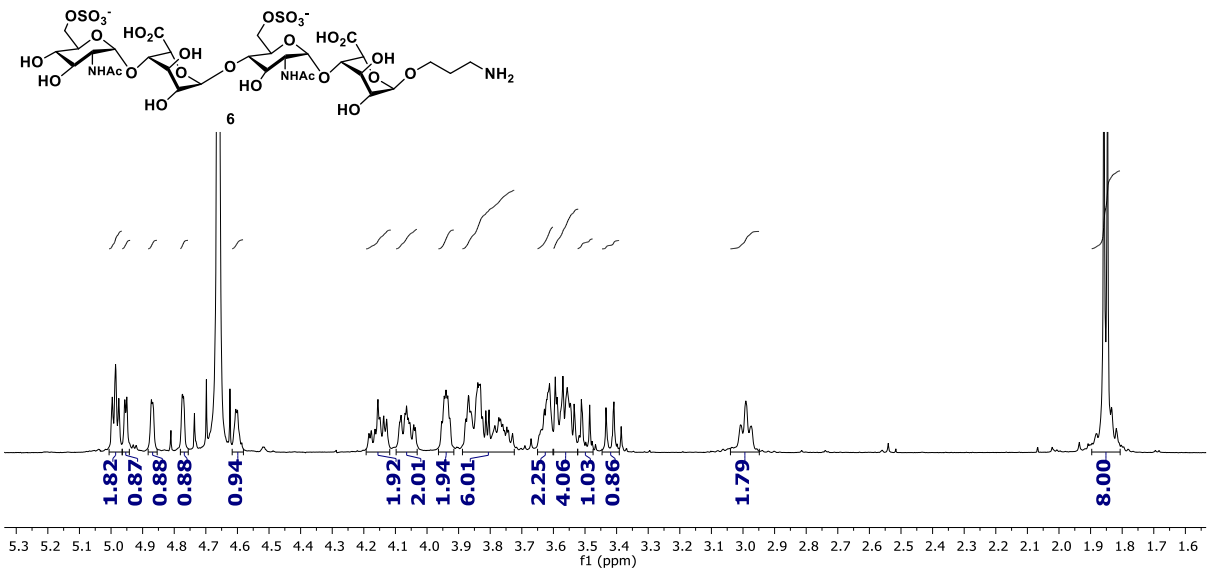
6
1.82
0.87
0.88
0.88
0.94
1.92
2.01
1.94
6.01
2.25
4.06
1.03
0.86
1.79
8.00
f1 (ppm)

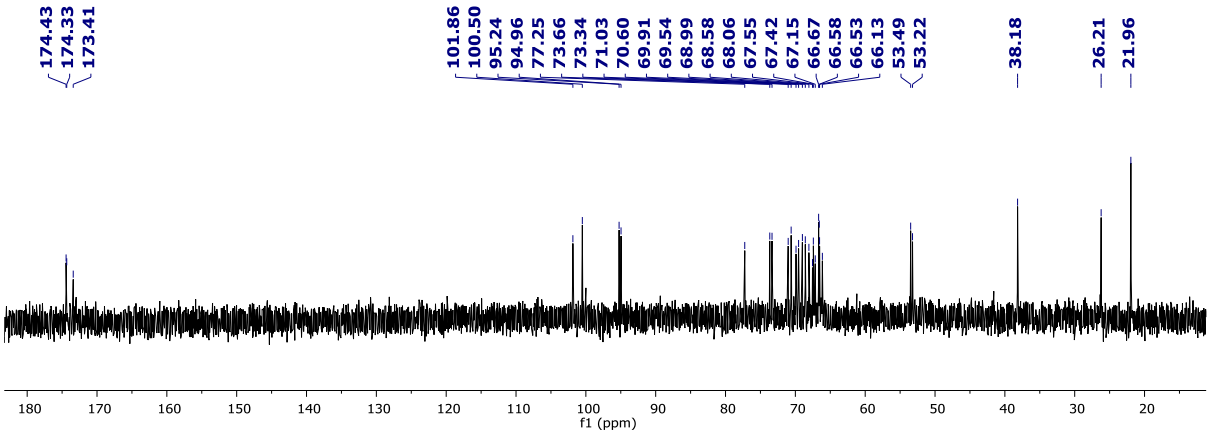
174.43
174.33
173.41
101.86
100.50
95.24
94.96
77.25
73.66
73.34
71.03
70.60
69.91
69.54
68.99
68.58
68.06
67.55
67.42
67.15
66.67
66.58
66.53
66.13
53.49
53.22
38.18
26.21
21.96
f1 (ppm)

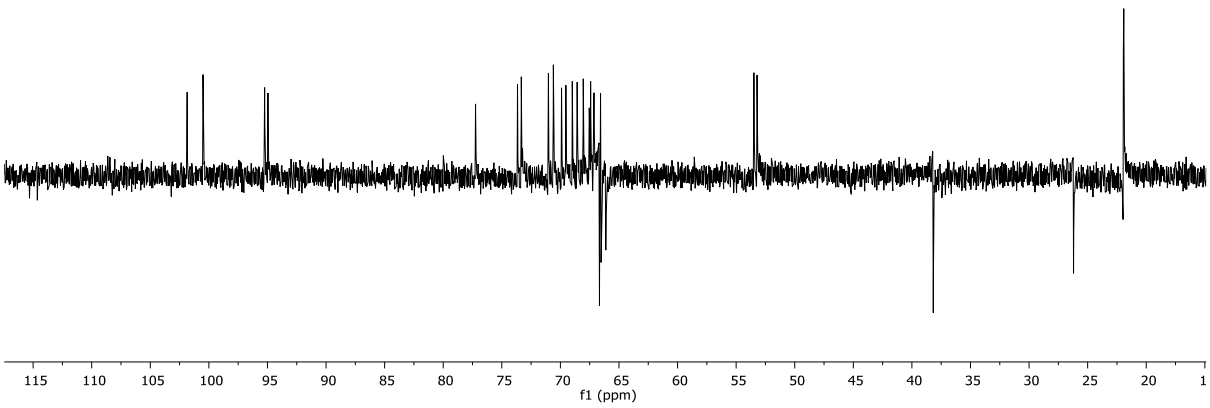
f1 (ppm)

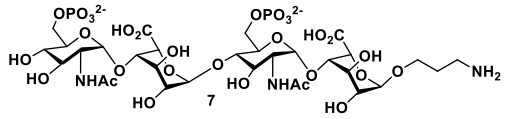
OPO3 2-
HO2C
OH
HO
NHAc
O
7
NH2

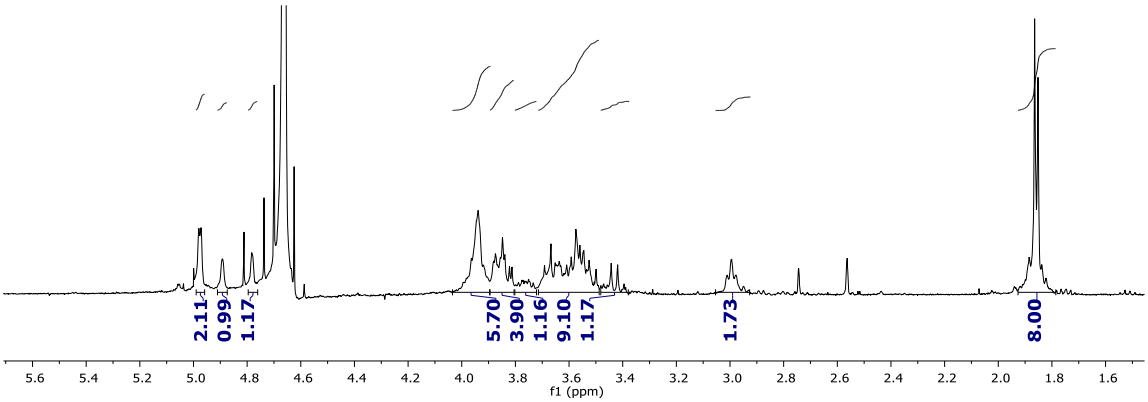
2.11
0.99
1.17
5.70
3.90
1.16
9.10
1.17
1.73
8.00
f1 (ppm)

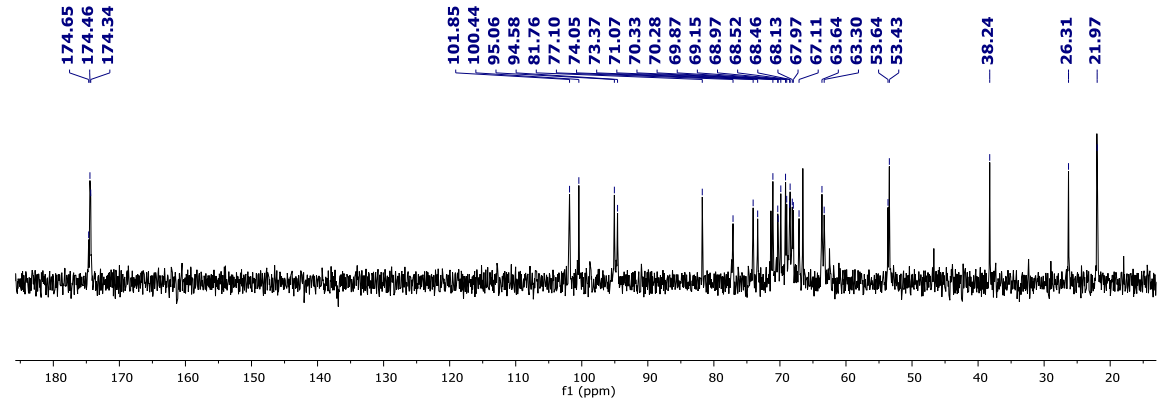
174.65
174.46
174.34
101.85
100.44
95.06
94.58
81.76
77.10
74.05
73.37
71.07
70.33
70.28
69.87
69.15
68.97
68.52
68.46
68.13
67.97
67.11
63.64
63.30
53.64
53.43
38.24
26.31
21.97
f1 (ppm)

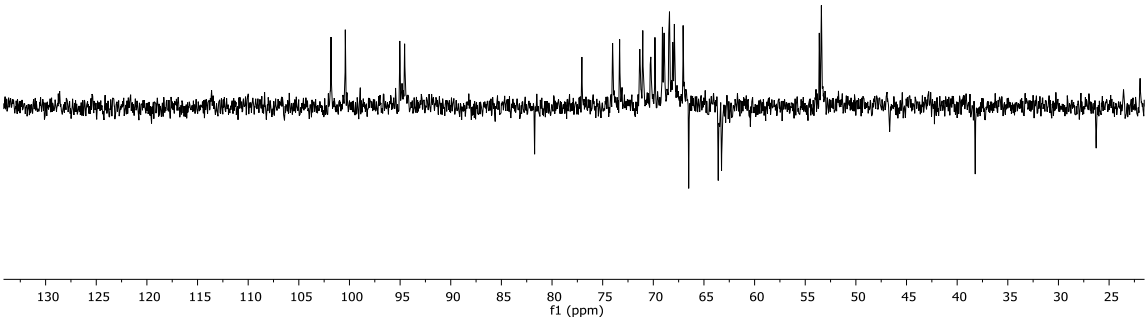
f1 (ppm)

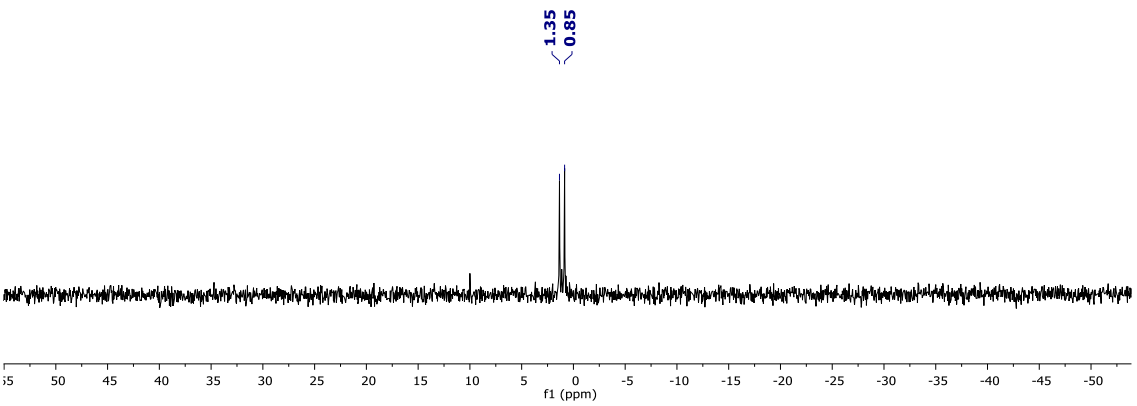
1.35
0.85
f1 (ppm)

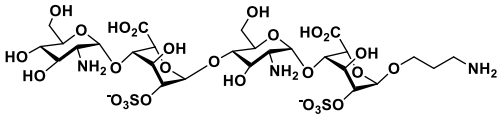

8

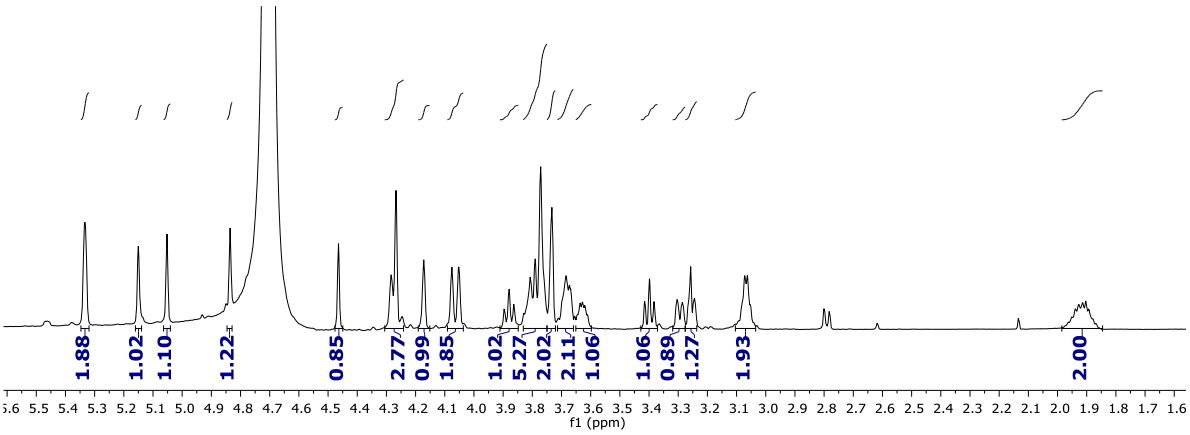
1.88
1.02
1.10
1.22
0.85
2.77
0.99
1.85
1.02
5.27
2.02
2.11
1.06
1.06
0.89
1.27
1.93
2.00
f1 (ppm)

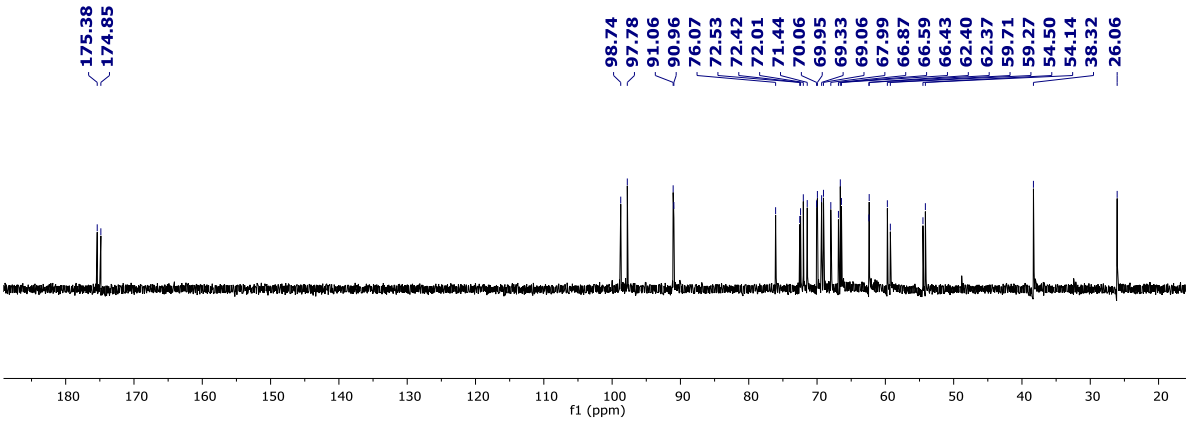
175.38
174.85
98.74
97.78
91.06
90.96
76.07
72.53
72.42
72.01
71.44
70.06
69.95
69.33
69.06
67.99
66.87
66.59
66.43
62.40
62.37
59.71
59.27
54.50
54.14
38.32
26.06
f1 (ppm)

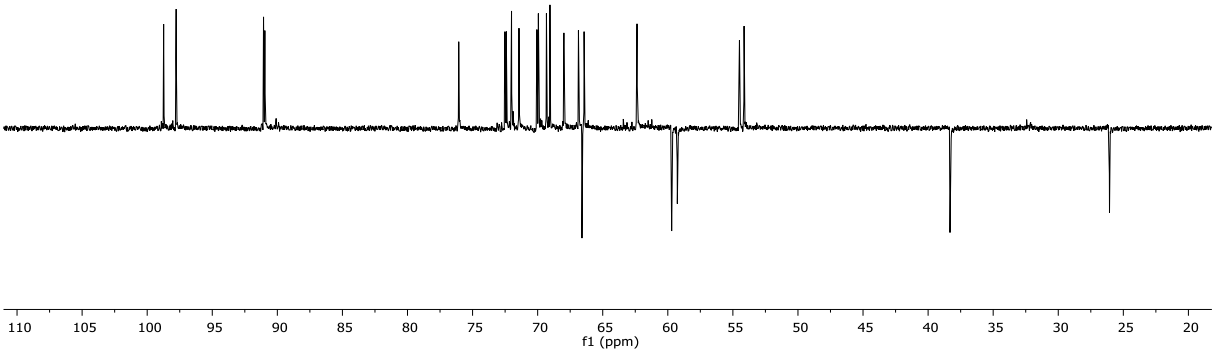
f1 (ppm)

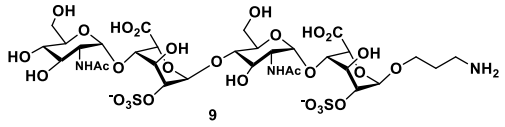
OH
HO
HO
O
NHAc
HO2C
OH
O
O3SO
O
NH2

9

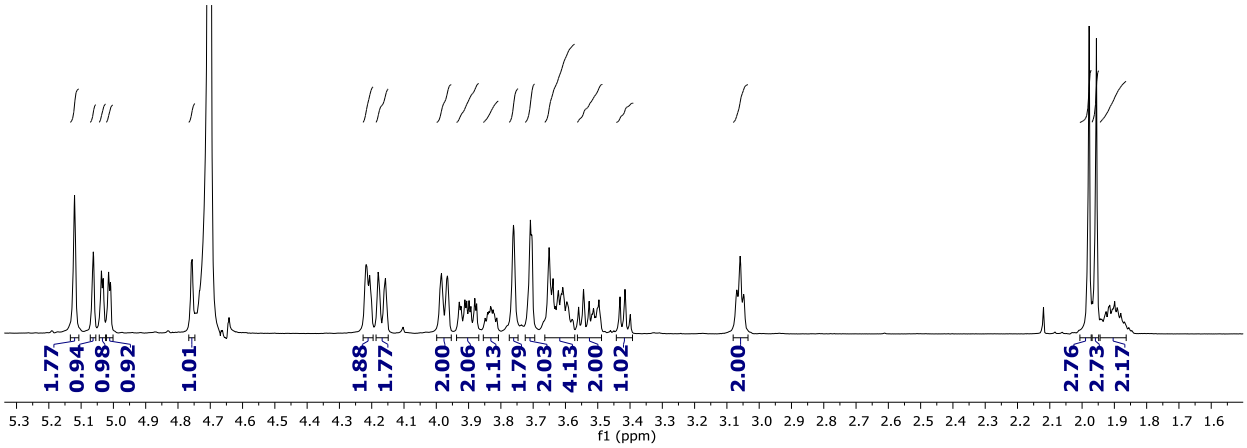
1.77
0.94
0.98
0.92
1.01
1.88
1.77
2.00
2.06
1.13
1.79
2.03
4.13
2.00
1.02
2.00
2.76
2.73
2.17
f1 (ppm)

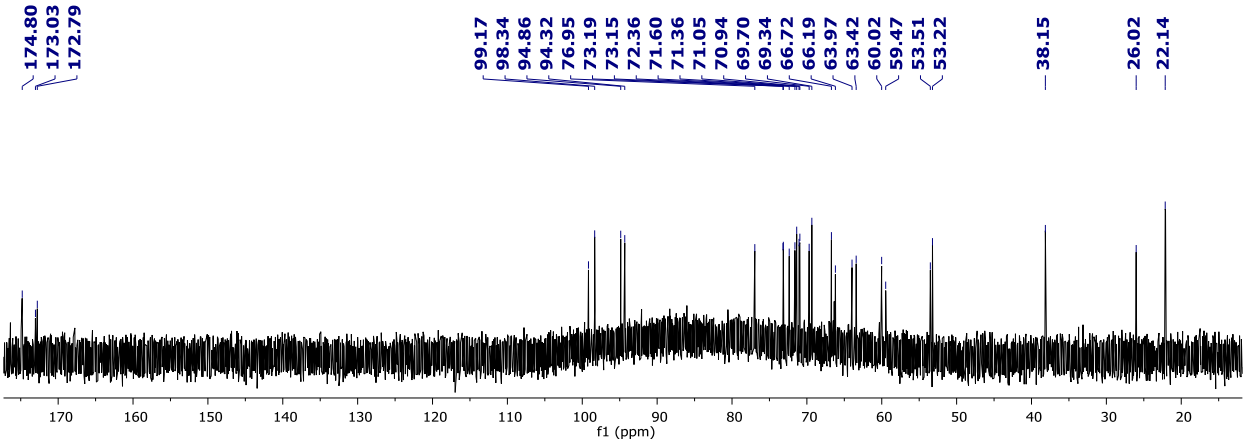
174.80
173.03
172.79
99.17
98.34
94.86
94.32
76.95
73.19
73.15
72.36
71.60
71.36
71.05
70.94
69.70
69.34
66.72
66.19
63.97
63.42
60.02
59.47
53.51
53.22
38.15
26.02
22.14
f1 (ppm)

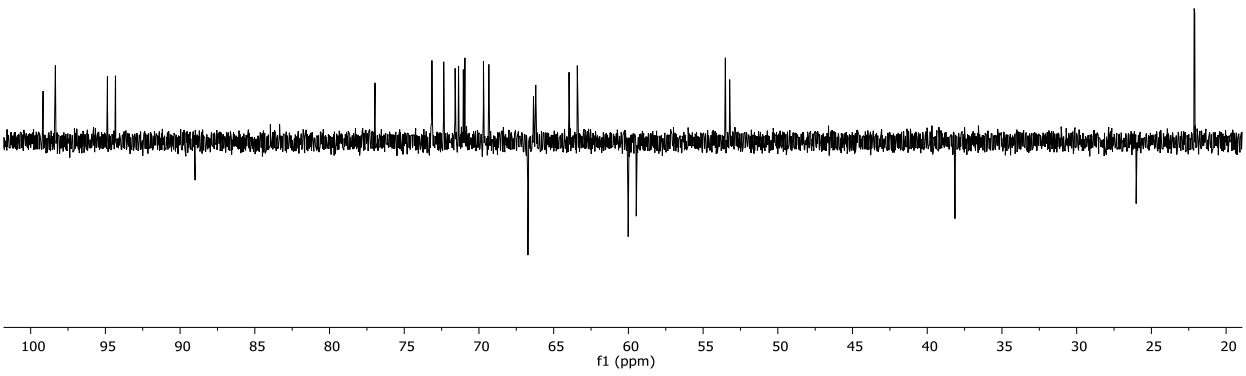
f1 (ppm)

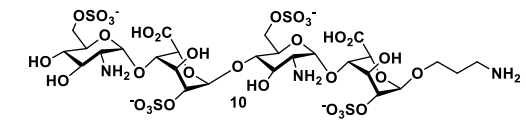
OSO3-
HO2C
OH
HO
NH2
O
-O3SO
10
NH2

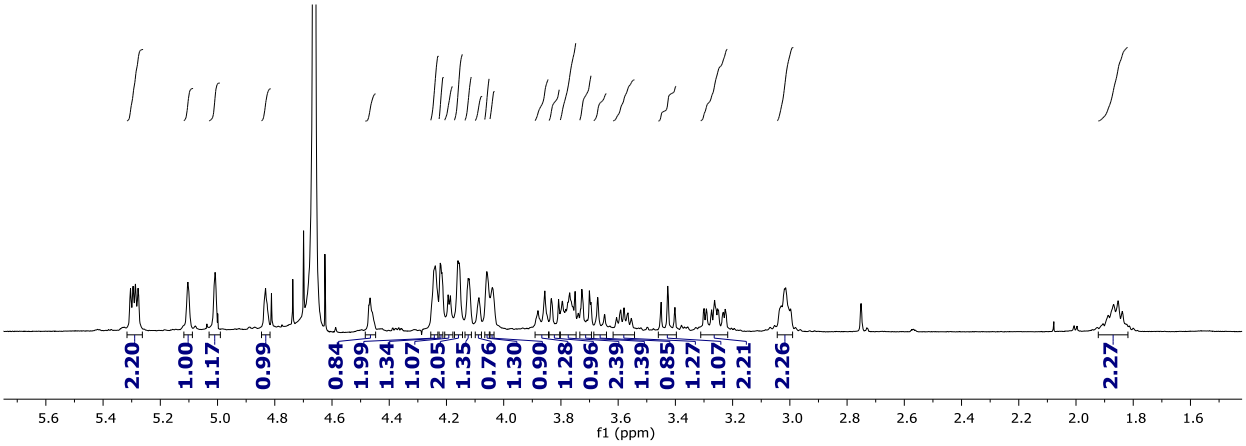
2.20
1.00
1.17
0.99
0.84
1.99
1.34
1.07
2.05
1.35
0.76
1.30
0.90
1.28
0.96
2.39
1.39
0.85
1.27
1.07
2.21
2.26
2.27
f1 (ppm)

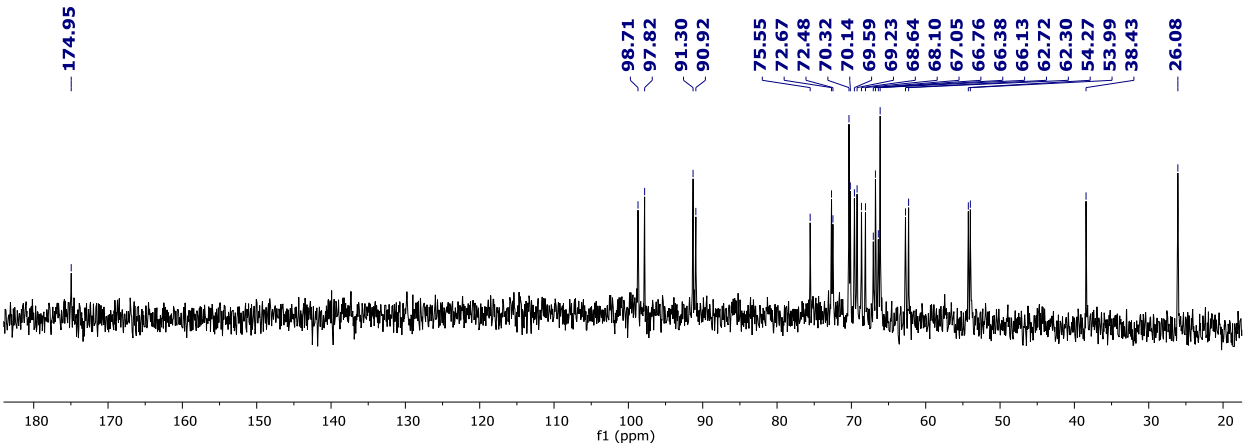
174.95
98.71
97.82
91.30
90.92
75.55
72.67
72.48
70.32
70.14
69.59
69.23
68.64
68.10
67.05
66.76
66.38
66.13
62.72
62.30
54.27
53.99
38.43
26.08
f1 (ppm)

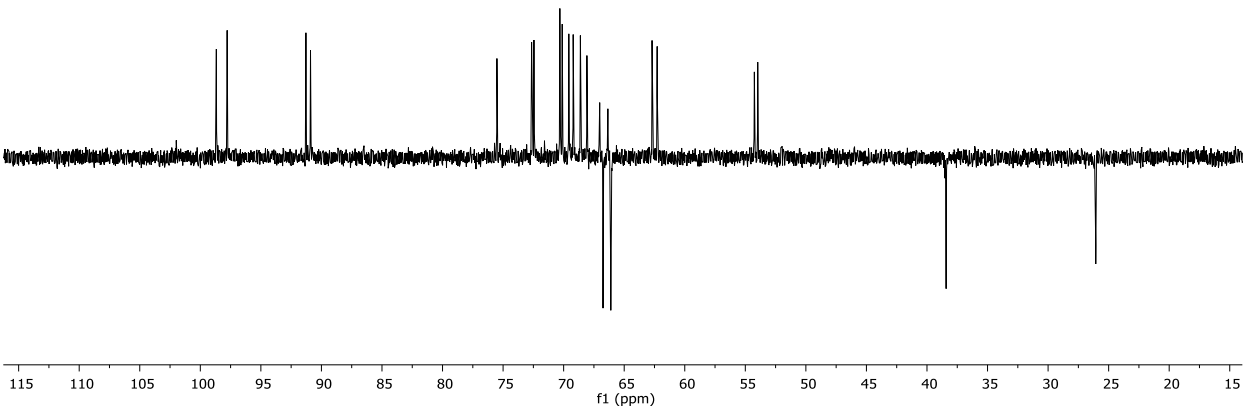
f1 (ppm)

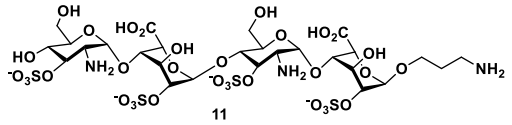
OH
HO
$^{-}O_3SO$
NH$_2$
HO$_2$C
OH
O
$^{-}O_3SO$
NH$_2$
HO$_2$C
OH
O
$^{-}O_3SO$
NH$_2$

11

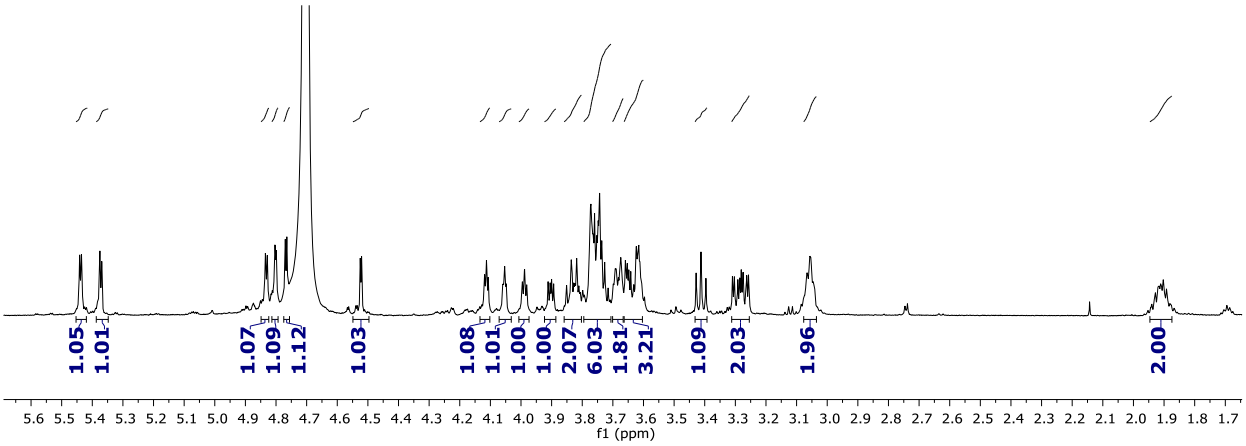
1.05
1.01
1.07
1.09
1.12
1.03
1.08
1.01
1.00
1.00
2.07
6.03
1.81
3.21
1.09
2.03
1.96
2.00
f1 (ppm)

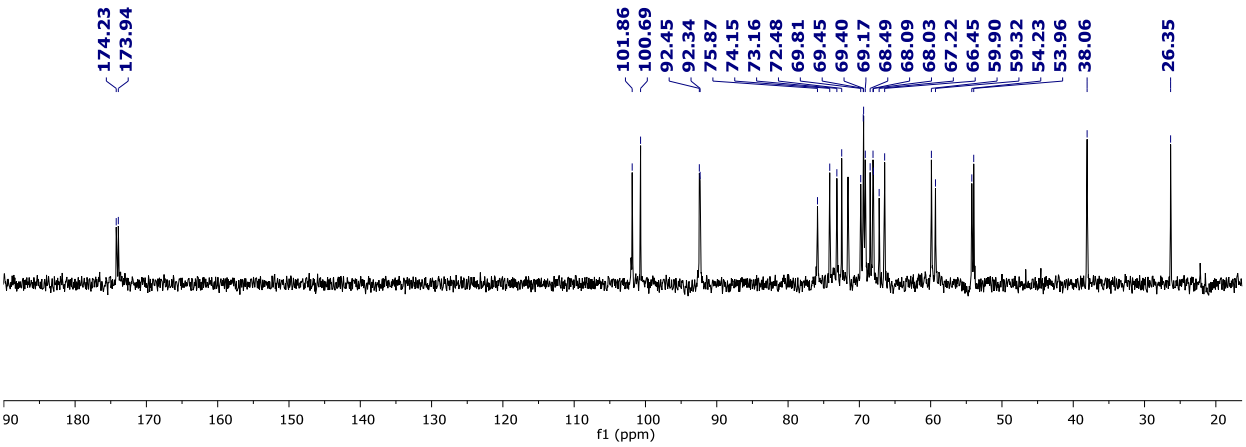
174.23
173.94
101.86
100.69
92.45
92.34
75.87
74.15
73.16
72.48
69.81
69.45
69.40
69.17
68.49
68.09
68.03
67.22
66.45
59.90
59.32
54.23
53.96
38.06
26.35
f1 (ppm)

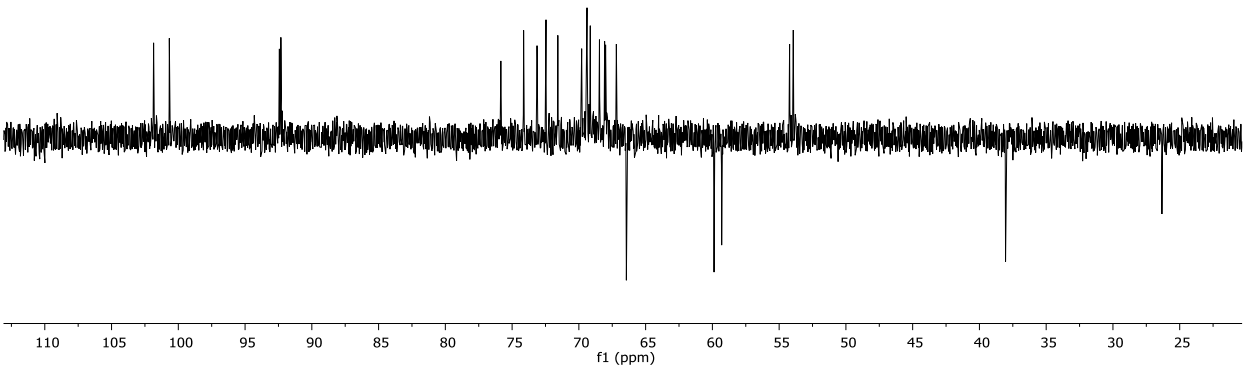
f1 (ppm)

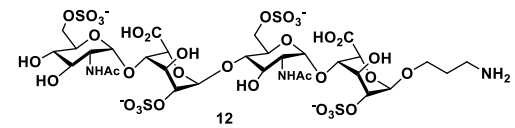
OSO3-
HO2C
OH
HO
NHAc
O
-O3SO
NH2

12

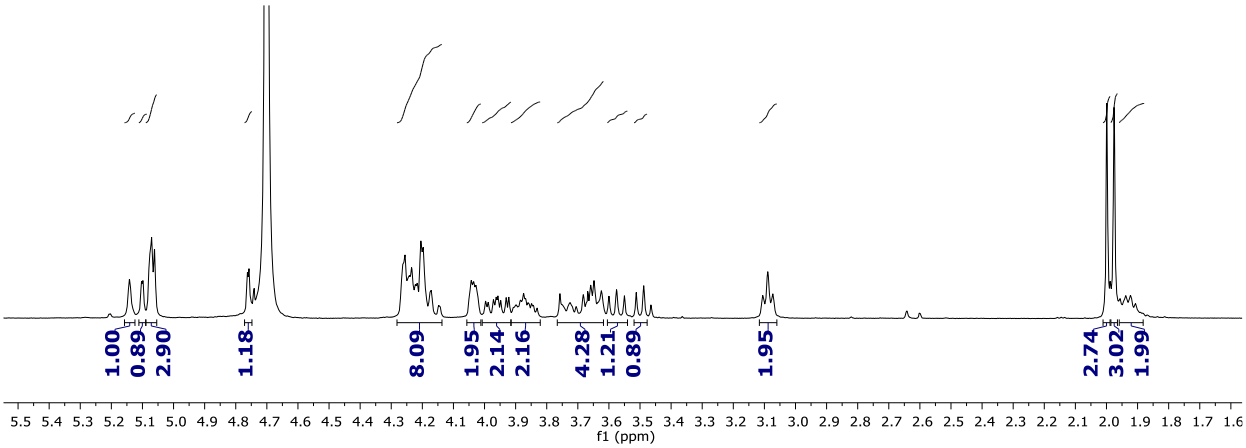
1.00
0.89
2.90
1.18
8.09
1.95
2.14
2.16
4.28
1.21
0.89
1.95
2.74
3.02
1.99
f1 (ppm)

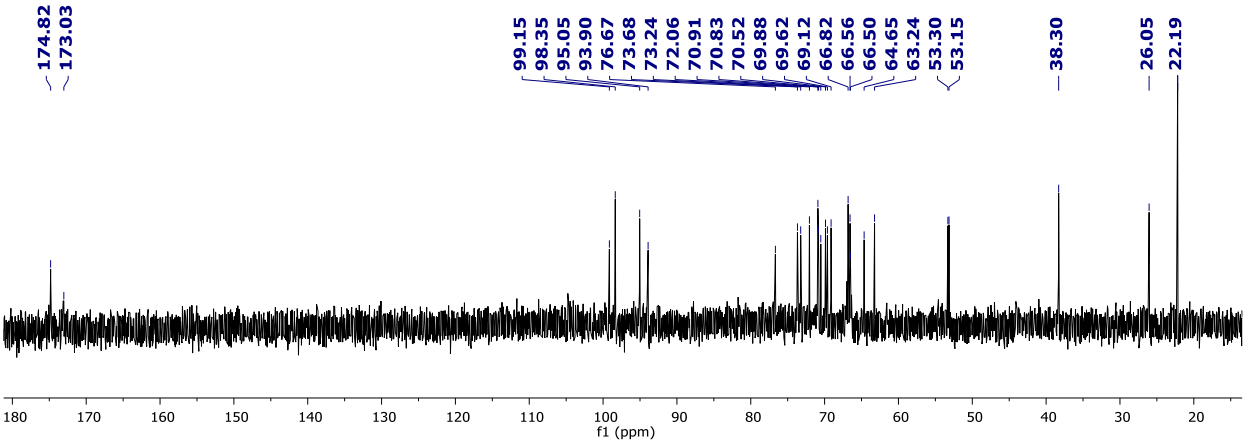
174.82
173.03
99.15
98.35
95.05
93.90
76.67
73.68
73.24
72.06
70.91
70.83
70.52
69.88
69.62
69.12
66.82
66.56
66.50
64.65
63.24
53.30
53.15
38.30
26.05
22.19
f1 (ppm)

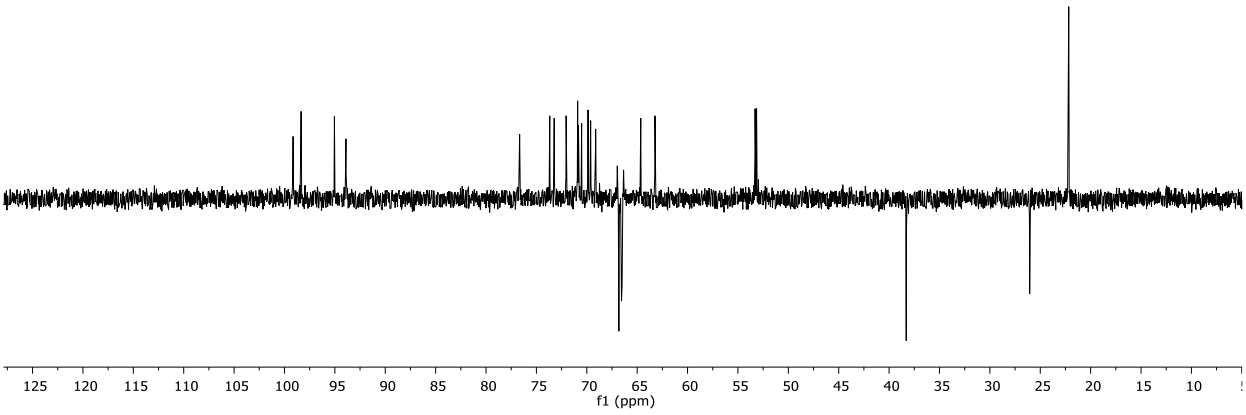
f1 (ppm)

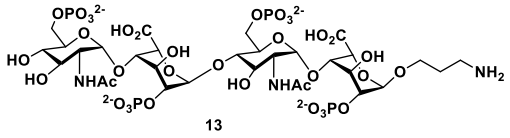
OPO3 2-
HO2C
OH
HO
NHAc
O
2-O3PO
NH2

13

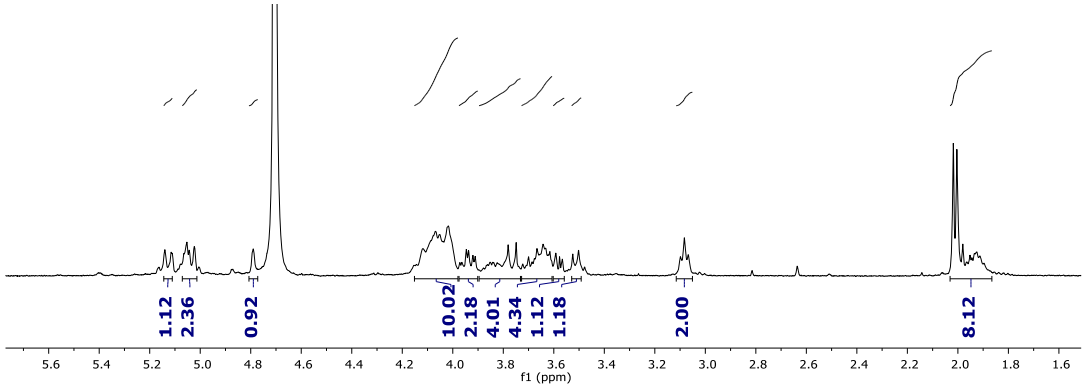
1.12
2.36
0.92
10.02
2.18
4.01
4.34
1.12
1.18
2.00
8.12
f1 (ppm)

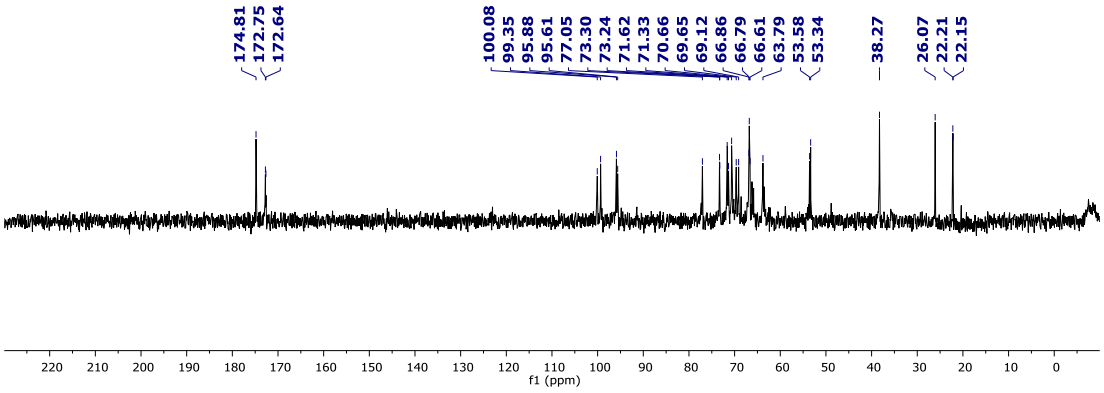
174.81
172.75
172.64
100.08
99.35
95.88
95.61
77.05
73.30
73.24
71.62
71.33
70.66
69.65
69.12
66.86
66.79
66.61
63.79
53.58
53.34
38.27
26.07
22.21
22.15
f1 (ppm)

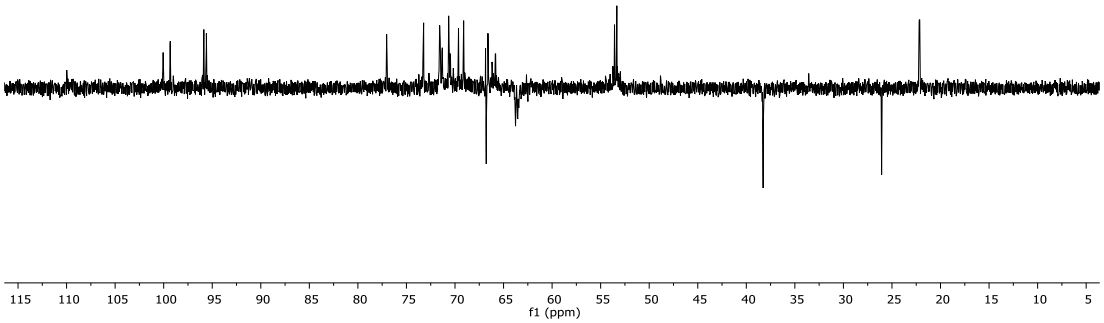
f1 (ppm)

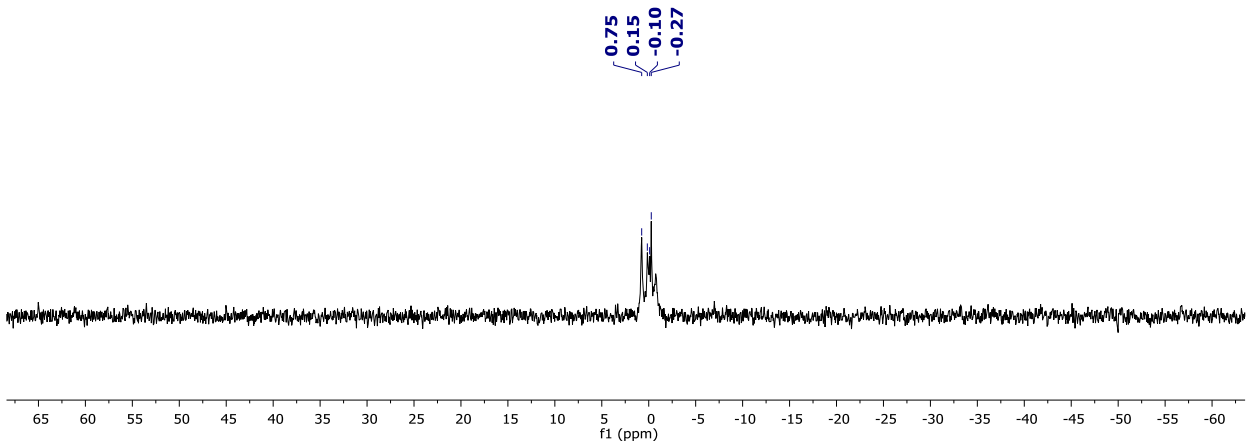
0.75
0.15
-0.10
-0.27
65 60 55 50 45 40 35 30 25 20 15 10 5 0 -5 -10 -15 -20 -25 -30 -35 -40 -45 -50 -55 -60
f1 (ppm)

# CHAPTER -3

## Identification of a High Affinity Heparan Sulfate Ligands for Vascular Endothelial Growth Factor to Modulate Angiogenesis

## Abstract:

We report the discovery of a potential heparan sulfate (HS) ligand to target several growth factors using 13 unique HS tetrasaccharide ligands. By employing an HS microarray and SPR, we deciphered the crucial structure-binding relationship of these glycans with the growth factors amphiregulin, BMP2, $VEGF_{165}$, HB-EGF, and FGF2. Notably, amphiregulin showed high affinity and selective binding to GlcNH(3-$OSO_3$)-IdoA(2-O-$SO_3$) **(HT-2,3S-NH)** ligand, whereas, GlcNHAc(6-$OSO_3$)-IdoA(2-O-$SO_3$) **(HT-2,6S-NAc)** tetrasaccharide showed strong binding with $VEGF_{165}$ growth factor. *In vitro* vascular endothelial cell proliferation, migration and angiogenesis in the presence of $VEGF_{165}$ and **HT-2,6S-NAc** or **HT-6S-NAc** revealed the potential therapeutic role of synthetic HS ligands.

## 3.1 Introduction:

Heparan sulfate (HS) is a linear, negatively charged polysaccharide, which is considered to be a member of the glycosaminoglycan family.[1-4] HS is a major component of the cell surface as well as of the extracellular matrix of all types of cells. Further, HS plays a fundamental role in many cellular events, including cell signalling, cell morphogenesis and pathophysiological functions.[5-10] However, the structural complexity of HS hinders the identification of its specific domain and, its therapeutic significance. HS is known to be associated with two types of structural variations: (i) a variation in the relative composition of the HS disaccharide units (D-glucosamine and uronic acid, with the variation involving either D-glucuronic acid or L-iduronic acid) and (ii) a variation in the sulfation substitutions at 6-OH, 3-OH of the glucosamine residue and 2-OH of the uronic acid residue. In addition, glucosamine also exists in the N-acetylated (NA) and N-sulfated (NS) forms.[11, 12] The structural diversity exhibited by various sulfation groups located on the HS chain results in interactions with a plethora of proteins,[13-21] thereby modulating a wide range of biological activities. For example, it has been shown that the 6-*O*-sulfated NS domain of the HS chain plays a pivotal role in fibroblast growth factor-1 (FGF1) activation and signalling.[22-25] Moreover, HS pentasaccharides featuring a 3-*O*-sulfated NS domain are known to significantly modulate the activity of antithrombin III.[26-29]

Similarly, the binding of several chemokines are regulated by a highly sulfated NS domain.[30-37] However, a systematic study of HS analogs with growth factors, particularly with rare *N*-unsubstituted (NU) domain and *N*-acetate domain HS ligands are not reported. Here, we show that synthetic HS ligands can effectively target growth factors; more importantly, NU and NA domain HS ligands markedly influence the growth factors binding and its activities.

## 3.2 Results and Discussion:

### 3.2.1 Microarray analysis:

A small library of HS tetrasaccharides (Figure 1) composed of different sulfation patterns and NU/NA-glucosamine residue were used for growth factors binding studies. These analogs were conjugated to microarray chips and then detected with various biotinylated growth factors followed by detection with Cy3-tagged streptavidin. The rationale of selection of growth factors is based on their binding affinity to native HS.[38- 48]

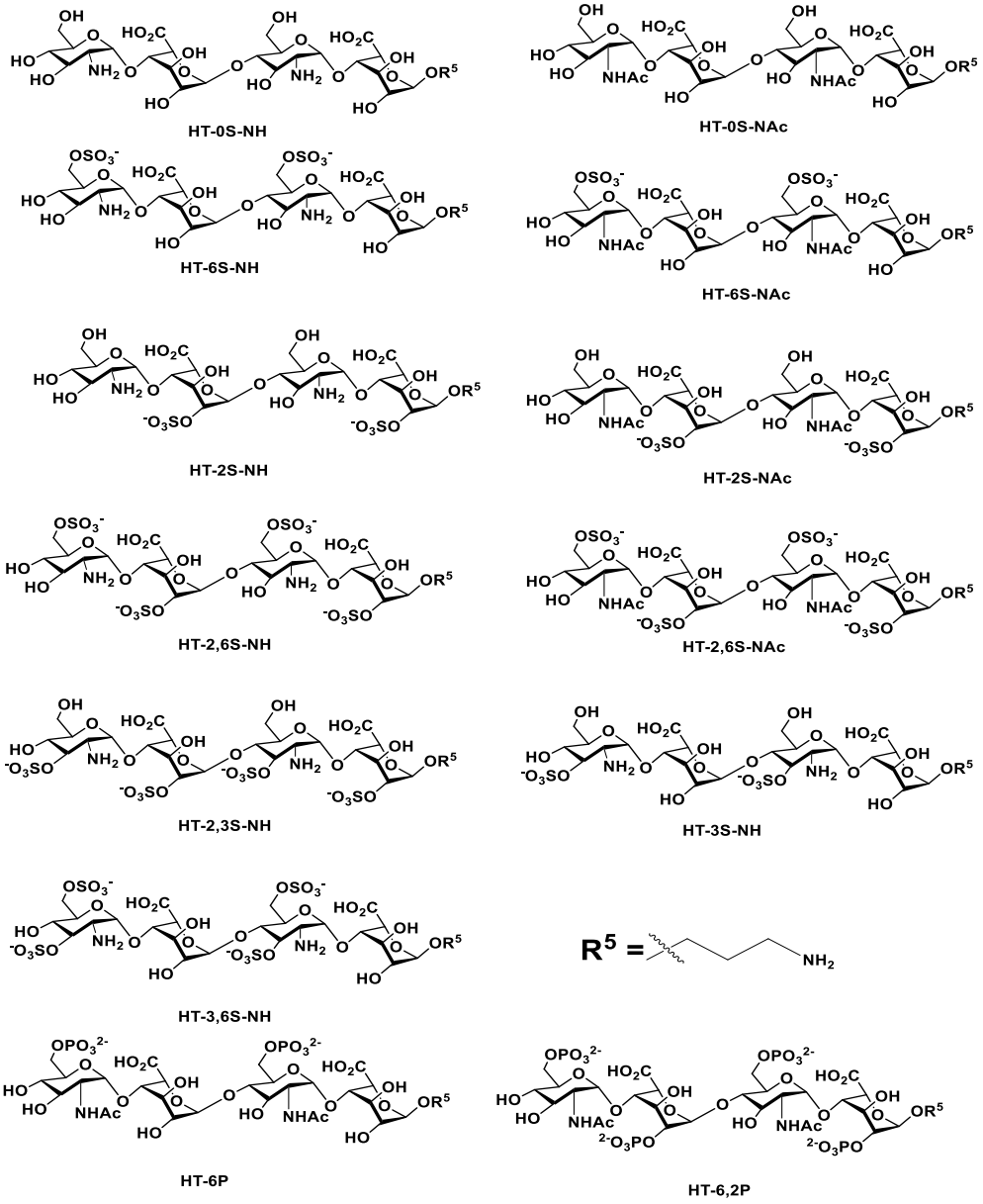


**Figure 1:** Structures of heparan sulfate tetrasaccharide.

To analyse the high-throughput array binding assays, each HS ligand-growth factor interaction was ranked, based on their fluorescent intensity with respect to maximal fluorescent intensity in each array block[49, 50] (Figure 2).

Amphiregulin showed distinctive binding pattern that is different from all the other tested growth factors (GFs; BMP2, $VEGF_{165}$, HB-EGF, FGF2), with high selectivity and strong binding to **HT-2,3S-NH** ligand, whereas non-sulfated, di- and tetra-sulfated, and phosphate HS ligands showed weak or moderate binding. This binding pattern clearly illustrates that

| Sulfation/ Phosphation | Substituent | ID | Amphiregulin | BMP2 | $VEGF_{165}$ | HB-EGF | FGF2 |
|---|---|---|---|---|---|---|---|
| None | None | HT-0S-NH | 36 | 42 | 32 | 32 | 46 |
| | None | HT-0S-NAc | 24 | 6 | 2 | 11 | 6 |
| Di-Sulfateted | IdoA(2S) | HT-2S-NH | 43 | 72 | 69 | 69 | 59 |
| | IdoA(2S) | HT-2S-NAc | 18 | 5 | 2 | 11 | 6 |
| | GlcNH(6S) | HT-6S-NH | 21 | 8 | 5 | 16 | 46 |
| | GlcNAc(6S) | HT-6S-NAc | 48 | 94 | 66 | 73 | 72 |
| | GlcNH(3S) | HT-3S-NH | 47 | 68 | 68 | 62 | 68 |
| Tetra-Sulfateted | GlcNH(6S)-IdoA(2S) | HT-2,6S-NH | 38 | 78 | 87 | 82 | 71 |
| | GlcNAc(6S)-IdoA(2S) | HT-2,6S-NAc | 33 | 85 | 88 | 84 | 73 |
| | GlcNH(3S, 6S) | HT-3,6S-NH | 64 | 74 | 82 | 83 | 68 |
| | GlcNH(3S)-IdoA(2S) | HT-2,3S-NH | 72 | 41 | 19 | 42 | 54 |
| Phosphated | GlcNAc(6P)-IdoA(2P) | HT-6,2P | 44 | 80 | 68 | 72 | 54 |
| | GlcNAc(6P) | HT-6P | 48 | 67 | 22 | 42 | 38 |

| % Rank |
|---|
| 100 |
| 75 |
| 50 |
| 25 |
| 0 |

**Figure 2.** Growth Factors glycan microarray binding assay. Binding was tested at 3 serial dilutions, then detected with the relevant biotinylated secondary antibody (1 µg/ml) followed by Cy3-strepavidin (1.5 µg/ml) (Table 2, experimental section). Arrays were scanned, relative fluorescent units (RFU) were obtained, and maximum RFU determined was set as 100% binding. Then rank binding (per printed glycan per concentration, per each growth factor dilution, per printed block) was determined. Since each glycans was printed at 2 concentration, 100% binding was set separately for each concentration. Then, binding to all the other glycans at the same concentration was ranked in comparison to the maximal binding, and the average rank binding and SEM for each glycan across the two glycan concentrations and three examined dilutions of each growth factor was calculated (n=6, 2 glycan concentrations across 3 growth factors dilutions). This analysis allowed to compare the glycan binding profiles of the different growth factors and dissect their binding preferences. The mean rank is shown as a heatmap of all the examined binding assays together (red highest, blue lowest and white 50$^{th}$ percentile of ranking).

2,3-*O*-disulfated *N*-unsubstituted glucosamine is an ideal ligand for selective targeting of the amphiregulin growth factor. Further studies on 2,3-*O*-disulfated NA and NS-based HS

analogs may fine-tune the structural information required for controlling amphiregulin function.

Interestingly, all the other growth factors, BMP2, $VEGF_{165}$, HB-EGF and FGF2 showed a similar binding pattern. For instance, among the 13 HS tetrasaccharides, the non-sulfated ones displayed weak binding. In contrast, the highly sulfated ligands (**HT-2,6S-NH**, **HT-2,6S-NAc** and **HT-3,6S-NAc**) and the di-sulfated ligands (**HT-2S-NH** and **HT-6S-NAc**) displayed strong binding (Figure. 2). Furthermore, **HT-2,3S-NH**, **HT-2S-NAc** and **HT-6S-NH** displayed weak binding, illustrating that NU/NA domains with GlcN(6S) and IdoA(2S) sulfation patterns synergistically improve GFs' binding. Among phosphate HS ligands, **HT-6,2P** displayed moderate to strong binding of these growth factors, whereas **HT-6P** displayed weak binding, with the exception of BMP2, illustrating that sulfate and phosphate groups mimic each other and that heparin phosphate ligands are interesting ligands for further study.

### 3.2.2 SPR analysis:

Although most of the GFs showed similar binding patterns with HS ligands, their fluorescent intensity was found to be three- to six-fold less than that of $VEGF_{165}$ (Figure 5, experimental section). Hence, a more detailed binding affinity of these HS ligands with $VEGF_{165}$ may establish a sensitive ligand to target $VEGF_{165}$-mediated angiogenesis. To validate the binding affinity of $VEGF_{165}$ with synthetic HS ligands, surface plasmon resonance (SPR) analysis was performed by immobilising five HS ligands (**HT-6S-NAc, HT-2,6S-NH, HT-2,6S-NAc, HT-3,6S-NH** and **HT-2S-NH**) independently on a CM5 sensor chip and treated with $VEGF_{165}$ at different concentrations (Figure 3a-3c).

| Substrate | Growth Factors | $K_D$ (μM) | $K_{on}$ ($M^{-1}S^{-1}$) | $K_{off}$ ($s^{-1}$) |
|---|---|---|---|---|
| **Direct binding Assay** | **HT-6S-NAc** | **6.98 ± 0.17** | $3.17 \pm 0.31 \times 10^4$ | $2.21 \pm 0.28 \times 10^{-1}$ |
| | **HT-2,6S-NH** | **3.16 ± 0.13** | $4.89 \pm 0.1 \times 10^4$ | $1.55 \pm 0.1 \times 10^{-1}$ |
| | **HT-2,6S-NAc** | **2.76 ± 0.32** | $5.07 \pm 0.32 \times 10^4$ | $1.45 \pm 0.21 \times 10^{-1}$ |
| | **HT-3,6S-NH** | **10.14 ± 0.23** | $2.37 \pm 0.41 \times 10^4$ | $2.40 \pm 0.48 \times 10^{-1}$ |
| | **HT-2S-NH** | **10.91 ± 0.19** | $2.87 \pm 0.18 \times 10^4$ | $3.13 \pm 0.26 \times 10^{-1}$ |
| **Competitive binding assay** | **HT-2,6S-NAc** | **62.3 ± 2.1** | $9.13 \pm 0.28 \times 10^2$ | $5.67 \pm 0.37 \times 10^{-2}$ |
| | **HT-2,6S-NH** | **63.7 ± 1.9** | $9.12 \pm 0.23 \times 10^2$ | $5.81 \pm 0.31 \times 10^{-2}$ |
| | **HT-6S-NAc** | **112.6 ± 3.7** | $8.35 \pm 0.31 \times 10^2$ | $9.39 \pm 0.61 \times 10^{-2}$ |

**Table 1.** SPR analysis of kinetic rate constants and equilibrium affinities for HS ligands binding to $VEGF_{165}$ growth factors.

The $K_D$ value calculated from the kinetics revealed that **HT-2,6S-NAc** and **HT-2,6S-NH** (3.19 μM and 2.76 μM, respectively) displayed three-fold stronger binding compared with the other two ligands (**HT-3,6S-NH** [10.14 μM] **HT-2S-NH** [9.88 μM]) (Table 1). Although there is a 2 magnitude difference between the pKa of $2^0$-amine of glucosamine (~8.5) and reducing end linker amine (~10.4) and at a given pH the reactivity of primary amine is much higher than glucosamine. The speculation of reaction between amine group of GlcNH and NHS of CM5 chip cannot be completely ruled out. To further validate binding affinity, we performed additional competitive binding assay using SPR. In this case, biotinylated heparin was immobilized on streptavidin coated chip and treated with varying concentration of HS oligosaccharides (0 to 1 mM) and $VEGF_{165}$ (10 nM). Our results demonstrated that apparent $K_D$ of HT-2,6S-NAc and HT-2,6S-NH remain same (62 μM and 63 μM respectively), reiterating the NU and NA-domain HS ligands showed similar binding strength. Whereas, HT-2,6S-NAc displayed 2-fold strong binding to HT-6S-NAc (112 μM), indicating the 2,6-O-disulfated HS ligands are ideal to target $VEGF_{165}$. The disparity in $K_D$ value of direct and competitive binding assay is due to multivalent vs monovalent binding affinity between HS ligand with growth factor.

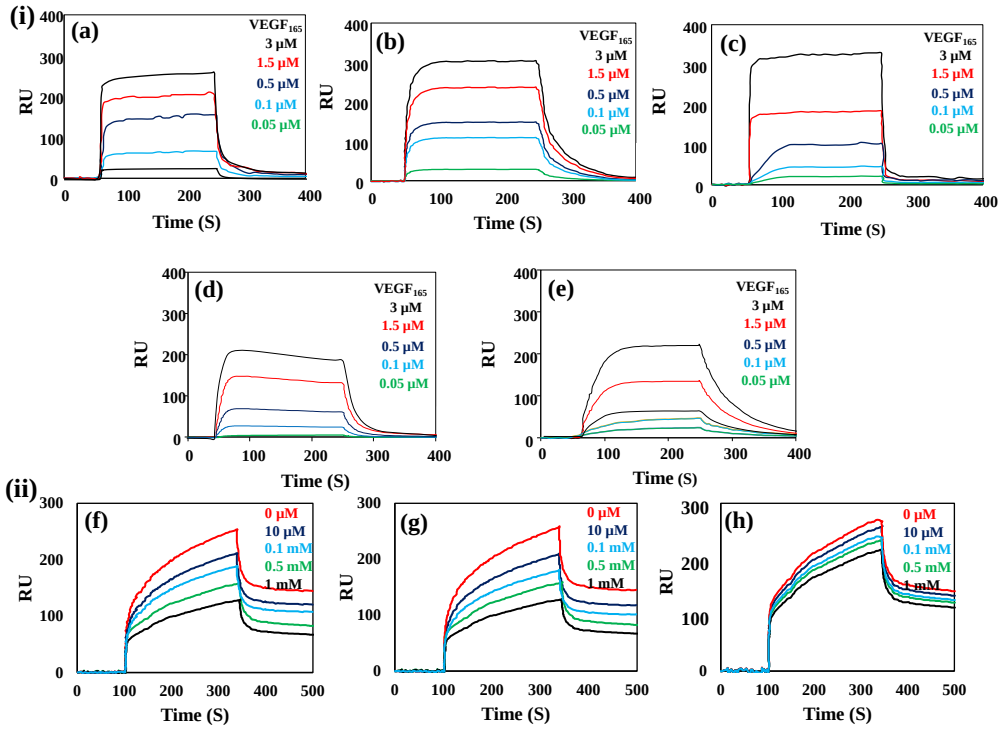


**Figure 3.** (i) SPR analysis of $VEGF_{165}$ binding profile on sensor chip having (a) HT-6S-NAc, (b) HT-2,6S-NAc, (c) HT-2,6S-NH, (d) HT-3.6S-NH and (e) HT-2S-NH respectively; (ii) SPR competitive binding measurement to heparin and $VEGF_{165}$ (5 nM) in the presence of varying concentration of HS tetrasaccharides (0 to 1 mM) (f) HT-2,6S-NAc; (g) HT-2,6S-NH and (h) HT-6S-NAc respectively.

.

### 3.3.3 Cell proliferation and migration assay:

Active binding between $VEGF_{165}$ and its native receptor VEGFR-2 is known to trigger several cellular events, including vascular cell proliferation, cell migration and angiogenesis.[51- 57] To confirm the inhibitory activity of HT-2,6S-NAc, we performed a systematic *in vitro* study using HUVEC cells. First, we performed a cell proliferation assay with $VEGF_{165}$ and HS ligands (**HT-6S-NAc** (**H-1**) and **HT-2,6S-NAc** (**H-2**)) (Figure 4a). It was observed that both HS ligands moderately reduced the cell proliferation in the presence of $VEGF_{165}$, illustrating the inhibitory activity of HS analogs.

Next, we studied the role of HS ligands in inhibiting the cell migration process by using a wound healing assay.[58] To this end, a monolayer of HUVEC cells was cultured and a wound was created. Then, the effect of $VEGF_{165}$ with or without HS ligand or native heparin was monitored. At 50 µg/ml concentration of HS ligands, we observed a substantial

reduction in the rate of cell migration (Figure 4b). It was observed that the addition of **HT-2,6S-NAc** induced nearly a 25% reduction in the cell migration process, in comparison to 21% of native **HT-6S-NAc**, illustrating the importance of NAc-domain in $VEGF_{165}$ activation.

### 3.3.4 Endothelial tube formation assay:

Finally, we evaluated the influence of the HS ligand on $VEGF_{165}$-dependent tube formation. $VEGF_{165}$ with or without HS ligands (**HT-2,6S-NAc HT-2,6S-NH** and **HT-6S-NAc**) were added to HUVECs cells cultured in matrigel. All three HS analogs showed the strong inhibition of the tube formation of HUVEC cells (Figure 4c). Among them 2,6-O-disulfation ligands showed strong activity compared to 6-O-sulfted HS ligands, a result which correlates with the cell migration assay. These results clearly showed that **2,6-disulfated HS ligands** are potential ligands for targeting $VEGF_{165}$.

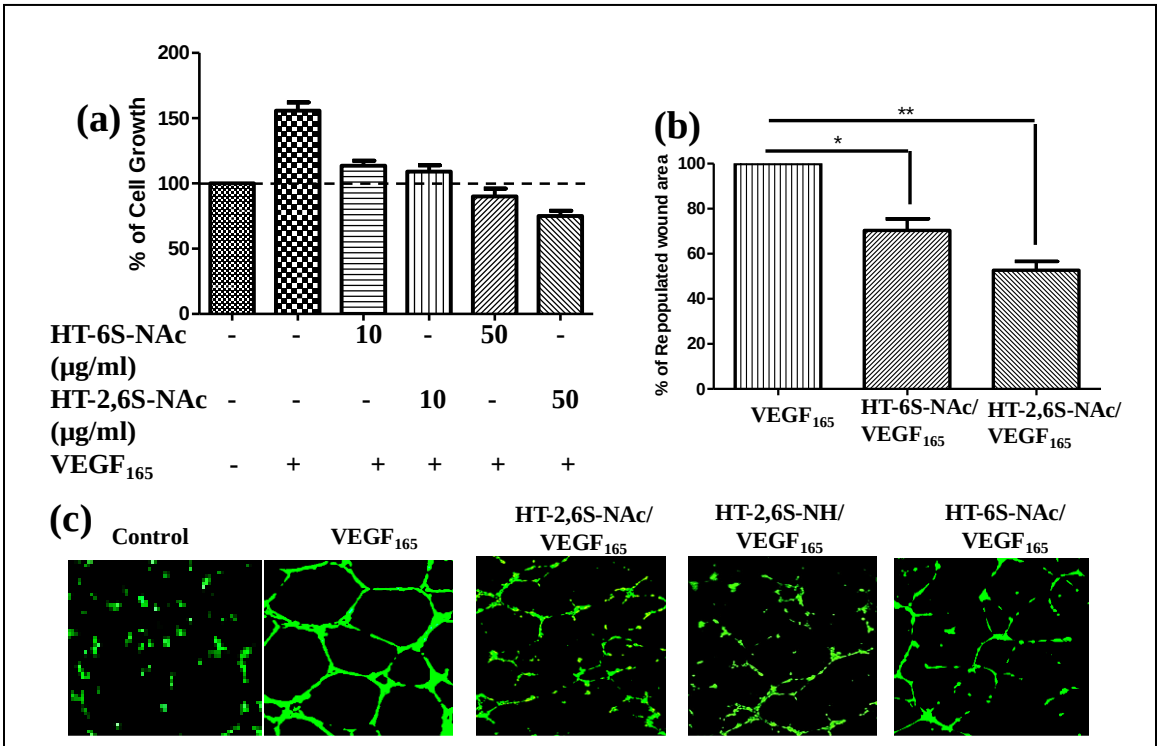


**Figure 4.** (a) WST assay was performed to assess HUVEC cell proliferation after 72 hrs. Concentration of $VEGF_{165}$ concentration is 50 ng/ml; (b) Wound healing assay with and with $VEGF_{165}$ and HS ligands (conc 50 µg/ml). The percentage of the effect of growth factors without HS mimics (= 100%) Data expressed as mean ± SD (n=3; *P<0.01); (c) Confocal images of tube formation assay in the presence and absence of HS ligand (50 µg/ml) and $VEGF_{165}$. After 24h cells were stained with Calcein AM and imaged scale bar 30 µm.

These results clearly showed that **HT-2,6S-NAc** and **HT-6S-NAc** are potential ligands for targeting $VEGF_{165}$.

## 3.3 Conclusions:

In conclusion, we constructed a carbohydrate microarray by using 13 HS ligands to generate binding profiles of several growth factors which are implicated in crucial cellular events. The array data provided important structure-binding patterns of GAGs needed to target specific growth factors. In particular, we demonstrated that amphiregulin revealed selective binding to the **HT-2,3S-NH** ligand, whereas other GFs displayed broad binding profiles with HS ligands. SPR analysis of the $VEGF_{165}$-mediated binding of HS ligands confirmed that **HT-2,6S-NAc** and **HT-6S-NAc** are a potential ligand for targeting $VEGF_{165}$-mediated cellular events. In vitro, HUVEC cells proliferation, migration and tube formation assays were used to assess the effect of HS ligands on cancer biology.

## 3.4 Experimental Part

### 3.4.1 Glycan Microarray:

**Materials**. Human $VEGF_{165}$ (AF-100-20), human HB-EGF (100-47), human Amphiregulin (100-55B), human BMP2 (AF-120-02), biotinylated-rabbit-anti-human $VEGF_{165}$ (500-P10BT), biotinylated-rabbit-anti-human HB-EGF (500-P329BT), biotinylated-rabbit-anti-human amphiregulin (500-P322BT), anti-human BMP2 (500-P195BT), were purchased from Peprotech. Human FGF2 basic recombinant (RP-8626) and polyclonal biotinylated-anti-human-FGF2 antibody (PA1-25521) were purchased from Thermo Fischer. Cy3-sterptavidin was purchased from Jackson ImmunoResearch.

**HS microarray fabrication.** HS Arrays were fabricated with NanoPrint LM-60 Microarray Printer (Arrayit) on epoxide-derivatized slides (PolyAn 2D) with four 946MP3 pins (5 µm tip, 0.25 µl sample channel, ~100 µm spot diameter; Arrayit) at 16 sub-array blocks on each slide (array VrHI.01). Glycoconjugates were distributed into 384-well source plates using 4 replicate wells per sample and 7 µl per well. Each glycoconjugate was printed at two different concentration (50 µM and 100 µM) at four replicate spots in

an optimized printing buffer (300 mM phosphate buffer, pH 8.4). AlexaFlour-555-hydraside was printed per block (Invitrogen A20501MP, at 1 ng/µl in 178 mM phosphate buffer, pH 5.5) to monitor printing and the humidity level in the arraying chamber was maintained at ~70% during the procedure. Upon printing, slides were left on arrayer deck over-night for allowing humidity to drop to ambient levels (40-45%). subsequent, slides had been packed, vacuum-sealed and stored at room temperature (RT) until used.

**HS microarray binding assay.** Slides were developed and analyzed as formerly described[59] with some adjustments. After rehydrating with $dH_2O$, slides were incubated for 30 min in a staining dish containing pre-warmed (50 °C) ethanolamine (0.05 M) in Tris-HCl (0.1 M, pH 9.0) to block the previously unreacted epoxy groups on the slide surface and washed finally with 50 °C pre-warmed $dH_2O$. Slides were centrifuged at 200×*g* for three min then fitted with ProPlate™ Multi-Array 16-well slide module (Grace Bio-lab) to divide into the sub-arrays (blocks). Slides were washed with PBST (PBS pH 7.3 + 0.1% Tween 20), aspirated and blocked with 200 µl/sub-array of blocking buffer (PBS pH 7.3 + 1% w/v Ovalbumin grade V, Sigma) for 1 hour at RT with gentle shaking. Next, the blocking solution was aspirated and 100 µl/block of primary detection proteins (for each detection, 3 serially decreasing concentrations were used, see Table 2) diluted in blocking buffer, were incubated with gentle shaking for 2 hours at RT. Slides were washed 4 times with PBST, then with PBS for 2 min. Bound antibodies were detected by incubating with biotinylated secondary detections (1 ng/µl, see Table 2) diluted in PBS, at 200 µl/block at RT for 1 hour. Slides were washed 4 times with PBST, then with PBS for 2 min and biotinylated antibodies detected with Cy3-sterptavidin (1.2µg/ml). Slides were washed 4 times with PBST, then with PBS for 10 min followed by removal from ProPlate™ Multi-Array slide module and immediately dipping in a staining dish with $dH_2O$ for 10 min with shaking. Slide then were centrifuged at 200×*g* for 3 min. and the dry slides immediately scanned.

**Table 2.** Primary detection and secondary biotinylated antibodies used on the array.

| **Primary Detection** | **Concentrations used (ng/µl)** | **Secondary Detection** |
|---|---|---|
| Human FGF2 (basic recombinant) | 20, 10, 5 | Biotinylated-FGF2 polyclonal antibody |
| Human $VEGF_{165}$ | 5, 2.5, 1.25 | Biotinylated-rabbit-anti-human $VEGF_{165}$ |
| Human HB-EGF | 20, 10, 5 | Biotinylated-rabbit-anti-human HB-EGF |
| Human Amphiregulin | 20, 10, 5 | Biotinylated-rabbit-anti-human Amphiregulin |
| Human BMP2 | 2, 1, 0.5 | Human BMP2 detection antibody |

**HS microarray slide processing.** Genepix 4000B microarray scanner (Molecular Devices) and Genepix Pro 4.0 analysis software (Molecular Devices) was used for the processed slides scanning (using 350 gain at 10 µm) and image analysis respectively. Spots were defined as circular features with a variable radius as determined by the software. RFU from each spot was calculated after subtracting local background. Ranking was done to compare the data between detections (3 dilutions for each detection). For each growth factor and at each dilution, the binding RFU's of the glycans were listed, maximum RFU was determined and set as 100% binding while all the others were calculated compared to the max. Next, the rank for each glycan was averaged between the three dilutions and SEM was calculated.

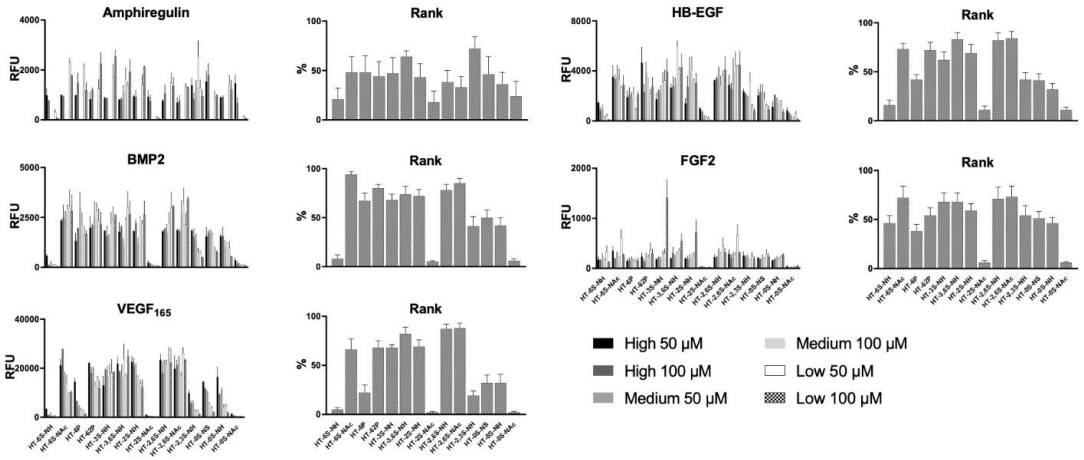


**Figure 5.** Growth Factors glycan microarray binding assay bar graphs for RFUs and rankings.

### 3.4.2 Surface Plasmon Resonance binding kinetics

HS tetrasaccharides were immobilized on CM5 sensor surface using a coupling reaction. $K_D$ values were analysed by treating the surface with different fraction of $VEGF_{165}$ at a flow rate of 50 µL/min and 25 °C. HBS-EP buffer flowed on the surface to perform dissociation for 3 mins. Binding kinetics was analyzed using the BIAevaluation software for T100 by adjusting the fitting curve with 1;1 interaction model. Finally, the sensor chip was regenerated by washing with 0.1% SDS and 0.085% $H_3PO_4$ injected for 3 min at a flow rate of 100 µl/min.

### 3.4.3 Cell proliferation assay

HUVECs were plated on 96 well plates in EBM-2 medium in 1% FBS without growth supplements. HS tetrasaccharides (10 and 50 µg/ml) with VEGF165 (50 ng/ml) were added to each well. After 48 h of incubation, cells were washed with PBS buffer and fixed with paraformaldehyde. Cells were stained with 2-(4-iodophenyl)-3-(4-nitrophenyl)-5-(2,4-disulfophenyl)- 2H-tetrazolium monosodium salt and cell proliferation was quantified by measuring the absorption intensity at 450 nm.

### 3.4.4 Wound healing assay

HUVEC cells were cultured on 24-well plates in EBM-2 media and allowed to grow till monolayer formation. Afterwards, a wound was created by using 1000 µl pipette tip. Cells were then treated with HS analogs (50 µg/ml) and $VEGF_{165}$ or $VEGF_{165}$ alone (50 ng/ml). After 12 h, $VEGF_{165}$ alone treated HUVECs showed complete wound healing, which was considered as 100% healing, and at that point, the percentage of cell migrated in other wells were quantified.

## 3.5 References:


1. Shriver, Z.; Capila, I.; Venkataraman, G.; Sasisekharan, R., Heparin and heparan sulfate: analyzing structure and microheterogeneity. In *Heparin-A Century of Progress*, Springer: 2012; pp 159-176.
2. Rabenstein, D. L., Heparin and heparan sulfate: structure and function. *Nat. Prod. Rep.* **2002,** *19* (3), 312-331.
3. Sarrazin, S.; Lamanna, W. C.; Esko, J. D., Heparan sulfate proteoglycans. *Cold Spring Harbor Perspect. Bio.* **2011,** *3* (7), a004952.
4. Gama, C. I.; Hsieh-Wilson, L. C., Chemical approaches to deciphering the glycosaminoglycan code. *Curr. Opin. Chem. Biol.* **2005,** *9* (6), 609-619.
5. Xu, D.; Esko, J. D., Demystifying heparan sulfate–protein interactions. *Ann. Rev. Biochem.* **2014,** *83*, 129-157.
6. Vlodavsky, I.; Gross-Cohen, M.; Weissmann, M.; Ilan, N.; Sanderson, R. D., Opposing functions of heparanase-1 and heparanase-2 in cancer progression. *Trends Biochem. Sci.* **2018,** *43* (1), 18-31.
7. Capila, I.; Linhardt, R. J., Heparin–protein interactions. *Angew. Chem. Int. Ed.* **2002,** *41* (3), 390-412.
8. Iozzo, R. V., Basement membrane proteoglycans: from cellar to ceiling. *Nat. Rev. Mol. Cell Biol.* **2005,** *6* (8), 646-656.
9. Lin, X., Functions of heparan sulfate proteoglycans in cell signaling during development. *Development* **2004,** *131* (24), 6009-6021.

10. Lindahl, U.; Kjellén, L., Pathophysiology of heparan sulphate: many diseases, few drugs. *J. Intern. Med.* **2013,** *273* (6), 555-571.
11. Whitelock, J. M.; Iozzo, R. V., Heparan sulfate: a complex polymer charged with biological activity. *Chem. Rev.* **2005,** *105* (7), 2745-2764.
12. Lindahl, U.; Couchman, J.; Kimata, K.; Esko, J. D., Proteoglycans and sulfated glycosaminoglycans. **2017**. *Essentials of Glycobiology, 3rd edition* (Eds: A. Varki, R.D.Cummings, J. D. Esko, P. Stanley, G. W. Hart, M. Aebi, A. G.Darvill, T. Kinoshita, N. H. Packer, J. H. Prestegard, R. L. Schnaarand P. H. Seeberger), Cold spring Harbor Laboratory press, 2015-2017, Chapter 17.
13. Sakamoto, K.; Ozaki, T.; Ko, Y.-C.; Tsai, C.-F.; Gong, Y.; Morozumi, M.; Ishikawa, Y.; Uchimura, K.; Nadanaka, S.; Kitagawa, H., Glycan sulfation patterns define autophagy flux at axon tip via PTPRσ-cortactin axis. *Nat. Chem. Biol.* **2019,** *15* (7), 699-709.
14. Meneghetti, M. C.; Hughes, A. J.; Rudd, T. R.; Nader, H. B.; Powell, A. K.; Yates, E. A.; Lima, M. A., Heparan sulfate and heparin interactions with proteins. *J. R. Soc. Interface.* **2015,** *12* (110), 20150589.
15. Bishop, J. R.; Schuksz, M.; Esko, J. D., Heparan sulphate proteoglycans fine-tune mammalian physiology. *Nature.* **2007,** *446* (7139), 1030-1037.
16. Zulueta, M. M. L.; Chyan, C.-L.; Hung, S.-C., Structural analysis of synthetic heparan sulfate oligosaccharides with fibroblast growth factors and heparin-binding hemagglutinin. *Curr. Opin. Struc. Biol.* **2018,** *50*, 126-133.
17. Wang, P.; Cascio, F. L.; Gao, J.; Kayed, R.; Huang, X., Binding and neurotoxicity mitigation of toxic tau oligomers by synthetic heparin like oligosaccharides. *Chem. Commun.* **2018,** *54* (72), 10120-10123.
18. Zulueta, M. M. L.; Lin, S.-Y.; Lin, Y.-T.; Huang, C.-J.; Wang, C.-C.; Ku, C.-C.; Shi, Z.; Chyan, C.-L.; Irene, D.; Lim, L.-H., α-Glycosylation by D-glucosamine-derived donors: synthesis of heparosan and heparin analogs that interact with mycobacterial heparin-binding hemagglutinin. *J. Am. Chem. Soc.* **2012,** *134* (21), 8988-8995.
19. Wang, Z.; Hsieh, P.-H.; Xu, Y.; Thieker, D.; Chai, E. J. E.; Xie, S.; Cooley, B.; Woods, R. J.; Chi, L.; Liu, J., Synthesis of 3-O-sulfated oligosaccharides to

understand the relationship between structures and functions of heparan sulfate. *J. Am. Chem. Soc.* **2017,** *139* (14), 5249-5256.

20. de Paz, J. L.; Noti, C.; Seeberger, P. H., Microarrays of synthetic heparin oligosaccharides. *J. Am. Chem. Soc.* **2006,** *128* (9), 2766-2767.
21. Hu, Y.-P.; Zhong, Y.-Q.; Chen, Z.-G.; Chen, C.-Y.; Shi, Z.; Zulueta, M. M. L.; Ku, C.-C.; Lee, P.-Y.; Wang, C.-C.; Hung, S.-C., Divergent synthesis of 48 heparan sulfate-based disaccharides and probing the specific sugar–fibroblast growth factor-1 interaction. *J. Am. Chem. Soc.***2012,** *134* (51), 20722-20727.
22. Noti, C.; de Paz, J. L.; Polito, L.; Seeberger, P. H., Preparation and use of microarrays containing synthetic heparin oligosaccharides for the rapid analysis of heparin–protein interactions. *Chem. Eur. J.* **2006,** *12* (34), 8664-8686.
23. Naticchia, M. R.; Laubach, L. K.; Tota, E. M.; Lucas, T. M.; Huang, M. L.; Godula, K., Embryonic stem cell engineering with a glycomimetic FGF2/BMP4 co-receptor drives mesodermal differentiation in a three-dimensional culture. *ACS Chem. Biol.* **2018,** *13* (10), 2880-2887.
24. Li, Y.-C.; Ho, I.-H.; Ku, C.-C.; Zhong, Y.-Q.; Hu, Y.-P.; Chen, Z.-G.; Chen, C.-Y.; Lin, W.-C.; Zulueta, M. M. L.; Hung, S.-C., Interactions that influence the binding of synthetic heparan sulfate based disaccharides to fibroblast growth factor-2. *ACS Chem. Biol.* **2014,** *9* (8), 1712-1717.
25. Thacker, B. E.; Xu, D.; Lawrence, R.; Esko, J. D., Heparan sulfate 3-O-sulfation: a rare modification in search of a function. *Matrix Biol.* **2014,** *35*, 60-72.
26. Langeslay, D. J.; Young, R. P.; Beni, S.; Beecher, C. N.; Mueller, L. J.; Larive, C. K., Sulfamate proton solvent exchange in heparin oligosaccharides: Evidence for a persistent hydrogen bond in the antithrombin-binding pentasaccharide Arixtra. *Glycobiology.* **2012,** *22* (9), 1173-1182.
27. Guerrini, M.; Elli, S.; Mourier, P.; Rudd, T. R.; Gaudesi, D.; Casu, B.; Boudier, C.; Torri, G.; Viskov, C., An unusual antithrombin-binding heparin octasaccharide with an additional 3-O-sulfated glucosamine in the active pentasaccharide sequence. *Biochem. J.* **2013,** *449* (2), 343-351.
28. Sankaranarayanan, N. V.; Strebel, T. R.; Boothello, R. S.; Sheerin, K.; Raghuraman, A.; Sallas, F.; Mosier, P. D.; Watermeyer, N. D.; Oscarson, S.; Desai,

U. R., A hexasaccharide containing rare 2-O-sulfate-glucuronic acid residues selectively activates heparin cofactor II. *Angew. Chem. Int. Ed.* **2017,** *56* (9), 2312-2317.

29. Kreuger, J.; Spillmann, D.; Li, J.-p.; Lindahl, U., Interactions between heparan sulfate and proteins: the concept of specificity. *J. Cell Biol.* **2006,** *174* (3), 323.
30. Collins, L. E.; Troeberg, L., Heparan sulfate as a regulator of inflammation and immunity. *J. Leukoc. Biol.* **2019,** *105* (1), 81-92.
31. Allen, S. J.; Crown, S. E.; Handel, T. M., Chemokine: receptor structure, interactions, and antagonism. *Annu. Rev. Immunol.* **2007,** *25*, 787-820.
32. Zong, C.; Venot, A.; Li, X.; Lu, W.; Xiao, W.; Wilkes, J.-S. L.; Salanga, C. L.; Handel, T. M.; Wang, L.; Wolfert, M. A., Heparan sulfate microarray reveals that heparan sulfate–protein binding exhibits different ligand requirements. *J. Am. Chem. Soc.* **2017,** *139* (28), 9534-9543.
33. de Paz, J. L.; Moseman, E. A.; Noti, C.; Polito, L.; von Andrian, U. H.; Seeberger, P. H., Profiling heparin–chemokine interactions using synthetic tools. *ACS Chem. Biol.* **2007,** *2* (11), 735-744.
34. Handel, T.; Johnson, Z.; Crown, S.; Lau, E.; Sweeney, M.; Proudfoot, A., Regulation of protein function by glycosaminoglycans—as exemplified by chemokines. *Annu. Rev. Biochem.* **2005,** *74*, 385-410.
35. Nonaka, M.; Bao, X.; Matsumura, F.; Götze, S.; Kandasamy, J.; Kononov, A.; Broide, D. H.; Nakayama, J.; Seeberger, P. H.; Fukuda, M., Synthetic di-sulfated iduronic acid attenuates asthmatic response by blocking T-cell recruitment to inflammatory sites. *Proc. Natl. Acad. Sci.* **2014,** *111* (22), 8173-8178.
36. Sheng, G. J.; Oh, Y. I.; Chang, S.-K.; Hsieh-Wilson, L. C., Tunable heparan sulfate mimetics for modulating chemokine activity. *J. Am. Chem. Soc.* **2013,** *135* (30), 10898-10901.
37. Jayson, G. C.; Hansen, S. U.; Miller, G. J.; Cole, C. L.; Rushton, G.; Avizienyte, E.; Gardiner, J. M., Synthetic heparan sulfate dodecasaccharides reveal single sulfation site interconverts CXCL8 and CXCL12 chemokine biology. *Chem. Commun.* **2015,** *51* (72), 13846-13849.

38. Ori, A.; Wilkinson, M. C.; Fernig, D. G., The heparanome and regulation of cell function: structures, functions and challenges. *Front Biosci* **2008,** *13*, 4309-4338.
39. Ashikari-Hada, S.; Habuchi, H.; Sugaya, N.; Kobayashi, T.; Kimata, K., Specific inhibition of FGF-2 signaling with 2-O-sulfated octasaccharides of heparan sulfate. *Glycobiology* **2009,** *19* (6), 644-654.
40. Johnson, G. R.; Wong, L., Heparan sulfate is essential to amphiregulin-induced mitogenic signaling by the epidermal growth factor receptor. *J. Biol. Chem.* **1994,** *269* (43), 27149-27154.
41. Billings, P. C.; Pacifici, M., Interactions of signaling proteins, growth factors and other proteins with heparan sulfate: mechanisms and mysteries. *Connective Tissue Res.* **2015,** *56* (4), 272-280.
42. Jiao, X.; Billings, P. C.; O'Connell, M. P.; Kaplan, F. S.; Shore, E. M.; Glaser, D. L., Heparan sulfate proteoglycans (HSPGs) modulate BMP2 osteogenic bioactivity in C2C12 cells. *J. Biol. Chem.* **2007,** *282* (2), 1080-1086.
43. Kuo, W.-J.; Digman, M. A.; Lander, A. D., Heparan sulfate acts as a bone morphogenetic protein coreceptor by facilitating ligand-induced receptor hetero-oligomerization. *Mol. Biol. Cell.* **2010,** *21* (22), 4028-4041.
44. Gdalevitch, M.; Kasaai, B.; Alam, N.; Dohin, B.; Lauzier, D.; Hamdy, R. C., The effect of heparan sulfate application on bone formation during distraction osteogenesis. *Plos One.* **2013,** *8* (2), e56790.
45. Higashiyama, S.; Abraham, J. A.; Klagsbrun, M., Heparin-binding EGF-like growth factor stimulation of smooth muscle cell migration: dependence on interactions with cell surface heparan sulfate. *J. Cell. Biol.* **1993,** *122* (4), 933-940.
46. Zhao, W.; McCallum, S. A.; Xiao, Z.; Zhang, F.; Linhardt, R. J., Binding affinities of vascular endothelial growth factor (VEGF) for heparin-derived oligosaccharides. *Biosci. Rep.* **2012,** *32* (1), 71-81.
47. Ashikari-Hada, S.; Habuchi, H.; Kariya, Y.; Itoh, N.; Reddi, A. H.; Kimata, K., Characterization of growth factor-binding structures in heparin/heparan sulfate using an octasaccharide library. *J. Biol. Chem.* **2004,** *279* (13), 12346-12354.

48. Casu, B.; Naggi, A.; Torri, G., Heparin-derived heparan sulfate mimics to modulate heparan sulfate-protein interaction in inflammation and cancer. *Matrix Biol.* **2010,** *29* (6), 442-452.
49. Padler-Karavani, V.; Song, X.; Yu, H.; Hurtado-Ziola, N.; Huang, S.; Muthana, S.; Chokhawala, H. A.; Cheng, J.; Verhagen, A.; Langereis, M. A., Cross-comparison of protein recognition of sialic acid diversity on two novel sialoglycan microarrays. *J. Biol. Chem.* **2012,** *287* (27), 22593-22608.
50. Ben-Arye, S. L.; Yu, H.; Chen, X.; Padler-Karavani, V., Profiling anti-Neu5Gc IgG in human sera with a sialoglycan microarray assay. *J. Vis. Exp.* **2017,** (125), e56094.
51. Carmeliet, P.; Jain, R. K., Angiogenesis in cancer and other diseases. *Nature.* **2000,** *407* (6801), 249-257.
52. Carmeliet, P., VEGF as a key mediator of angiogenesis in cancer. *Oncology* **2005,** *69* (Suppl. 3), 4-10.
53. Ferrara, N., VEGF as a therapeutic target in cancer. *Oncology* **2005,** *69* (Suppl. 3), 11-16.
54. Rapisarda, A.; Melillo, G., Role of the VEGF/VEGFR axis in cancer biology and therapy. In *Adv. Cancer Res.*, Elsevier: 2012; Vol. 114, pp 237-267.
55. Hicklin, D. J.; Ellis, L. M., Role of the vascular endothelial growth factor pathway in tumor growth and angiogenesis. *J. Clin. Oncol.* **2005,** *23* (5), 1011-1027.
56. Hoff, P. M.; Machado, K. K., Role of angiogenesis in the pathogenesis of cancer. *Cancer Treat. Rev.* **2012,** *38* (7), 825-833.
57. Tugues, S.; Koch, S.; Gualandi, L.; Li, X.; Claesson-Welsh, L., Vascular endothelial growth factors and receptors: anti-angiogenic therapy in the treatment of cancer. *Mol. Asp. Med.* **2011,** *32* (2), 88-111.
58. Sangabathuni, S.; Murthy, R. V.; Gade, M.; Bavireddi, H.; Toraskar, S.; Sonar, M. V.; Ganesh, K. N.; Kikkeri, R., Modeling Glyco-Collagen Conjugates Using a Host–Guest Strategy To Alter Phenotypic Cell Migration and in Vivo Wound Healing. *ACS Nano.* **2017,** *11* (12), 11969-11977.
59. Bashir, S.; Leviatan Ben Arye, S.; Reuven, E. M.; Yu, H.; Costa, C.; Galiñanes, M.; Bottio, T.; Chen, X.; Padler-Karavani, V., Presentation mode of glycans affect

recognition of human serum anti-Neu5Gc IgG antibodies. *Bioconjug. Chem.* **2018,** *30* (1), 161-168.

# CHAPTER- 4

## Rational Designing of Glyco-nanovehicles to Target Cellular Heterogeneity

# Abstract

The aberrant expression of endocytic epidermal growth factor receptors (EGFR) on cancer cells has emerged as a key target for therapeutic intervention. Here, a broad synthetic heparan sulfate (HS)-tetrasaccharide library is synthesized to evaluate binding affinity with EGFR specific growth factors and thereby develop the HS-nanovehicle to target cancer cells in tumor model. ELISA binding assay of structurally well-defined HS oligosaccharides shows that 6-*O*-sulfation (6-*O*-S) and 6-*O*-phosphorylation (6-*O*-P) of HS tetrasaccharides significantly enhances EGFR cognate growth-factor binding. To highlight the oncogenic activities, synthetic HS-tetrasaccharides are conjugated on multivalent fluorescent gold nanoparticles and measured the phenotypic cancer-cell-uptake mechanism. Hierarchical clustering of the cellular update assay with different degrees of EGFR-expressed cancer cells showed native 6-*O*-S residues of HS as powerful scaffold in EGFR mediated nanovehicle delivery. Finally, the 6-*O*-S HS-conjugated nanovehicle showed selective homing of the nanoparticles in cancer cells in 3D-co-culture spheroids, thus providing a novel target for cancer therapy and diagnostics in tumor microenvironment.

## 4.1 Introduction:

Cancer is a devastating and multifactorial disease. Recent studies have confirmed that over-expression of certain cell-surface receptors, growth factors, and suppression of tumor-specific genes are primary causes of cancer phenotype development.[1-3] Therefore, developing suitable markers for these functional changes may provide new diagnostic tools and lead to new delivery systems. Over the past two decades, epidermal growth factor receptors (EGFRs) have emerged as potential oncogenes that are commonly found in various cancer types.[4, 5] Thus, EGFRs targeted small molecules and EGFR-neutralizing monoclonal antibodies have impressive clinical significance.[6, 7] The EGFR binds to and is activated by its autocrine growth factors, such as EGF and heparin-binding EGF-like growth factors (HB-EGFs) that are often governed by heparan sulfate (HS), which is ubiquitous on both cell surfaces and the extracellular matrix.[8, 9] Hence, deciphering the structure-function relationship between HB-EGF or EGF and HS could be a new tool for selectively targeting cancer cells in tumor microenvironments. Structurally, HS is composed of α(1-4)-linked disaccharide repeating units of D-glucosamine and hexuronic acid, which could be either D-glucuronic acid (GlcA) or L-iduronic acid (IdoA).

The structural diversity of HS comes from the degree of *O*-sulfation and *N*-sulfation/acetylation on the glucosamine and hexuronic acid ligands.[10, 11] Several research groups have synthesized broad well-defined HS oligosaccharides libraries to elucidate the active ligand for growth factors, chemokines and biologically active molecules.[12- 22] The majority of these HS libraries are able to determine the sulfation code, uronic acid composition and oligosaccharide lengths of the HS during protein recognition. However, to the best of our knowledge, it is still unclear what is the HS chemically defined epitope(s) of EGFRs specific growth factors.

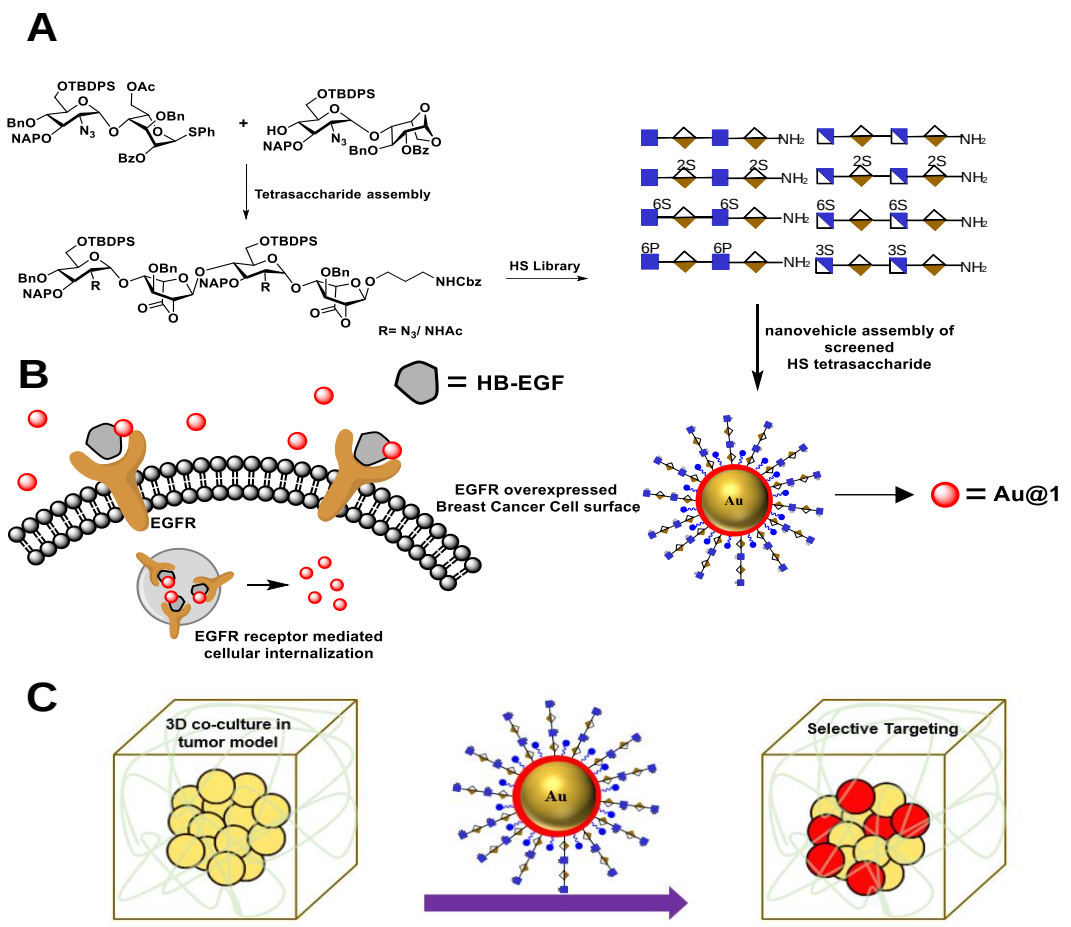


**Figure 1.** (A) Synthetic heparan sulfate based nanovehicle assembly and cancer cells targeting via EGFR in 2D and 3D-coculture model. (B) EGFR mediated uptake of nanovehicle by breast cancer cell. (C) Schematic representation of tumor model and selective targeting of cancer cells in the presence of stromal cells and extracellular matrix.

Herein, we report a new set of HS-tetrasaccharides with well-defined sulfation codes to determine the structure-functional relationship between EGFR binding growth factors. An ELISA assay with HB-EGF and EGF growth factors rationalized the molecular code of HS for EGFR activation. We have also synthesized the phosphate analog of super-active HS-tetrasaccharides in order determine why nature prefers sulfate pattern of HS during molecular recognition. The active ligands were functionalized on fluorescent gold nanoparticles to highlight the endocytosis process in different cancer cell lines with variable EGFR expression. Finally, we developed a three-dimensional coculture spheroid

model to demonstrate selective targeting of cancer cells in the presence of stromal cells and the extracellular matrix (Figure 1). Although HS/heparin polymer-based nanoparticles targeting cancer cells have been reported in the literature[23- 26], however, structure heterogeneity of HS polymer rendered native ligand less specific to cancer cells. Here, we report the first example of well-defined HS oligosaccharide-based nanovehicle construction to target specific cancer cells, followed by a 3D-coculture assay to establish selective targeting of cancer cells in the tumor microenvironment

## 4.2 Results and Discussion:

With the aim of identifying HS oligosaccharides ligand for EGFR specific growth factors, we selected *N*-unsubstituted and *N*-acetate derivative of glucosamine (synthesized previously in Chapter 2) with sulfation substitution at 6-OH, 3-OH and 2-OH of iduronic acid residue respectively. The rationale behind this sulfation patterns is that they exhibit common binding pocket for various growth factors and chemokines (Figure 2).

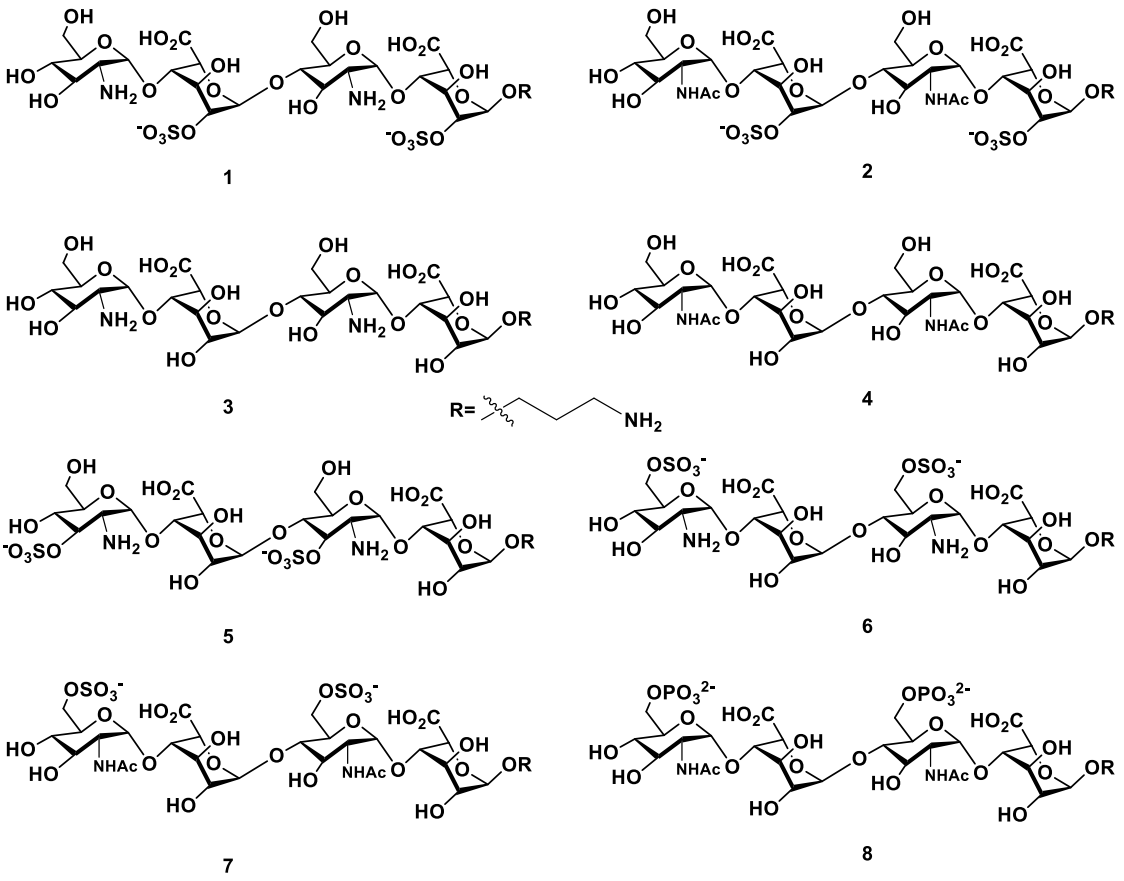


**Figure 2**: HS oligosaccharides 1-8.

### 4.2.1 ELISA Assay:

Next, we confirmed the HB-EGF binding affinity of **1**-**7** HS-tetrasaccharides. To this end, native heparin was immobilized on an ELISA plate and standard competition assay with heparinoids (**1**-**7**) was performed using HB-EGF, and EGF proteins. The ELISA analysis revealed that the only 6-*O*-S HS tetrasaccharide **(7)** showed strong inhibition with HB-EGF binding to native HS ($IC_{50}$ = 126.6 μM) (Figure 3c) compared to 2-*O*-S, 3-*O*-S and non-sulfated HS-tetrasaccharide analogs **(1-6)** at a concentration between 0 to 1 mg/L. In contrast, EGF protein showed no binding with synthetic HS-tetrasaccharides. An additional surface Plasmon resonance (SPR) binding experiment of **7** with HB-EGF revealed a $K_D$ of 11.12 μM (Figure 3a, Table 2 (experimental section)), clearly illustrating that the 6-*O*-S HS tetrasaccharide functioned as an active ligand for HB-EGF. Also, HS ligand **6** and **7** displayed the contrasting binding preferences as expected based on the microarray binding

profiles obtained for HB-EGF in chapter 3. To determine whether comp **7** and HB-EGF interactions differentiate between charge species geometrically close to sulfate group,[27] we also chose HS tetrasaccharide **8** and checked ELISA and SPR profiles. The ELISA assay and SPR binding showed strong binding with HB-EGF ($IC_{50}$ = 97.13 µM) (Figure 3d) and $K_D$ of 11.06 µM (Figure 3b, Table 2), These results demonstrated that the sulfated and phosphated HS tetrasaccharides functioned as active ligands of HB-EGF. It would be interesting to determine whether both ligands target cancer cells by activating the EGFR through autocrine HB-EGF signaling.

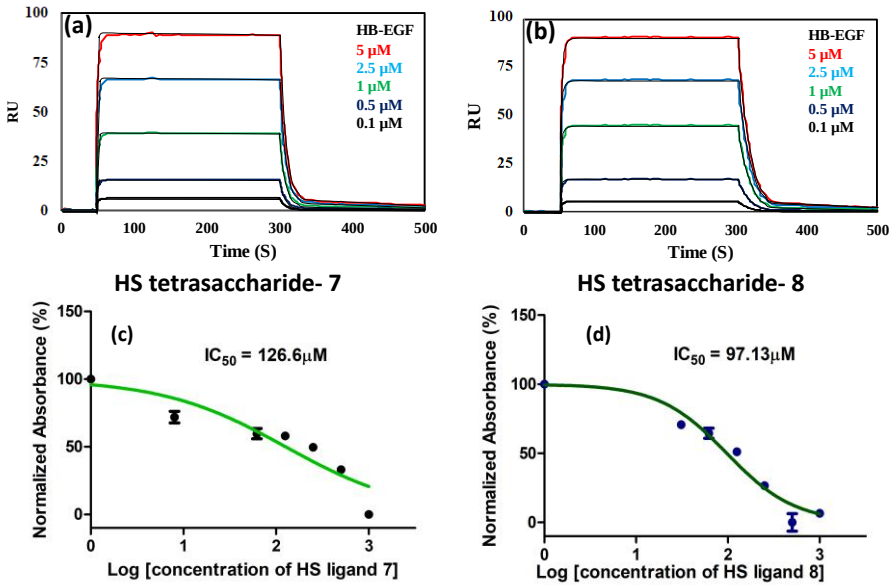


**Figure 3:** SPR binding analysis for the interaction between HB-EGF with (a) HS tetrasaccharide **7**; (b) HS tetrasaccharide **8;** HB-EGF binding to heparin coated plate measured by competitive ELISA with (c) HS ligand **7**; (d) HS ligand **8**

### 4.2.2 Glyco-nanovehicle construction:

To assess the efficacy of HS-tetrasaccharide ligands in activating EGFR, we functionalized them with commercial *N*-hydroxysuccinimide-active fluorescent gold nanoparticles **($AF_{555}Au$)**, which served as optical and non-toxic probes.[28], [29] The nanoparticle functionalization was performed by mixing ligands **7** and **8** at RT in 0.01 M PBS buffer with a pH of 7.5 for 12 h. (Scheme 1). Finally, the remaining NHS groups were neutralized with ethanolamine to afford heparinoid-capped fluorescent gold nanoparticles

(**AF$_{555}$Au@1** (HS ligand **7**) **and AF$_{555}$Au@2** (HS ligand **8**), respectively, altogether these are collectively represented as heparinoid-AuNPs).

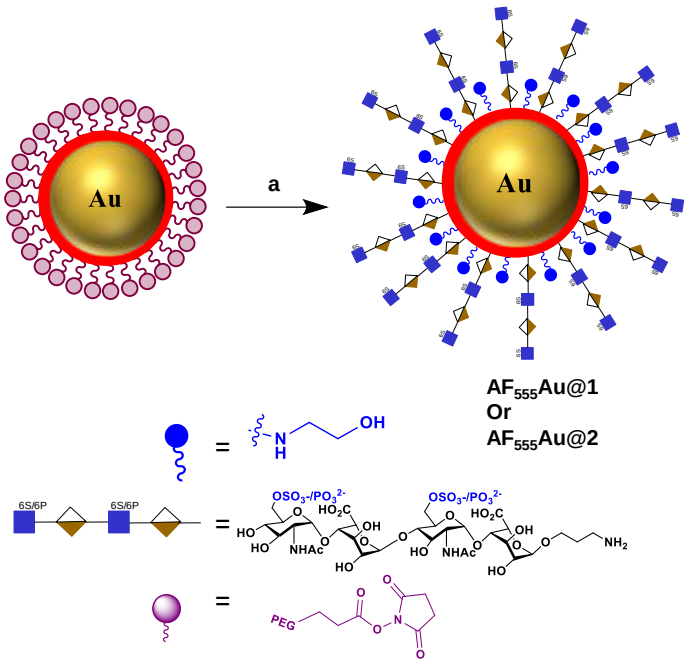


**Scheme 1.** Synthesis of heparinoid AuNPs: Reagents and conditions: (a) **7** or **8**, PBS, rt, 12 h.

The physical properties of the **AF$_{555}$Au@1 and AF$_{555}$Au@2** were confirmed by means of Transmission Electron Microscopy (TEM), UV-visible, fluorescence spectroscopy and zeta potential measurements (Table 1, Figure 9 (experimental section)). As a control, native heparin sulfate was conjugated with Texas Red (T-HP) and characterized (Figure 8 (experimental section)).

| Properties | Before Conjugation | After Conjugation | |
|---|---|---|---|
| | AF$_{555}$Au | AF$_{555}$Au | |
| | | Au@1 | Au@2 |
| Size (nm) | 10 | 15 | 15 |
| $\lambda_{max}$(nm) | 521 | 526 | 521 |
| $E_{max}$ (nm) | 580 | 573 | 573 |
| ζ (mV) | -20 | -56.3 | -59.4 |

**Table 1:** Physical Characterization of Heparinoid-AuNPs

### 4.2.3 Cellular uptake studies:

Next, a cellular uptake assay was performed using the standard protocol described in the experimental section. Breast cancer cell lines were selected based on the EGFR expression level (MDA-MB-468 high degree; MDA-MB-231, T-47D and MCF-7: moderate to low degree; and SK-BR-3 least EGFR expression[30]). The cancer cells and NIH-3T3 (as normal cells) were seeded on eight-well glass chamber slides and allowed to grow until they reached 70–80% confluency at 37 ºC in a 5% $CO_2$ incubator. Heparinoid-AuNPs (15 μg/ml) and T-HP (10 μg/ml) were added to the wells, and live images were recorded at two different time intervals (4 h and 24 h). (Figure 4(ii) & Figure 10 (experimental section)) To demonstrate HB- EGF-mediated uptake, the uptake mechanism was tested in the presence of 0.1 ng/ml of the HB-EGF proteins (Figure 11, experimental section). Hierarchical clustering (HCA) was developed based on the fluorescent intensity of the heparinoid-AuNPs inside the cells (Figure 4(i)). To ensure the consistency of the findings, all tests were performed in triplicate. The HCA of the heparinoid-AuNPs cellular internalization assay indicated the presence of a distinct disparity in uptake rates. As expected, the MDA-MB-468 cell line showed stronger cellular internalization responses than the other breast cancer cell lines and normal cells. Among the heparinoids, the uptake rate of **$AF_{555}$Au@1** was approximately 70-80 % stronger after 4 h (Figure 4(ii)), and the uptake rate significantly enhanced in the presence of the HB-EGF protein (Figure 11). This trend continued after 24 h. MDA-MB-468 showed preferential uptake of the sulfated heparinoid over phosphate analog, confirming the critical role of 6-O-sulfation of glucosamine in HB-EGF/EGFR signaling.

The uptake rate in the other breast cancer cell lines was weak as compared to that of MDA-MB-468. Moreover, T-HP exhibited a weak cellular uptake rate when compared to the heparinoid-AuNPs, indicating that synthetic ligand **7** might be a better functional ligand in terms of targeting the EGFR than the native HS sequence. We also performed FACS assays with MDA-MB-468 and NIH-3T3 to quantify the percentage cell uptake of the heparinoid-AuNPs. The FACS analysis clearly revealed potential uptake of **$AF_{555}$Au@1** in the MDA-MB-468 and no uptake in the normal NIH-3T3 cells. (Figure 4(iv), Figure 7 (experimental

section)). On the basis of these results, we hypothesized that **$AF_{555}$Au@1** could serve as a potential nanovehicle for targeting breast cancer cells.

To elucidate the mechanism underlying endocytosis, we performed live confocal imaging studies in the presence of endocytic pathway inhibitors. First, we evaluated the energy-dependent pathway. To this end, we incubated MDA-MB-468 with sodium azide so as to deplete the ATP and then administered the **$AF_{555}$Au@1** treatment for 4 h. We observed a substantial decrease in cellular internalization of the nanoparticles, indicating the presence of receptor-mediated endocytic pathways (Figure 4 (iii-b)). To analyze EGFR-mediated endocytosis, Gefitinib (an EGFR Inhibitor) (30 µM) was added. The blockage of the receptor resulted in a strong decrease in the cellular uptake of **$AF_{555}$Au@1** (Figure 4 (iii-c)). These findings suggested that **$AF_{555}$Au@1** undergoes receptor-mediated endocytosis.

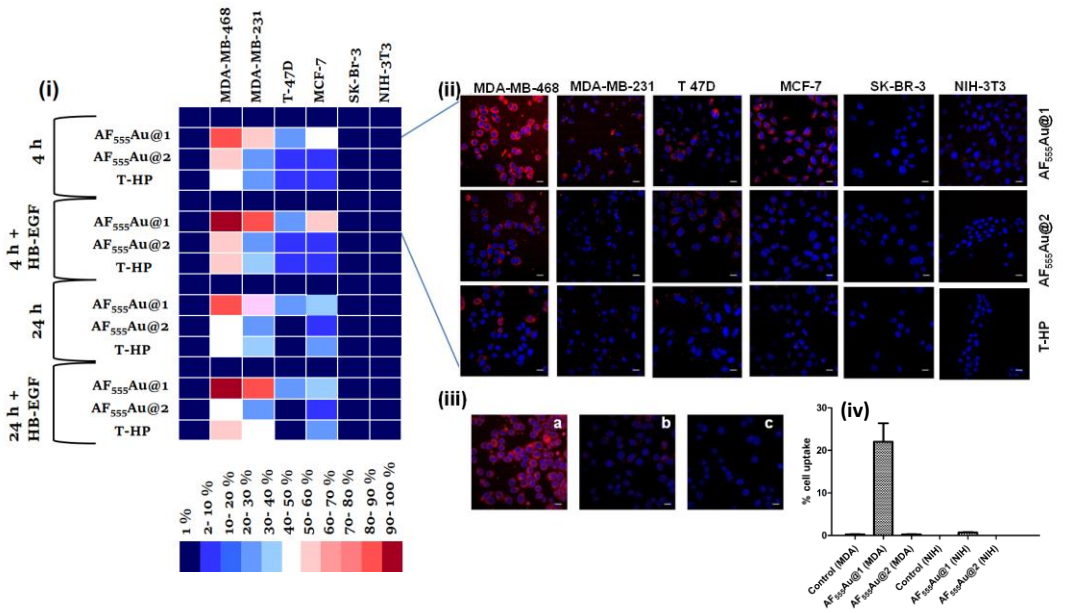


**Figure 4. (i)** Hierarchical clustering analysis (HCA) of cellular internalization of heparinoid-AuNPs with different breast cancer cells and normal cells after 4 and 24 h in presence and absence of EGF proteins (HB-EGF mediated uptake of **$AF_{555}$Au@1** after 24 h was considered as 100%); **(ii)** Confocal images of nanoparticles internalization by different cells lines after 4 h (scale bar: 20 $\mu$m); **(iii)** Confocal images of **$AF_{555}$Au@1** in the presence of different endocytotic pathways inhibitors (scale bar: 20 $\mu$m) :(a) **$AF_{555}$Au@1**; (b) **$NaN_3$ + $AF_{555}$Au@1**; (c) **EGF inhibitor + $AF_{555}$Au@1. (iv)** (c) Quantification of cellular uptake in MDA-MB-468 and NIH-3T3 for **$AF_{555}$Au@1** and **$AF_{555}$Au@2** using flow cytometry**.**

### 4.2.4. 3D- cell culture model:

Recently, it has been established that a two-dimensional (2D) monolayer cell assay does not replicate the *in vivo* tumor model to evaluate the efficacy of nanovehicles in cancer therapy.[31] Alternatively, a three-dimensional (3D) spheroids can provide an attractive *in vitro* model that accurately mimics the tumor microenvironment (TME) for the purposes of drug discovery and tumor targeting.[32] The TME comprises tumor cells encapsulated by a dense extracellular matrix (ECM) as well as heterogeneous cells types such as stromal cells, immune cells, and endothelial cells. These cell lines, together with the composition of the ECM, support the enhancement of cancer cells motility, activate different signaling pathways, and modulate targeting efficacy of nanovehicles.[33] Thus, it is important to examine the activity of heparinoid-AuNPs in a 3D-spheroid model so as to demonstrate the efficacy. We first constructed MDA-MB-468 and SK-BR-3 cell microspheriods using ECM matrigel. After eight days of culture, we observed the formation of spheroids that were uniform in size (40-42 μm) and contained approximately 10–15 cells per spheroid. We added **$AF_{555}$Au@1** at an optimum concentration of 50 μg/ml. Confocal microscopy revealed the strong uptake of the **$AF_{555}$Au@1** by the MDA-MB-468 cells (Figure 5). However, the SK-BR-3 did not uptake **$AF_{555}$Au@1**. The well-organized hoechst stained nuclei and the red fluorescent **$AF_{555}$Au@1** were co-localized through a 3D reconstruction of the confocal Z-stack images. These results confirmed that **$AF_{555}$Au@1** can diffuse the ECM and selectively target the EGFRs on MDA-MB-468.

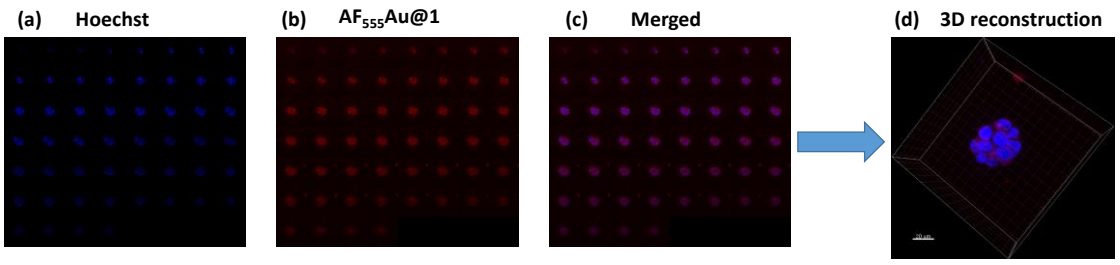


**Figure 5**: Z-stack montage for MDA-MB-468 spheroids (total slices- 52); (a) Nuclei staining (blue channel); (b) $AF_{555}$Au@1 (red channel); (c) Merged (blue and red); (d) 3D reconstruction of the z-stacked images (scale bar: 20 $\mu$m)

Next, we investigated whether cancer cells can be selectively targeted in the presence of stromal cells such as fibroblast cells. Fibroblast cells are one of the prominent cells in the TME and they play a pivotal role in ECM remodeling and causing resistance to the uptake

mechanism of nanovehicles.[34] To this end, we constructed 3D co-culture models by mixing 2:1 of MDA-MB-468 and GFP tagged NIH-3T3 respectively. After five days, we observed the presence of multicellular spheroids. These spheroids were much larger in size then the MDA-MB-468 alone. To these co-culture model, we added **$AF_{555}$Au@1** (50 μg/ml) and then performed the imaging after 4 h. As shown in (Figure 6) the multicellular spheroid featuring GFP-NIH-3T3 displayed nanoparticle sequestration in the interior part after successfully crossing the fibroblast barrier outside the spheroid. Moreover, the absence of **$AF_{555}$Au@1** from NIH-3T3 could be easily seen in the Z- stacked slices. These results suggest that the **$AF_{555}$Au@1** targeted the cancer cells in the presence of the high concentration of fibroblast cells, thus demonstrating the efficacy of nanovehicle in targeting cancer cells in the TME. The selective targeting was a result of high expression of EGFRs present on the cancer cells.

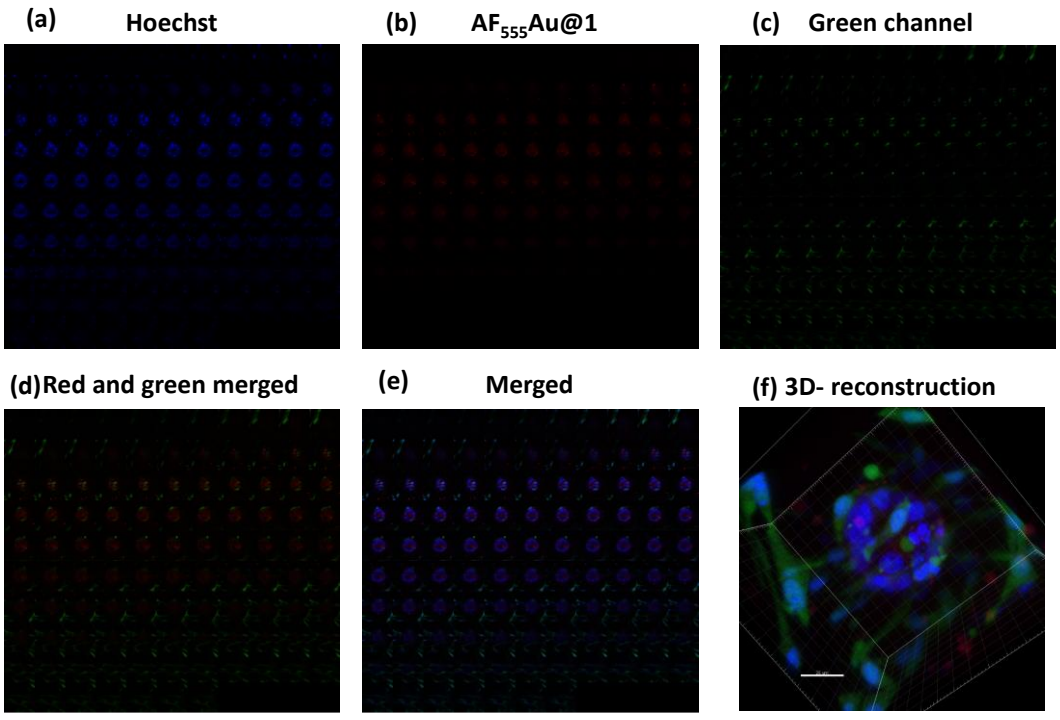


**Figure 6**: Z-stack montage for MDA-MB-468 and GFP stable NIH-3T3 cells spheroids (total slices-106); (a) Nuclei stain (blue channel); (b) $AF_{555}$Au@1 (red channel); (c) GFP-NIH-3T3 (green channel); (d) Merged (red and green); (e) Merged (blue, red and green); (f) 3D reconstruction of Z-stacked images (scale bar: 25 $\mu$m)

## 4.3 Conclusions:

In conclusion, we have identified a structurally well-defined 6-*O*-S HS tetrasaccharide as the most active ligand among the series when the binding affinity with EGFR cognate growth factors was tested. The study also confirmed that 6-*O*-phsophate is a potential ligand of HB-EGF. Using these two ligands, we have constructed HS-based fluorescentnanovehicles that are intended to target breast cancer cells in tumor microenvironment. As validated by a series of confocal imaging techniques, we found that 6-*O*-sulfated HS-tetrasaccharide exhibits enhanced uptake by EGFR-overexpressed cancer cells, whereas their phosphate derivatives show weak EGFR-mediated uptake rates. These results, confirm the critical role of HS sulfation groups in EGFR activation. The HS-nanoparticles targeted the breast cancer cells via HB-EGF/EGFR-mediated interactions in both the 2D monolayer and in the 3D-complex coculture tumor model, which underscores their potential use in cancer therapies.

## 4.4 Experimental Part:

### 4.4.1 General Information:

All the confocal microscopy images were captured on a Zeiss LSM710 confocal microscope and processed using ImageJ software. Human HB-EGF, amphiepiregulin, EGF and its respective biotinylated antibody was purchased from Peprotech. Gefitinib (EGFR inhibitor) was purchased from Sigma-aldrich. GFP stable NIH-3T3 cells were purchased from Biogenuix.

### 4.4.2 ELISA, SPR and FACS protocol:

**ELISA:** $IC_{50}$ value of heparinoids **7** & **8** with HB-EGF were evaluated using standard competitive ELISA protocol. First, commercially available Heparin sodium salt in PBS at a concentration of 10 µg/mL was added on 96 well flat bottomed (Nunc MaxiSorp) plate with 100 µL in coating buffer and incubated at RT for 16 h. For positive control HB-EGF at a concentration of 0.1 µg/mL was also coated and incubated. Next day, after blocking (at 37 $^{o}$C) , pre-incubated mixture of HB-EGF (0.1 µg/mL) with an increasing heparinoid

concentration (0- 1 mg/L, 100 µL) were added and incubated for 2 h at RT. After 2 h, normal washing procedure was followed and wells were incubated with biotinylated anti HB-EGF antibody (1 µg/mL, 100 µL) at RT for another 2 h. Next, plate was washed 3-4 times and incubated with streptavidin-HRP conjugate (0.05 µg/mL, 100 µL) for 30 minutes. Finally, TMB liquid substrate (100 µL) was added to wells after washing and incubated in dark at RT for 20 minutes for the color development. The reaction was stopped using 1 N HCl and absorbance was recorded at 450 nm and analysed using GraphPad Prism Software. A similar experiment with EGF and amphiregulin didn't showed any competitive binding in the presence of heparinoids concentration (0- 1 mg/L, 100 µL), indicating weak/no-binding affinity.

**SPR:** Heparin tetrasaccharide ligands (**7** and **8**) were immobilized onto a CM5 chip (BIACORE) using standard amine coupling procedures. Briefly, the CM5 chip was activated by injecting a mixture of NHS/EDC mixture with a contact time of 300 S at a flow rate of 20 µL/min, followed by multiple injections of HS ligands (0.5 mM) dissolved in HBS-EP buffer. On the control channel, a propanol amine linker was injected. Different HB-EGF growth factors at a flow rate of 50 µL/min and 25 °C in HBS-EP buffer were injected for 250 secs. After that, dissociation was performed by injected the HBS-EP without growth factors. The binding was measured after reference subtraction of control. All data evaluation was performed using BIAevaluation.

| **HS Tetrasaccharide** | **$K_D$ (µM)** | **$K_{on}$ ($M^{-1}S^{-1}$)** | **$K_{off}$ ($S^{-1}$)** |
|---|---|---|---|
| **7** | 11.12 ± 0.3 | $4.26 \pm 0.2 \times 10^4$ | $4.75 \pm 0.32 \times 10^{-1}$ |
| **8** | 11.06 ± 0.15 | $4.29 \pm 0.11 \times 10^4$ | $4.72 \pm 0.22 \times 10^{-1}$ |

**Table 2:** SPR analysis of kinetic rate constants and equilibrium affinities for HS tetrasaccharides **7** and **8** binding to HB-EGF.

**FACS:** MDA-MB-468 cells ($0.24 \times 10^5$) were seeded in 24 well plate and allowed to grow at 37 °C in 5 % $CO_2$ atmosphere till 70- 80 % confluency. After that heparinoid AuNPs (10 µg/ml) were added and incubated for 4 h. Upon incubation, wells were washed with PBS to remove the excess NPs. Finally, cells were trypsinized and resuspended in 0.5 ml PBS for FACS

measurements. Cells without NPs were taken as a control and fluorescence with respect to that were measured to quantify the uptake in PE-A channel using yellow green (561 nm) laser.

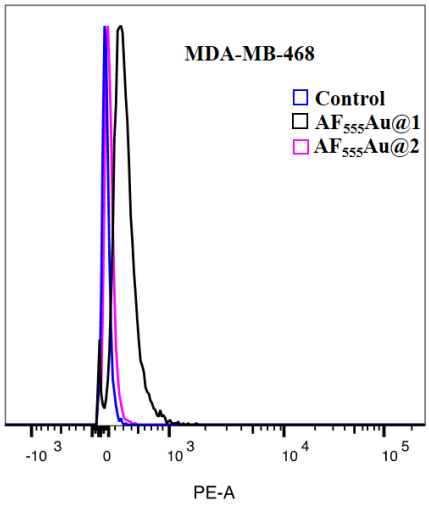


**Figure 7:** Histograms representing the cell uptake of **$AF_{555}$Au@1** and **$AF_{555}$Au@2** in MDA-MB-468 at 4 h.

### 4.4.3 Synthesis of heparinoid-gold nanoparticles ($AF_{555}$Au@1 and $AF_{555}$Au@2):

The NHS activated-$Alexa_{555}$ fluorescent gold nanparticles (**$AF_{555}$Au**) were purchased from NanoPartz. The $AF_{555}$Au were suspended in PBS buffer in 1.5 mL centrifuge tube and incubated with **7** and **8** (3 mg) at 25 ºC for 12 h. After amide functionalization, the remaining NHS groups were neutralized with ethanolamine (0.05 µL) for 12 h. Subsequently, the nanoparticles were centrifuge at 15000 rpm for 5 minutes to precipitate functionalized AuNPs. Next, nanoparticles were washed with PBS (3 X 1 ml) to remove unreacted heparinoids, ethanolamine and NHS. Finally, heparinoid-AuNPs were dissolved in PBS buffer and stored at 4 ºC till further use.

### 4.4.4 Synthesis and characterization of Texas red conjugated Heparin (T-HP)

To a solution of commercially available Heparin sodium salt (5 mg/ mL) (H4784 Sigma) in 0.1 M sodium bicarbonate buffer (pH= 8.3) was added 100 µL of Texas Red™-X, Succinimidyl Ester (0.5 mg) in a drop wise manner and left for stirring for 1 h at room

temperature. After 1 h, the solution was dialyzed against 1 kD dialysis membrane for 24 h to remove the unreacted dye solution. Finally, the dialysed solution was lyophilized and stored at -20 ºC till further use.

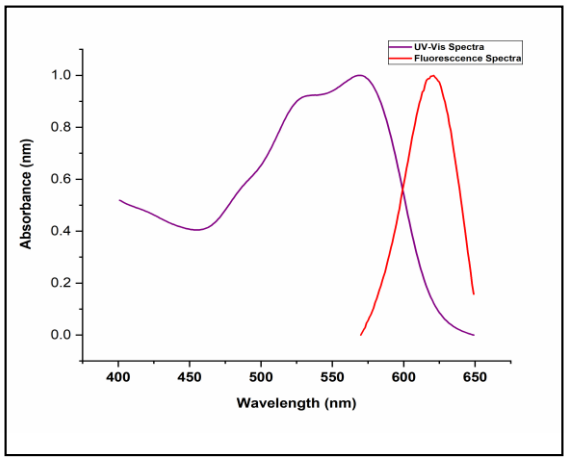


**Figure 8**: T-HP characterization.

### 4.4.5 TEM, UV and Fluorescence measurements:

TEM measurements of heparinoid- AuNPs were performed on a Jeol, JEM 2200FS. The samples were prepared by vacuum drying of 5 µl of the sample drop casted on carbon type-B 200 mesh copper grid.

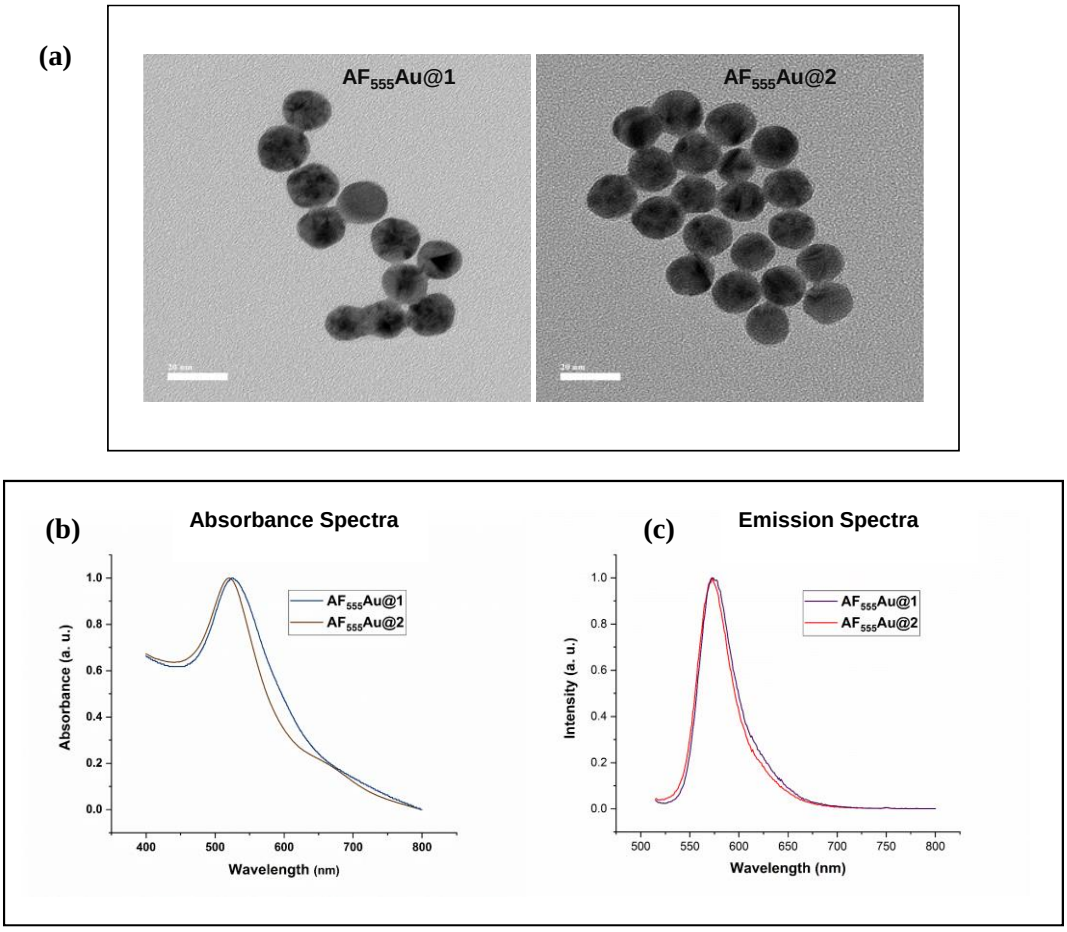


**Figure 9**: (a) TEM Images (scale bar: 20 nm); (b) UV-Visible; (c) Fluorescence Spectra

### 4.4.6 Zeta potential measurements:

Zeta potential was used to measure the electrophoretic mobility of heparinoid nanoparticles. We applied a unit field of 1 volt per meter to the nanoparticle solution and employed Helmholtz-Smoluchowski equation to quantify the zeta potentials.

### 4.4.7 Cell Viability assay:

MDA-MB-468 and NIH-3T3 ($1 \times 10^5$ cells/well) were seeded in 96-well microtiter plate and incubated overnight in a 5% $CO_2$ incubator at 37 °C for attachment. Cells were then treated with heperinoid-AuNPS in different concentrations (0, 0.5, 1 μg/ml) for 24 h. Then

20 µL of MTT reagent (5 mg/mL) were added and incubated at 37 °C in the $CO_2$ incubator. After 4 h, 100 µL of DMSO was added. Absorbance was measured with spectrophotometer at 550 nm. The percent cell viability was calculated considering the untreated cells as 100% viability.

### 4.4.8 Cellular internalization of heparinoid-AuNPs:

| Cell line | Growth Media |
|---|---|
| MDA-MB-468, MDA-MB-231, T47D, MCF-7, SK-BR-3 and NIH-3T3 | Cells were grown at 37 °C in 5% $CO_2$ atmosphere in DMEM medium containing 10% fetal bovine serum and 0.1% streptomycin |

All cells (2 x $10^4$ cells per well) were seeded on 8-well chamber slides and allowed to grow for 24 h. Then heparinoid-AuNPs (10 µg/mL) was added in presence and absence of HB-EGF (20 ng/mL) for 4 h and 24 h respectively. Later the cells were washed three times with PBS buffer and placed in fresh media. Nuclei were stained with Hoechst 33342 reagent (2 µg/mL). Fluorescence measurements were performed using excitation with an argon laser, $I$ = 405 & 561 nm, and the emission was collected at 450- 500 nm (for blue), 550- 650 nm (for red).

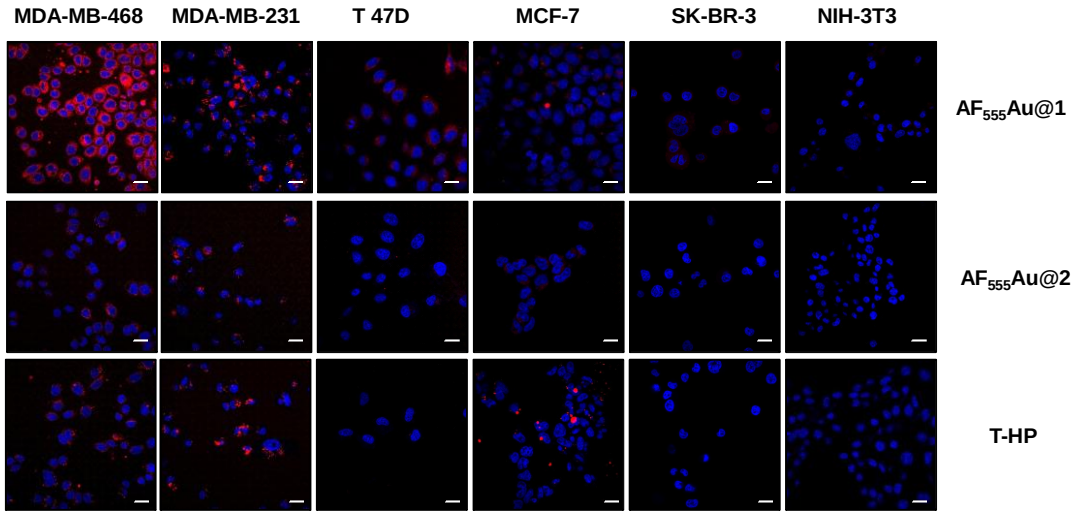


**Figure 10:** Confocal images of nanoparticles internalization by different cells lines after 24 h (scale bar- 20 $\mu$m)

### 4.4.9 HB-EGF-Mediated uptake for MDA-MB-468:

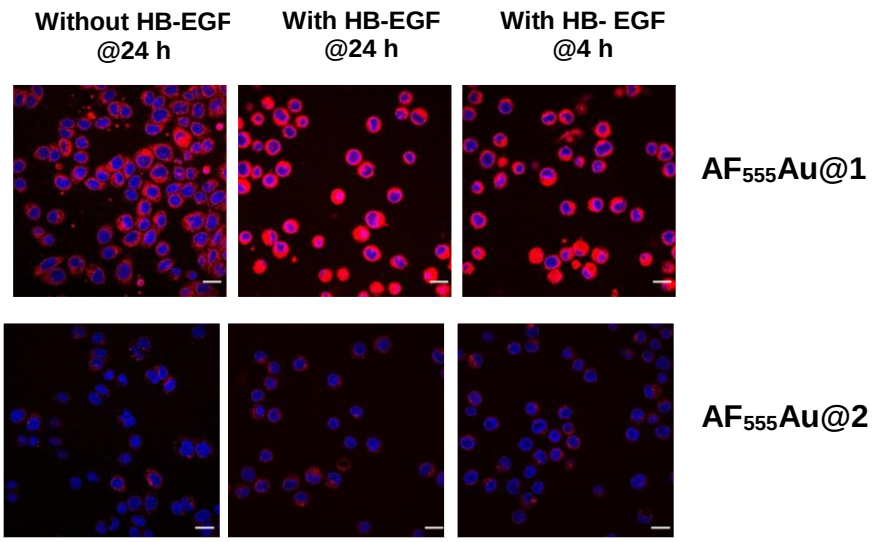


**Figure 11**: Cellular internalization of nanoparticles in presence of HB-EGF at 4 and 24 h. (scale bar: 20 $\mu$m)

### 4.4.10 Cellular internalization mechanism studies of $AF_{555}$Au@1 in MDA-MB-468:

To prove the endocytosis pathway, we utilized EGFR inhibitor to prove the mechanism. We incubated MDA-MB-468 cells ($2 \times 10^4$ cells/well) in 8-well chamber slides and treated with $NaN_3$ (50 mM) for 30 min to deplete ATP, followed by the addition of **$AF_{555}$Au@1** for 4 h and imaged. To confirm EGFR mediated cellular internalization of nanoparticles, cells were treated with Gefitinib (EGFR inhibitor) at a concentration of 30 µM and incubated for 30 min h, followed by **$AF_{555}$Au@1** addition and imaged after 4 h.

### 4.4.11 3D spheroid formation:

3D spheroids for MDA-MB-468 were formed using Matrigel (ECM Gel from Engelbreth-Holm-Swarm murine sarcoma) using manufacturer's protocol. Briefly, at first a monolayer

of 100 % matrigel (~55 µL) was coated on 8-well chamber slides and kept for polymerization at 37 °C for 15 min. Next, mono-dispersed freshly trypsinized MDA-MB-468 (~4000 cells/well) in growth medium containing 2% matrigel was plated on top of the pure matrigel layer and incubated at 37 °C for 7-8 days. Growth Medium was replaced every 2$^{nd}$ day. After spheroid formation heparinoid-AuNPs (50 µg/mL) were added and incubated for 4 h. Later, the cells were washed three times with PBS buffer and placed in fresh media. Nuclei were stained with Hoechst 33342 reagent (2 µg/mL). Fluorescence measurements were performed using excitation with an argon laser, $I$ = 405 and 450 nm, with the emission collected through 403–452 nm and 550–650 nm filters. 3D spheroids for co-culture were formed following the same protocol as described above keeping the cell number constant (~ 4000 cells/ well).

## 4.5 References:


1. Anastas, J. N.; Moon, R. T., WNT signalling pathways as therapeutic targets in cancer. *Nature Reviews Cancer* **2013,** *13* (1), 11-26.
2. Ellis, L. M.; Hicklin, D. J., VEGF-targeted therapy: mechanisms of anti-tumour activity. *Nature reviews cancer* **2008,** *8* (8), 579-591.
3. Schroeder, A.; Heller, D. A.; Winslow, M. M.; Dahlman, J. E.; Pratt, G. W.; Langer, R.; Jacks, T.; Anderson, D. G. Treating metastatic cancer with nanotechnology. *Nat. Rev. Cancer*. **2011**, *12*, 39–50.
4. Tebbutt, N.; Pedersen, M. W.; Johns, T. G., Targeting the ERBB family in cancer: couples therapy. *Nature reviews Cancer* **2013,** *13* (9), 663-673.
5. Wells, A., EGF receptor. *The international journal of biochemistry & cell biology* **1999,** *31* (6), 637-643.
6. Ali, R.; Wendt, M. K. The paradoxical functions of EGFR during breast cancer progression. *Signal. Transduct. Target.Ther*. **2017**, *2*, 16042.
7. Sigismund, S.; Avanzato, D.; Lanzetti, L. Emerging functions of the EGFR in cancer. *Mol. Oncol*. **2018**, *12*, 3–20.

8. Henriksen, L.; Grandal, M. V.; Knudsen, S. L. J.; Deurs, B. V.; Grøvdal, L. M. Internalization mechanisms of the epidermal growth factor receptors after activation with different ligands. *PLoS One*. **2013**, *8*, e58148
9. Yotsumoto, F.; Sanui, A.; Fukami, T.; Shirota, K.; Horiuchi, S.; Tsujioka, H.; Yoshizato, T.; Kuroki, M.; Miyamoto, S. Efficacy of ligand-based targeting for the EGF system in cancer. *Anticancer Res*. **2009**, *29*, 4879-4885.
10. Whitelock, J. M.; Iozzo, R. V. Heparan sulfate: a complex polymer charged with biological activity. *Chem. Rev.* **2005**, *105*, 2745-2764.
11. Lindahl, U.; Couchman, J.; Kimmata K.; Esko, J. D. *Essentials of Glycobiology*, *3rd edition* (Eds: Varki, A.; Cummings, R. D.; Esko, J. D.; Stanley, P.; Hart, G. W.; Aebi, M.; Darvill, A. G.; Kinoshita, T.; Packer, N. H.; Prestegard, J. H.; Schnaar, R. L.; Seeberger P. H.), Cold spring Harbor Laboratory press, **2015-2017**, Chapter 17.
12. Mende, M.; Bednarek, C.; Wawryszyn, M.; Sauter, P.; Biskup, M. B.; Schepers, U.; Bräse, S. Chemical synthesis of glycosaminoglycans. *Chem. Rev*. **2016**, *116*, 8193-8255.
13. Lu, W.; Zong, C.; Chopra, P.; Pepi, L. E.; Xu, Y.; Amster, I. J.; Liu, J.; Boons, G. J. Controlled chemoenzymatic synthesis of heparan sulfate oligosaccharides. *Angew. Chem. Int. Ed*. **2018**, *57*, 5340-5344.
14. Hansen, S. U.; Miller, G. J.; Cliff, M. J.; Jayson, G. C.; Gardiner, J. M. Making the longest sugars: a chemical synthesis of heparin-related [4]n oligosaccharides from 16-mer to 40-mer. *Chem. Sci*. **2015**, *6*, 6158-6164.
15. Hu, Y. P.; Lin, S. Y.; Huang, C. Y.; Zulueta, M. M. L; Liu, J. Y.; Chang, W.; Hung, S. C. Synthesis of 3-*O*-sulfonated heparan sulfate octasaccharides that inhibit the herpes simplex virus type 1 host-cell interaction. *Nat. Chem*. **2011**, *3*, 557–563.
16. Zhang, X.; Pagadala, V.; Jester, H. M.; Lim, A. M.; Pham, T. Q.; Goulas, A. M. P.; Liu, J.; Linhardt, R. J. Chemoenzymatic synthesis of heparan sulfate and heparin oligosaccharides and NMR analysis: paving the way to a diverse library for glycobiologists. *Chem. Sci*. **2017**, *8*, 7932–7940.

17. Noti, C.; de Paz, J. L.; Polito, L.; Seeberger, P. H. Preparation and use of microarray containing synthetic heparin oligosaccharides for the rapid analysis of heparin-protein interactions. *Chem.: Eur. J.* **2006**, *12*, 8664-8686.
18. De Paz, J. L.; Noti, C.; Seeberger, P. H. Microarrays of synthetic heparin oligosaccharides. *J. Am. Chem. Soc.* **2006**, *128*, 2766-2767.
19. Zong, C.; Venot, A.; Li, X.; Lu, W.; Xiao, W.; Wilkes, J. L.; Salanga, C. L.; Handel, T. M.; Wang, L.; Wolfert, M. A.; Boons, G. J. Heparan sulfate microarray reveals that heparan sulfate-protein binding exhibits different ligand requirements. *J. Am. Chem. Soc*. **2017**, *139*, 9534-9543.
20. Pawar, N. J.; Wang, L.; Higo, T.; Bhattacharya, C.; Kancharla, P. K.; Zhang F.; Baryal, K.; Huo, C. X.; Jian, J. L.; Linhardt, R. J.; Xuefei, X. H.; Hsieh-Wilson, L. C. Expedient synthesis of core disaccharide building blocks from natural polysaccharides for heparan sulfate oligosaccharide assembly. *Angew. Chem. Int. Ed. Engl.* **2019**. ASAP. doi: 10.1002/anie.201908805.
21. Boothello, R. S.; Sarkar, A.; Tran, V. M.; Nguyen, T. K.; Sankaranarayanan, N. V.; Mehta, A. Y.; Alabbas, A.; Brown, S.; Rossi, A.; Joice, A. C.; Mencio, C. P.; Quintero, M. V.; Kuberan, B.; Desai, U. R. Chemoenzymatically prepared heparan sulfate containing rare 2-*O*-sulfonated glucuronic acid residues. *ACS Chem. Biol.* **2015,** *10*, 1485-1494.
22. Sankarayanarayanan, N. V.; Strebel, T. R.; Boothello, R. S.; Sheerin, K.; Raghuraman, A.; Sallas, F.; Mosier, P. D.; Watermeyer, N. D.; Oscarson, S.; Desai, U. R. A hexasaccharide containing rare 2-*O*-sulfate-glucuronic acid residues selectively activates heparin cofactor II. *Angew. Chem. Int .Ed. Engl*. **2017**, *56*, 2312-2317.
23. Yang, X.; Du, H.; Liu, J.; Zhai, G., Advanced nanocarriers based on heparin and its derivatives for cancer management. *Biomacromolecules* **2015,** *16* (2), 423-436
24. Wang, Y.; Wang, Y.; Xiang, J.; Yao, K., Target-specific cellular uptake of taxol-loaded heparin-PEG-folate nanoparticles. *Biomacromolecules* **2010,** *11* (12), 3531-3538.
25. Wang, L.; Gong, T.; Brown, Z.; Randle, C.; Guan, Y.; Ye, W.; Ming, W., Ascidian-Inspired Heparin-Mimetic Magnetic Nanoparticles with Potential for Application

in Hemodialysis as Recycling Anticoagulants. *ACS Biomater. Sci. Eng.* **2020,** *6* (4), 1998-2006.

26. Groult, H.; Poupard, N.; Herranz, F.; Conforto, E.; Bridiau, N.; Sannier, F. d.; Bordenave, S. p.; Piot, J.-M.; Ruiz-Cabello, J. s.; Fruitier-Arnaudin, I., Family of bioactive heparin-coated iron oxide nanoparticles with positive contrast in magnetic resonance imaging for specific biomedical applications. *Biomacromolecules* **2017,** *18* (10), 3156-3167.
27. Van Boeckel, A. A.; Petitou, M. The unique antithrombin III binding domain of heparin: a lead to new synthetic antithrombotics. *Angew. Chem. Int. Ed.* **1993**, *32*, 1671-1818.
28. Yang, X.; Yang, M.; Pang, B.; Vara, M.; Xia, Y. Gold nanomaterials at work in biomedicine. *Chem. Rev.* **2015**, *115*, 10410-10488.
29. Sangabathuni, S.; Murthy, R. V.; Chaudhary, P. M.; Surve, M.; Banerjee, A.; Kikkeri, R. Glyco-gold nanoparticle shapes enhance carbohydrate-protein interactions in mammalian cells. *Nanoscale*, **2016**,*8*, 12729-12735.
30. Konecny, G. E.; Pegram, M. D.; Venkatesan, N.; Finn, R.; Yang, G.; Rahmeh, M.; Untch, M.; Rusnak, D. W.; Spehar, G.; Mullin, R. J.; Keith, B. R.; Gilmer, T. M.; Berger, M.; Podratz, K. C.; Slamon, D. J. Activity of the dual kinase inhibitor lapatinib (GW572016) against HER-2-overexpressing and trantuzumab-treated breast cancer cells. *Cancer Res.* **2006,** *66*, 1630-1639.
31. Dai, Q.; Wilhelm, S.; Ding, D.; Syed, A. M.; Sindhwani, S.; Zhang, Y.; Chen, Y. Y.; MacMillan, P.; Chan, W. C. W. Quantifying the ligand-coated nanoparticle delivery to cancer cells in solid tumors. *ACS Nano*. **2018**, *12*, 8423−8435.
32. Nath, S.; Devi, G. R.; Three-dimentional culture systems in cancer research: focus on tumor spheroid model. *Pharmacol. Ther*. **2016**, *163*, 94-108.
33. Miao, L.; Huang, L. Exploring the tumor microenvironment with nanoparticles. *Cancer Treat Res.* **2015**, *166*, 193-226.
34. Alkasalias, T.; Galceran, L. M.; Henriksson, M. A.; Lehti, K. Fibroblasts in the tumor microenvironment: shield or shear? *Int. J. Mol. Sci.* **2018**, *19*, 1532.

# CHAPTER- 5

## Deciphering Sulfation Code Required for Modulating P-selectin and Tau Protein Activities Using Glycan Microarray

## 5.1 Introduction:

Heparan Sulfate regulates its biological activity upon binding with the function-specific proteins.[1, 2] For instance, anticoagulant activity is regulated upon antithrombin binding with heparin. Similarly, binding of cell surface HS with chemokines and growth factors are responsible for maintaining homeostasis. The importance of identifying the optimal structural requirements for regulating these processes and their therapeutic significance has been discussed throughout the thesis. However, HS is known to bind with a myriad of proteins owing to its structural diversity.[3] Studying the structural-activity relationship of every single protein/ biomolecule that HS interacts with is beyond the human limits. We have studied the binding profiles of newly synthesized HT ligands with a broad library of chemokines and growth factors in previous chapters to push this limit. In this chapter, we have chosen P-selectin and Tau protein as our target proteins that have not been studied earlier in search of some novel binding characteristics.

P-selectin (CD62) is a transmembrane glycoprotein with an approximate size of 140kD. Like its other family members (L and E selectin), it works synergistically with other cell adhesion molecules (ICAM-1, etc.) to mediate platelets' adhesive interactions. Selectins are known to regulate their biological activities through their carbohydrate-binding domains (lectin domain) upon binding with sialylated and sulfated carbohydrate ligands. Sialyl lewis$^X$ containing glycoprotein (PSGL-1/ ESL-1) was thought to be the *numero uno* ligands for all three selectins until the 1990s.[4, 5] However, breakthrough research by Varki et al. revealed HS glycans' existence as one of the selectin's ligand candidates.[6, 7] More importantly, they have demonstrated the significance of the NU domain in selectin binding for the first time.[8] Since then, there have not been any reports in the literature that have validated the theory. The reason could be partially attributed to the NU domain's rare presence (0.7 to 4 % of total glucosamine residues) in the HS backbone, limiting its bioavailability and further studies.[9, 10] To validate this three-decade-old theory, with a comprehensive NU domain carrying HS library in hand, we have carried out the microarray analysis of HT ligands with P-selectin.

In addition to that, we have further extended our studies to establish a structure-activity relationship between HS and Tau protein. The rise in the literature suggesting the role of

HS in mitigating tau-related pathology has intrigued us to find the optimal structural requirements for modulating heparin-tau interactions.[11- 13]

## 5.2 Results and Discussion:

### 5.2.1 Selectins:

HT ligands library constructed in chapter 2 was used for P and E selectin binding studies. Both NU/NA domains carrying HT ligands were conjugated on microarray chips and then detected with recombinant human P and E selectin, followed by detection with APC conjugated secondary antibody. To analyze the high-throughput array binding assays, each HT ligand-selectin interaction was ranked based on their fluorescent intensity with respect to maximal fluorescent intensity in each array block. As a control, sialylated ligands were also conjugated to the chips and analyzed. Based on rankings data, the ligands were divided into three groups, i.e., Group A, B, and C for both P and E selectins.

P-Selectin: In group A, ligands showed weak/ no binding with P-selectin. HT ligands with phosphate and N-acetate backbone, namely, **HT-62P, HT-6P, HT-0S-NAc, HT-6S-NAc, HT-2S-NAc, HT-3S-NH, HT-2,6S-NAc** were among the major ligands present in group A. The results suggest that phosphated ligands that are geometrically and structurally equivalent to sulfate groups might not be the appropriate modification for fine-tuning the heparin selectin interactions. It also signifies nature's preference for choosing sulfate groups in HS backbone during molecular recognition and evolution. Further non-binding with acetate derivatives of HT ligands suggested that glucosamine residue in the HS backbone could be an additional factor along with the sulfate moieties to regulate selectin binding (Figure 1).

Group B ligands **HT-0S-NH, HT-6S-NH, HT-2,3S-NH,** and **HT-3,6S-NH**, showed moderate binding with P-selectin. The results clearly demonstrated the importance of free glucosamine residues for selectin recognition. The binding percentage was slightly higher for HT ligands with higher-order sulfation.

Finally, in group C, exclusive and robust binding of HT ligands **HT-2S-NH and HT-2,6S-NH** with P-selectin unraveled HS's hidden structural features that were unknown for

decades. Notably, **HT-2S-NH** ligand with low order sulfation (disulfate) ranked 100 percent in the group than **HT-2,6S-NH** (ranked 82 %, tetrasulfate). The results clearly highlight the importance of IdoA 2-*O*-sulfate along with the NU domain for modulating P-selectin activities. Further, quantification of binding using SPR and *in vitro* studies are in progress.

No/ weak binding with sialylated ligands was in good agreement with previously reported literature (Figure 2).

| | P- Selectin | | E- Selectin | | |
|---|---|---|---|---|---|
| Code | Mean | SEM | Mean | SEM | Group |
| HT-62P | 0 | 0 | 1 | 0 | A |
| HT-6P | 2 | 0 | 2 | 0 | |
| HT-0S-NAc | 9 | 5 | 6 | 3 | |
| HT-6S-NAc | 11 | 0 | 9 | 6 | |
| HT-2S-NAc | 18 | 11 | 29 | 4 | |
| HT-2,6S-NAc | 27 | 4 | 38 | 6 | |
| HT-3S-NH | 7 | 3 | 15 | 8 | |
| HT-0S-NH | 43 | 1 | 32 | 5 | B |
| HT-6S-NH | 41 | 4 | 35 | 5 | |
| HT-2,3S-NH | 60 | 3 | 47 | 5 | |
| HT-3,6S-NH | 67 | 7 | 77 | 14 | |
| HT-2S-NH | 100 | 0 | 86 | 0 | C |
| HT-2,6S-NH | 82 | 4 | 100 | 0 | |
| Hep | 2 | 1 | 13 | 7 | Control |

| % |
|---|
| 100 |
| 75 |
| 50 |
| 25 |
| 0 |

**Figure 1:** P and E- Selectin glycan microarray binding assay. Binding was tested at 3 serial dilutions (100, 50, 25 µg/ ml), then detected with the APC conjugated secondary antibody. Arrays were scanned, relative fluorescent units (RFU) obtained, and maximum RFU determined and set as 100% binding. The mean rank is shown as a heat map of all the examined binding assays together (red highest, blue lowest and white 50th percentile of ranking).

E- Selectin: The binding pattern for E-selectin was similar to that of P-selectin. Similar binding preferences for both the selectins could be attributed to the structural homology between them, especially in the lectin domain that binds with sugars.

| | | | | P-Selectin µg/ml | | | | | |
|---|---|---|---|---|---|---|---|---|---|
| Skeleton | TYPE | Name | ID | 100 | 50 | 25 | 12.5 | 6.2 | 3.1 |
| 6S-Lex | Gc | Neu5Gc-α-2-3-Gal-β1-4(Fuc-α1-3-)-GlcNAc6SO3-βProNH2 | 58 | 35 | 35 | 51 | 42 | 34 | 14 |
| | Ac | Neu5Ac-α-2-3-Gal-β1-4(Fuc-α1-3-)-GlcNAc6SO3-βProNH2 | 57 | 49 | 43 | 36 | 31 | 41 | 47 |
| Lea | Gc | Neu5Gc-α2,3-Lea βProNH2 | 86 | 47 | 19 | 33 | 40 | 29 | 45 |
| | | Neu9Ac5Gc-α2,3-Lea βProNH2 | 88 | 36 | 26 | 37 | 43 | 9 | 31 |
| | Ac | Neu5Ac-α2,3-Lea βProNH2 | 83 | 23 | 52 | 48 | 21 | 34 | 32 |
| | | Neu5,9Ac2-α2,3-Lea βProNH2 | 87 | 24 | 35 | 22 | 19 | 19 | 52 |
| | Sc | Lea βProNH2 | 84 | 22 | 37 | 56 | 4 | 53 | 38 |
| Lex | Gc | Neu5Gc-α-2-3-Gal-β1-4(Fuc-α1-3-)-GlcNAc-βProNH2 | 56 | 56 | 28 | 33 | 34 | 39 | 16 |
| | Ac | Neu5Ac-α-2-3-Gal-β1-4(Fuc-α1-3-)-GlcNAc-βProNH2 | 55 | 34 | 34 | 49 | 35 | 23 | 38 |
| Leb | Sc | Leb βProNH2 | 85 | 38 | 60 | 40 | 48 | 17 | 37 |

**Figure 2:** P selectin glycan microarray binding assay with Sia glycans

### 5.2.2 Tau Protein:

Microarray chips conjugated with HT ligands were detected with fluorescently labeled (Atto 655) monomeric Tau protein (K-18 construct), and binding profiles were measured. Similar to other proteins, the binding intensities were ranked with respect to maximal fluorescent intensity in each array block. Natural heparin was used as a control and analyzed.

Interestingly, natural heparin displayed a continuous decrease in binding intensities with increased protein concentration, thereby suggesting that HS requires an optimum Tau concentration for efficient binding. Further, except for **HT-3,6S-NH**, all other HT ligands showed an increase in the fluorescent intensity with increased protein concentration. No clear trend or binding pattern was observed for these ligands, suggesting that Tau protein might require a larger oligosaccharide library for determining accurate HS binding epitopes (Figure 3).

| Code | 0.0375 | 0.075 | 0.15 | 0.3125 | 0.625 | 1.25 | 2.5 | 5 |
|---|---|---|---|---|---|---|---|---|
| HT-0S-NAc | 1 | 2 | 7 | 8 | 25 | 7 | 6 | 6 |
| HT-2S-NAc | 2 | 4 | 13 | 12 | 14 | 5 | 3 | 4 |
| HT-6S-NH | 2 | 3 | 9 | 9 | 6 | 12 | 16 | 35 |
| HT-2,3S-NH | 2 | 4 | 11 | 15 | 11 | 15 | 21 | 58 |
| HT-0S-NH | 3 | 8 | 22 | 24 | 26 | 21 | 23 | 53 |
| HT-6P | 7 | 12 | 22 | 26 | 31 | 27 | 33 | 65 |
| HT-6,2P | 7 | 8 | 30 | 42 | 32 | 49 | 40 | 56 |
| HT-3S-NH | 8 | 18 | 42 | 19 | 44 | 60 | 48 | 50 |
| HT-6S-NAc | 7 | 13 | 28 | 45 | 32 | 59 | 55 | 100 |
| HT-2S-NH | 6 | 15 | 25 | 36 | 39 | 48 | 60 | 70 |
| HT-2,6S-NAc | 8 | 16 | 24 | 65 | 69 | 69 | 67 | 64 |
| HT-2,6S-NH | 34 | 35 | 62 | 56 | 43 | 81 | 52 | 41 |
| HT-3,6S-NH | 34 | 32 | 76 | 98 | 69 | 65 | 40 | 35 |
| Hep | 100 | 100 | 100 | 76 | 67 | 49 | 25 | 29 |

| % |
|---|
| 100 |
| 75 |
| 50 |
| 25 |
| 0 |

**Figure 2:** Tau protein glycan microarray binding assay. Protein concentration was varied from 0.0375- 5 µg/ml.

HT-3,6S-NH showed a gaussian-like distribution for binding profiles with different protein concentrations. After reaching the maxima (at 0.3125 ug/ml protein concentration), the continuous decrease in the fluorescent intensity suggests that HT-3,6S-NH could behave similarly to natural heparin. However, further studies and a broad library is required to find the precise tau binding HS epitopes.

## 5.3 Conclusions:

In conclusion, we have identified **HT-2S-NH** and **HT-2,6S-NH** as potential targeting for P-selectin. The results supported the requirement of the NU domain for selectin binding. Additionally, we have also identified HT-**3,6S-NH** ligand that could behave similarly to natural heparin; however, further detailed analysis is required to support the hypothesis. Overall, the results demonstrate the potential of synthetic glycan library and glycan microarray technology to identify precisely well-defined HS analogs to fine-tune heparin-protein interactions.

## 5.4 Experimental Part:

### 5.4.1 Glycan microarray:

Materials: Recombinant Human P-selectin (ADP3-050), E-selectin (ADP1-050) and APC-anti Human P/E selectins (FAB6169A) were purchased from R&D systems. Atto 655 conjugated Tau protein was isolated and purified by Dr. Harish Kumar at IISER Pune, Biology department.

HT microarray fabrication and slide processing: Experimental conditions similar to chapters 2 and 3 were used.

## 5.5 References:


1. Lamanna, W. C.; Kalus, I.; Padva, M.; Baldwin, R. J.; Merry, C. L.; Dierks, T., The heparanome—the enigma of encoding and decoding heparan sulfate sulfation. *J. Biotechnol.* **2007,** *129* (2), 290-307.
2. Sattelle, B. M.; Shakeri, J.; Almond, A., Does microsecond sugar ring flexing encode 3D-shape and bioactivity in the heparanome? *Biomacromolecules* **2013,** *14* (4), 1149-1159.
3. Nagamine, S.; Tamba, M.; Ishimine, H.; Araki, K.; Shiomi, K.; Okada, T.; Ohto, T.; Kunita, S.; Takahashi, S.; Wismans, R. G., Organ-specific sulfation patterns of heparan sulfate generated by extracellular sulfatases Sulf1 and Sulf2 in mice. *J. Biol. Chem.* **2012,** *287* (12), 9579-9590.
4. Bevilacqua, M. P.; Nelson, R. M., Selectins. *J. Clin. Investig.* **1993,** *91* (2), 379-387.
5. McEver, R. P., Selectins. *Curr. Opin. Immunol.* **1994,** *6* (1), 75-84.
6. Norgard-Sumnicht, K. E.; Varki, N. M.; Varki, A., Calcium-dependent heparin-like ligands for L-selectin in nonlymphoid endothelial cells. *Science* **1993,** *261* (5120), 480-483.
7. Koenig, A.; Norgard-Sumnicht, K.; Linhardt, R.; Varki, A., Differential interactions of heparin and heparan sulfate glycosaminoglycans with the selectins.

Implications for the use of unfractionated and low molecular weight heparins as therapeutic agents. *J. Clin. Investig.* **1998,** *101* (4), 877-889.

8. Norgard-Sumnicht, K.; Varki, A., Endothelial heparan sulfate proteoglycans that bind to L-selectin have glucosamine residues with unsubstituted amino groups. *J. Biol. Chem.* **1995,** *270* (20), 12012-12024.
9. Van Den Born, J.; Gunnarsson, K.; Bakker, M. A.; Kjellén, L.; Kusche-Gullberg, M.; Maccarana, M.; Berden, J. H.; Lindahl, U., Presence of N-unsubstituted glucosamine units in native heparan sulfate revealed by a monoclonal antibody. *J. Biol. Chem.* **1995,** *270* (52), 31303-31309.
10. Westling, C.; Lindahl, U., Location of N-unsubstituted glucosamine residues in heparan sulfate. *J. Biol. Chem.* **2002,** *277* (51), 49247-49255.
11. Zhao, J.; Zhu, Y.; Song, X.; Xiao, Y.; Su, G.; Liu, X.; Wang, Z.; Xu, Y.; Liu, J.; Eliezer, D., 3-O-Sulfation of Heparan Sulfate Enhances Tau Interaction and Cellular Uptake. *Angew. Chem. Int. Ed.* **2020,** *59* (5), 1818-1827.
12. Wang, P.; Cascio, F. L.; Gao, J.; Kayed, R.; Huang, X., Binding and neurotoxicity mitigation of toxic tau oligomers by synthetic heparin like oligosaccharides. *Chem. Commun.* **2018,** *54* (72), 10120-10123.
13. Rauch, J. N.; Chen, J. J.; Sorum, A. W.; Miller, G. M.; Sharf, T.; See, S. K.; Hsieh-Wilson, L. C.; Kampmann, M.; Kosik, K. S., Tau internalization is regulated by 6-O sulfation on heparan sulfate proteoglycans (HSPGs). *Sci. Rep.* **2018,** *8* (1), 1-10.